Characterisation of Alloantibody-Human Leukocyte Antigen Interactions to Improve Immunological Risk Assessment in Solid Organ Transplantation

Ashley J. Priddey

Primary Supervisor: Dr. Vasilis Kosmoliaptsis

Secondary Supervisor: Dr. Andrew Leach

Department of Surgery, University of Cambridge

This dissertation is submitted to the University of Cambridge for the degree of

Doctor of Philosophy

Queens' College August 2022

Declaration

I, Ashley James Priddey, hereby declare that except where specific reference is made to the work of others, the contents of this dissertation are original and have not been submitted in whole or in part for consideration for any other degree or qualification in this, or any other University. This dissertation is the result of my own work and includes nothing which is the outcome of work done in collaboration, except where specifically indicated in the text. This dissertation contains less than 65,000 words including appendices, bibliography, footnotes, tables, and equations and has less than 150 figures.

Ashley Priddey

August 2022

I dedicate this thesis to my wife, Ann Elizabeth Priddey, who throughout the period of these studies has provided me with all the love, support, and inspiration needed to get me to this point. You have been the perfect role model in demonstrating how to tackle adversities in all aspects of life head-on, whilst maintaining positivity and a forward-thinking mentality throughout. You are my rock!

Abstract

Characterisation of Alloantibody-Human Leukocyte Antigen Interactions to Improve Immunological Risk Assessment in Solid Organ Transplantation

Antibody mediated rejection remains a major challenge in solid organ transplantation, where the development of immunoassays for characterisation a recipient's donor HLA-specific antibodies has revolutionised the field of solid organ transplantation. These immunoassays are essential for patient evaluation, immune monitoring, and antibody-related immunological risk assessment, however uncertainties concerning data interpretation often prevents determination of an antibody's clinical significance. The initial aim of this research was to expand the knowledge on the properties of HLA-specific antibodies that govern their pathogenic potential. Luminex single antigen beads (SABs), SAB-C1q, flow cytometry (FC) and complement dependent cytotoxicity (CDC) assays were used to determine the reactivity and complement fixing capacities of human monoclonal antibodies, whilst biolayer interferometry (BLI) was used for real-time quantification of alloantibody-HLA kinetics. Outputs from each immunoassay were found to be dependent on antibody concentration, [Ab], where the degree of CDC was proportional to the antibody's affinity, K_D. The strongest affinity for each antibody was measured with the sensitising antigen. Solid-phase assays offered a higher sensitivity of antibody detection, however stronger interactions could not be distinguished from one another. In attempt to further assess the relationship between antibody-HLA interaction affinity and effector function, the ability to establish an *in vitro* model of alloantibody-mediated endothelial cell activation and tissue injury was explored. Lastly, using the principles of microfluidic diffusional sizing and Bayesian inference, microfluidic antibody affinity profiling (MAAP) was developed to enable in-solution, simultaneous determination of the K_D and [Ab] of antibodies directly in patient serum samples. Quantification of purified monoclonal antibodies spiked into both PBS and blank serum provided a proof-of-principle before moving into HLA antibody-incompatible transplant sera. Here, MAAP was able to quantify the affinity and concentration of antibodies in real-life patient sera, whilst also providing examples of how this information may be used as a tool in clinic to improve transplant-related decision-making processes. Overall, this work provides evidence for the importance of antibody abundance and affinity in clinically relevant humoral alloresponses and, through development of MAAP, outlines a path towards in depth profiling of antibody responses in patient sera.

Acknowledgements

I would firstly like to acknowledge my supervisors, Dr. Vasilis Kosmoliaptsis and Dr. Andrew Leach, where without their help, guidance and support, this project would not have been possible. I would specifically like to express my gratitude to Dr. Kosmoliaptsis, for his continuous positivity and belief in my skills as a researcher, which pushes me further each day. The dedication and effort that you have put into the discipline of clinical transplantation is inspirational and has fuelled my desire to be a part of this field.

I thank my family for giving me the love, support, and encouragement to get me to where I am today. I would not be here if I did not have the relationships and support structure you have provided for me that defines my personality.

I am extremely grateful to have been given the opportunity to work and study at the University of Cambridge Department of Surgery, attributed to grants awarded by the Addenbrooke's Charitable Trust (2016-2018) and the National Institute of Health Blood and Transplant Research Unit (2018-2021), who have supported my employment within the department.

I would like to thank Prof. M.L. Nicholson who has and continues to support me throughout my posts within the Department of Surgery, somewhere I have always felt accepted and valued.

Thank you to all members of the Department of Surgery, you have made my time within this department very enjoyable and somewhere I will always be grateful of having worked. I would also like to say a special thank you to members of the Kosmoliaptsis lab group and Hosgood lab group, our daily interactions can make the dullest days brighter.

Thank you to my first-year examiners, Dr. Nicholas Torpey and Prof. Chris Watson, for their knowledge and advice when deciding the most interesting and suitable questions to direct my research projects.

I would also like thank the following individuals, collaborators, and institutions for their contribution to the research projects which has led to the submission of this thesis:

- To Prof. Frans Claas, Dr. Sebastiaan Heidt, Dr. Gonca Karahan, and Dr. Cynthia Kramer at Leiden University Medical Centre, for providing monoclonal antibodies,

protein sequences, and assay protocols, and their collaboration and contribution to T-cell flow cytometry and complement-dependent cytotoxicity experiments in chapter 3.

- To the members of the Addenbrooke's Hospital Histocompatibility and Immunogenetics Laboratory, specifically Sarah Peacock, Gemma Brewin, Sophie Bossingham, Jessie Martin, and Owen Vennard, who have provided access to equipment, patient samples and clinical data, whilst also offering aid with Luminex experiments.
- To Prof. Tuomas Knowles and various members of his group at the University of Cambridge Department of Chemistry; Dr. Georg Meisl, Dr. Catherine Xu, Dr. Tom Schiedt, Matthias Schneider and Mengsha Hu, for their collaboration on the MAAP project and contribution to the work outlined in chapter five.
- To employees of Fluidic Analytics Ltd. who provided the Fluidity One-W Serum instrument, but more specifically to Sean Devenish, the research and development team, and the applications team who have continuously offered support, help, troubleshooting and advice on assay development throughout the microfluidic studies.
- To Prof. Kourosh Saeb-Parsey and members of the Cambridge Biorepository for Translational Medicine, particularly Krishnaa Mahbubani, for supplying primary human vessel tissue for endothelial cell isolation.
- To Sarah Hosgood for supplying porcine renal artery tissue needed for development of the endothelial cell isolation protocol.
- To Katherine Stott in the Department of Biochemistry Biophysics Facility for her ongoing support and advice with biolayer interferometry studies.
- To Rico Buchli at PureProtein LLC, and the NIH tetramer core facility-Leiden for supplying the purified HLA monomers needed for these studies to go ahead.
- To Dr Josan Marquez and members of his team at the EMBL Grenoble for their support, training and collaboration with other projects stemming from these studies.
- To Dr. Elaine Reed and members of her group at UCLA for providing protocols and help with regards to the primary endothelial cell studies.

Finally, I would like to say a huge thank you to the donors, their families, and their friends, who this work is aimed to support. The struggles of your life are widely recognised throughout the medical community, and I hope the outcomes of this work will go on to better these issues.

Publications and Presentations

Publications arising from this work:

- Kramer CSM, Franke-van Dijk MEI, **Priddey AJ**, Pongrácz T, Gnudi E, Car H, et al. Recombinant human monoclonal HLA antibodies of different IgG subclasses recognising the same epitope: Excellent tools to study differential effects of donor-specific antibodies. *HLA*, 94(5):415-424, 2019. (See appendices)

In review (* = joint first authors):

- Schneider MM*, Scheidt T*, **Priddey AJ***, Xu CK*, Hu M*, Devenish SR, et al. Microfluidic Antibody Affinity Profiling for In-Solution Characterisation of Alloantibody-HLA Interactions in Human Serum. *bioRxiv*, 2020. (See appendices)

In preparation:

- Affinity profiling to assess the clinical significance of HLA-specific antibodies.

Pending Patents:

- PCT international application number PCT/GB2021/051244

  Patent submitted to protect the intellectual property concerning the development and use of Microfluidic Antibody Affinity Profiling. (See appendix 17)

Abstracts/Conferences:

- British Transplant Society Congress (2022) - Medawar Medal Presentation - Winner

  Abstract Title: '*Direct alloantibody affinity profiling in patient sera to improve immunological risk assessment in transplantation*'
- 20th European Society of Organ Transplantation Congress (2021)

  Abstract Title: '*Detection and characterization of immunologically relevant alloantibody-HLA interactions using microfluidic antibody affinity profiling*'
- 2020 American Transplant Congress
- Blood and Transplant Research Unit in Organ Donation and Transplantation Meetings (2018-2021)

- 18th European Society of Organ Transplantation Congress (2017)

  Abstract Title: '*Quantitation of alloantibody-HLA binding kinetics using a novel biosensor assay to improve immunological risk assessment in transplantation*'

- British Transplant Society Annual Congress (2017)

Abbreviations

[Ab]	Concentration of antibody
+ve	Positive
-ve	Negative
AAMR	Acute antibody-mediated rejection
Ab	Antibody
ABC	ATP-binding cassette
Abs	Absorbance
ADCC	Antibody-dependent cell-mediated cytotoxicity
AF647	Alexa Fluor 647
Ag	Antigen
AHC	Anti-human IgG Fc capture
Akt	Serin/threonine protein kinase / Protein kinase B
AlloAb	Alloantibody
AMC	Anti-murine IgG Fc capture
AMR	Antibody-mediated rejection
APC	Antigen presenting cell
APC*	Allophycocyanin
Asn	Asparagine
ATP	Adenosine triphosphate
AV	Allograft vasculopathy

B2M	Beta-2 microglobulin
BCA	Bicinchoninic acid
Bcl-2	B-cell lymphoma 2
Bcl-xL	B-cell lymphoma extra large
BCR	B-cell receptor
bFGF	basic fibroblast growth factor
BLI	Biolayer Interferometry
BSA	Bovine serum albumin
C1q	Complement component 1q
cAMP	Cyclic adenosine monophosphate
CAMR	Chronic antibody-mediated rejection
CAN	Chronic allograft nephropathy
CD3	Cluster of differentiation 3
CD4	Cluster of differentiation 4
CD8	Cluster of differentiation 8
CD31	Cluster of differentiation 31/ Platelet endothelial cell adhesion molecule I (PECAM-I)
CDC	Complement-dependent cytotoxicity
CDR	Complementarity-determining region
C_H	Constant heavy domain
C.I.	Confidence interval
C_L	Constant light chain domain
CLIP	Class II-associated invariant chain peptide

CMR	Cell-mediated rejection
CNX	Calnexin
CREB	cAMP response element-binding protein
CREG	Cross-reactive group
CRT	Calreticulin
CSR	Class-switch recombination
CTL	Cytotoxic T lymphocyte
Cys	Cysteine
DAMP	Disease activated molecular pattern
DBD	Deceased brain dead
DC-SIGN	Dendritic cell-specific intracellular adhesion molecule-3-grabbing non-integrin
DCD	Deceased cardiac dead
ddH2O	Double-distilled water
DMSO	Dimethyl sulphoxide
DNA	Deoxyribonucleic acid
DSA	Donor-specific antibody
DTT	1,4-Dithiothreitol
EBV-LCL	Epstein-Barr virus transformation of immortalised lymphoblastoid cell line
EC	Endothelial cell
ECGS	Endothelial cell growth supplement
EDTA	Ethylenediaminetetraacetic acid

EECGM	Enriched endothelial cell growth medium
EGF	Epidermal growth factor
eIF4A1	Eukaryotic translation initiation factor 4A1
ELISA	Enzyme-linked immunosorbent assay
EMS-3D	Electrostatic mismatch score 3-dimensional
EndMT	Endothelial-to-mesenchymal transition
ER	Endoplasmic reticulum
ERAAP	Endoplasmic reticulum aminopeptidase associated with antigen processing
ERp57	Endoplasmic reticulum protein 57
ERK/Erk	Extracellular signal-regulated kinase
Fab	Fragment antigen-binding
FACS	Fluorescence-activated cell sorting
FAK	Focal adhesion kinase
Fc	Fragment crystallisable
FC	Flow cytometry
FcR	Fragment crystallisable receptor
FCS	Foetal calf serum
FIDA	Flow-induced dispersion analysis
FITC	Fluorescein isothiocyanate
FR	Framework region
Fv	Fragment variable
GC	Germinal centre

GlcNAc	N-acetylglucosamine
GTP	Guanosine triphosphate
GVHD	Graft-versus-host disease
H-2	Histocompatibility system 2
HAoEC	Human aortic endothelial cell
HAoSMC	Human aortic smooth muscle cell
HAR	Hyperacute rejection
HI	Heat-inactivated
HLA	Human leukocyte antigen
HO-I	Haem oxygenase I
hr	Hour
HR	Hinge region
HRP	Horseradish peroxidase
HUVEC	Human umbilical vein endothelial cell
ICAM-I	Intercellular adhesion molecule-I
IFN	Interferon
Ig	Immunoglobulin
IgA/D/E/G/M	Immunoglobulin class A/D/E/G/M
IGF-1	Insulin-like growth factor 1
IgG1/2/3/4	Immunoglobulin class G, subclass 1/2/3/4
IMDM	Iscove's modified Dulbecco's medium
ITAM	Immunoreceptor tyrosine-based activation motif
ITIM	Immunoreceptor tyrosine-based inhibitory motif

JAM-1	Junction adhesion molecule 1
K_D	Equilibrium dissociation constant
kDa	Kilodalton
k_{off}	Dissociation constant
k_{on}	Association constant
LA	Leukocyte antigen
LD	Lymphocyte-defined
M	Molar
M199	Medium 199
MAAP	Microfluidic antibody-affinity profiling
mAb	Monoclonal antibody
MAC	Membrane attack complex
MAPK	Mitogen-activated protein kinase
MAPKAP1	MAPK-associated protein 1
MDS	Microfluidic diffusional sizing
MFI	Mean fluorescence intensity
MFI-FC	Mean fluorescence intensity fold-change
µg	Microgram
mg	Milligram
MHC	Major histocompatibility complex
µl	Microlitre
ml	Millilitre
MLC	Mixed lymphocyte culture

MLCK	Myosin light chain kinase
mLST8	mTOR-associated protein LST8 homolog
µM	Micromolar
mM	Millimolar
mTOR	mechanistic target of rapamycin kinase
N_2	Nitrogen
NHS	N-hydroxysuccinimide
NK	Natural killer
NLSQ	Non-linear least squares
nm	Nanometre
nM	Nanomolar
NP-40	Nonidet P-40
OD	Optical density
PAMP	Pathogen-associated molecular pattern
PBMC	Peripheral blood mononuclear cells
PBS	Phosphate buffered saline
PBS-T	Phosphate buffered saline + 0.2% Tween-20
PCR	Polymerase chain reaction
PDGF	Platelet-derived growth factor
PDI	Protein disulphide isomerase
PE	Phycoerythrin
pg	Picogram
PI3K	Phosphoinositide 3-kinase

PKA	Protein kinase A
PLC	Peptide loading complex
pM	Picomolar
PMA	Phorbol 12-myristate 13-acetate
PMSF	Phenylmethylsulphonyl fluoride
PPI	Protein-protein interaction
PRR	Pattern recognition receptors
R_{eq}	Response at equilibrium
R_H	Hydrodynamic radius
Rho-GTP	Rho family of GTPases
Rictor	rapamycin-insensitive companion of mTOR
RNA	Ribonucleic acid
ROK	Rho kinase
rpm	Revolutions per minute
RT	Room temperature
S6K	S6 kinase
S6RP	S6 ribosomal protein
SA	Streptavidin
SAB	Single antigen bead
SC	Secretory component
SD	Serologically defined
SDS	Sodium dodecyl sulphate
SDS-PAGE	Sodium dodecyl sulphate-polyacrylamide gel electrophoresis

SEC	Size exclusion chromatography
SHC	Somatic hyperconversion
SHIP	Src homology region 2 domain-containing inositol polyphosphate 5 phosphatase
SHM	Somatic hypermutation
SHP	Src homology region 2 domain-containing phosphatase
SLO	Secondary lymphoid organs
SMC	Smooth muscle cell
SRP	Signal recognition particle
SRPR	Signal recognition particle receptor
STA	Stop-transfer sequence
TAP	Transporter associated with antigen processing
TAP-BPR	Transporter associated with antigen processing-binding protein related
TBS	Tris buffered saline
TBS-T	Tris buffered saline + 0.1% Tween-20
TCR	T-cell receptor
Tfh	T follicular helper cell
Th	T helper cell
TMB	Tetramethylbenzidine
TNF	Tumour necrosis factor
Treg	T regulatory cell
TRIM21	Tripartite motif-containing protein 21
VCAM-I	Vascular cell adhesion molecule-1

VEGF	Vascular endothelial cell growth factor
V_H	Variable heavy chain domain
V_L	Variable light chain domain
vWF	Von Willebrand factor
XM	Cross-match

Contents

Schneider MM*, Scheidt T*, **Priddey AJ***, Xu CK*, Hu M*, Devenish SR, et al. Microfluidic Antibody Affinity Profiling for In-Solution Characterisation of Alloantibody-HLA Interactions in Human Serum. *bioRxiv*, 2020.

(* = joint first authors)

Kramer CSM, Franke-van Dijk MEI, **Priddey AJ**, Pongrácz T, Gnudi E, Car H, et al. Recombinant human monoclonal HLA antibodies of different IgG subclasses recognising the same epitope: Excellent tools to study differential effects of donor-specific antibodies. *HLA*, 94(5):415-424, 2019.

List of Figures

List of Tables

Chapter One

General Introduction

1.1. Histocompatibility in Transplantation

1.1.1. A Brief History of Organ Transplantation

Organ transplantation is defined as the transfer of organ tissue from one person to another to replace the recipient's current organ function and is currently the best treatment for end-stage organ failure [1]. Despite the practice of tissue transplantation dating back to 600 B.C., as documented in the Sushruta Samhita, where autogenous skin flaps were used to replace noses as part of disciplinary procedures [2], the first successful whole organ transplant was not performed until 1902 by the Austrian surgeon E. Ullmann [3]. This procedure involved the autotransplantation of a canine kidney using vascular suturing techniques developed by M. Jaboulay, J. Dörfler and A. Carrel [4,5]. This feat was later followed by the first renal xenotransplantation attempts in which caprine and porcine kidneys were transplanted into human patients suffering from chronic kidney failure by Jaboulay (1906) [6], and later using simian kidneys by E. Unger (1910) [7], all of which failed. The first human-to-human allotransplantation was attempted by Soviet surgeon Y.Y. Voronoy in 1933, in which failure was attributed to major blood group mismatch between donor and recipient [8].

Following several failed transplants throughout the 1930s and 1940s, it wasn't until 1954 when J. Murray performed the first successful human-to-human renal transplant between identical twins [9]. Although this feat was celebrated by surgeons worldwide, this success did not advance the scientific knowledge in the field as skin graft transplants were being frequently performed across identical twins in surgical practice [10, 11]. The first breakthrough came in

1958, when Murray then went on to complete the first successful non-identical twin transplant by irradiating the recipient's whole body to deplete their bone marrow [12]. This procedure fulfilled a larger scientific accomplishment of overcoming the genetic barrier between non-identical humans and paved the way for modern age transplantation.

1.1.2. Transplant Science Through the Years

The transplantation of organs across different animals and species was performed readily throughout the early 20th century with no fruitful outcomes. Despite this, the emerging immunological understanding during this period enabled popularity to grow around the transplant field, providing hope that the prospect of a successful transplant could be achieved. In 1912, the researcher G. Schöne made the first directly transplant-related medical observation, in that skin allografts would always fail, and subsequent grafts from the same donor result in an accelerated rate of failure [13]. This finding would later be documented by many others including P. Medawar and T. Gibson, who in 1943 coined the term 'second-set response' [14]. Medawar went on to receive the 1960 Nobel Prize in physiology and medicine for his findings [15]. Other discoveries by J. Murphy between 1912-1921 showed that depleting lymphocytes through various methods could extend the life of a homograft [16], conclusively establishing the role of lymphocytes in graft rejection and opening the doors for therapies that may aid in successful transplantation.

C.C. Little and E. Tyzzer's studies on genetics and Mendelian inheritance guided their interest to the transplant field, where they found that rejection was dependent on the strain of the graft-versus-host (disease; GVHD) [17]. They suggested that tissue rejection is related to the codominant expression of products encoded by several loci, where rejection occurs when the recipient does not express the same products of these loci as the donor tissue. Further experiments carried out by P. Gorer (1936) led to the discovery of these products in inbred mice [18-20], where collaborative research with G. Snell identified a locus of these encoded products. This locus was given the term the histocompatibility locus 2 (H-2) [21], which is now known as the major histocompatibility complex (MHC) across the animal kingdom. MHC molecules were first discovered in humans around the same time as the first successful transplant in 1958, when J. Dausset observed leuko-agglutination to be caused by antibodies against human MHC, what was then known as MAC (now HLA-A2) [22]. This was closely followed by similar observations by J. Van Rood and R. Payne, who went on to further analyse the reaction patterns of sera from multiparous women against a panel of donor leucocytes [23,

24]. Van Rood found that this system was diallelic, which he called alleles 4a and 4b [25], while Payne together with her associates were able to detect two alternative individual leucocyte antigens (LAs) which they named LA1 and LA2 [26]. Due to the complexity of the subjects involved with these studies, various international histocompatibility workshops were set up throughout the 1960s to develop and carry out various serological typing methods to detect different leukocyte antigens [27]. This effort led to the development of the antibody microcytotoxicity assay by P. Terasaki (1964), which later emerged as the gold standard for serological typing and crossmatching [28]. F. Kissmeyer-Nielsen was able to establish two separate genetic loci within the same coding region of a single chromosome that encode different antigens, called LA and Four after their previous designations (now HLA-A and HLA-B) [29]. Further studies to detect new antigens carried out by this group also uncovered a novel antigen, AJ, which was proven to be independent of the LA and 4 loci and was designated to a third human leukocyte antigen (HLA) locus, the AJ locus (now HLA-C) [30]. These three loci are now known as the constituents of the HLA class I antigens.

As well as the success of Terasaki's microcytotoxicity assay, another method that assessed the immunogenicity of lymphocytes was also developed by F. Bach and D.B. Amos, known as the mixed lymphocyte culture (MLC) [31, 32]. By observing the morphology and division patterns of leukocytes from two separate individuals upon mixing, they were able to show that the outcome of this reaction was controlled by the HLA-encoding region of the chromosome, but not linked to the serological typing of the HLA antigens [33]. This brought about Bach's theory that there are two determinants encoded by the HLA complex, those that are serologically defined (SD) and those that are lymphocytically defined (LD) [34]. Through primed LD typing [35], these determinants were found to be encoded at a separate locus on the HLA chromosomal region, called HLA-D, and were later found to be a collection of three separate but closely linked loci (HLA-DR, -DP and -DQ) now called the class II antigens [36].

Within the scientific field, the progression of knowledge is often dependent on the development of newer and improved techniques/assays. In terms of transplantation, it is widely believed that the discovery of the HLA system and the introduction of the International Histocompatibility Workshops in 1964 are two of the most pivotal turning points which aided the rapid improvement of solid organ transplantation success throughout this time.

1.2. Human Leukocyte Antigen

The human leukocyte antigen complex is an evolutionarily conserved set of genes that encode a collection of highly polymorphic glycoproteins which play major roles in the mammalian adaptive immune system. Located on the short arm of chromosome 6, a 7.6 megabase-pair-long DNA sequence encodes 252 different genes that can be transcribed into numerous antigens and immunological proteins, around 28% of which have an immune system function [37]. The antigens encoded by these genes can be split into 2 main classes: class I and class II (Figure 1.1), each consisting of classical and non-classical sub-classes [27]. Classical HLA molecules have a main role of presenting antigenic peptides at the cell surface of antigen presenting cells (APCs) [38], whilst non-classical antigens function to carry out various regulatory functions [39, 40]. When expressed, intracellular classical HLA molecules can bind complimentary polypeptide antigen fragments within their peptide binding groove, where they can then translocate to the cell surface to present these to be recognised by clonally derived T-cells [41]. The purpose of this peptide presentation is to enable the human body to distinguish 'self' from 'non-self' so that an immune response can be initiated upon the introduction of foreign antigens into the body [42].

1.2.1. HLA Class I

Class I HLAs can be found on almost all nucleated somatic cells and consist of the classical HLA-A, -B and -C, and the non-classical HLA-E, -F and -G molecules [43]. The structure of these class I molecules was solved by P. Bjorkman et al (1987) [44], where they showed these molecules to be composed of 2 subunits; a ~45kDa transmembrane α-chain containing 3 extracellular domains (α1, α2 and α3) with the C-terminus on the cytosolic side of the membrane, and a ~12kDa β-chain known as β-2 microglobulin (B2M) which makes up the fourth, non-covalently linked domain (Figure 1.1.A). Between the two α-helix and eight anti-parallel β-strand platform of the membrane-distal α1 and α2 domains, lies the peptide binding groove which is predominantly involved with the binding of 8-10 residue-long intracellular peptides.

Upon transcription of type I membrane protein genes, such as the HLA Class I heavy chain, ribosomes in the cytosol synthesise the first amino acid residues of the thermally unstable HLA

heavy chain peptide. The first 25 residues of this gene, encode hydrophobic signal sequence at the N-terminus of the heavy chain peptide, is recognised by the signal recognition particle (SRP) and binds the ribosome to pause translation [45]. This peptide is then targeted to the secretory pathway where the ribosome/SRP complex then translocates from the cytosol to the endoplasmic reticulum (ER) compartment. SRP can be recognised by a GTP-binding SRP receptor (SRPR) on the ER surface, causing the ribosome to dock at the ER membrane. Here, the ribosome continues translation of the RNA sequence where the synthesised amino acids are immediately passed across the ER membrane N-terminal first, through the Sec61 translocon channel and into the ER lumen [46]. As the peptide passes through the ER membrane, SRP and SRPR can hydrolyse their bound GTPs, releasing them from the ribosome [47]. Signal peptidase located on the ER membranes cleaves the signal peptide, freeing up the N-terminus of the HLA protein [48]. The peptide continues to pass through the Sec61 channel until a hydrophobic stop-transfer sequence (STA) is reached, where it forms an alpha helix and inserts the protein into the ER membrane [49]. Once in the ER lumen, calnexin (CNX), calreticulin (CRT) and other chaperone proteins aid in folding of the HLA polypeptide, where the glutathione-rich oxidative environment enables the thioredoxin protein disulphide isomerase (PDI) to catalyse disulphide bond formation between cysteine residues of the heavy chain [50]. The first disulphide bond rapidly forms between the membrane proximal Cys203 and Cys259 residues, stabilising the HLA α3 immunoglobulin fold domain with the disulphide bond buried at its core [51]. The HLA light chain, B2M, previously synthesised and translocated through the same secretory pathway also contains a disulphide bond between Cys25 and Cys80. This B2M associates with the heavy chain whilst assembly of the peptide loading complex occurs in tandem, thus stabilising a relatively unstable disulphide bond between heavy chain residues Cys101 and Cys164 to form the HLA α2 domain. This equates three disulphide bonds in total throughout the whole HLA structure.

Antigenic peptides that have been processed through the class I pathway via endoplasmic reticulum aminopeptidase associated with antigen processing (ERAAP) are translocated to the ER lumen through the recruitment of the transporter associated with antigen processing (TAP) 1 and 2 protein complex [52, 53]. These complexes transport degradation products from the proteasome to the ER lumen where they can combine with the HLA heterodimer, tapasin, the ATP-binding cassette (ABC) transporter, CRT, PDI and the thiol oxidoreductase ERp57 to form the peptide loading complex (PLC). The PLC is a key component in regulating the oxidation state of HLA molecules [54, 55]. Here, PDI and ERp57 are responsible for

stabilisation of peptide-free HLA complexes, whilst the alternating redox state of the α2 disulphide bond at the fringe of the peptide binding groove modulates the conformation of the HLA's peptide binding site [56]. The ability for antigenic peptide to be loaded onto the exposed peptide binding groove of HLA is determined by the complementarity of the two sequences, where the association of peptide with the HLA dimer can stabilise the entire complex, from which it is then released. Following a process of peptide editing modulated by the intracellular MHC class I chaperone TAPBPR [57, 58], this now free HLA molecule is then able to translocate in an anterograde fashion via the Golgi, to the cell surface, where the loaded peptide can then be presented exclusively to CD8+ T-cells to initiate a response [42].

1.2.2. HLA Class II

Class II molecules consist of the classical HLA-DR, -DP and -DQ, and the non-classical -DM and -DO antigens [43]. In contrast to class I, class II molecules are expressed exclusively on immunocompetent cells under normal physiological conditions, however their expression can be induced in most cell types [59]. Like the classical class I antigens, classical class II molecules are associated with peptide presentation. HLA-DM on the other hand is thought to act as a chaperone involved with efficient peptide loading of the classical antigens, whilst HLA-DO is known to assist this process in B-cells [60]. The structure of class II antigens is like that of class I in that they consist of a homodimer making up 4 extracellular domains, however unlike class I antigens, class II molecules are constructed from two transmembrane peptides: a ~34kDa α-chain making up 2 domains (α1 and α2), and a ~27kDa β-chain making up the final 2 domains (β1 and β2) (Figure 1.1.B) [61]. Compared to nonameric peptide preference of class I antigens, the peptide binding groove in class II molecules spans the membrane-distal α1 and β1 domains where it predominantly binds 13-25-residue-long, phagocytically/endocytically-internalised, endosomal/lysosomal-processed exogenous peptides [62]. Once internalised and resident within class-II containing compartments such as late endosomes, antigenic peptides can bind within the peptide groove, enabling the release of the stabiliser protein class II-associated invariant chain peptide (CLIP) [63]. This HLA is then able to translocate to the cell surface and present the bound peptide to CD4+ helper T-cells [64].

1.2.3. HLA Polymorphism

Despite the similarities amidst HLA molecules, amino acid substitutions within the primary peptide sequences gives rise to numerous allelic variants of each gene. The location of these substitutions will not only determine the ability of an antibody to recognise two HLA molecules that share a similar epitope but may also influence the ability of these HLAs to present specific antigenic peptides should these substitutions occur within the HLA's peptide binding groove [65]. Each person can express all three isotypes of classical HLA antigens, with the potential of expressing two allelic variants of each isotype, one passed down from each parent in a heterozygous or homozygous manner. This means that each human has the potential to express six different HLA molecules per class, making a total of twelve individual antigens that make up our unique (for the most part) tissue type. This, along with the documenting of over 22,000 different class I and over 8,000 different class II alleles to date (IPD-IMGT/HLA database; accessed 01/09/2021, https://www.ebi.ac.uk/ipd/imgt/hla/stats.html), details the complexity of the HLA system and the effectiveness it grants to initiate a specific and efficient immune response, whilst simultaneously making this a major barrier to overcome in the context of solid organ transplantation.

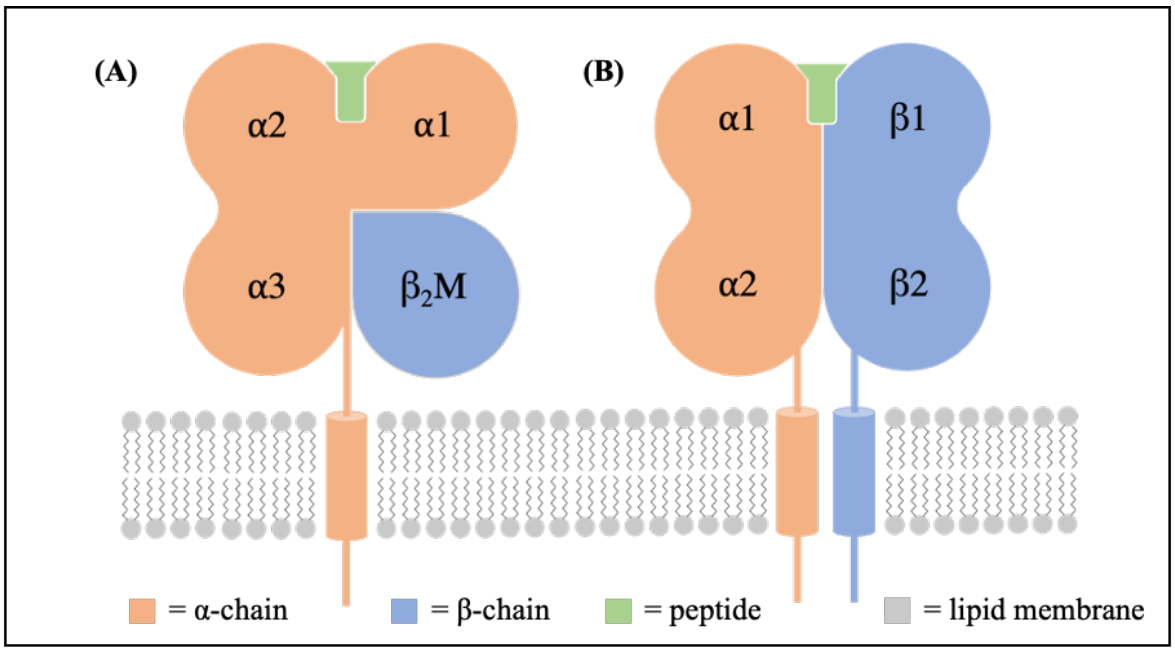

Figure 1.1. HLA class I and class II molecules. A diagrammatical representation displaying the general structure of A) HLA class I antigens, and B) HLA class II antigens. Orange represents the alpha-chain of each molecule. Blue represents the beta-chain of each molecule. Green represents the antigenic peptide. Grey represents the phospholipid bilayer of the cellular membrane.

1.3. Antibodies and Immunoglobulins

Almost 100 years after E. Jenner's first demonstration of smallpox vaccination, the first ever reference to the presence of molecules within our blood which help us fight infection (antibodies) came in 1890, when E. von Behring and S. Kitasato demonstrated that the serum of an animal immune to diphtheria could be transferred to an animal suffering from the infection to cure the disease [66, 67]. This was soon found to be directly translational in humans, for which Behring was later awarded the Nobel Prize in Physiology and Medicine (1901) [15]. Almost a decade after Behring's initial findings, J. Bordet (1899) discovered that there is a component of sera that is responsible for specific immunity against microorganisms [68]. P. Ehrlich went on to name this serum component 'complement' and one year later proposed a model known as the 'side-chain' concept, in which a branched receptor (antibody) on a cell could bind multiple sites of a pathogen and permit complement activation [69]. This, along with the 'lock and key' theory for enzymes proposed by E. Fischer (1894) [70] led to further speculation into how these antibodies work. J. Marrack's work on the chemistry of antigen-antibody (Ag-Ab) interactions (1934) detailed the physio-chemical aspects of these protein-protein interactions (PPI) [71], inspiring R. Goldberg's theory of antibody-antigen complementarity and specificity (1952) [72, 73].

The first document detailing the basis of antibody generation was by A. Fagraeus (1948), where she described plasma B-cells to be the exclusive source of antibodies [74]. This was followed by the clonal selection theory by F. Burnet and D. Talmage (1957), where they described that an antibody's specificity to an antigen is pre-determined and occurs before the antigen is present [75]. With the first composition of an immunoglobulin molecule being published by R. Porter and G. Edelman (1959) [76, 77], later followed by the first published crystallographic structures of antibodies [78, 79], as well as the invention of monoclonal antibodies by G. Köhler and C. Milstein (1975) [80], these monumental discoveries laid the foundations for understanding the biology of antibodies. This revolutionised the field of science, marking the beginning of a new era in antibody research.

1.3.1. Immunoglobulin Structure

Immunoglobulin (Ig) monomers exist as heterodimeric molecules consisting of four polypeptide chains: two identical ~50 kDa heavy chains and two identical ~25 kDa light chains linked by multiple disulphide bonds that can be separated by cleavage with papain and/or pepsin [81, 82]. Each polypeptide chain forms tandem ~12-13 kDa domains of two tightly packed anti-parallel beta-pleated sheets connected and stabilised by a conserved disulphide bond, aptly named immunoglobulin folds [83]. Heavy chains are comprised of one variable and up to four constant domains (V_H, C_H1, C_H2, C_H3 and C_H4) depending on the immunoglobulin class [84]. The combined C_H2-C_H4 domains from both heavy chains make up the crystallisable fragment (Fc) region at the base of the molecule. Light chains consist of two domains each, one variable and one constant (V_L and C_L), that together with the V_H and C_H1 domains of the heavy chain make up individual fragment antigen binding (Fab) regions, of which there are two. These three main tetrahedral-shaped structural regions within immunoglobulins are connected through a flexible hinge region (HR) that gives the molecule a distorted 'Y' shape (Figure 1.2.A) [85].

Whilst the constant regions of the Fc fragment determine the class of the immunoglobulin and is concerned with the effector function through its interaction with other constituents of the immune system (see section 1.3.3), the Fab regions of Ig molecules contain polymorphic residues within the two variable domains (Fv) of the structure which determine the Ig's specificity [79]. Each variable domain is encoded by V(D)J gene segments and contains an Ig fold of nine beta strands (A, B, C', C'', C''', D, E, F and G), consisting of framework regions (FRs) and three hypervariable loops between strands B-C, C'-C'' and F-G, better known as complementarity determining regions (CDRs) 1, 2 and 3 respectively (Figure 1.2.C) [84, 86, 87]. Whilst CDR-3 is the most variable of these CDRs and is thought to be central for antigen recognition, somatic hypermutation within all three of these small loops enables antibodies to recognise different antigenic targets [88, 89]. The ability of an Ig to bind its antigen is dependent on the overall complementarity of the target sequence of the antigen (epitope) to the total six CDRs within each whole Fab region (paratope).

As well as varying in their specificity, Igs are also able to be post-translationally modified at the constant domains of the Fc region (C_H2 in IgG) [90]. Covalently linked to asparagine residues of the Ig (Asn297 of human IgG1) is a common core of two tandem N-acetyl-glucosamine (GlcNAc) residues from which three mannose residues branch (Figure 1.2.B).

The addition of various other oligosaccharide chains such as fucose, galactose, sialic acid, or bisecting GlcNAc to this common core brings about large heterogeneity between antibodies. These modifications have been found to be important for maintaining the structural integrity of the immunoglobulin molecule, whilst regulating the downstream immunological response upon interaction establishment with a cellularly-expressed Fc receptor [91].

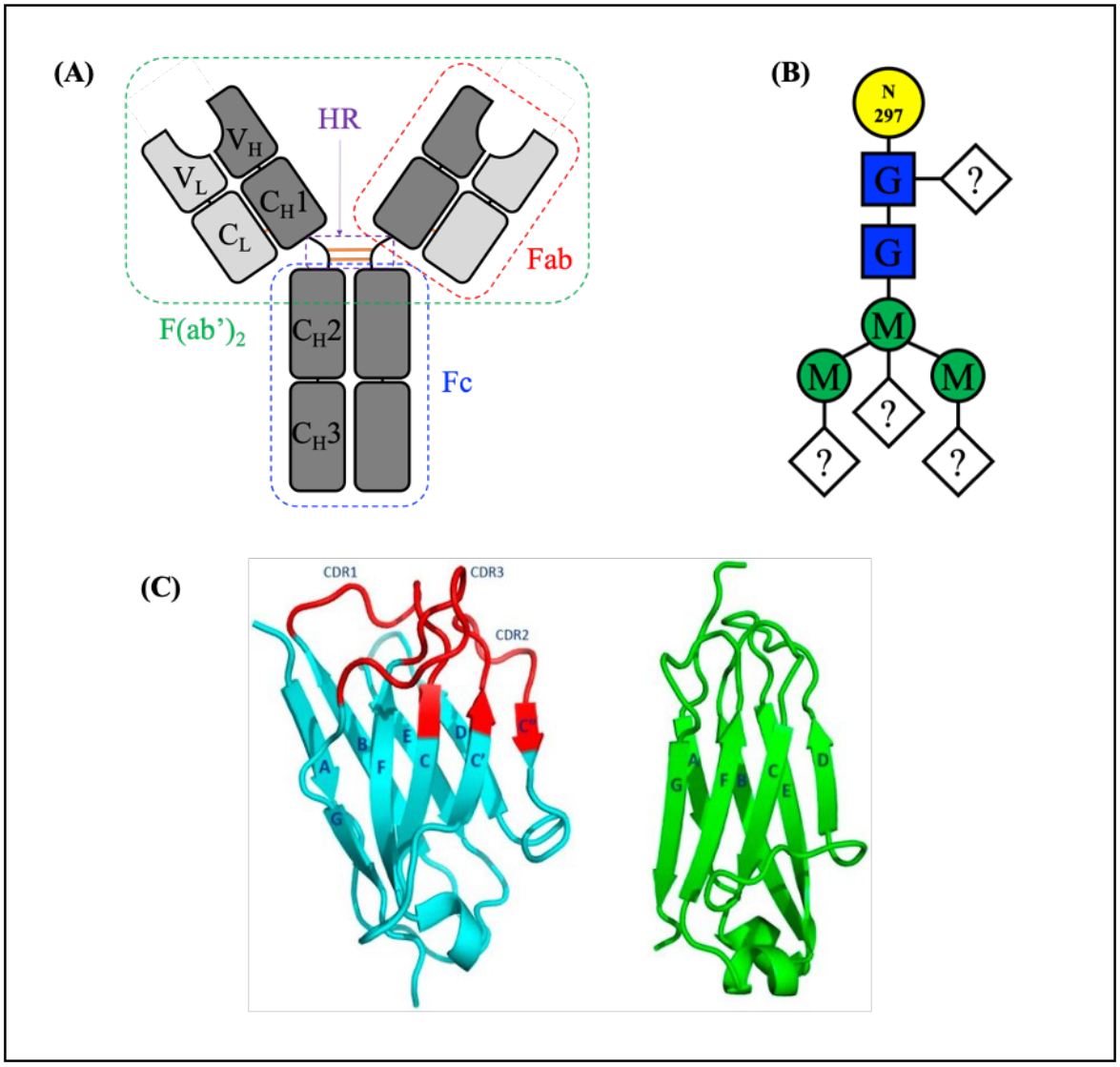

Figure 1.2. Immunoglobulins and their structure. A) A diagrammatical representation of general structure of immunoglobulin G molecules, consisting of two light chains (light grey) and two heavy chains (dark grey) that make up two identical Fab domains (red/green) and are connected by a hinge region (purple) to the Fc domain (blue). B) The common core polysaccharide made up of two N-acetyl-glucosamine residues and three branched mannose residues which are post-translationally, covalently attached to asparagine 297 of IgG1. C) Each immunoglobulin fold is made up of a nine-stranded beta strands which make up the variable (cyan/red) and constant (green) regions. Variable regions contain the three encoded antigen-recognising CDR loops (red). C is Reproduced from Chiu et al. (2019) [86].

1.3.2. Classes, Subclasses, and Isotypes of Immunoglobulin Molecules

Whilst residues within the paratopes of Ig Fab regions classify the antibody's idiotype, each Ig can also be categorised based on the heavy and light chains that the molecule is composed of. In general, mammalian antibodies can be one of five classes: IgA, IgD, IgE, IgG or IgM (Figure 1.3.A), each of which differ in their size and composition corresponding to the heavy chains polypeptides they contain: alpha (α), delta (δ), epsilon (ε), gamma (γ) or mu (μ), respectively [92]. Whilst α and γ heavy chains consist of ~450 amino acid residues that make up three constant domains, ε and μ heavy chains consist of ~550 amino acid residues which fold into four constant domains, the extra domain replacing the hinge region seen in IgA and IgG. δ is like α and γ in that it contains three constant domains, however its composition of 512 amino acids and its extended hinge region makes it unique to the other four classes.

In normal human sera IgG is the most abundant class of antibody, making up ~75% of the entire Ig pool, where it exists in monomeric form secreted from plasma cells [93]. Within this category of immunoglobulins however, there is a further sub-classification of the molecules into IgG1, IgG2, IgG3 and IgG4, that make up ~60-70%, ~20-30%, ~5-8% and ~1-3% of the total IgG pool respectively [94]. These subclasses were assigned based on amino acid differences in their heavy chains, but also vary structurally. Ig hinge regions contain a common carboxy-terminal disulphide bond within the CxxC motif, at C220 in IgG1 and C131 in IgG2/3/4, but each IgG subclass differs in the number of residues within their hinge region and amount of total disulphide bonds that connects the two heavy chains (Figure 1.3.B) [84, 94-98]. The hinge region of IgG3 is the longest of all subclasses, connected by eleven disulphide bonds and made up of up to 62 amino acids encoded by up to four exons, in comparison to only one encoding exon at the other three subclass loci. A single G235 deletion within IgG2's lower hinge region means this subclass has the shortest hinge region, consisting of 12 amino acids connected by four disulphide bonds and stabilised by a poly-proline helix. IgG2 has also been shown to have various hinge isomers, where the inter-disulphide bonds between heavy chains and intra-disulphide bonds between heavy and light chains can reorganise to form either A/A, A/B or B/B conformations [99, 100]. IgG1 and IgG4 both have two inter-chain disulphide bonds composed of fifteen and twelve residues respectively, however IgG4 does not contain the glycine deletion seen in IgG2 which enables more flexibility in its hinge region. Like IgG2, IgG4 has also been shown to have various isomers due to its ability to form half-molecules upon inter- to intra- chain bond rearrangement of the two disulphide bridges that link the heavy

chains together [101]. The ability to rearrange both disulphide bonds that keep this molecule whole means that these IgG4 molecules can not only exist as half molecules consisting of one heavy and one light chain, but also enables them to recombine with other half molecules to form bispecific immunoglobulins, a process known as Fab arm exchange [102].

IgA is the next most abundant class in human serum making up ~15% of the entire Ig pool [93]. Whilst also being secreted by plasma cells, these Igs can be further classified into IgA1 and IgA2 [103]. In serum, IgA exists in monomeric form, however it is the most prevalent class in various other bodily fluid secretions where it can be present as a dimer, connected at the Fc regions by a secretory component (SC) and a disulphide-bonded joining (J) peptide chain [104]. IgM makes up 10% of the total immunoglobulin pool in sera, once again connected by a series of disulphide bonds and a joining peptide across neighbouring Fc regions [105]. Additionally, an extra hydrophobic domain at the C-terminus of IgM heavy chain peptides enables membrane anchorage of IgM monomers where it can act as a B-cell receptor (BCR) [98]. While IgD and IgE together make up a combined < 1% of the immunoglobulin pool, they also only exist as one subclass in monomeric form [93]. IgD is very similar in structure to IgG, however its extended hinge region contains only one disulphide bond which makes it very susceptible to proteolytic cleavage. IgD can also be commonly found as a BCR expressed on the surface of B-cells [98]. IgE on the other hand is very similar in structure to monomeric IgM, in that the fourth constant domain of each heavy chain replaces the hinge region seen in other Ig classes. Whilst IgE is the scarcest of all immunoglobulin molecules in sera, it can be found primarily fixed to FcεRI receptors on the surface of eosinophils, basophils, and mast cells [106].

As well as the alternative heavy chain peptides encoded on chromosome fourteen, Igs can also vary in their light chains [107]. In humans there are two possible variants, kappa (κ) and lambda (λ), which are genetically located at chromosome two and twenty-two respectively and only differ by a few amino acids in their constant domains [108, 109]. While individual B-cells are limited to expressing only one of these chains for all the antibodies it produces, of which κ is found to be the most abundant [110], the functional differences in these chains are not completely understood but have been linked to several conditions such as kidney disease and myeloma [111, 112]. Lastly, the documentation of numerous single amino acid substitutions within γ1, γ2, γ3, γ4 and α2 heavy chains across different ethnic groups means that there is also allotypic variation within IgG and IgA subclasses [113]. While the amino acid variations of γ2 and γ4 heavy chains can also be found in other Ig subclasses (isoallotypes) [114], the

unique amino acid variations of γ1, γ3 and α2 heavy chains between individuals means that if a person were to encounter antibodies of a different allotype, it is possible for an anti-allotypic response to be induced [115, 116].

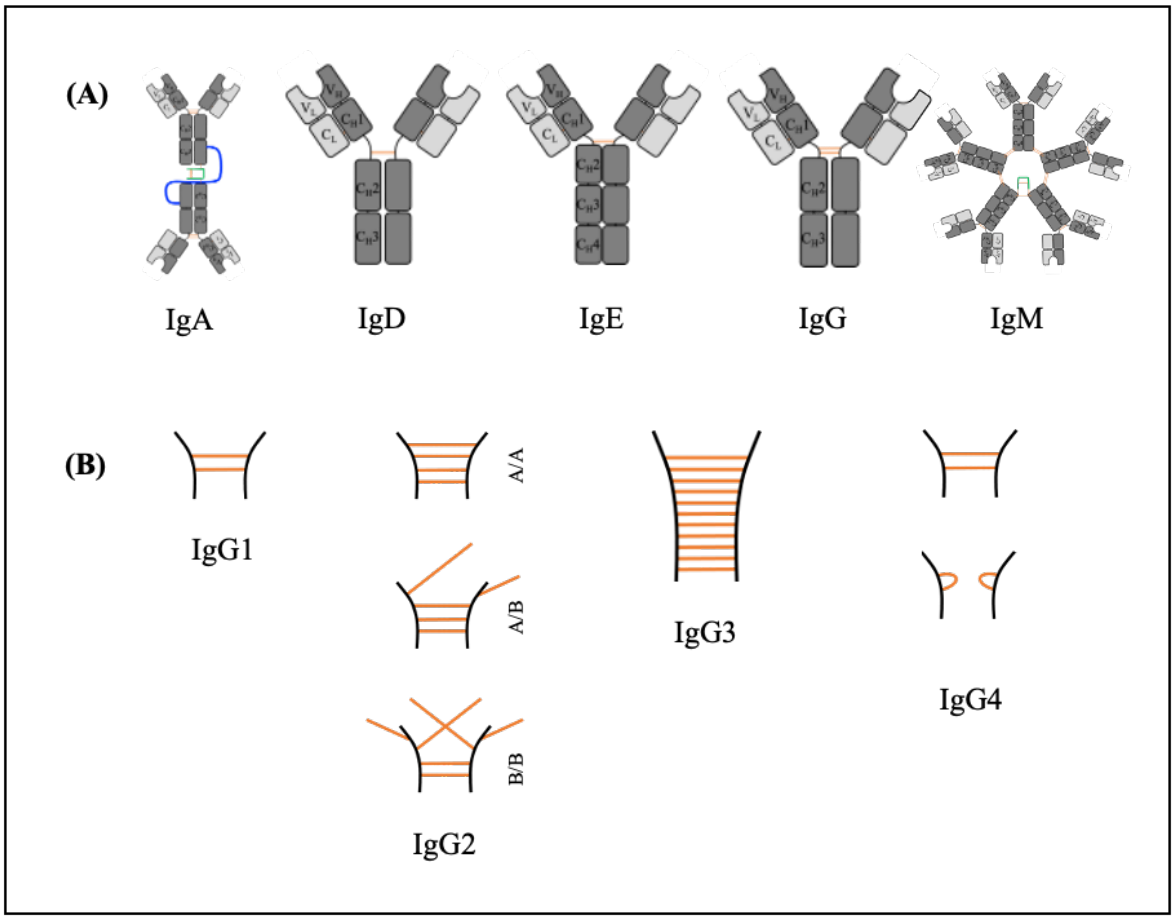

Figure 1.3. Immunoglobulin species and variability. A) Diagrammatical representation of the five structures of the immunoglobulin classes; IgA, IgD, IgE, IgG and IgM. B) The variable disulphide bond arrangements within the hinge region of IgG molecules that further categorises this class of Igs into subclasses IgG1, IgG2, IgG3 and IgG4, and the further species within these subclasses.

1.3.3. Roles, Interaction Partners, and Effector Functions of Antibodies

An immunoglobulin's primary function is to act as a specific antigen detector, bridging the recognition mechanisms of adaptive immunity to the effector responses of the innate system, where their diverse functions and roles in many different immune response processes have been documented. Cell-surface/membrane-bound immunoglobulins (mIg), such as B-cell/T-cell receptors etc., may commonly act as antigen-specific cell activators capable of initiating various intracellular signalling pathways upon antigen recognition. Secreted immunoglobulins (sIg), known as antibodies, are a major component of the humoral immune system which aids in foreign antigen detection and immune confrontation within bodily fluids.

In their simplest form, antibodies can act as protein-blocking molecules inhibiting the formation of various protein-protein interactions, preventing responses after ligand-receptor complex formation. Whilst bound to an antigen, antibodies also act as molecular connector/docking sites for various effector proteins, for which the Ab's Fc region has a complementary epitope. One of these proteins is the complement protein C1q, which when docked to a cell's surface activates the classical complement cascade, leading to target cell lysis (see section 1.4.3). Whilst both IgM and IgG molecules can efficiently bind C1q, the hexameric structure of the complement protein implies that multiple C1q-Ig interactions must occur for stabilisation of the complex to initiate the cascade [117]. Since IgM is pentameric and exists as one isotype, the capacity of the Ag-Ab interaction to initiate a response is dependent on the stability of the Ag-Ab complex. In terms of IgG however, the presence of multiple isoforms of this class gives rise to a varying ability of each IgG subclasses to fix C1q and initiate the complement cascade, with IgG3 having the strongest complement-fixing capacity, followed by IgG1, IgG2 then IgG4 [94].

Thought to be the most crucial group of antibody-recognising immune regulatory proteins is the membrane-bound Fc receptor (FcR) family, which forms the connection between antigen, antibody, and effector immune cell. Cells express different types of FcRs determining which antibody class they can recognise; FcαR, FcδR, FcεR, FcγR and FcμR recognise IgA, IgD, IgE, IgG and IgM respectively [118, 119]. Within the IgG-specific FcγR class of receptors encoded on the long arm of chromosome 1, there are three subtypes; FcγRI, FcγRII and FcγRIII, where FcγRI can bind IgG Fc with higher affinity than the others [120]. FcγRII and FcγRIII receptors can be further categorised into three and two groups respectively: FcγRIIa, FcγRIIb and FcγRIIc, and FcγRIIIa and FcγRIIIb [121]. After docking with IgG following

recognition of an antigen, FcγRs that bear the YxxL/Ix(6-8)YxxL/I immunoreceptor tyrosine-based activation motif (ITAM) within their cytoplasmic tail domain become phosphorylated at both tyrosine residues by the Src family tyrosine kinases [122]. This activates downstream intracellular signalling events leading to a response such as phagocytosis or ADCC (see sections 1.4.2 and 4.1). In the case that the receptor contains the immunoreceptor tyrosine-based inhibitory motif (ITIM) S/I/V/LxxYxxI/V/L, such as in the FcγRIIb receptor, phosphorylation of only one tyrosine is not sufficient to activate the cell. This does however regulate Src homology region 2 domain-containing phosphatase (SHP) and Src homology 2 domain-containing inositol polyphosphate 5 phosphatase (SHIP), which work to counteract the magnitude of these activating signals through dephosphorylation of the motif's tyrosines [119, 122-124]. Considering the FcγR binding site within the N-terminus of the IgG's C_H2 domain partially overlaps with the C1q docking site, it comes as no surprise that the ability of each IgG class to initiate a cellular immune response is like that of the IgG subclass' ability to initiate the complement cascade, however this does slightly vary across different FcγR sub-types [119].

IgAs are predominantly found in mucosal secretions such as in the gastrointestinal, respiratory, and urogenital tracts where they play a major role in preventing the build-up of potentially harmful pathogens in these vulnerable areas [84]. Once bound to an antigen, IgA can dock with FcαRI and facilitate internalisation and recycling of the receptor molecule [125]. In the case that the FcαRI receptor is associated with two FcγRI receptor signalling chains that bear the ITAM motif, phagocytosis may be induced to clear the recognised pathogen [126]. While the true roles of IgD-FcδR and IgM-FcμR complex formation remain relatively unexplored, the C_H3 domain of IgE has been shown to be crucial for the binding of the FcεR, where its role in allergy-specific responses through release of pro-inflammatory signals such as histamine, proteoglycans and various cytokines has been uncovered [127, 128]. One final member of the FcR family that has been shown to be up- and down-regulated by TNF-α and IFN-γ, respectively, is the FCGRT gene-encoded neonatal FcR (FcRn) [129-131]. This receptor is unique in that it is expressed on endothelial, epithelial, and myeloid cells and shares structural similarities to that of MHC class I molecules, such as its B2M light chain. In early life, this receptor is essential for the transport of IgG molecules from mother to child, firstly across the placenta in the antenatal stage, and then postpartum by providing these IgGs with protection from degradation in the gut of breast-fed children [132]. Upon maturity, these receptors become downregulated in gastrointestinal tissues, however they remain expressed on epithelial

cells into maturity to aid in antigen sampling and IgG transport across epithelial barriers [133, 134].

As well as the above-mentioned interacting partners, many other proteins have also been found to bind Ig Fc regions, including: the cytosolic tripartite motif-containing protein 21 (TRIM21) which aids in antibody-dependent intracellular neutralization of IgG-opsonised virus and bacteria by the ubiquitin-dependant proteasome [135-136], dendritic cell-specific ICAM-3 grabbing non-integrin (DC-SIGN) which is a c-type lectin that recognises the mannose-rich glycosylation of the Ig Fc region to activate phagocytosis [137], and also many bacterial surface proteins such as Protein A and Protein G, where their interaction with various immunoglobulin molecules aims to aid in immune evasion within the host [138].

1.4. The 'Slow Response' of Acquired Immunity

Despite HLA playing a profoundly important role in the regulation of the human humoral immune system, the polymorphic intricacy of HLA offers a major problem to overcome in the context of solid organ transplantation. Mismatching of HLA between donor and recipient may result in the recognition of 'non-self' antigens by immune cells, a process known as allorecognition or the afferent arm of adaptive immunity [139]. Once this allorecognition occurs, the immune response becomes initiated which then enables the efferent arm of adaptive immunity to carry out its functions through either cell- or antibody-mediated mechanisms, potentially leading to tissue rejection and/or graft loss.

1.4.1. Allorecognition

Allorecognition is the detection of a foreign molecule by immune cells and occurs in T-cells through direct, indirect, or semi-direct mechanisms (Figure 1.4) [140, 141]. During the short-term direct allorecognition process [142], intact HLA molecules on donor antigen presenting cells (APCs) are recognised by T-cell receptors (TCRs) on resident CD4+ and CD8+ T-cells which initiate the response (Figure 1.4.A) [143]. The indirect pathway occurs in a similar fashion to standard antigen peptide presentation, whereby internalised donor alloantigenic peptide fragments are recognised by CD4+ T-cells after it has been processed and presented on the class II HLAs of recipient APCs (Figure 1.4.B) [144, 145]. Although indirect allorecognition primarily concerns HLA class II peptide presentation, this phenomenon may also involve CD8+ T-cell recognition of class I molecules that present internalised soluble peptides that have processed through the class I pathway, a process known as cross-presentation [146, 147]. Finally, the semi-direct process is believed to occur upon acquisition of intact donor HLA molecules into the membrane of recipient APCs, mediated through cell-to-cell contact with donor APCs (Figure 1.4.C) [148]. These MHC recipient cells then can trigger both direct and indirect pathways depending on whether it is the native or foreign HLA molecule that the T-cell recognises. Although the semi-direct pathway is implicated in the allorecognition process and has been supported by the demonstration of alloantigen transfer between cultured dendritic cells [149], the *in vivo* roles of this model for inducing allograft rejection are yet to be determined. As well as T-cells being able to detect foreign molecules,

B-cells are also capable of this feat in an antigen presentation-independent manner through their BCRs. This is further discussed in section 1.4.3. One final way in which allorecognition may occur within the human body is through pattern recognition receptors (PRRs) on the surface of various immune cells [150]. These receptors recognise conserved pathogen- or disease- associated molecular patterns (PAMPs or DAMPs) which when activated leads to upregulation of their HLA genes [151]. These cells then mature into APCs capable of presenting the foreign peptide necessary to activate T-cells and initiate the immune response. Although the recognition of PAMPs/DAMPs is implicated in the allorecognition process, PAMPs are predominantly associated with immunity against microbial infection and does not apply in the context of organ transplantation.

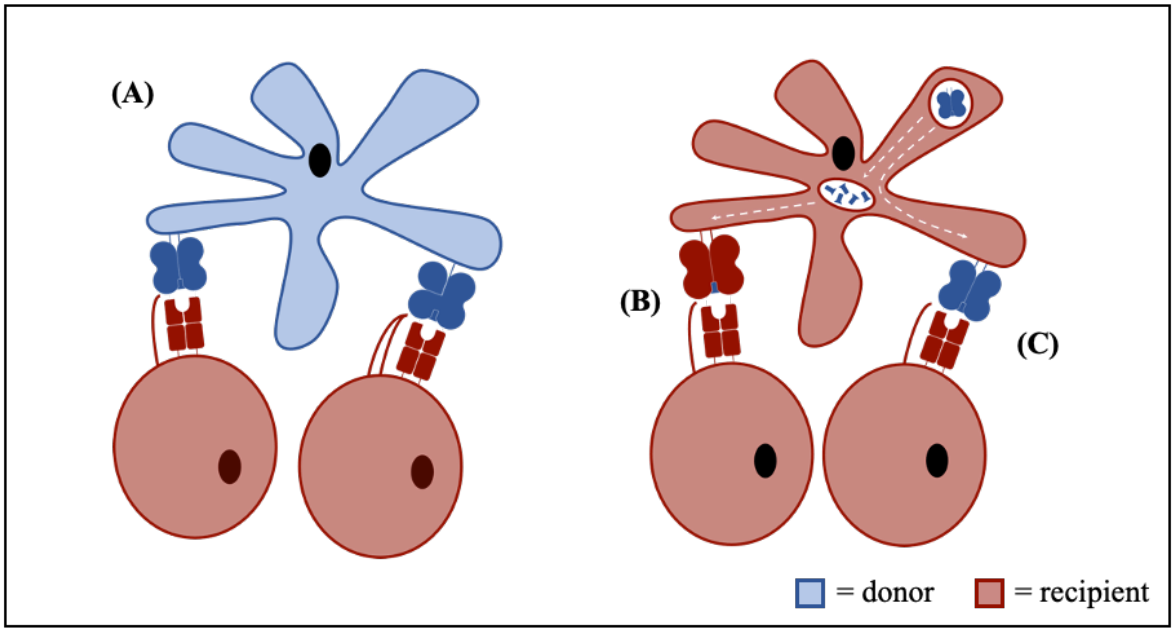

Figure 1.4. Allorecognition pathways. Detection of a foreign molecule by immune cells can be carried out through direct (A), indirect (B) or semi-direct (C) mechanisms. The direct pathway relies on recipient cell recognition of donor HLA on donor cells. The indirect pathway relies on recognition of donor HLA peptides presented by recipient APCs. Semi-direct allorecognition relies on the the acquisition of donor HLA on recipient APCs where can they activate either of the other two pathways.

1.4.2. Cell-Mediated response

Upon allorecognition by the T-cell receptor, T-cells become activated and can differentiate to specify the immune response that will be produced [152]. Recognition of HLA class I molecules by CD8+ T-cells results in the production of various inflammatory cytokines such as interferon-gamma (IFNγ), interleukin 12 (IL-12) and tumour necrosis factor (TNF) [153]. This cellular activation triggers differentiation of these T-cells into cytotoxic T-lymphocytes (CTLs) capable of degranulation, releasing various proteases and cytolytic proteins that can bind and lyse the recognised cell. The increasing presence of inflammatory cytokines may also induce upregulation of adhesion molecules at the surface of the recognised target to facilitate recruitment of other resident immune cells to the site [154]. In the instance that naïve CD4+ T-cells can activate in response to recognition of peptides bound to class II molecules, these cells can differentiate into various T helper sub-types depending on the cytokine composition of the microenvironment and the internal signalling events that follow. Among these sub-types are T-helper 1 cells (Th1), T-helper 2 cells (Th2), T-helper 9 cells (Th9), T-helper 17 cells (Th17), induced T-regulatory cells (iTreg), regulatory type 1 cells (Tr1) and follicular helper T-cells (Tfh), all with their own unique characteristic cytokine profile [155]. Once activated these T helper cells can release inflammatory cytokines, such as interleukins, resulting in the activation and mobilisation of other immune cells, such as B-cells, macrophages, natural killer (NK) cells and CTLs, which can then carry out their respective effector functions. Activated B-cells differentiate into either antibody-producing plasma cells or memory B-cells (see section 1.4.3), whereas other cells such as NK cells can migrate to and infiltrate at the site of allorecognition to carry out their functions whilst simultaneously releasing more cytokines to aid in the process [156]. All together, these processes enable an effective response to allorecognition, resulting in target cell lysis and tissue injury.

1.4.3. Antibody-Mediated Response

Antibody mediated rejection (AMR) also relies on the allorecognition of HLA by a lymphocyte, only this time it is recognition of a structural epitope of a protein through the BCR on B-cells within secondary lymphoid organs (SLOs) [157, 158]. Once an epitope is recognised, some of these antigen-specific B-cells differentiate into short-lived plasmablasts which produce allo-specific/donor-specific antibodies (DSAs) in the form of IgM. Other activated B-cells migrate into the follicles of SLOs with the aid of T-helper cells, where they form germinal centres (GCs) [159]. Within these GCs, dendritic and T-follicular helper cells

promote the activated B-cells to undergo clonal expansion and activate somatic hypermutation (SHM) and somatic hyperconversion (SHC) of the genetic immunoglobulin variable region. SHM is driven through one of two mechanisms; one which targets mutation-prone regions containing the RGYW motif, and the other which incorporates error-prone DNA synthesis that causes nucleotide mismatches that can be translated into amino acid substitutions [88, 89]. The result of this process is diverse clonal populations of B-cells with a range of affinities against the priming antigen [160]. Throughout this process these B-cells go through selection, whereby dendritic cells assess them for their specificity to the antigen, promoting survival of only those cells which have high affinity/avidity, a process known as affinity maturation [161, 162]. Cells that survive this selection then enter a process known as immunoglobulin class switch recombination (CSR). Cytokine signals trigger the clonally selected B-cells to alter the heavy chain constant portion of their produced immunoglobulin molecules through variable activation of an intervening exon preceding the C_H1 domain, irreversibly altering the Igs class, e.g., from IgM to IgG [162, 163]. The outcome of this is the production of one of two types of high affinity, antigen-binding, T-cell activation-independent cells: memory B-cells and long-lived plasma cells [164].

Once in circulation, affinity-matured antibodies can bind their specific target where they can either mediate allograft injury through complement-dependent or -independent mechanisms. The complement-independent mechanism utilises the ability of FcR-expressing cells, such as NK cells and macrophages, to recognise the Fc portion of antigen-bound antibodies and activate their cytotoxic functions to mediate antibody-dependent cell-mediated cytotoxicity (ADCC) [165]. Although complement proteins may aid in the recruitment of immune cells to a site of inflammation [166], the ability of an antibody to carry out its complement-dependent cytotoxic function is not reliant on the recognition of a target-bound antibody's Fc region by an FcR on an immune cell, but the capacity of the Fc to fix complement component C1q and initiate the complement cascade via the classical pathway (Figure 1.5) [167]. Through this pathway, the stabilised C1q-Fc complex can activate the 'early event' of the cascade in which C2 and C4 components are both enzymatically cleaved into two fragments, a, and b, whereby C2a and C4b combine to form C2aC4b, also known as C3 convertase. This activated protease is then able to cleave C3 into inflammatory mediator anaphylatoxin C3a and the main complement effector molecule, C3b. C3b can bind C3 convertase to form C5 convertase whilst also being deposited on the target cell surface, acting as an opsonin, and targeting the cell for destruction by phagocytes. C5 convertase can now cleave C5 into two fragments: a second

inflammatory mediator anaphylatoxin C5a and the 'late' event initiator C5b. The late event progression of this cascade involves the association of C5b with complement components C6, C7, and C8, where this complex can disrupt the plasma membrane of the target protein. Once inserted into the membrane, C8 associates with multiple C9 molecules to form a pore in the membrane known as the membrane attack complex (MAC), leading to the release of the cell's contents and subsequent cell lysis [168]. Other studies have also described the ability of immune cells to produce their own complement proteins such as to initiate this pathway [169].

Alloantibody in patient sera can have an immediate effect on graft function, however in many cases alloantibody mediated graft injury has an indolent course for a significant time prior to clinical manifestation [170]. The timeframe at which allograft injury occurs post-implantation may sub-categorise humoral rejection into three classifications; hyperacute rejection (HAR) which usually occurs within minutes of the implant, acute antibody-mediated rejection (AAMR) which can occur after weeks to months, and chronic antibody-mediated rejection (CAMR) which causes the loss of graft function in the long term [171-173]. While HAR occurs due to the high titre of pre-existing DSAs within the recipient prior to transplant, this has been overcome through implementation of several antibody characterisation assays in clinic (see section 1.5.2). AAMR occurs due to an increase in alloantibody titre post-transplant, which can be put down to either a memory B-cell response via allorecognition in a pre-sensitised recipient or the formation of new antibody *de novo* [174]. Whilst options for reducing the risk of HAR and AAMR exist [17], it is CAMR which presents a major cause of late-stage graft loss [175, 176].

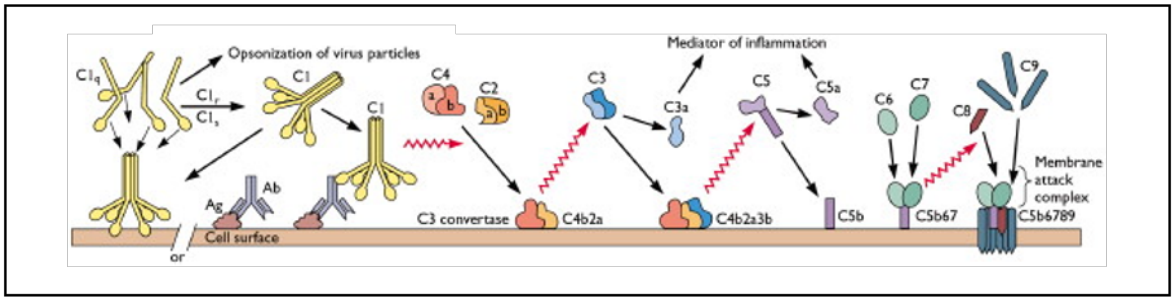

Figure 1.5. Classical complement cascade. A schematic representation of the steps involved in the activation of the classical complement pathway. Reproduced from: Racaniello V. The complement system virology blog. 2009 [Available from: https://www.virology.ws/2009/09/28/the-complement-system/].

1.5. Immunological Risk Assessment in Transplantation

When selecting a suitable donor-recipient tissue match for organ transplantation, it is well-known that minimising HLA incompatibilities between recipient and donor has a positive effect on transplantation outcome [177]. Histocompatibility is most often assessed at the antigenic rather than the allelic level, and in the context of renal transplantation it is the HLA-A, -B and -DR loci that are analysed for discrepancies [178-181]. Despite this relatively low level of HLA resolution, matching six HLA molecules is often unrealistic given the shortage of donor organs and the competing demand for equity of access to transplantation [182]. Where serological methods of tissue typing have assisted in determining potential useful donor-recipient matching, the development of polymerase chain reaction (PCR)-based DNA sequencing has fuelled the rapid discovery of many more HLA alleles and individual isotypic variants, underpinning the complexity of defining a well-matched organ [183, 184].

In addition to identifying the donor's and recipient's expressed HLAs, the recipient's pre-existing antibody repertoire also needs to be analysed to determine whether any prior HLA sensitisation event has occurred that could also lead to graft rejection. Whether or not the donor/recipient pairing is perceived to be a good match or not, the presence of recipient alloantibodies with specificity against the donor HLA prior to transplantation may increase the immunological risk [185]. Re-exposure to an antigen which can be recognised by the recipient's immune compartments may lead to a potential immunological memory response through memory B-cells/T-cells, causing graft rejection [186].

1.5.1. HLA matching

In attempt to determine donor antigen mismatches that may be better tolerated by a particular recipient, various studies have been carried out to explore the similarities and differences in the properties of individual HLAs. Some of the first attempts to determine the effect of HLA mismatching intended to identify specific HLA mismatches that may be tolerated by the recipient based on retrospective analysis of transplant outcomes [187-189]. Other studies on HLA mismatching looked at the presence of shared epitopes found on multiple HLA molecules, known as cross reactive groups (CREGs) (Appendix 2) [190, 191]. This angle was able to shed light on the disparity of individual HLA mismatches and why some donor-recipient

matches may be preferable due to shared epitopes, however, this method did not account for an individual antigen's uniqueness and the potential for an antibody to be raised against any epitope of an individual HLA molecule. In more recent years, alternative approaches to HLA matching have been introduced whereby the amino acid sequence of a donor antigen would be directly compared to that of the recipient's antigens using a computer algorithm called HLA Matchmaker, which excludes those residues that are not surface accessible [192]. Although HLA Matchmaker has been documented to be a very valuable tool in predicting the extent of alloantibodies that arise in response to mismatched HLA [193, 194], this method does not account for the epitopes formed by non-neighbouring amino acids due to the protein's tertiary structure. Another method developed for analysing the immunogenicity of HLA mismatches is the three—dimensional electrostatic mismatch score (EMS-3D). EMS-3D is used to quantitatively assess the differences in the physical properties of HLA molecules at the tertiary structure level [195]. Here, the contribution of polar and charged residues within the HLA molecule is mapped using continuum electrostatics to give an overall electrostatic potential at any point on the HLAs exterior. The surface electrostatic potential of a particular HLA can then be superimposed on to that of another HLA to identify and/or quantify the differences between the two molecules, which is measured as an overall mismatch score [196].

1.5.2. Alloantibody Detection and Evaluation

To determine the alloantibody-related immunological risk associated with a potential donor organ, the recipient is screened for the presence and specificity of alloantibodies in their sera. While alloantibody binding to its priming antigen is expected to lead to immune reactivity and initiation of effector functions, the structural conservation of HLA means that an alloantibody primed against a conserved epitope on one HLA may also cross-react against third-party HLA that expresses the same epitope [197]. This cross-reactivity may affect the ability of alloantibodies to carry out their effector function, often meaning that the identity of the priming antigen cannot be determined. Various methods have been developed for the purpose of identifying alloantibody specificities and understanding their pathogenic potential, including flow cytometry (FC), complement-dependent cytotoxicity (CDC), and Luminex single antigen bead (SAB) assays (Figure 1.6) [198-209]. These techniques enable a profile of a potential transplant recipient's serum to be evaluated where it can be used to assess the reactivity of their antibodies against the potential donor pool. Accurate assessment of the immunological risk assigned to serum reactivity against specific donor HLA is of paramount importance as it

determines the recipient's access to the donor pool, the necessity for additional interventions to facilitate transplantation (e.g., antibody removal from serum via plasmapheresis), and influences the choice of immunosuppression treatment. Detection of DSA post-transplantation can also be used as a prognostic biomarker, lending itself to the diagnostic criteria for AMR whilst also helping determine the intensity of clinical monitoring and future immunosuppression treatment [210-212].

1.5.2.1. Flow Cytometry Assays

Flow cytometry assays examine the ability of a recipient's alloantibody to bind HLA expressed on donor lymphocytes. The output is measured as a mean fluorescence intensity (MFI) which is determined by the amount of fluorophore-tagged secondary reporter antibody that detects the cell-bound alloantibody. This assay can either be carried out as a screen using panels of donor lymphocytes expressing the most frequently found HLA a given population, or as a crossmatch (XM) to determine the reactivity of recipient serum to a specific donor [200, 204, 206]. FC allows for detection of clinically relevant antibodies present in patient sera; however, it should also be noted that the presence of autoantibodies may give rise to false-positive results, and this should be accounted for accordingly [207, 213].

1.5.2.2. Luminex Single Antigen Bead Assays

In recent years, alloantibody detection and specificity resolution has been increasingly relying on solid-phase assays, such as that implemented in Luminex technology. Luminex uses the principles of FC to observe the binding of alloantibodies to recombinant HLA-coated microbeads [214]. Upon detection of a bead using a flow cytometer, two distinct fluorescent signals are recorded which reveal two separate parameters; the identity of the bead (nature of HLA) and the amount of bound alloantibody to that specific bead, measured as an MFI. When compared to cell-based assays, this technique enables higher-throughput, higher sensitivity, antigen-specific determinations of alloantibodies present in patient sera. Although this technology has revolutionised antibody detection in clinical practice, significant caveats remain. Luminex output is semi-quantitative as the amount of HLA on the surface of the beads is unknown [215]. Moreover, the titre of antibody in sera at a specific time point has a major effect on MFI output which in turn is used to determine the immunological risk associated with a specific alloantibody-HLA interaction [216]. As mentioned in section 1.3.2, it has also been documented that IgG molecules of each subclass have differing capabilities to fix complement

and activate the classical pathway [94]. These characteristics are not accounted for in Luminex SAB assays as the secondary detection antibody does not distinguish between molecules of each IgG subclass, something that may be useful in determining their pathogenic potential. By adapting the protocol to incorporate C1q, this assay can also be used to observe the complement-fixing capabilities of antigen-bound antibodies [201]. Although Luminex SAB assays may be supported by Luminex C1q-binding assays which are expected to provide further information on the complement fixing abilities of DSAs, Luminex C1q is not heavily employed in clinical practice and comes with its own limitations [217]. As a result, the clinical significance of Luminex detected alloantibodies and the interpretation of MFI values from these assays are the subject of debate within the transplant field [218], where thresholds that define a positive interaction are often quite arbitrary.

1.5.2.3. Complement-Dependent Cytotoxicity Assays

CDC assays have been rapidly developed based on the principles of Terasaki's microcytotoxicity assay and are currently seen as the gold standard for immunological risk assessment in transplantation [28]. CDC assays, like FC assays, use donor T-cells expressing HLA class I and donor B-cells expressing both HLA class I and II to assess antibody binding where they can be used as a crossmatch. The main advantage to CDC assays over FC assays is that not only does CDC uncover the ability of antibodies to bind cell-surface-expressed HLA, but also assesses their capacity to fix complement and cause cytotoxic death through cell lysis [206]. Upon antibody introduction to the cells, the sample is then incubated with complement protein to observe the cytotoxic lysis of cells which is measured as an overall percentage cell death. The major limitation of both FC and CDC assays pertains to the fact that cellular targets express a combination of multiple HLA class I and II antigens and, therefore, resolution of serum alloantibody reactivity against specific HLA is difficult. Although CDC assays enable insight into the pathogenic potential of alloantibodies to be gained, it is also known to be of low sensitivity and is limited to the detection of complement-fixing alloantibodies. This remains an issue when analysing a potential recipients' serum as although it may contain clinically relevant antibodies, if the levels of antibody are below the sensitivity limits of the CDC assay, then they will not be detected [219].

1.5.2.4. Clinical Interpretation of Alloantibody Assessment

Although the introduction of methods for antibody-related clinical immunological risk assessment have contributed to the advancements in successful transplantation outcome, the complexity of data interpretation has led to non-uniformity among clinical laboratories, introducing significant variation in clinical practice and decision-making processes between transplant centres. This is especially the case for those patients with antibodies that interact with HLA at the lower end of the spectrum for positive immunoassay detection. Alloantibodies that bind cross-reactive HLA are commonly detected with high-sensitivity assays such as Luminex, however the true clinical significance of these cross-reactive interactions are more difficult to ascertain which accounts for much of the current uncertainty with Luminex output interpretation [220]. For this reason, outputs of each assay can be ranked based on the assay sensitivity and the relevance of a positive result to confer a higher immunological risk [219]. Patient sera that yield a positive result in CDC assays raise an automatic veto to transplantation, whilst DSA detected via Luminex solid phase assays alone are more difficult to interpret and may or may not increase the immunological risk associated with a particular transplant. When positive results for Luminex assays are combined with positive FC results, this is said to offer an intermediate level immunological of risk, which can then be bumped up to a high immunological risk category with a positive CDC result.

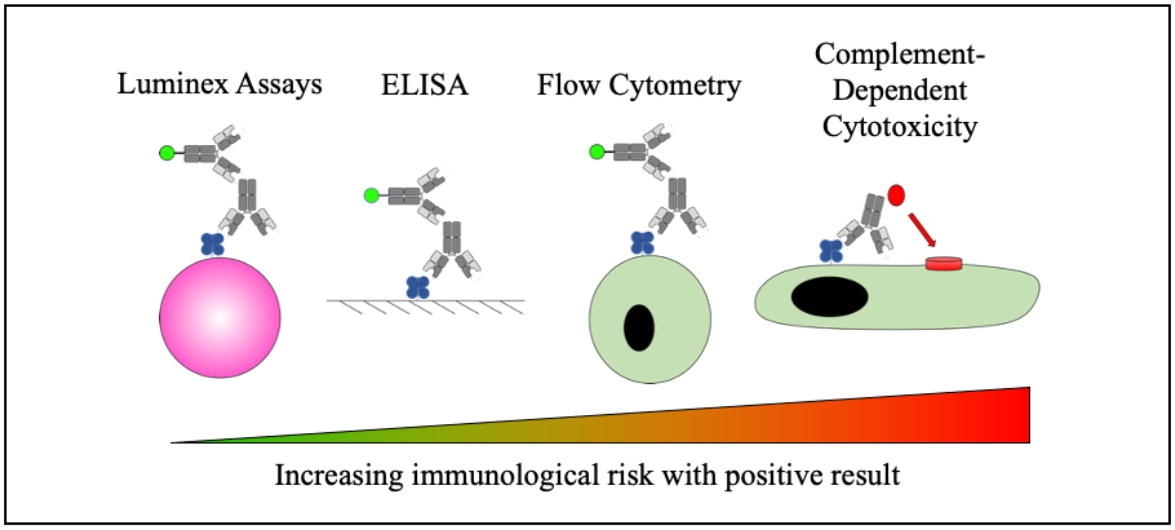

Figure 1.6. Methods of donor-specific antibody immunological risk assessment. A diagrammatical representation of the methods currently used to assess alloantibodies within a transplant recipient's sera. Luminex and ELISAs use HLAs immobilised to a solid surface, whilst flow cytometry and CDC assays rely on the natural expression of HLAs on cell samples. Assay sensitivity decreases from left to right, correlating with the increased immunological risk upon a positive output from the assay in question.

1.6. Thesis Aims, Objectives, and Hypotheses

Upon allorecognition, development of a mature humoral response entails germinal centre formation, somatic hypermutation, and affinity maturation, culminating in the secretion of high-affinity antibodies [157-164]. DSA development and antibody recognition of donor HLA are major factors influencing graft survival in the context of solid organ transplantation, and although modern immunosuppression regimens and pre-transplant interventions have helped reduce the incidence of short-term graft loss, CAMR remains a major challenge with a significant impact on long-term graft survival [176]. Despite pre-existing DSA being well associated with worse graft outcomes in most solid organ transplants, it is well documented that not all alloantibodies lead to graft injury and in some cases the presence of DSA may be tolerated [221, 222]. This is particularly the case for alloantibodies detected solely by high sensitivity solid-phase assays, such as Luminex, where interpretation of the data remains contentious. Overall, there is an unmet need to accurately assess the HLA-related immunological risk associated with a particular transplant as this information influences a person's access to transplant donors for those patients already sensitised against HLA pre-transplant, whilst also permitting individualised immune monitoring and management of immunosuppression post-transplant. The principle aims of this work are to provide insights into the clinical significance of alloantibodies, the factors that determine their pathogenicity, and the molecular signalling pathways that govern these characteristics. Such understanding may enable improved immunological risk assessment in transplantation and offer opportunities to develop new methods for assessment of HLA-specific antibodies beyond what is currently possible using currently available immunoassays. An overview of this thesis is described below.

- **Investigation into the potential of alloantibody-HLA kinetic analysis to inform the interpretation of currently used assays for detection and characterisation of human HLA-specific antibodies (Chapter 3).**

  Solid phase assays such as Luminex SAB are widely used to assess the alloantibody profile of sensitised patients and to perform immunological risk analysis, however interpretation of assay output is not always straight forward with wide variation in practice among clinical laboratories. This uncertainty can have important clinical

implications including determining an individual patient's access to transplantation and on post-transplant immunological monitoring. It is established that an antibody increases its specificity through a process known as affinity maturation and evidence from other fields support the critical contribution of antibody-antigen interaction affinity to the antibody effector function [223, 224], however, this has not yet been fully explored in the transplant setting. The objectives of this work are to examine the relationship between alloantibody-HLA interaction affinity and antibody effector functions as assessed by complement-dependent cytotoxicity assays, and to provide insights into the effect of alloantibody affinity on interpretation of the output of currently used immunoassays for alloantibody detection and characterisation.

Hypothesis: The affinity of alloantibody-HLA binding is a major determinant of the antibody effector function; alloantibody affinity determination enables better interpretation of the output of clinically used immunoassays for alloantibody detection.

- **Examining the relationship between alloantibody-HLA interaction affinity and the activation of intracellular signalling pathways that lead to endothelial cell activation (Chapter 4).**

Antibody recognition of cell-surface HLA has previously been observed to initiate a cascade of protein kinase signals, resulting in proliferation, migration, gene upregulation and protein translocation in various cell types [233-275]. To delve further into the effects that these alloantibodies have on the cells they interact with, various *in vitro* assays were employed to assess the magnitude of antibody adhesion, protein signalling transduction, and cell adhesion molecule presentation upon the establishment of varying affinity alloantibody-HLA complexes on the surface of primary human aortic endothelial cells.

Hypothesis: The magnitude of a cellular response upon antibody ligation to cell surface HLA is dependent on the affinity that the antibody has for its antigen, where stronger interactions will induce a larger cellular response.

- **Development of a novel method for HLA-specific antibody affinity and concentration quantification in patient sera to improve immunological risk assessment. (Chapter 5)**

  Detecting and assessing the pathogenic potential of HLA-specific antibodies in transplant patients is an important process in evaluating the immunological risk associated with a particular transplant. Current methods for immunological risk assessment measure the reactivity of antibodies against immobilised HLA via a reporter and/or their ability to exert their cytotoxic function with addition of complement. Nevertheless, the semi-quantitative, amalgamated outputs of these assays often make it difficult to accurately determine their clinical significance [219]. Moreover, current methods to assess protein-protein interaction kinetics often necessitate the immobilisation of one interacting molecule. This is particularly problematic when complex media such as human serum is being evaluated. To enable full quantification of alloantibody-HLA interactions using non-purified samples, a novel in-solution method was established using the principles of microfluidic diffusional sizing (MDS) and Bayesian inference analysis. The ability of this approach to simultaneously measure the concentration of antibodies within a serum sample and the alloantibody interaction affinity against HLA targets was determined.

  Hypothesis: Developing a method that can quantitatively detect the formation of alloantibody-HLA complexes in solution will enable the fundamental parameters of antibody binding to be determined in non-purified samples.

Chapter Two

Materials and Methods

2.1. HLA Proteins, Antibodies and Ethical Approvals

2.1.1. Recombinant HLA Proteins

Purified, soluble, recombinant HLA proteins were provided from two separate sources. Proteins received from Pure Protein LLC (Oklahoma City, OK, USA) were used in affinity assessments for Chapter 4, whilst the National Institute of Health Tetramer Core Facility (Emory University, Atlanta, GA, USA) provided antigens for studies carried out in Chapter 5 (Table 2.1). HLA molecules were received in both biotinylated and unbiotinylated form. The concentrations of each protein were determined prior to use via either BCA protein assay (ThermoFisher Scientific, Cat. #23227) or Nanodrop OneC (ThermoFisher Scientific, Waltham, MA, USA). Protein concentrations quantified by Nanodrop were calculated by employing the Beer-Lambert Law (Equation 1) using the absorbance measured at 280nm (Abs280) and the molecular extinction coefficients (ε) for each protein as calculated from the protein sequences.

$$\mathbf{Abs_{280}} = \boldsymbol{\varepsilon}\, \mathbf{c}\, \mathbf{l}$$

Equation 1. Beer-Lambert Law. Where Abs_{280} is the absorbance measured at 280 nm, ε is the molar extinction coefficient (M^{-1} cm^{-1}), c is the concentration (M), and l is the pathlength of light (cm).

Table 2.1. Recombinant monomeric HLA molecule inventory. A list of the soluble, recombinant HLA monomers acquired for these studies. All Proteins were available in biotinylated and non-biotinylated forms.

Source	Expression System	Class	Locus	Allele	Variant	Nomenclature
Pure Protein LLC	Human Embryonic Kidney (HEK) 293	I	A	01	01	A*01:01
				02	01	A*02:01
				11	01	A*11:01
				11	02	A*11:02
				23	01	A*23:01
				24	02	A*24:02
				25	01	A*25:01
				31	01	A*31:01
				66	02	A*66:02
				68	01	A*68:01
				69	01	A*69:01
				80	01	A*80:01
			B	07	02	B*07:02
				08	01	B*08:01
				13	02	B*13:02
				15	01	B*15:01
				15	10	B*15:10
				27	05	B*27:05
				40	01	B*40:01
				40	02	B*40:02
				48	01	B*48:01
				57	01	B*57:01
				58	01	B*58:01
NIH Tetramer Core	*E. coli*	I	A	01	01	A*01:01
				02	01	A*02:01
				03	01	A*03:01
				11	01	A*11:01
			B	08	01	B*08:01
		II	DR	07	01	DRB1*07:01

2.1.2. HLA Antibodies

Human monoclonal HLA-specific antibodies (mAbs) were provided by Prof. Frans Claas and Dr. Sebastiaan Heidt at Leiden University Medical Centre (Table 2.2). Anti-HLA class I mAbs originated from alloantibody-positive, multiparous, post-natal women where the sensitising event is known. These mAbs were stably expressed in human heterohybridoma cells produced via Epstein-Barr virus transformation of immortalised lymphoblastoid cell lines (EBV-LCL) prior to fusion and sub-cloning. Anti-HLA-DR7 mAbs also originated from post-natal women where B-cells enriched from PBMC samples were positively selected for HLA reactivity via FACS using HLA-DR tetramers. RNA isolated from expanded individual HLA-DR-reactive B-cell clones were then sequenced to determine the Ab chain sequences. V_H and V_L domain sequences were cloned into separate pcDNA3.3 expression vectors alongside the constant domains of IgG1 (IGHG1*03), κ (IGKC), or λ (IGLC2*01). These constructs were then co-transfected into Expi293F cells, from which the Abs were purified from their supernatants. W6/32 was produced in hybridoma HB-95 cell lines and purified from the supernatants.

Table 2.2. HLA-specific human monoclonal antibody inventory. A list of the purified human monoclonal anti-HLA antibodies used to carry out these studies.

mAb	IgG Isotype	Expression System	Immunising HLA
WIM8E5	IgG1, κ	B-cell heterohydridoma	A*11:01
WK1D12	IgG1, κ	B-cell heterohydridoma	B*07:02
SN230G6	IgG1, λ	B-cell heterohydridoma	A*02:01/B*57:01
SN607D8	IgG1, κ	B-cell heterohydridoma	A*02:01
GV5D1	IgG1, λ	B-cell heterohydridoma	A*01:01
OUW4F11	IgG1, λ	B-cell heterohydridoma	B*08:01
BVK1F9	IgG1, κ	B-cell heterohydridoma	B*08:01
DR7 Ab 1	IgG1, λ	Expi293F	DRB1*07:01
DR7 Ab 2	IgG1, κ	Expi293F	DRB1*07:01
DR7 Ab 3	IgG1, κ	Expi293F	DRB1*07:01

2.1.3. Ethical Approvals

Human serum samples were routinely taken from transplant patients within Addenbrooke's hospital that were undergoing immunological risk assessment at Addenbrooke's Hospital Histocompatibility and Immunogenetics Laboratory. Ethical approval for the use of clinical patient sera for research was granted by the National Research Ethics Committee in the United Kingdom (REC Ref: 15/NE/0081). 100 µl aliquots were taken from 8 individual samples for these studies.

Primary human aortic tissue was collected from deceased human organ donors after circulatory death (DCD) or brainstem death (DBD) by the Cambridge Biorepository for Translational Medicine team. Informed consent from the donor's family was obtained prior to sample collection. Ethical approval for the use of human tissues in scientific research was granted by the National Research Ethics Committee in the United Kingdom (REC Ref: 15/EE/0152). A total of twelve aortic rings from individual donors were acquired for these studies.

Renal arteries were dissected from porcine kidneys procured from adult female Landrace pigs under Schedule 1 of the Animals (Scientific Procedures) act. All surgical procedures were carried out at a designated establishment in the United Kingdom.

2.2. Materials and Methods for Chapter 3

2.2.1. Biolayer Interferometry

2.2.1.1. Reagents and Consumables

Anti-human IgG Fc capture (AHC) (FortéBio, Cat. #18-5060), anti-murine IgG Fc capture (AMC) (FortéBio, Cat. #18-5088), streptavidin (SA) kinetic biosensors (FortéBio, Cat. #18-5019), Biocytin (Sigma, Cat. #B4261), Casein (Acros Organics, Cat. #276071000). All assays were carried out in black 96-well plates (Greiner, Cat. #655209).

2.2.1.2. General Protocol

Kinetic analysis of each mAb-HLA interaction was carried out on the OctetRED96 platform (FortéBio, Fremont, CA, USA) using the Octet55 Data Acquisition 9 software. BLI sensors were calibrated by soaking in standard BLI buffer (1 X PBS, 0.1% BSA, 0.02% Tween-20) from 30 minutes to overnight. Samples and sensors were loaded into the instrument and left for >10 minutes for the samples to reach the 30 °C set temperature. Sensors were initially incubated for 100 seconds in standard BLI buffer to establish a baseline for each sensor. Ligand was loaded onto the sensor by dipping into a well containing a previously determined optimal concentration of ligand in standard BLI buffer, allowing a threshold of 0.6 nm for all sensors in to be reached. A second baseline was established using standard BLI buffer over 100 seconds. In the association step, parallel sensors were dipped into wells containing one concentration of a 2-fold dilution series of purified soluble HLA, diluted in standard BLI buffer. Sensors were returned to the well in which the second baseline was established to allow dissociation of the complex to be measured. The optimal conditions were found to be using a loading density cut-off of 0.6 nm, a plate shake speed of 1000 rpm, temperature of 30 °C, with no need for sensor blocking steps (see section 3.2.2). Data analysis was carried out in FortéBio's Data Analysis 9 software.

2.2.1.3. Antibody-HLA-Screening Assay

mAbs were loaded onto calibrated AHC sensors prior to baseline establishment. Association of analyte was allowed to occur for 300 seconds in wells containing 50 μg/ml HLA before dissociation in BLI buffer-containing wells for a further 300 seconds. Affinities were calculated by fitting of the initial 100 seconds of association and dissociation phases using a 1:1 stoichiometry model, where K_D was measured as a function of k_{off}/k_{on}.

2.2.1.4. Interaction Affinity Determination

mAb-loaded AHC sensors were dipped into wells containing HLA until interaction equilibrium had been reached. Dissociation was allowed to proceed for 1000 seconds or until a significant, quantifiable amount of dissociation had been observed. Two parallel reference sensors; one sensor loaded with isotype control IgG and dipped into a well containing the HLA molecule in question during the association step (non-specific binding), and the other sensor loaded with the antibody in question and dipped into a well containing no HLA (curve drift), were subtracted from each test sensor prior to K_D determination. Data was fitted using global fitting and a 1:1 stoichiometry binding model from which the association rate (k_{on}), dissociation rate (k_{off}) and response at equilibrium (R_{eq}) were determined. K_D was measured as a function of k_{off}/k_{on}. During assay optimisation experiments, K_D was determined using steady state analysis as a function of 50% R_{MAX}.

2.2.2. Human PBMCs for HLA Targets

Human peripheral blood monocytic cells (PBMCs) were isolated from buffy coats obtained from healthy, HLA-typed individuals after informed consent (Sanquin Blood Supply, Amsterdam, the Netherlands). PBMCs were isolated by Ficoll-Hypaque density gradient centrifugation and cryopreserved in liquid nitrogen (N_2) until further use. Upon thawing, CDC and FC assays were performed simultaneously using the same PBMC sample as the HLA target (Table 2.3).

Table 2.3. Peripheral blood monocytic cell inventory. A list of the human peripheral blood mononuclear cells used for CDC and FC assays in chapter 3, their HLA types and the mAbs that were used against them. Grey filling signifies the expressed HLA target(s) of interest. ND = not determined. * = no allelic typing available. - = homozygous allele.

PBMC sample	HLA Class I Type						mAb(s) Tested
	A*	A*	B*	B*	C*	C*	
1	01:01	03:01	07:02	08:01	07:01	07:02	WIM8E5, WK1D12
2	01:01	32:01	15:01	37:01	03:03	06:02	WIM8E5
3	01:01	32:01	40:02	53:01	02:02	04:01	WIM8E5
4	02:01	03:01	07:02	13:02	06:02	07:02	WIM8E5, SN230G6, SN607D8
5	03:01	11:01	07:02	55:01	ND	ND	WIM8E5
6	03:01	24:02	35:03	44:05	02:02	04:01	WIM8E5
7	03:01	25:01	18:01	49:01	07*	12*	WIM8E5
8	31:01	32:01	07:02	40:01	03:04	07:02	WIM8E5
9	01:01	11:01	07:02	51:01	04:01	07:02	WK1D12
10	01:01	02:01	07:02	08:01	07:01	07:02	WK1D12
11	02:01	11:01	15:01	27:05	02:02	03:04	WK1D12
12	01:01	24:02	40:01	51:01	03:04	14:02	WK1D12
13	02:01	02:01	40:02	51:01	02:02	-	WK1D12
14	01:01	11:01	08:01	48:01	01:02	07:01	WK1D12
15	01:01	03:01	08:01	44:02	05:01	07:01	WIM8E5, OUW4F11
16	03:01	26:01	44:02	51:01	05:01	07:01	OUW4F11
17	02:01	-	44:02	58:01	05:01	07:01	OUW4F11

2.2.3. Control Reagents in Cell-Based Assays

Positive control serum was a pool of patient serum with HLA antibodies against Bw4 or Bw6 epitopes and were used as positive controls in every CDC and FC test. Negative control serum was pooled serum from 8 non-immunised males. Medium control was Iscove's modified Dulbecco's medium (IMDM) containing 10% FCS. This was used as an alternative negative control as it was the buffer used for dilution of monoclonal antibodies in FC and CDC assays. HLA-specific controls were human monoclonal HLA antibodies specific to the HLA in question, in the form of supernatants taken from hybridomas. Specific positive controls were used at a concentration of 10 μg/ml in every CDC test to confirm the expression of target HLA on the PBMCs.

2.2.4. Luminex Assays

All antibodies were tested for specificity against HLA class I molecules using LABScreen single antigen beads (SABs) (OneLambda, Cat. #LS1A04) following the suggested protocol (One Lambda, Canoga Park, CA, USA). In brief, mAbs were incubated with LABScreen SABs for 30 minutes on a rocker, washed with wash buffer (OneLambda, Cat. #LSPWABUF) and subsequently incubated with PE-conjugated anti-human IgG detection antibody (OneLambda, Cat. #LS-AB2) for a further 30 minutes. Samples were washed three more times before data collection. The ability of antibodies to fix complement protein C1q was measured using C1qScreen (OneLambda, Cat. #03C1Q). In brief, mAb, C1q and SABs were combined into one tube and gently rocked for 20 minutes before the addition of the provided PE-conjugated anti-C1q antibody. Samples were incubated for a further 20 minutes before being washed and analysed. Data collection was carried out on the Luminex 200 machine using xPOENENT software. Data analysis was carried out using OneLambda Fusion 4.1 software, referenced against the negative control beads and samples.

2.2.5. Flow Cytometry Assays

5 x 10^5 HLA-typed PBMCs as isolated in section 2.2.2 were incubated with 25 μl mAb or control for 30 minutes at RT. After washing three times with cold PBS, samples were stained with PE-conjugated mouse anti-human CD3 (clone:SK7; BD Biosciences, the Netherlands) and FITC-conjugated rabbit anti-human IgG F(ab')2 (Dako, Leiden, the Netherlands) in the dark, at 4 °C, for 30 minutes. Following two more washes, cells were fixed with 1% paraformaldehyde and acquired on an Accuri C6 flow cytometer (BD Biosciences). Only PE-

positive cells (T-cells) were analysed for each sample (Appendix 8). Interactions were considered positive if the ratio of FITC MFI between that of the test sample and negative control was greater than 1.6. PBMC FC assays were designed and planned by me and carried out by Gonca Karahan at Leiden University Medical Center.

2.2.6. Complement-Dependent Cytotoxicity Assays

1 µl of mAb or control antibody were added to triplicate wells in a pre-oiled 60-well Terasaki microtiter tray (Greiner, the Netherlands). 1 µl HLA-typed PBMCs were added to each well at a concentration of 3000 cells/µl and incubated at RT for 1 hour. 5 µl rabbit complement (Innotrain, Kronberg, Germany) was added to each well and incubated for a further 1 hour at RT. To visualise cytotoxicity, 5 µl propidium iodide (Sigma) was added to each well and incubated in the dark for 15 minutes. Microtiter trays were scanned by an automated inverted microscope (Leica DMI 4000B) and images were taken using microscope imaging software Leica QWin Patimed 2 V2.9.1 (Leica Microsystems, Switzerland). The reactivity in each tray was scored according to the percentage of dead cells: 0-10 % scoring 1, 10-20 % scoring 2, 20-40 % scoring 4, 40-80 % scoring 6 and 80-100 % scoring 8. CDC assays were designed and planned by me and carried out by Gonca Karahan at Leiden University Medical Center.

2.3. Materials and Methods for Chapter 4

2.3.1. Reagents and Consumables

Accutase enzyme cell detachment medium (eBioscience, Cat. #00-4555-56), Autoradiography film, UltraCruz (Santa Cruz, Cat. #sc-201696), Bromophenol blue sodium salt (Fluka, Cat. #18740), Casein (Acros Organics, Cat. #276071000), Cell dissociation buffer, enzyme-free (Gibco, Cat. #13151-014), Collagenase Type II (Gibco, Cat. #17101-015), Dimethyl sulphoxide (DMSO; Sigma, Cat. #D8418), 1,4-Dithiothreitol (DTT; Sigma, Cat. #10197777001), Endothelial cell growth supplement (ECGS; Fisher, Cat. #CB-40006B), Epidermal growth factor, Human (hEGF; Miltenyi Biotech, Cat. #130-093-825), Foetal calf serum (FCS; Hyclone, Cat. #SH30070-03), Gelatin (Sigma, Cat. #G1890), Heparin sodium salt (Sigma, Cat. #H3149), Histamine (Sigma, Cat. #H7125), Medium 199 (Corning, Cat. #10-060-CVR), Milk, Marvel Dried (Premier Foods Group Ltd, London, UK), Nitrocellulose membrane 0.45 μm (Bio-Rad, Cat. #1620115), Nonidet P-40 substitute (NP-40; Fluka, Cat. #74385), NP-40 lysis buffer (Alfa Aesar, Cat. #J62805), Paraformaldehyde (PFA; Alfa Aesar, Cat. #043368), Penicillin-streptomycin (Sigma, Cat. #P0781), Phorbol 12-myristate 13-acetate (PMA; Cambridge Bioscience, Cat. #10008014), phenylmethylsulphonyl fluoride (PMSF; Alpha Diagnostic, Cat. #PMSF16-S), Ponceau S solution (Sigma, Cat. #P7170), Protease and phosphatase inhibitor mini tablets, Pierce (Thermo Scientific, Cat #88669), Proteome profiler human phosphokinase array kit (R&D systems, Cat. #ARY003B), Sodium dodecyl sulphate (SDS; Sigma, Cat. #L4509), Sodium pyruvate (Gibco, Cat. #11360-070), Thrombin (Sigma, Cat. #T7326), TMB Substrate reagent pack (R&D, Cat. #DY999), TMB Western lightning ECL pro (PerkinElmer, Cat. #NEL121001EA), Triton X-100 (Sigma, Cat. #T8787), Trizma base (Sigma, Cat. #T6066), Trypsin-EDTA solution, 0.25% (Sigma, Cat. #T4049), Tumour necrosis factor α (TNFα; Peprotech, Cat. #300-01A).

2.3.2. Antibodies and Controls

Akt, pan (Cell Signalling, Cat. #4691), Akt, Phospho-473 (Cell Signalling, Cat. #4060), A-tubulin (Cell Signalling, Cat. #2144), CD31/PECAM-I-Biotin (eBioscience, Cat. #MA1-82378), ERK1/2, pan (Cell Signalling, Cat. #4695), ERK1/2, Phospho-202/204 (Cell Signalling, Cat. #4370), ICAM-1/CD54 (Cell Signalling, Cat. #4914), IgG1, κ isotype control,

human (Abcam, Cat. #ab206198), IgG1, λ isotype control, human (Abcam, Cat. #ab206203), IgG2a isotype control, mouse (Abcam, Cat. #ab18414), anti-human IgG-biotin (Bio-Rad, Cat. #STAR126B), anti-mouse IgG-FITC (Bio-Rad, Cat. #STAR70), anti-mouse IgG-HRP (Cell Signalling, Cat. #7076), anti-sheep IgG-HRP (R&D, Cat. #HAF016), P-Selectin/CD62P (Abcam, Cat. #ab6632), P-Selectin/CD62P (R&D, Cat. #AF137), Streptavidin-APC* (Thermo, Cat. #SA1005), VCAM-I (Cell Signalling, Cat. #13662), Vinculin (Cell Signalling, Cat. #4650).

2.3.3. Primary Endothelial Cell Isolation

Porcine renal artery tissues were provided by Dr. Sarah Hosgood at University of Cambridge Department of Surgery, where they had been dissected from an *ex vivo* perfused kidney. Human aortic tissue was received from the Cambridge Biorepository for Translational Medicine after procurement from DBD or DCD donors and stored at 4 °C in PBS or University of Wisconsin solution before processing. All tissues were acquired under full ethical approval as per section 2.1.3. Vascular tissue was placed into a petri dish containing pre-warmed PBS under a Microflow biological safety cabinet and was cut laterally to open the vessel into a flat sheet. Adventitia was removed from the outer layer of the vessel and the remaining tissue was rinsed to remove debris and erythrocytes. Tissue was placed endothelial side down into a new dish containing pre-warmed cell dissociation buffer (0.2 % (w/v) collagenase in 1:1 PBS/M199) and left to digest at 37 °C for 15 minutes. The digestion reaction was removed from the incubator and the endothelial side of the tissue was sprayed with 20 ml enriched endothelial cell growth media (EECGM; M199, 20 % HI FCS, 1 % sodium pyruvate, 36 μg/ml ECGS, 2400 U heparin, 0.1 μg/ml EGF) using a syringe connected to a 27-gauge needle. Media and dissociated cells were transferred into a 50 ml falcon tube and centrifuged at 300 x g for 7 minutes. Supernatants were discarded and the cell pellet was re-suspended in 15 ml EECGM before being equally transferred into each well of a 6-well gelatinised plate. After 24 hours, cells were rinsed with M199 medium to remove debris before addition of 2 ml EECGM per well. HAoEC patches were observed daily, where images were taken using an Olympus IX81 microscope. 1 ml of EECGM media was replaced every other day while the cells grew to confluence.

2.3.4. Cell Culture

Primary human aortic endothelial cells (Table 2.4) isolated in-house or purchased in vials at passage 2 (Promocell GmbH, Cat. #C-12271) were cultured in EECGM or endothelial cell growth medium MV (Promocell GmbH, Cat. #C-22020), respectively. Human umbilical vein endothelial cells (HUVEC; Promocell GmbH, Cat. #C-12200) and smooth muscle cells (SMC; Promocell GmbH, Cat. #C-12533) were cultured in endothelial cell growth medium (Promocell GmbH, Cat. #C-22010) or smooth muscle cell growth medium 2 (Promocell GmbH, Cat. #C-22062) respectively. Frozen cells were thawed for 2 minutes in a 37 °C water bath, washed with PBS, and pelleted via centrifugation at 300 x g for 5 minutes. Cells were re-suspended in growth media and seeded into T75 flasks which had been pre-coated with 0.2 % gelatin for >30 minutes. Cells were incubated at 37 °C, 5 % CO_2 in Sanyo O_2/CO_2 incubators where they were monitored daily with replenishment of media every 2-3 days. Once cells had reached 85 % confluence, media was removed from flasks and cells were washed with 10 ml 1 X PBS. 3 ml 0.25 % Trypsin-EDTA was added to the flask and incubated until cells were observed to dissociate under a Leitz Labovert FS microscope. After dissociation from the flask, 10 ml FCS/PBS (1:10) was added to flasks to inhibit trypsin activity. Cells were transferred into a 15 ml falcon tube and pelleted by centrifugation at 300 x g for 5 minutes. Supernatant was discarded and pellets were washed with 1 X PBS before being re-pelleted via centrifugation. Pelleted cells could then either be re-suspended in growth media and continually cultured or frozen for storage. To freeze cells, cell pellets were resuspended in freeze media (50 % FCS, 40 % M199, 10 % DMSO) to a concentration of 1 X 10^6 cells/ml. Cells were transferred into cryovials and placed into a Cryo 1°C Freezing Container (Nalgene, Cat. #5100-0001) and stored at -80 °C for 24 hours before transferral into a liquid N_2 Dewar for long-term storage. Unless stated, cells used for experiments were grown to 80 % confluence at passage 3-6 and were never left to exceed passage 6 to limit cell differentiation and sub-culturing effects. If starvation was needed, growth media was removed from plates, washed with 1 x PBS, and then replaced with starvation media (in-house-isolated HAoEC = M199+0.2% HI FCS, commercial cells = growth/basal media with adjusted FCS concentration to 0.2% and no addition of provided growth supplements) 6 hours to overnight prior to treatment.

Table 2.4. Primary cell sample inventory. A list of the primary cells used for *in vitro* cell signaling experiments. * = cells that have not been typed at a molecular level. ND = cells that have not been typed for their expressed HLA.

Cell Type	Source	Lot./ Donor #	HLA Type			
			A	A	B	B
HAoEC	Donor	335B	02:01	31:01	27:02	44:02
HAoEC	Promocell	415Z025	02:01	68:01	15:01	27:05
HAoEC	Promocell	422Z037	02*	26*	35*	27*
HAoEC	Promocell	422Z038	02*	03*	07*	49*
HUVEC	Promocell	422Z029	ND	ND	ND	ND
HAoSMC	Promocell	431Z013	ND	ND	ND	ND

2.3.5. Flow Cytometry

For analysis of cell surface molecules via flow cytometry, cells were removed from culture flasks through trypsinisation, incubation with accutase or with enzyme-free cell dissociation buffer. Pelleted cells were washed with FACS buffer (1 X PBS, 0.1 % BSA, 0.01 % Tween-20) and transferred into microfuge tubes. Cells were blocked with FcR blocking reagent (Miltenyi Biotech, Cat. #130-059901) at a 1:50 dilution in FACS buffer, for 20 minutes, on ice prior to centrifugation and washing. Primary and secondary antibody incubations were carried out for 30 minutes on ice, proceeded by three washes with FACS buffer following each incubation step. Cell samples were analysed on a BD FACSCanto II instrument using BD FACSDiva software. Analysis of data was carried out using FlowJo V10 software.

2.3.6. Cell Lysate Preparation, SDS-PAGE and Western Blot

Adherent treated cells were lysed on ice by direct addition of NP-40 lysis buffer (25 mM Tris pH 8.0, 150 mM NaCl, 1 % NP-40/Triton-X, 1 X PMSF, 1 inhibitor cocktail tablet per 10 ml) and scraping. Lysates were transferred into microfuge tubes and incubated on ice for >20 minutes before centrifugation at 13,000 rpm, at 4 °C, for 10 minutes to pellet cell debris. Supernatants were transferred into new tubes and lysate protein concentrations were analysed via BCA protein assay kit and the provided albumin standard. Samples were either used

instantly or frozen at -20 °C for later use. To carry out SDS-PAGE, consistent amounts of cell lysate (generally 10-20 µg) was mixed with 4X gel loading buffer (200 mM Tris pH 6.8, 400 mM DTT, 8 % SDS, 0.4 % Bromophenol Blue, 40 % Glycerol), incubated for 3 minutes at 100 °C on a heat block and loaded into each well of a 4-20 % Mini-Protean TGX stain-free pre-cast SDS gel (Bio-Rad Laboratories, Hercules, CA, USA). Gels were run at 120 V until the dye reached the end of the gel. For total protein staining, gels were rinsed with ddH2O and incubated with SimplyBlue SafeStain (Invitrogen, Cat. #LC6060) for 2 hours followed by de-staining in ddH2O for 24 hours. Images of gels were taken using a Syngene Ingenius 3 camera using GeneSys software. For observing individual protein expression/phosphorylation, western blot analysis was used. To do this, separated protein within SDS-gels was transferred on to nitrocellulose membrane via western transfer using the mini Trans-Blot cell (Bio-Rad Laboratories, Hercules, CA, USA). Samples were transferred at a voltage of 90 V for 90 minutes using 1 X transfer buffer (10 % methanol, 190 M glycine, 25 mM Tris, pH 8.3). Transfer success was observed via staining of membrane-bound protein with ponceau S solution. Ponceau stain was removed by washing with 1 X TBS-T (TBS; 50 mM Tris, 150 mM NaCl, pH to 7.5. TBS-T; TBS + 0.1 % Tween-20) and membranes were blocked with 5 % BSA in TBS-T for 1 hour before addition of primary antibody and incubation overnight, on a rocker, at 4 °C. The next day, membranes were washed 4 times with TBS-T for 5 minutes before the addition of HRP-conjugated secondary antibody in 5 % milk in TBS-T. After gentle rocking at RT for 1-2 hours wash steps were then repeated before membranes were incubated with 5 ml ECL substrate per membrane for 3 minutes. The presence of luminescent bands (target protein) was visualised via exposure to autoradiography film and/or using the ChemiDoc MP imaging system (Bio-Rad Laboratories, Hercules, CA, USA). Densitometry analysis of bands was carried out using ImageJ software.

2.3.7. Cell-Based ELISA Assay

To analyse the level of cell surface markers in response to treatment, cell-based enzyme-linked immunosorbent assays (ELISA) were utilised. 6 x 10^3 HAoECs were seeded into gelatin-coated 96-well tissue culture-treated plates and left to reach 100 % confluence before treatment. Directly after treatment, wells were washed once with 200 µl PBS and cells were fixed by incubation with 4 % paraformaldehyde at RT for 5 minutes before a further 2 washes. For permeabilisation of cells (total cellular protein), wells were incubated with 100 µl PBS + 0.1 % Triton-X 100 for a further 5 minutes. All wells were blocked with 5 % BSA in PBS for 1-2

hours at RT. 100 µl of the primary antibody in 5 % BSA/PBS (+0.1 % Triton-X 100 for total protein) was added to each well before being gently rocked at 4 °C overnight. Wells were washed 3 times with PBS before incubation with HRP-conjugated secondary antibody in PBS on a rocker at RT for 1-2 hours. Wells were washed a further 3 times before output detection via addition of 100 µl TMB substrate per well. To measure the levels of target protein for each well in response to treatment, the occurrence of precipitate was measured over time or at an endpoint using a FLUOstar OPTIMA microplate reader. For the kinetic assay, absorbance at OD_{620} (blue) was used, whereas the end-point measurement quantified the absorbance at OD_{450} (yellow) upon addition of 100 µl stop solution (160 mM H_2SO_4).

2.4. Materials and Methods for Chapter 5

2.4.1. Patient Serum Sample Acquisition

Aliquots of human serum samples were taken from a cohort of patients within Addenbrooke's hospital that were undergoing immunological risk assessment in preparation for a future transplant and/or immune monitoring for the occurrence of DSA post-transplant. Samples were selected based on their HLA reactivity and MFI output when analysed via Luminex SAB which was routinely carried out within the Addenbrooke's Hospital Histocompatibility and Immunogenetics Laboratory. All samples taken for research were under full ethical approval as per section 2.1.3.

2.4.2. Alexa Fluor™ 647 Labelling of HLA Monomers

100 µg of HLA monomer was aliquoted into a microcentrifuge tube. Buffer exchange was required in cases where proteins are stored in amine-containing solutions e.g., Tris. Here, samples were added to a 3 kDa Amicon® Ultra 0.5 ml centrifugal filter device (Merck, #UFC500324), where PBS was added in sequential concentration steps until the end concentration of original storage buffer was below 1 %. The pH of the HLA-containing solution was adjusted to 8.3 by addition of 1 M $NaHCO_3$ to a final concentration of 200 mM (1 in 5 dilution). Alexa Fluor 647 (AF647) N-hydroxysuccinimide ester (ThermoFisher Scientific, #A37573) was then added to a molar ratio of 1:3 (HLA to fluorophore) before being incubated at room temperature for 1 hour. The incubated labelling reaction was subject to size exclusion chromatography (SEC) using an ÄKTA pure system (Cytiva, Marlborough, MA, U.S.A) attached to either a Superdex 75 Increase 3.2/300, Superdex 75 Increase 10/300, or Superdex 200 Increase 10/300 column (Cytiva, Marlborough, MA, U.S.A). Here, PBS at pH 7.4 was used as the buffer at a flow rate of 0.1 ml/min (3.2/300 column) or 0.5 ml/min (10/300 column), where fractions were collected every 100 µl or 500 µl, respectively. Fractions were analysed via SDS-PAGE and microfluidic diffusional sizing (MDS) to select the desired fractions, which were then pooled. Pooled fractions were concentrated to a volume between 80-120 µl using a 3 kDa Amicon® Ultra 0.5ml centrifugal filter device before being further purified using a 7 k MWCO Zeba™ Spin desalting column (ThermoFisher Scientific, Cat. #89882) to remove any further free label that may have not been purified away via SEC. The

now labelled, purified, and concentrated HLA sample was quantified by Nanodrop using the extinction coefficient calculated from the full protein sequence (Equation 1). Proteins were either used straight away or aliquoted, flash frozen in liquid nitrogen, and then stored at −80 °C in PBS pH 7.4 + 10% Glycerol.

2.4.3. Microfluidic Diffusional Sizing

Samples containing the desired concentrations of labelled protein and unlabelled interaction partner(s) were prepared in microcentrifuge tubes and were made up to a total of 18 µl using a standard buffer of PBS, pH 7.4 supplemented with 0.2 % Tween-20. Samples were incubated on ice, in the dark, for a minimum of 60 minutes to enable interaction equilibrium to be reached. For MDS analysis, the Fluidity One-W (Digby model; Fluidic Analytics, Cambridge, U.K.) was used, where 5 µl of sample was added to the pedestal of a microfluidic chip (Fluidic Analytics, #1003-90003). This chip was then inserted into the instrument where samples were run at the required flow rate (1-8 nm or 50 µl/hr for HLA class I, 2-20 nm or 20 µl/hr for HLA class II) to yield the average hydrodynamic radius (R_H) of the labelled protein/complex.

2.4.4. MDS Background Fluorescence Correction

To account for the background autofluorescence of serum and/or other autofluorescent samples, tubes were prepared containing 100 %, 50 % and 25 % serum, containing 0.2 % Tween-20 and diluted in PBS-T where necessary. These samples were analysed by MDS in triplicate, whereby a standard curve was created by plotting the fluorescence intensities measured in each diffused/undiffused channel for each serum concentration. Upon acquisition of sample data, background fluorescence in both diffused and undiffused chambers was corrected for by deducting the standard curve-extrapolated autofluorescence values for that specific concentration of sample from the raw fluorescence values output by MDS, prior to data analysis. The python script used for background fluorescence correction was created by Sean Devenish at Fluidic Analytics Ltd.

2.4.5. Interaction Stoichiometry Determination via MDS

To determine the stoichiometry of an interaction, samples containing 100 nM AF647-labelled HLA (conc. needs to be significantly above K_D) were incubated with a dilution series of mAb, between 0-250 nM, and analysed by MDS in triplicate. Plotting a graph of hydrodynamic radius against antibody concentration yields a saturation curve, where the ratio of antibody to antigen

at the concentration which results in the curve becoming saturated (or 'kinked') directly determines the stoichiometry of the interaction (Equation 2).

$$\textit{Stoichiometry of Interaction} = \frac{\textit{Concentration of Labelled HLA}}{\textit{Concentration of Ab at Plateau}}$$

Equation 2. Calculating the stoichiometry of an interaction via saturation curve

2.4.6. Interaction Affinity Determination – Equilibrium Binding Curve

To determine the affinity of an Ab-HLA interaction via generation of a full binding curve, individual samples containing the desired concentration of AF647-labelled HLA (conc. needs to be below K_D) were incubated with one concentration of a two-fold dilution series of antibody before being analysed by MDS in triplicate. In cases where serum was used, the background autofluorescence of serum was measured in the absence of labelled protein and used to correct the raw MDS data as stated in 2.4.4. Data which spanned the entire binding curve (from minimum to maximum hydrodynamic radius) was plotted on a graph of hydrodynamic radius against antibody concentration. Binding curves were fitted using Prism 9 software (GraphPad Software, San Diego, CA, U.S.A) using equation 4 (see Appendix 3 for derivation), assuming this interaction follow the principles of a binary reaction model as depicted in equation 3. From this the equilibrium dissociation constant (K_D) could be deduced.

$$[\boldsymbol{A}] + [\boldsymbol{B}] \overset{\boldsymbol{K_D}}{\leftrightarrow} [\boldsymbol{AB}]$$

Equation 3. General Chemical Equation for a Binary Reaction. Where [A] is the concentration of the AF647-labelled, unbound reactant, [B] is the concentration of the other unbound reactant, [AB] is the concentration of the complexed molecule, and K_D is the equilibrium dissociation constant.

$$\boldsymbol{R_{h,x}} = \left(\left(\frac{[\boldsymbol{Ab}] + \boldsymbol{n} \cdot [\boldsymbol{Ag}] + \boldsymbol{K_D}}{2} - \sqrt{\left(\frac{[\boldsymbol{Ab}] + \boldsymbol{n} \cdot [\boldsymbol{Ag}] + \boldsymbol{K_D}}{2} \right) - [\boldsymbol{Ab}] + \boldsymbol{n} \cdot [\boldsymbol{Ag}]} \right) \frac{\boldsymbol{R_{h,Ag}} - \boldsymbol{R_{h,AgAb}}}{\boldsymbol{n} \cdot [\boldsymbol{Ag}]} \right) + \boldsymbol{R_{h,Ag}}$$

Equation 4. Fitting of MDS Equilibrium Binding Curves. The equation used to calculate interaction affinity in solution via equilibrium binding curve, where $R_{h,x}$ is the effective hydrodynamic radius at equilibrium in the presence of Ab at concentration x, $R_{h,Ag}$ is the hydrodynamic radius of free antigen, $R_{h,AgAb}$ is the size of the antigen in complex with antibody, [Ab] is the total concentration of antibody, [Ag] is the total concentration of antigen, K_D is the affinity constant, and n is the number of antigen binding sites with respect to the antibody.

2.4.7. Interaction Affinity Determination – MAAP

Samples were prepared using varying ratios of AF647-labelled HLA (1-500 nM) and antibody-containing sample (0-90 %) before being analysed by MDS in triplicate. In cases where serum was used, the background autofluorescence of serum was measured in the absence of labelled protein and used to correct the raw MDS data as described in section 2.4.4. The concentration of antibody binding sites, [Ab], and equilibrium dissociation constant, K_D, were determined using Bayesian analysis using sequential MDS measurements until the 95% confidence intervals of the -log value for each parameter were constrained within 0.5 of each other (or as constrained as the values could be within the limitations of the experiment). The complete method and equations derived for determination of these parameters is protected under patent application number (PCT/GB2021/051244, filed on 21/05/21, Appendix 17). The python script developed for MAAP was created by Dr. Catherine Xu and Dr. Georg Meisl in the University of Cambridge Department of Chemistry.

Chapter Three

Assessment of Alloantibody-HLA Interactions: The Role of Antibody Affinity and Concentration

3.1. Introduction

Alloimmunity occurs following a priming event such as a blood transfusion, pregnancy and/or transplantation, where a person is exposed to non-self HLA. Should this exposure result in allorecognition of an epitope by the BCR [157, 158], an alloimmune response may be induced which results in the production of mature, developed antibodies through processes of clonal selection and affinity maturation, from which an antibody gains its specificity for the recognised antigen [88, 89, 160-163]. Once DSAs are secreted from the immune cells into the blood, they will remain circulating within the vascular system to carry out their specific functions whilst their titres naturally decline over time, a process known as resolution. To add further complexity, conservation of structural topographies between HLA molecules may enable an antibody that is primed against one antigen to recognise other antigens due to similarities in the physiochemical properties of epitopes at their surface. Thus, one sensitisation event has the capability to build immunity against multiple HLA molecules [197]. Should a sensitised individual receive a graft in which the donor-expressed HLA can be recognised by their resident antibodies, this could lead to antibody-mediated rejection and potentially loss of the graft. To prevent this situation from occurring, the antibodies present within a recipient's sera need to be analysed prior to transplant to determine which donor HLA molecules should

be avoided [198-209], whilst regular immune monitoring aids in the detection of any DSAs that may necessitate intervention to prevent graft damage post-transplantation [210-212].

To charaterise DSAs present in a patient's blood, various antibody assessment assays, such as Luminex single antigen beads (SAB), enzyme-linked immunosorbent assay (ELISA), flow cytometry (FC), and complement-dependent cytotoxicity (CDC) have been developed. Luminex, ELISA and FC assays aim to detect the presence and specificity of any anti-HLA Abs, where assay outputs are determined by the antibody's ability to recognise and specifically bind to its antigenic targets governed by its Ig Fab regions. CDC assays measure the ability of these alloantibody-HLA interactions to induce cytotoxic death through complement engagement [28]. Outputs of CDC assays are not only reliant on the establishment of a stable interaction between HLA and the antibody's Fab region but are additionally dependent on the ability of the Ig's Fc region to fix complement, where immunoglobulin class/subclass identity and Fc glycosylation have been documented to influence an antibody's complement-fixing capabilities [94]. Implementation of HLA-specific antibody analyses and immunological risk assessment have had a significant impact on transplant outcomes by limiting the risk of rejection due to detection of pre-existing immunity. Nevertheless, donor HLA recognition post-transplant and development of AMR remains a major cause of graft loss [225]. Due to the limitations of currently available assays, such as sensitivity, interpretation of assay outputs is not always standardised and vary between laboratories. For example, it cannot currently be determined with confidence whether an antibody-HLA interaction that yields a positive output in Luminex SAB, but also measured to be negative in cell-based assays, is due to the presence of clinically irrelevant antibodies at a high titre (e.g., due to cross-reactivity or non-specific binding), or due to clinically significant antibodies at a titre below the threshold for CDC detection [226]. This means that should a patient receive an organ where the latter scenario is applicable, a secondary immunological-memory response against the donor-expressed antigen(s) may be induced after transplantation, potentially resulting in graft injury and rejection. In addition, most assays detect the presence of DSAs using a reporter antibody that does not discriminate between IgG subclasses, and therefore does not provide any information on effector functions that is governed by antibody subclass [227].

To understand the importance of individual AlloAb-HLA interactions and delve further into the biological function of antibodies and the properties that determine whether an interaction is clinically significant, selected AlloAb-HLA interactions were analysed to establish the role

of interaction affinity on their ability to carry out specific effector functions. Initially, experiments were designed to uncover the unique specificity of various purified human monoclonal anti-HLA antibodies (mAbs). Upon selection of individual interactions to be assessed, an optical analytical method called biolayer interferometry (BLI) was adapted to enable the quantification of the kinetics associated with each interaction. BLI works by detecting the changes in wavelength of reflected light from the optical sensor's contact surface, which is directly proportional to the amount of organic material bound to it [228] (Figure 3.1.A). Using this principle, the association and subsequent dissociation of free protein from its binding partner immobilised to the surface of the optical sensor can be measured over time (Figure 3.1.B, C). From this, the association rate, k_{on}, dissociation rate, k_{off}, and affinity constant, K_D, of the interaction can be deduced. Analysing these same interactions using the immunoassays that are implemented in clinic for antibody-related immunological risk assessment (FC, Luminex and CDC assays) enables the binding and complement-fixing abilities of each interaction to be established. Using this approach, the main purpose of this study was to broaden our understanding around the fundamental parameters of antibodies that underpin immunoassay output, thus enabling us to identify which areas of study can be developed to help improve how we interpret the assays used for HLA-specific antibody assessment.

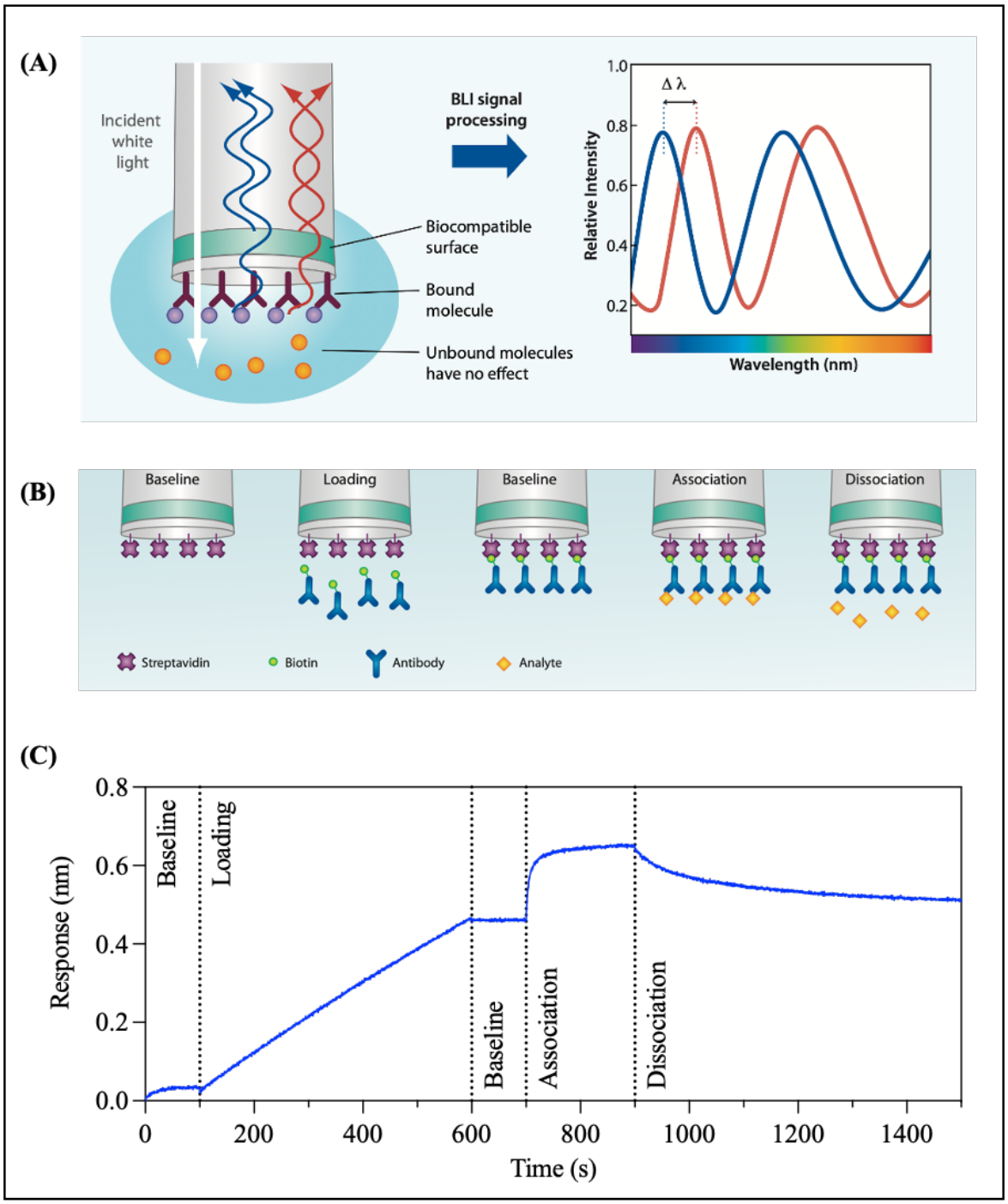

Figure 3.1. The principles of biolayer interferometry. Diagrammatical representation of the fundamental principles of the BLI method. (A) Binding of organic molecules to the surface of the BLI sensor causes a shift in wavelength due to the change in the distance light needs to travel in order to be reflected off the extremity of the sensor, measured as a response (nm). (B) A visualised example of loading a ligand onto the BLI sensor's surface, followed by the association and dissociation of analyte from the immobilised ligand, yielding a sensorgram such as in (C) (A*01:01-WIM8E5). A and B were reproduced from: Tobias, S. and Kumaraswamy, R. Biomolecular Binding Kinetics Assays on the Octet Platform. ForteBio. 2013.

3.2. Results

3.2.1. Screening of Alloantibody-HLA Interactions

Human monoclonal immunoglobulins, previously documented to bind HLA class I molecules and induce cytotoxicity *in vitro* were characterised as part of an international histocompatibility workshop (data not shown). Individual Abs were selected based on their ability to induce cytotoxic death of donor lymphocytes, were of IgG1 isotype, and were previously shown to bind HLAs that could be obtained in purified, soluble, recombinant form. To identify interactions of interest that could be taken forward for further assessment, selected monoclonal antibodies were preliminarily screened using Luminex class I SABs to determine their reactivity, and then via biolayer interferometry to gain an estimate of the kinetics that underpin the observed binding event.

3.2.1.1. Screening Antibody Reactivity against HLA Class I via Luminex Single Antigen Beads

Monoclonal antibodies were assessed via Luminex assay at a concentration of 1 μg/ml using class I SABs to reveal their unique HLA binding profiles so that interactions of interest could be identified. All antibodies displayed high reactivity against their sensitising antigen (>20,000 MFI), however their ability to recognise non-priming HLA molecules varied (Figure 3.2, Appendix 1). Where cross-reactivity was observed, the non-immunising antigens were often found to contain a potential common CREG with that of the priming antigen (Appendix 2). WIM8E5, OUW4F11 and WK1D12 were revealed to be the most cross-reactive antibodies, where the differing MFI values generated against HLAs within the class I SAB panel demonstrated the varying ability of each antibody to recognise non-priming antigens. SN607D8, SN230G6 and GV5D1 showed a narrower range of reactivity against class I SABs, generating positive MFI values against <10 SABs each. BVK1F9 was the only antibody found to have a unique specificity for its sensitising antigen, B*08:01 (MFI=24,653), without displaying cross-reactivity to any of the other antigens assessed within the SAB class I panel.

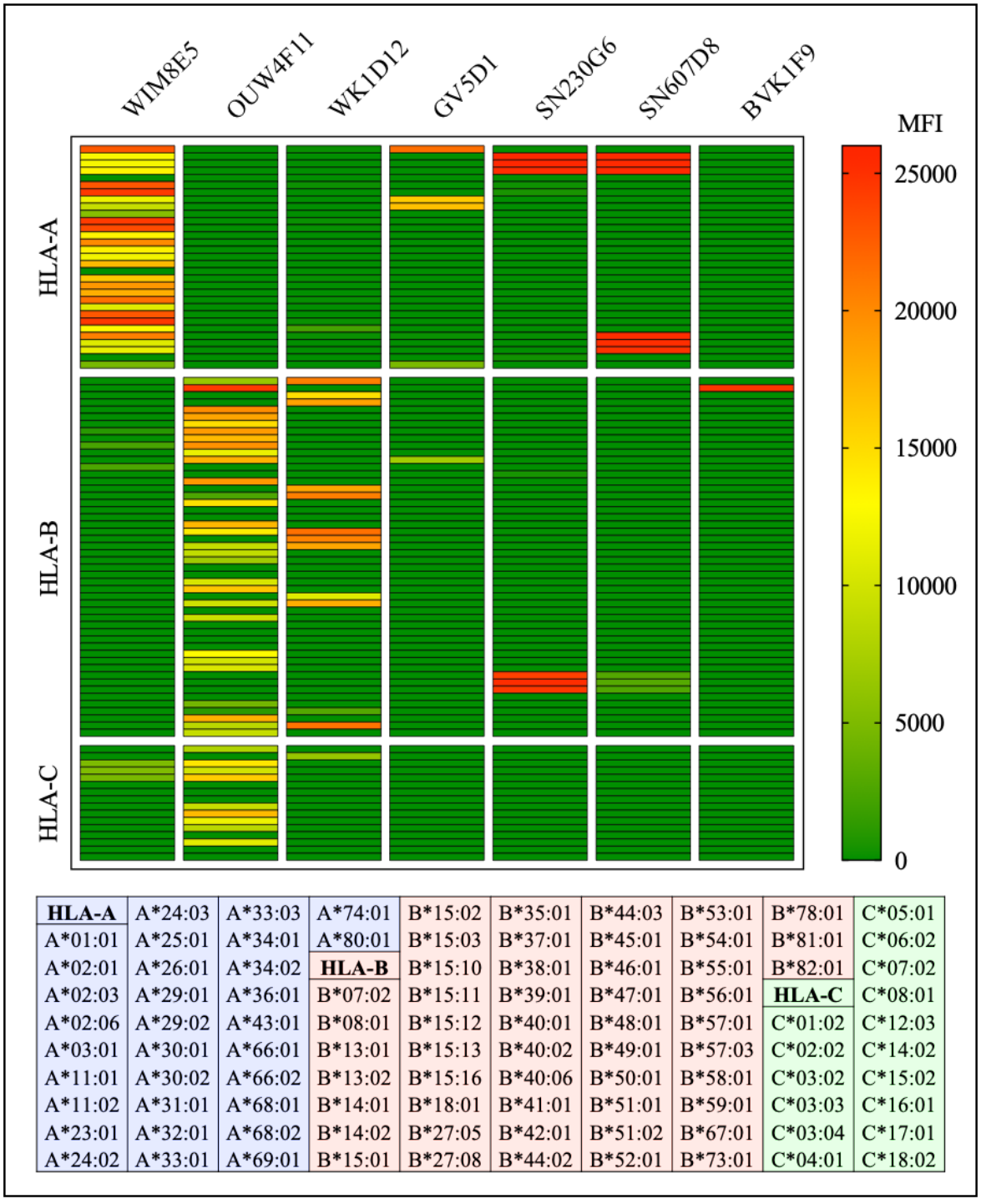

HLA-A	A*24:03	A*33:03	A*74:01	B*15:02	B*35:01	B*44:03	B*53:01	B*78:01	C*05:01
A*01:01	A*25:01	A*34:01	A*80:01	B*15:03	B*37:01	B*45:01	B*54:01	B*81:01	C*06:02
A*02:01	A*26:01	A*34:02	HLA-B	B*15:10	B*38:01	B*46:01	B*55:01	B*82:01	C*07:02
A*02:03	A*29:01	A*36:01	B*07:02	B*15:11	B*39:01	B*47:01	B*56:01	HLA-C	C*08:01
A*02:06	A*29:02	A*43:01	B*08:01	B*15:12	B*40:01	B*48:01	B*57:01	C*01:02	C*12:03
A*03:01	A*30:01	A*66:01	B*13:01	B*15:13	B*40:02	B*49:01	B*57:03	C*02:02	C*14:02
A*11:01	A*30:02	A*66:02	B*13:02	B*15:16	B*40:06	B*50:01	B*58:01	C*03:02	C*15:02
A*11:02	A*31:01	A*68:01	B*14:01	B*18:01	B*41:01	B*51:01	B*59:01	C*03:03	C*16:01
A*23:01	A*32:01	A*68:02	B*14:02	B*27:05	B*42:01	B*51:02	B*67:01	C*03:04	C*17:01
A*24:02	A*33:01	A*69:01	B*15:01	B*27:08	B*44:02	B*52:01	B*73:01	C*04:01	C*18:02

Figure 3.2. Alloantibody screening via Luminex Single Antigen Beads. Each mAb was screened against Luminex class I SABs at a concentration of 1 µg/ml (n=1) to determine their unique specificities. Each row within the heatmap represents one HLA allele as labelled in the table. The colour of each cell represents the mean fluorescence intensity taken from >100 beads due to antibody binding and subsequent secondary detection.

WIM8E5 generated positive MFIs (>1,500) against 33 of the 97 (34%) HLA molecules assessed (HLA-A=28, HLA-B=2, HLA-C=3). Along with its sensitising antigen, HLA-A11 (MFI: A*11:01=22,900; A*11:02=24,550), WIM8E5 showed the substantial ability to bind other HLA molecules that share epitopes within 1C/A1C/1C2/1C3 and 10C/28C CREG assignments (Figure 3.3). WIM8E5 was discovered to have considerable reactivity against HLA-A2 (MFIs: A*02:01=12,609; A*02:03=12,390; A*02:06=13,307), despite there being no assigned CREG that is shared between HLA-A2 and its priming antigen HLA-A11. HLA-A2 does however share epitopes with members of the HLA-A9 and HA-A28 broad serotypes within the 2C/A2/2C2 CREG assignments, which along with HLA-A11 are also assigned to the 1C/1C2 and 10C/28C CREGs, respectively. The lesser magnitude MFIs produced against beads expressing HLA alleles from the HLA-A9 and HLA-28 broad serotypes (HLA-A9: A*23:01=11,753; A*24:02=9,233, A*24:03=5,458, and HLA-A28; A*68:01=20,594, A*68:02=10,760, A*69:01=11,372) were comparable to that of HLA-A2 SABs in that many they could generate positive yet non-saturating MFIs. This suggests that WIM8E5 may recognise an unassigned epitope that is partially conserved across HLA-A11, HLA-A2, HLA-A9 and HLA-28 molecules, offering a potential explanation as to why this antibody is able to recognise antigens that are otherwise distinctly dissimilar to that of its sensitising antigen. OUW4F11 displayed the widest range of reactivity against Class I SABs, generating positive MFIs against 39 (40%) of the SABs, to which all were either HLA-B or -C alleles (Figure 3.4: HLA-B=30, HLA-C=9). All but one interaction involving HLA-B molecules belong to the Bw6 classification, where the only positive interaction against a Bw4-expressing bead (B*27:08) was measured to have a very low positive MFI value of 2,478. OUW4F11's interactions with beads containing the sensitising antigen, B*08:01, were able to generate saturating MFI levels (MFI=24,513), whilst cross-reactive interactions were observed to generate significantly decreased MFIs, all <20,000. WK1D12 antibodies were also found to a have a specificity for HLA-B antigens (Figure 3.5: HLA-A=1, HLA-B=12, HLA-C=1), where a broadly conserved epitope on its priming antigen, B*07:01, enables the antibody to recognise antigens from both Bw4 and Bw6 classifications. Unlike OUW4F11, WK1D12 was able to generate MFI values against cross-reactive HLAs like that of its sensitising antigen at this antibody concentration (B*07:02=20,666, B*27:08=20,654, B*40:01=21,488, B*40:02=20,389, B*81:01=21,336), suggesting a high conservation of the epitope between these molecules. When observing the narrower reactivity of GV5D1 (Figure 3.6.A), it was found to generate significant MFIs against its sensitising antigen (A*01:01=21,559), however

the MFIs generated against its three cross-reactive antigens within the 1C/A1C/1C2 CREG were significantly reduced (A*23:01=16,016, A*24:02=16,728, A*80:01=4,776). GV5D1's interaction with B*15:12-expressing beads was also noteworthy (MFI=7,029), although HLA-B*15:12 does not belong to this CREG and suggests a potential false positive measurement and/or an unassigned epitope that may be responsible for the initial priming event. SN230G6 and SN607D8 also displayed cross-reactive properties, but unlike the antibodies discussed above, all positive MFI values generated were measured at saturating levels like that of the sensitising antigen. This suggests that these antibodies recognise a highly conserved epitope present on both the sensitising and cross-reactive antigens (Figure 3.6.B-C). One interesting observation was the differing reactivity patterns of SN230G6 and SN607D8 despite being isolated from the same post-natal individual following two distinct A*02:01 sensitising events.

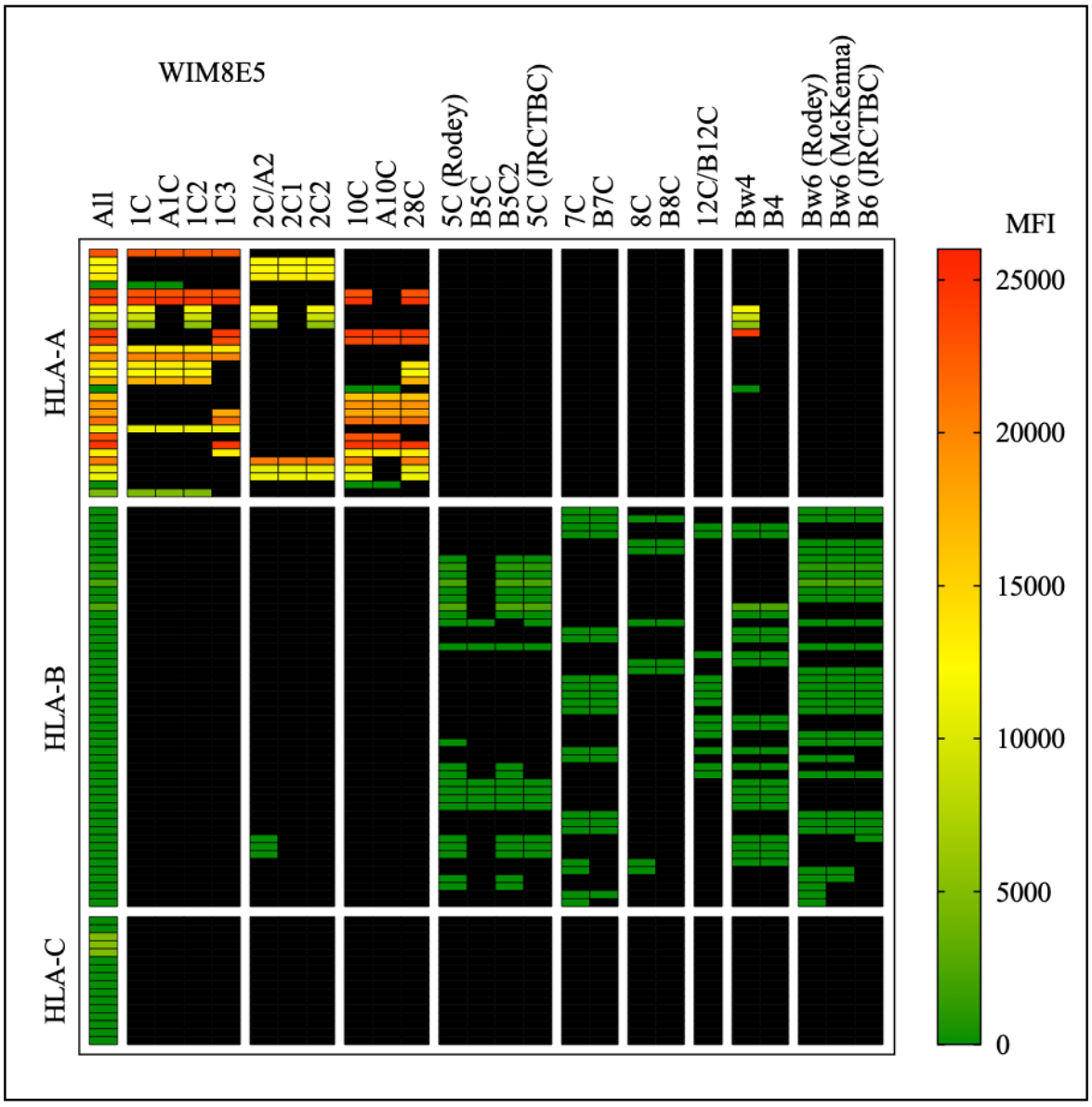

Figure 3.3. Luminex MFIs measured for WIM8E5 within each CREG. Assessing the Luminex Class I SAB outputs from incubation with 1 µg/ml WIM8E5 (n=1) to determine any patterns in binding that relate to any assigned cross-reactive group (see Appendix 2). WIM8E5 was observed to bind antigens belonging to 1C, 2C and 10C CREGs. Each row represents one HLA allele as labelled in the table in Figure 3.2. The colour of each cell represents the mean fluorescence intensity taken from >100 beads due to antibody binding and subsequent secondary detection. Black-filled cells represent antigens that do not belonging to that assigned CREG.

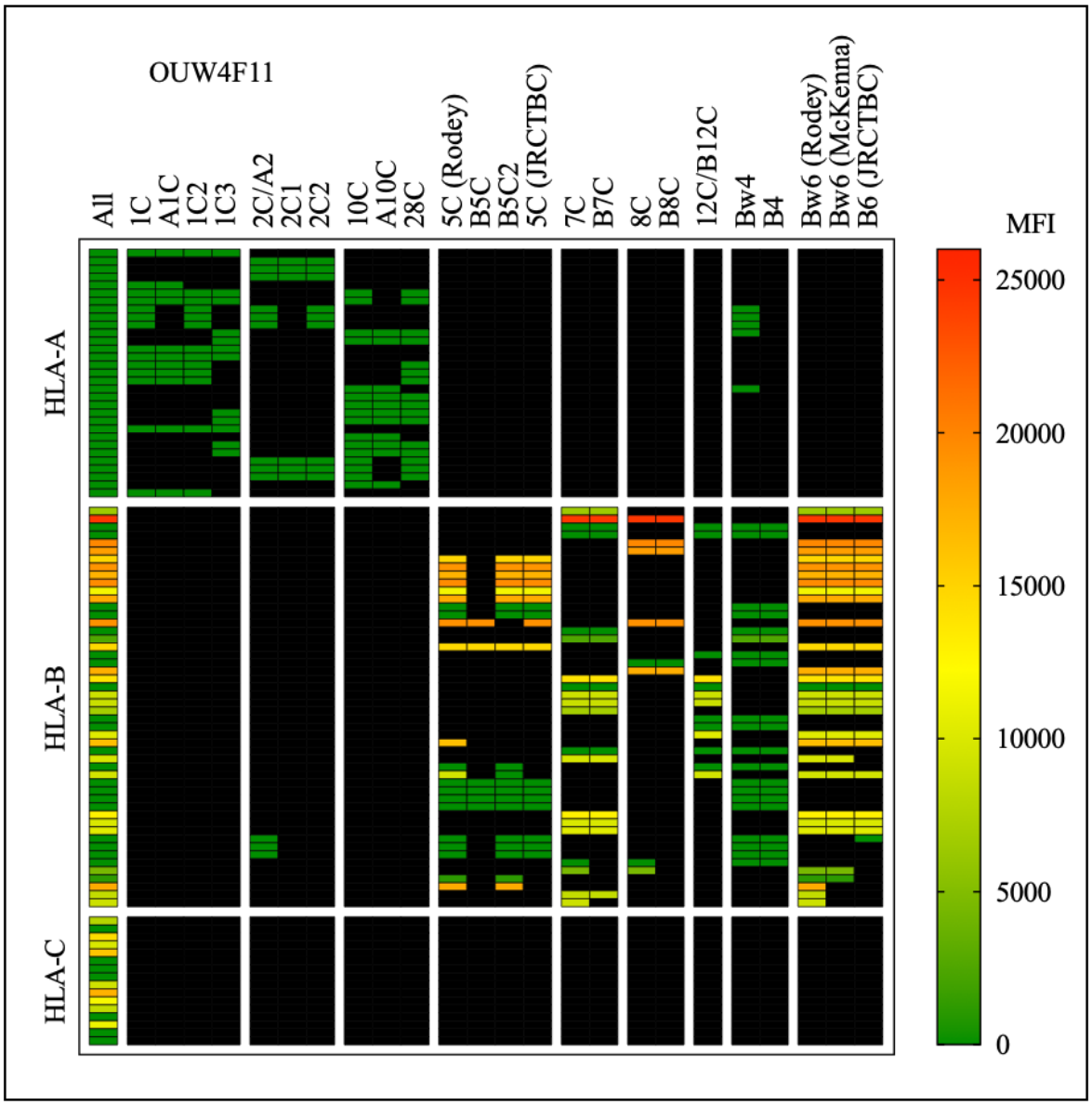

Figure 3.4. Luminex MFIs measured for OUW4F11 within each CREG. Assessing the Luminex Class I SAB outputs from incubation with 1 µg/ml OUW4F11 (n=1) to determine any patterns in binding that relate to any assigned cross-reactive group (see Appendix 2). OUW4F11 was observed to bind antigens belonging to 5C, 7C, 8C and Bw6 CREGs. Each row represents one HLA allele as labelled in the table in Figure 3.2. The colour of each cell represents the mean fluorescence intensity taken from >100 beads due to antibody binding and subsequent secondary detection. Black-filled cells represent antigens that do not belonging to that assigned CREG.

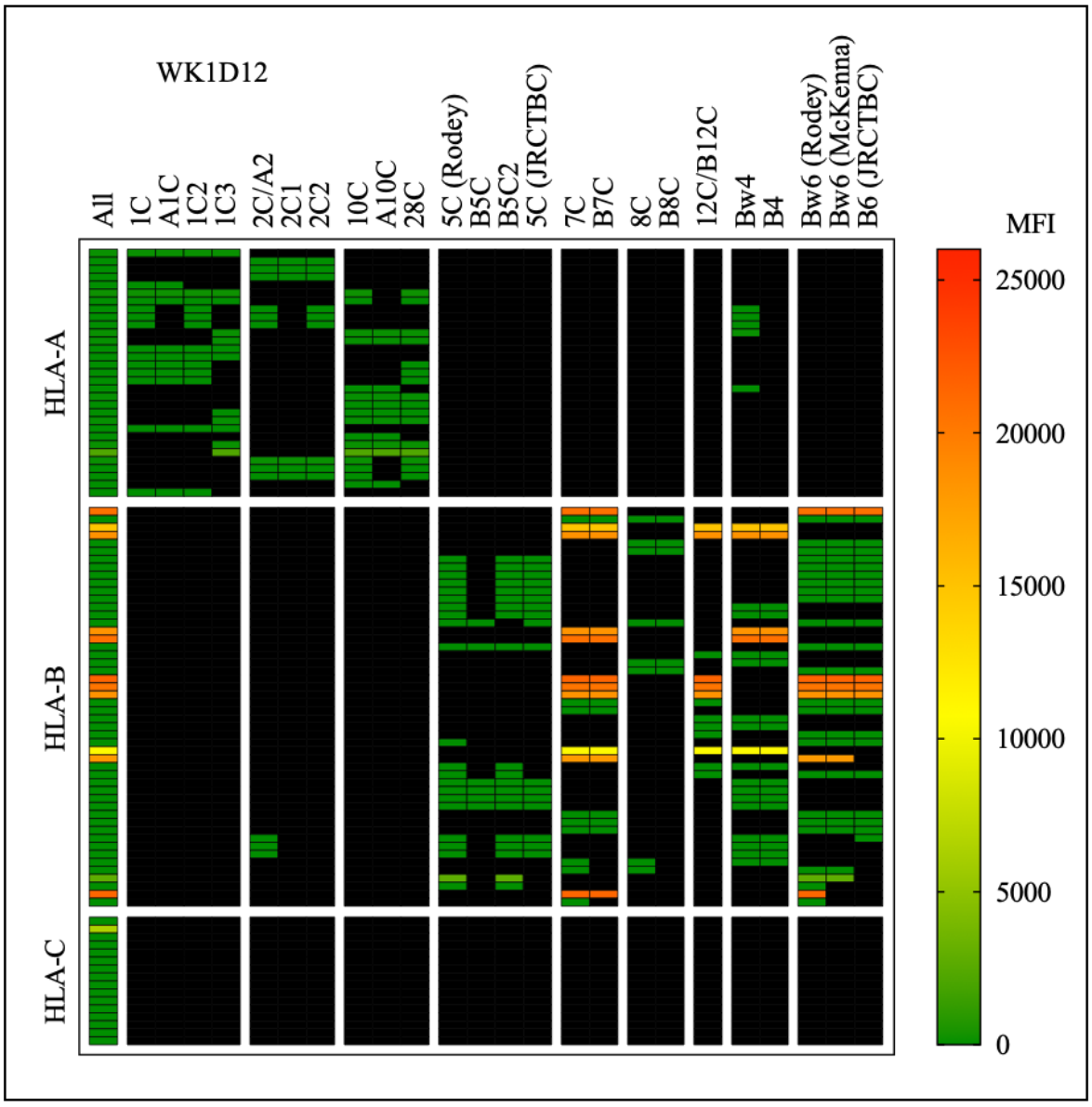

Figure 3.5. Luminex MFIs measured for WK1D12 within each CREG. Assessing the Luminex Class I SAB outputs from incubation with 1 µg/ml WK1D12 (n=1) to determine any patterns in binding that relate to any assigned cross-reactive group (see Appendix 2). WK1D12 was observed to bind antigens belonging to 7C, 12C, Bw4 and Bw6 CREGs. Each line represents one HLA allele as labelled in the table in Figure 3.2. The colour of each cell represents the mean fluorescence intensity taken from >100 beads due to antibody binding and subsequent secondary detection. Black-filled cells represent antigens that do not belonging to that assigned CREG.

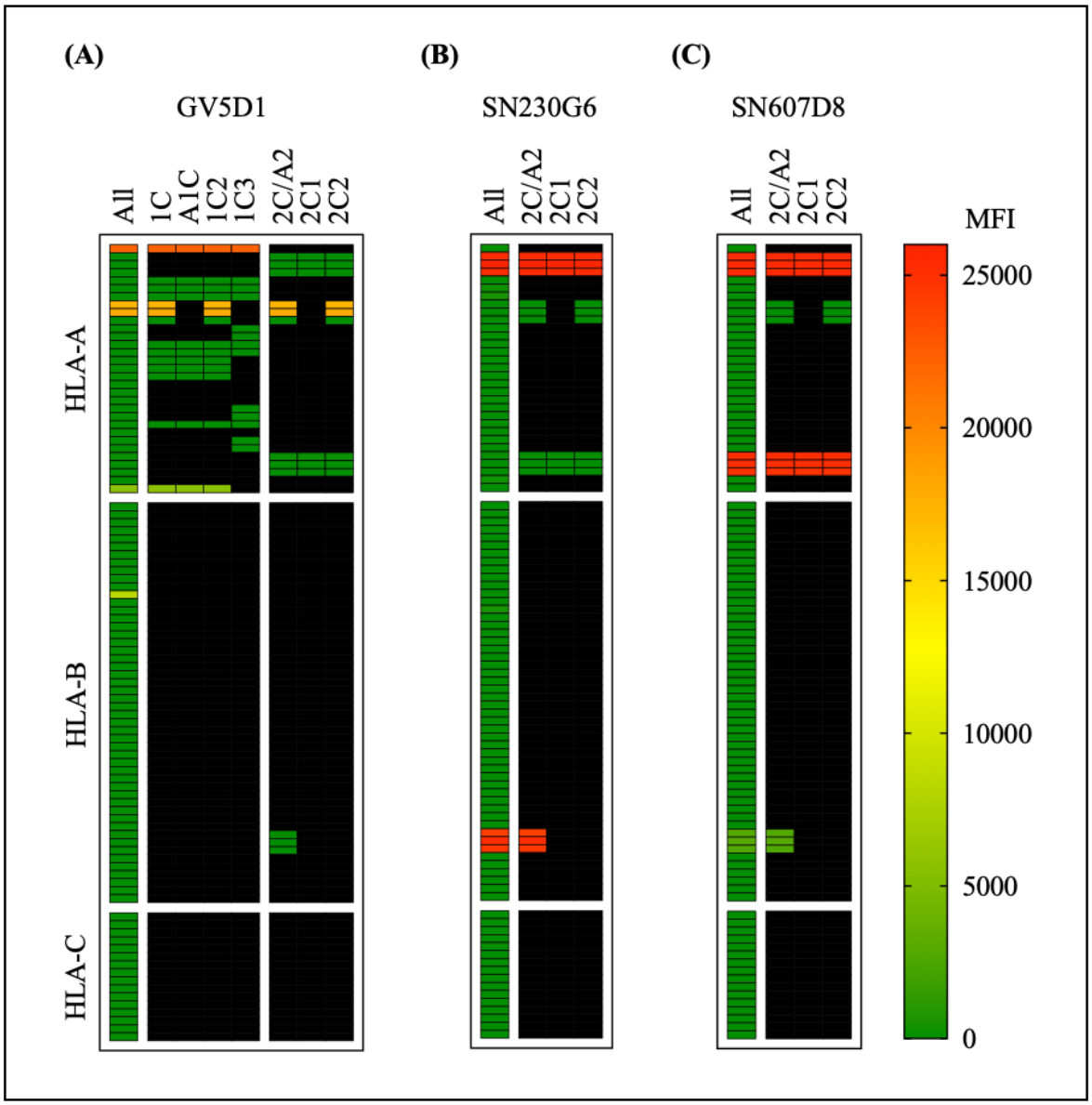

Figure 3.6. Luminex MFIs measured for GV5D1, SN230G6 and SN607D8 within each CREG. Assessing the Luminex Class I SAB outputs from incubation with A) GV5D1 (n=1), B) SN230G6 (n=1) or C) SN607D8 (n=1) at a concentration of 1 µg/ml to determine any patterns in binding that relate to any assigned cross-reactive group (see Appendix 2). GV5D1 was observed to bind antigens 1C and 2C CREGs. Both SN230G6 and SN607D8 only bound antigens within the 2C CREGs, however both showed differing reactivity patterns. Each line represents one HLA allele as labelled in the table in Figure 3.2. The colour of each cell represents the mean fluorescence intensity taken from >100 beads due to antibody binding and subsequent secondary detection. Black-filled cells represent antigens that do not belonging to that assigned CREG.

3.2.1.2. Screening Interaction Affinity via Biolayer Interferometry

Luminex-positive AlloAb-HLA interactions were selected to be further assessed via kinetic analysis using biolayer interferometry based on the availability of HLA reagents (Table 2.1). 50 μg/ml HLA was incubated with antibody immobilised to a sensor surface where the association (k_{on}) and dissociation (k_{off}) rates were measured and used to gain an estimation of the interaction affinity (K_D) (Figure 3.7, Table. 3.1). A total of 38 interactions were screened across the seven different antibodies combined. The K_D was successfully acquired for 24 interactions, with values ranging between 3.4×10^{-8} and 5.9×10^{-6} M (Figure 3.7, black sensorgrams). 14 interactions were unable to generate responses >0.06 nm and/or produced largely heterogenous sensorgrams and so could not be used to accurately determine the association, dissociation, and affinity constants (Figure 3.7, red sensorgrams).

Interestingly, interactions observed to be unquantifiable due to low BLI responses were also unable to generate Luminex SAB MFIs >17,000, whilst most of the quantified interactions produced MFI values beyond this mark. In cases where lower response sensorgrams were able to produce quantifiable sensorgrams, these binding events were measured to have weaker affinities despite possessing the potential to generate larger MFI values on Luminex (e.g. A*01:01-GV5D1; r=0.0714, K_D=1.6 μM, MFI = 21,559). Moving forward, several interactions representative of the varying outputs of Luminex and/or BLI screening methods for each individual antibody were selected for further, more in-depth analysis (Table 3.1, grey shading). Further optimisation of the BLI method also needs to be carried out to enable reliable quantification of interaction affinity as well as to be able to obtain quantifiable kinetic analysis of those interactions in which lower responses were observed.

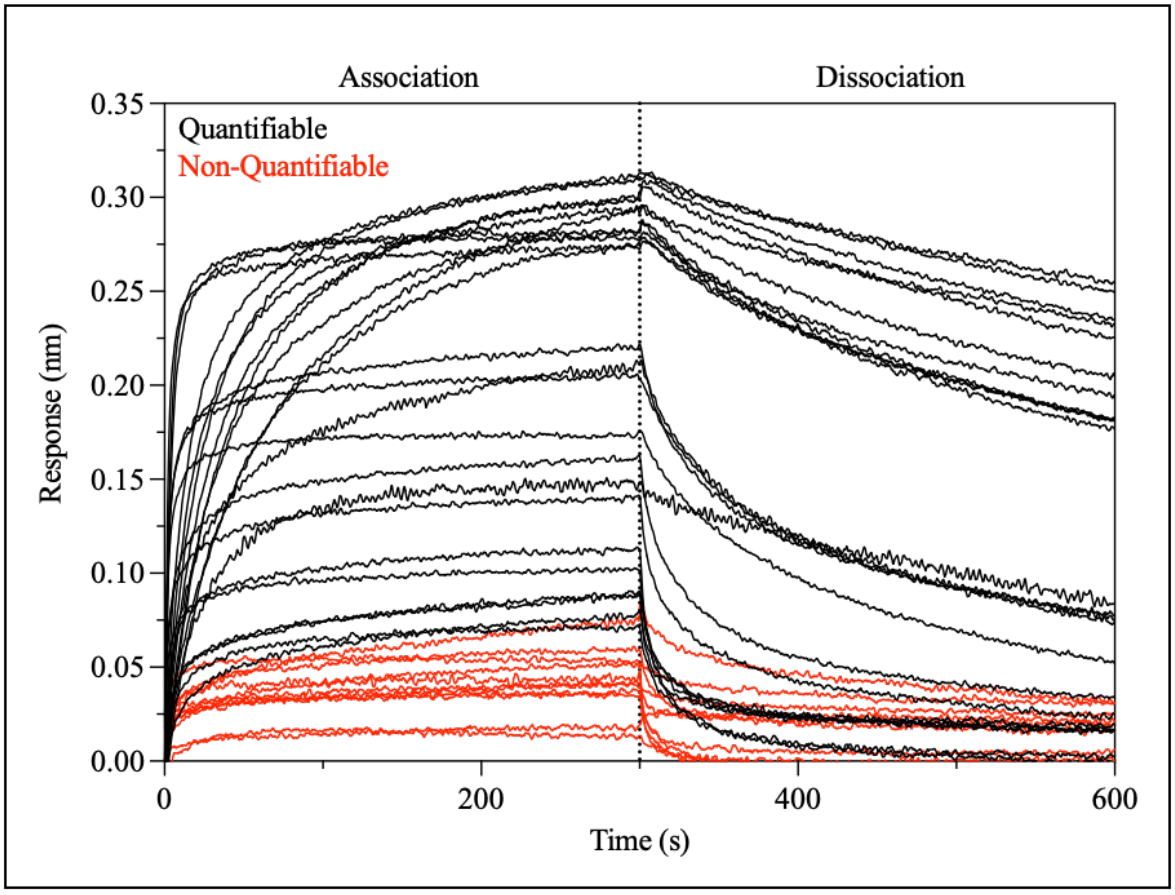

Figure 3.7. Screened binding kinetics of alloantibody-HLA interactions via biolayer interferometry. 38 Luminex-positive interactions selected for further kinetic assessment were screened via BLI using a standardised concentration of HLA to gain estimations of the interaction affinity. Briefly, AHC sensors loaded with mAb up to 0.6 nm were incubated with 50 µg/ml HLA (concentrations used for OUW4F11 interactions may vary, see Table 3.1) for 300 seconds, before being left to dissociate in standard BLI buffer for 300 seconds to yield the presented sensorgrams. Sensorgram data was fitted via partial analysis using the first 100 seconds of association and first 100 seconds of dissociation steps to gain the interaction affinity constant, K_D (see Figure 3.8 for values). Note interactions that showed positive, quantifiable binding were deemed trustworthy if they exceeded a 0.06nm response in the first 100 seconds of association (Quantifiable, black sensorgrams). Interactions that yielded a response less than 0.06nm in the first 100 seconds of association and/or produced heterogenous curves in the association phase that could not be reliably fit were deemed untrustworthy and were excluded from analysis (Non-quantifiable, red sensorgrams).

Table 3.1. Screening of individual alloantibody-HLA interactions. A list of the numerical values output from both screening methods as documented in Figures 3.2-3.7. Briefly, human mAbs were screened via Luminex class I single antigen beads at a concentration of 1 µg/ml to determine their reactivity, measured as MFI output. Where HLA was available in recombinant form, interactions were further screened via BLI using 50 µg/ml HLA to gain an estimation of the interaction affinity (K_D). Grey filling represents the interactions selected for further, in-depth assessment via BLI and clinical immunoassays. Red colouring represents the known immunising antigen. ▲ and ■ represent interactions which were screened via BLI using antigen concentrations of 41 µg/ml and 61.5 µg/ml, respectively. INDET = indeterminable due to untrustworthy sensorgrams (see Figure 3.7).

mAb	HLA Identity	Screened Luminex MFI	Screened K_D by BLI (M)
WIM8E5	A*11:02	24550	7.3×10^{-8}
	A*11:01	22900	9.8×10^{-8}
	A*25:01	24318	1.9×10^{-7}
	A*31:01	17126	5.2×10^{-7}
	A*01:01	22700	5.6×10^{-7}
	A*68:01	20594	9.5×10^{-7}
	A*66:02	13115	INDET
	A*02:01	12609	INDET
	A*23:01	11753	INDET
	A*69:01	11372	INDET
	A*24:02	9233	INDET
	A*80:01	4617	INDET
WK1D12	B*27:05	18282	7.2×10^{-8}
	B*40:01	21488	1.3×10^{-7}
	B*40:02	20389	1.4×10^{-7}
	B*07:02	20666	3.5×10^{-7}
	B*13:02	18517	6.4×10^{-7}
	B*48:01	17867	8.3×10^{-7}
	A*66:02	2170	INDET
OUW4F11	B*08:01	24513	6.9×10^{-7}▲
	B*15:10	19595	1.6×10^{-6}▲
	B*15:01	14901	1.8×10^{-6}■
	B*40:02	11542	4.7×10^{-6}■
	B*40:01	13923	5.9×10^{-6}■
	B*48:01	9775	INDET■
SN230G6	B*58:01	24550	3.4×10^{-8}
	B*57:01	24048	4.4×10^{-8}
	A*02:01	25718	5.5×10^{-8}
SN607D8	A*02:01	25433	1.3×10^{-7}
	A*69:01	24864	3.0×10^{-7}
	A*68:01	25194	3.5×10^{-7}
	B*57:01	2816	INDET
	B*58:01	2658	INDET
GV5D1	A*01:01	21559	1.6×10^{-6}
	A*24:02	16728	INDET
	A*23:01	16016	INDET
	A*80:01	4776	INDET
BVK1F9	B*08:01	24653	INDET

3.2.2. Development of an Optimised Method for the Assessment of Alloantibody-HLA Binding Kinetics using Biolayer Interferometry

To efficiently measure individual AlloAb-HLA interaction kinetics using BLI technology, an optimised assay needed to be established. It should be noted that the kinetic values obtained during optimisation experiments are not comparable to subsequent kinetic analysis experiments involving the same interactions. This is due to minimal controls being used in optimisation assays to maximise cost-efficiency.

3.2.2.1. Optimisation of BLI Sensor Loading Density

For an interaction to be measured, one of the interacting proteins needs to be immobilised to the sensor's surface so that the occurrence of an interaction can be clearly detected upon exposure to its interacting partner free in solution. Too much immobilised protein can lead to crowding, steric hindrance, aggregation, mass transport issues, and/or increased non-specific binding due to the need for a higher analyte concentration, whereas too little immobilised ligand may result in an undetectably low signal. To establish a threshold at which the amount of ligand immobilised to each sensor would give reliable, high quality, analysable data, the affinity of HLA-A11 to anti-human IgG Fc (AHC) sensors loaded with varying amounts of WIM8E5 was measured. Here, sensors were either incubated with BLI buffer containing 1 μg/ml, 0.75 μg/ml, 0.5 μg/ml, 0.375 μg/ml, 0.25 μg/ml, or 0.125 μg/ml antibody for a time of 500 seconds, or a fixed concentration of 1.5 μg/ml WIM8E5 was used to differentially load the sensors by incorporating thresholds of 1.0 nm, 0.8 nm, 0.6 nm, 0.4 nm, and 0.2 nm (Figure 3.8.A-B). Decreasing the amount of loaded ligand in both experiments caused a reduction in the signal response and a lower K_D output to be determined (Figure 3.8.C-D). Analysis of the sensorgrams for visual cleanliness and optimal curve fitting resulted in the decision for all future kinetic characterisation experiments to be run at a loading density of 0.6nm, where a loading threshold would be used to enable better control of sensor loading.

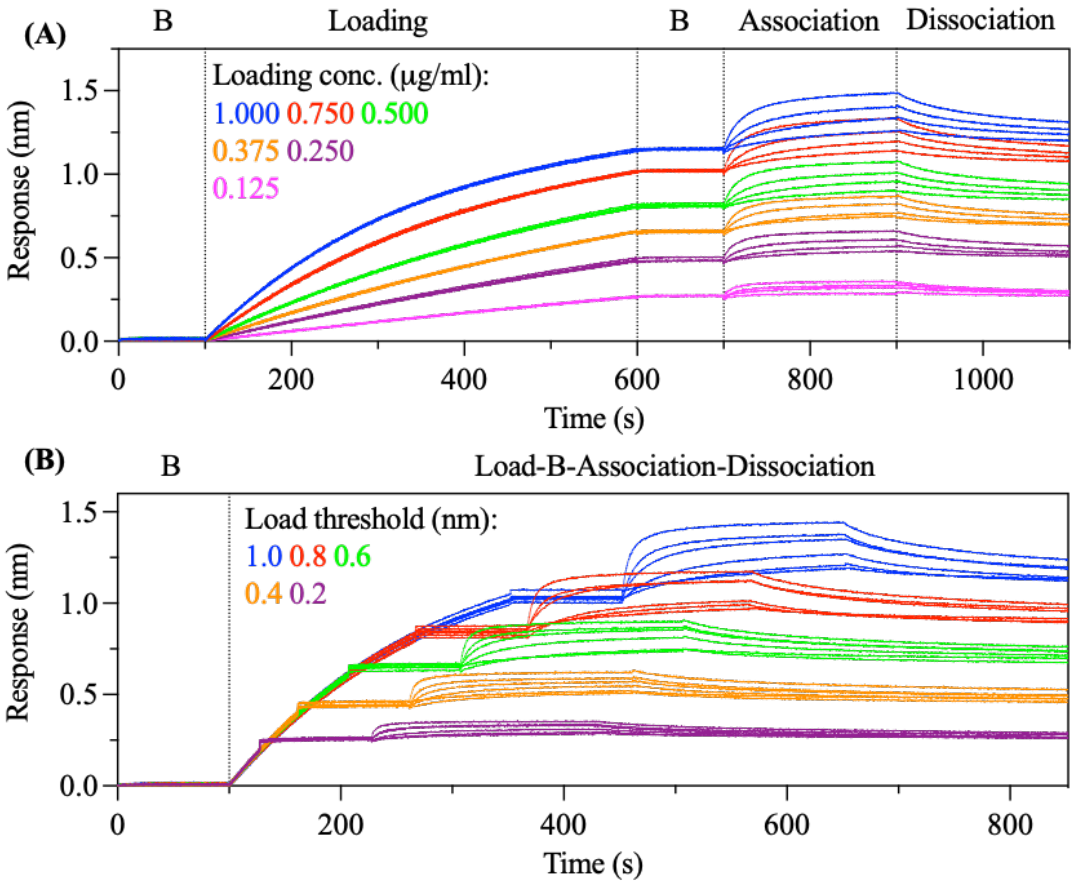

(C)

Interaction	Load Conc. (µg/ml)	K_D (nM)
WIM8E5 vs HLA-A*11:02	1.000	50
	0.750	48
	0.500	41
	0.375	39
	0.250	36
	0.125	38

(D)

Interaction	Load Threshold (nm)	K_D (nM)
WIM8E5 vs HLA-A*11:01	1.0	31
	0.8	30
	0.6	28
	0.4	27
	0.2	24

Figure 3.8. Determining the optimal BLI sensor loading density. The binding kinetics of the A11-WIM8E5 interaction was assessed using varied ligand loading densities to see how this would affect the resultant data. Briefly, sensorgrams were produced by A) setting a constant loading time of 500 seconds and loading WIM8E5 into parallel sensors using 1.0 µg/ml (blue), 0.75 µg/ml (red), 0.5 µg/ml (green), 0.375 µg/ml (orange), 0.25 µg/ml (purple) or 0.125 µg/ml (pink) antibody concentrations, or B) incubating parallel AHC biosensors with 1.0 µg/ml WIM8E5 and using thresholds of 1.0 nm (blue), 0.8 nm (red), 0.6 nm (green), 0.4 nm (orange) or 0.2nm (purple). Loaded sensors were exposed to 2-fold dilutions of HLA-A11 to yield the presented sensorgrams. Interaction affinities (C = variable ligand loading concentration, D = variable loading threshold) were calculated using steady state analysis from data fitted using a 1:1 stoichiometry model. The effect of variable loading on output data was assessed by visual sensorgram quality and optimal curve fitting, where using a loading threshold of 0.6nm was chosen as optimal. B = Baseline.

3.2.2.2. Optimisation of Ligand Loading Concentration

To control the amount of ligand that is loaded onto the sensor surface, an optimal concentration of protein needed during the loading step needed to be determined. To do this, parallel sensors were dipped into their corresponding wells containing a 2-fold dilution series of ligand, from 3.00 µg/ml to 0.19 µg/ml, for 500 seconds. The highest protein concentration that gave a steady, proportional rate of loading was selected as optimal for each individual loaded protein (Figure 3.9). The optimal concentrations of IgG and biotinylated-HLA selected to load AHC and SA sensors, respectively, was 0.375 µg/ml (darker sensorgrams).

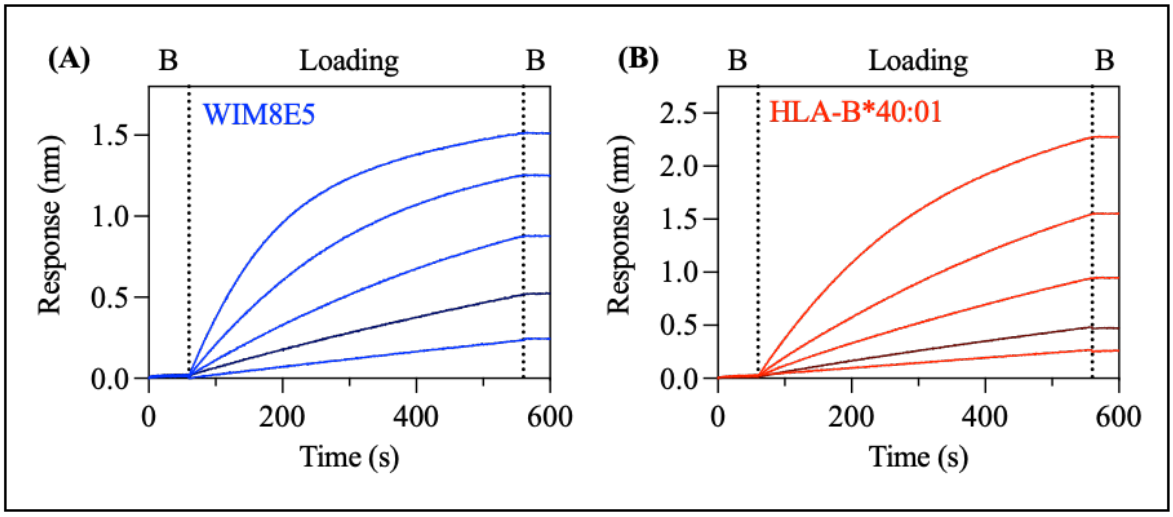

Figure 3.9. Optimisation of ligand concentration for BLI sensor loading. Sensorgrams showing the variable rates of protein immobilisation over a 500 second period upon exposure of parallel biosensors to one concentration of a 2-fold dilution of ligand. The loading of human IgG onto AHC sensors was optimised by observing the variable loading rates of WIM8E5 (A). The loading of HLA onto SA sensors was optimised using biotinylated B*40:01 as the ligand (B). In both scenarios, the optimal ligand loading concentrations that yielded steady rates of loading was 0.375 µg/ml (darker coloured sensorgrams). B = Baseline.

3.2.2.3. Affinity vs Avidity – Selecting the Interaction Orientation on the Sensor

Using the A*02:01-SN230G6 interaction as a model, two potential methods to analyse alloantibody-HLA interactions were proposed: immobilisation of HLA to the sensor and using mAb as the analyte, or immobilising mAb to the sensor surface and using HLA as the analyte (Figure 3.11). In the first instance, biotinylated HLA-A*02:01 was immobilised to streptavidin (SA)-coated sensors and SN230G6 was used as the free analyte. Although the A*02:01-SN230G6 complex was able to rapidly form in the association phase, only minimal detachment of the mAb from the sensor was seen during dissociation, thought to be due to the avidity effects of the bivalent analyte. This prevented a value of k_{off} from being measured, which is required for subsequent K_D determination (Figure 3.11, blue). Despite attempts to assist dissociation of antibody from the sensor by the addition of non-biotinylated HLA-A*02:01 into wells in the dissociation step (Figure 3.10), the alloantibody persisted to remain in complex with the immobilised HLA at the sensor surface, preventing the significant dissociation that is required for complete quantification of interaction kinetics. By reversing the orientation of this interaction, immobilising SN230G6 to AHC sensors and using non-biotinylated HLA-A*02:01 as the analyte, both association and dissociation of the mAb-HLA complex could be observed at the sensor surface which enabled the determination of the interaction kinetics (Figure 3.11, red). Moving forward, the orientation used to assess the affinity of alloantibody-HLA interactions was to immobilise mAb to AHC sensor surface and use HLA as the free analyte.

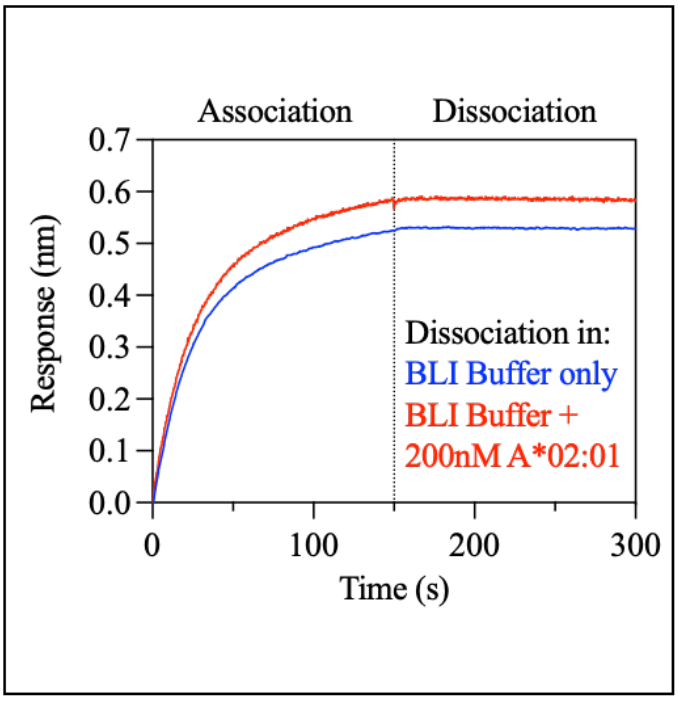

Figure 3.10. Addition of HLA does not improve antibody dissociation in BLI. Immobilisation of HLA in BLI experiments prevented determination of K_D due to the inability to measure complex dissociation (blue). Addition of HLA to dissociation wells to prevent analyte re-binding does not improve the dissociation (red). Briefly, HLA-A*02:01-loaded SA sensors were incubated with 200 nM W6/32 for 150 seconds prior to dissociation for a further 150 seconds. Dissociation wells contained BLI buffer alone or BLI buffer with 200nM unbiotinylated A*02:01 added. Neither condition resulted in measurable dissociation of antibody from the sensor surface.

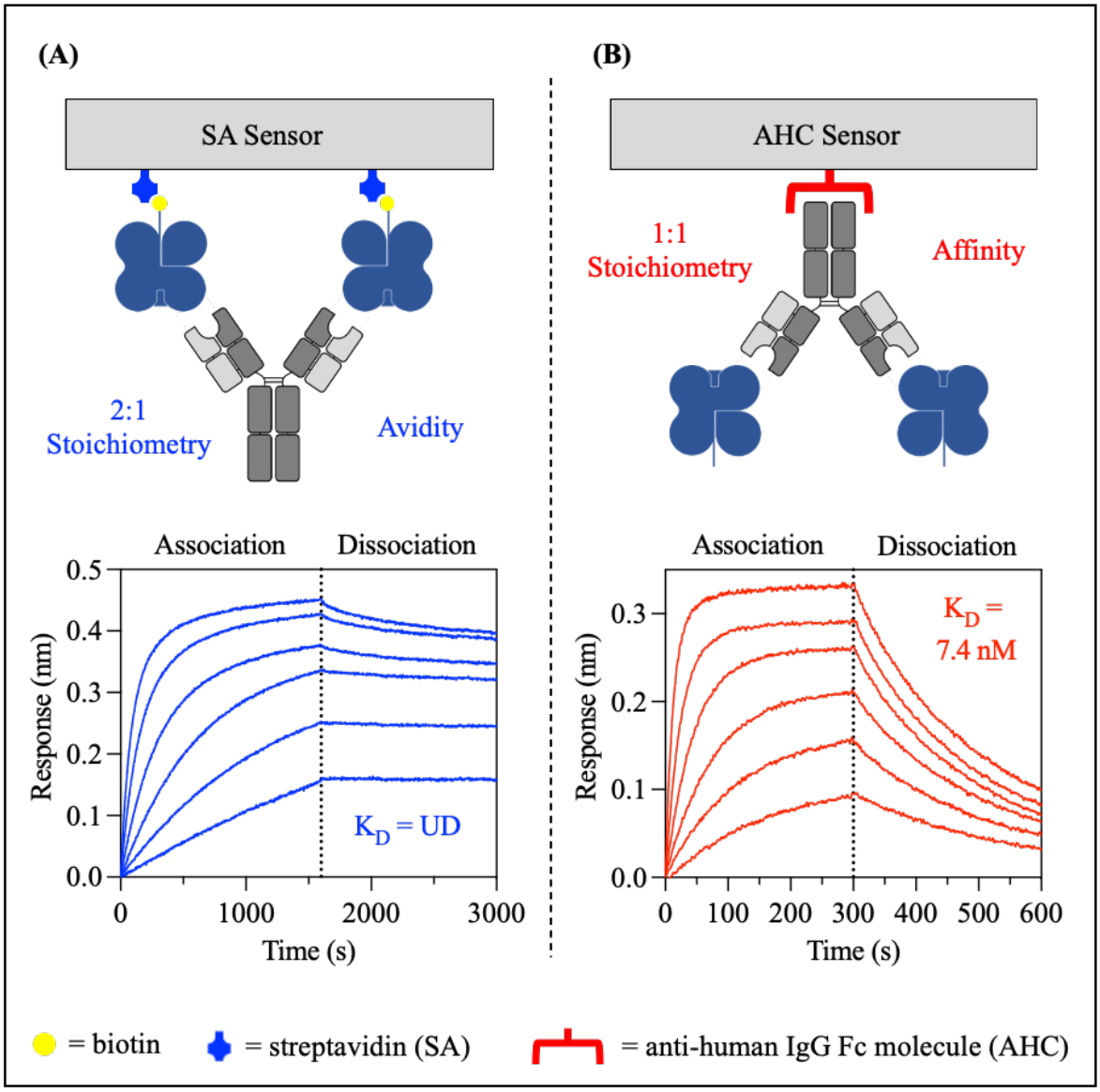

Figure 3.11. Affinity vs avidity – reversing the interaction orientation with biolayer interferometry. Diagrammatical representations of the two possible interaction orientations that can be achieved by assessing the A*02:01-SN230G6 interaction via BLI, and their resultant binding kinetics. (A) Immobilisation of biotinylated HLA-A*02:01 using streptavidin (SA) sensors results in the lack of SN230G6 dissociation from the sensor surface preventing K_D determination. (B) Immobilisation of antibody using anti-human IgG Fc (AHC) sensors allowed dissociation non-biotinylated HLA-A*02:01 from the protein complex which enabled the interaction affinity to be determined. K_D values were calculated as a function of k_{off}/k_{on} from data fitted using global fitting and a 1:1 stoichiometry model. UD = Undeterminable.

3.2.2.4. Effect of Temperature of Interaction Measurements

To further optimise the BLI assay set-up and assess how the temperature at which kinetic measurements are taken may influence the quality of the data yielded, the A*11:01-WIM8E5 interaction was selected as a model and the kinetics of this interaction were measured at temperatures between 25-40 °C (Figure 3.12). When measured at lower temperatures, the interaction was found to have a lower measured K_D values, suggesting the nature of this interaction is an exothermic process. Negative drift was also observed in sensorgrams produced at higher temperatures, suggesting a greater instability of the AHC sensors and/or protein immobilised to it. Moreover, greater evaporation within the wells was also observed at higher temperatures, meaning the true concentration of protein within the wells may change during experiments that take longer to complete. Due to the evidence suggesting lower quality data was yielded at higher temperatures, along with the natural fluctuation of ambient air temperature within the laboratory between 20-26°C, a consistent temperature of 30 °C was selected to carry out all further experiments.

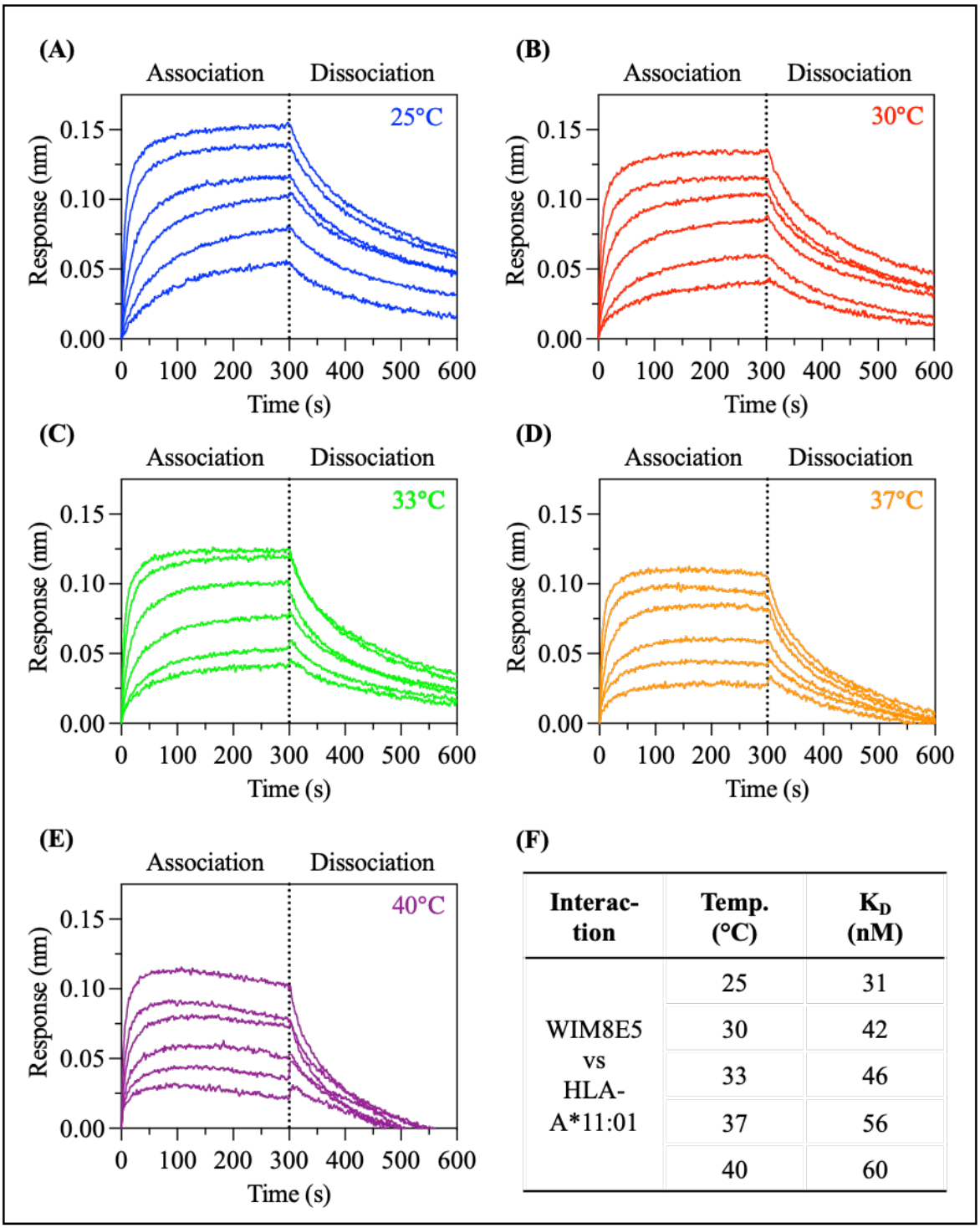

(F)

Interac-tion	Temp. (°C)	K_D (nM)
WIM8E5 vs HLA-A*11:01	25	31
	30	42
	33	46
	37	56
	40	60

Figure 3.12. BLI data quality is decreased at higher temperatures. Sensorgrams produced from assessment of the WIM8E5-A*11:01 interaction at temperatures of 25°C (A, blue), 30°C (B, red), 33 °C (C, green), 37°C (D, orange), and 40°C (E, purple), and the corresponding measured affinities (F). AHC sensors loaded with WIM8E5 were incubated with with two-fold dilutions of HLA-A*11:01 (starting from 500 nM). K_D values were calculated using steady state analysis from data fitted using a 1:1 stoichiometry model. The effect of temperature on output data was assessed by visual sensorgram quality and optimal curve fitting, where an optimal concentration of 30°C was selected.

3.2.2.5. Investigating the Effect of Sensor Blocking

Blocking steps aim to limit the amount of non-specific binding that can occur, preventing the formation of any unwanted complexes which may contribute to the measured binding response. To assess whether the addition of blocking steps was necessary for alloantibody-HLA interaction quantification, an experiment was carried out to test the ability of several blocking agents to improve the quality of the data acquired (Figure 3.14). Blocking AMC/AHC sensors with isotype control IgG molecules prior to ligand association prevented the establishment of a second baseline, causing interference with the sensorgram that contributed to the measured interaction kinetics (Figure 3.14.A). This was also observed when blocking AHC sensors with biocytin, casein, or a combination of both, albeit to a lesser extent (Figure 3.14.B-E). Despite being able normalise this baseline step this with the addition of a reference sensor, the incorporation of blocking steps to the assay did not yield any significant improvement in the quality of the data gathered (not shown). During these experiments, it was also ascertained that when incubated with biotinylated-HLA, these molecules were able to out-compete biocytin on at the sensor surface even after the presumed complete blockade of all SA binding sites (Figure 3.14.F). In addition, biotinylated HLA was also found to bind AHC and AMC sensors in the absence of HLA-specific antibody (Figure 3.13), suggesting that these sensors may be modified from streptavidin sensors. This finding was not something that is disclosed in the manufacturer's product description and so biotinylated proteins should be strictly avoided when using AMC/AHC sensors. The results of these experiments showed that there were no improvements in alloantibody-HLA interaction data quality when blocking steps were incorporated into the method, therefore no blocking steps were used in further experiments.

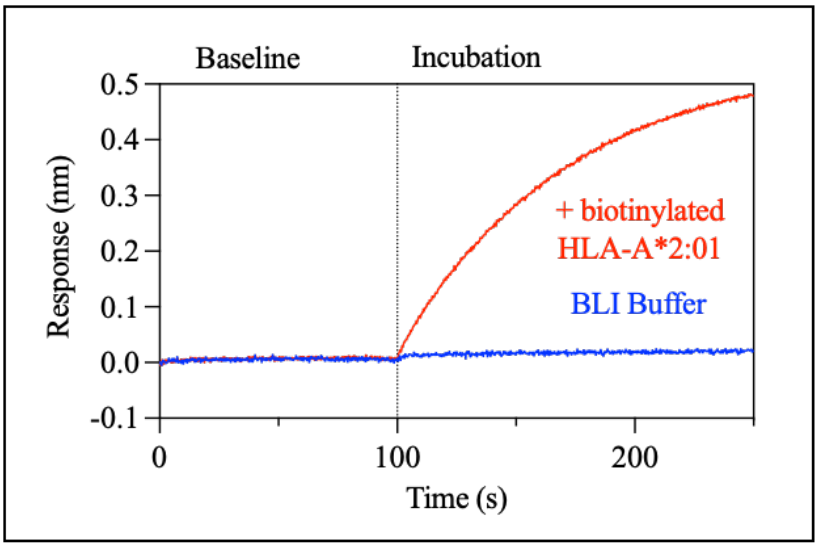

Figure 3.13. Anti-IgG capture sensors bind biotinylated A*02:01. Exposing calibrated AMC sensors to 200nM biotinylated HLA-A*02:01 resulted in antigen immobilisation to the sensor surface. This suggests that AMC/AHC sensors have an affinity for biotin and therefore using biotinylated HLA as a ligand should be avoided when using these sensors.

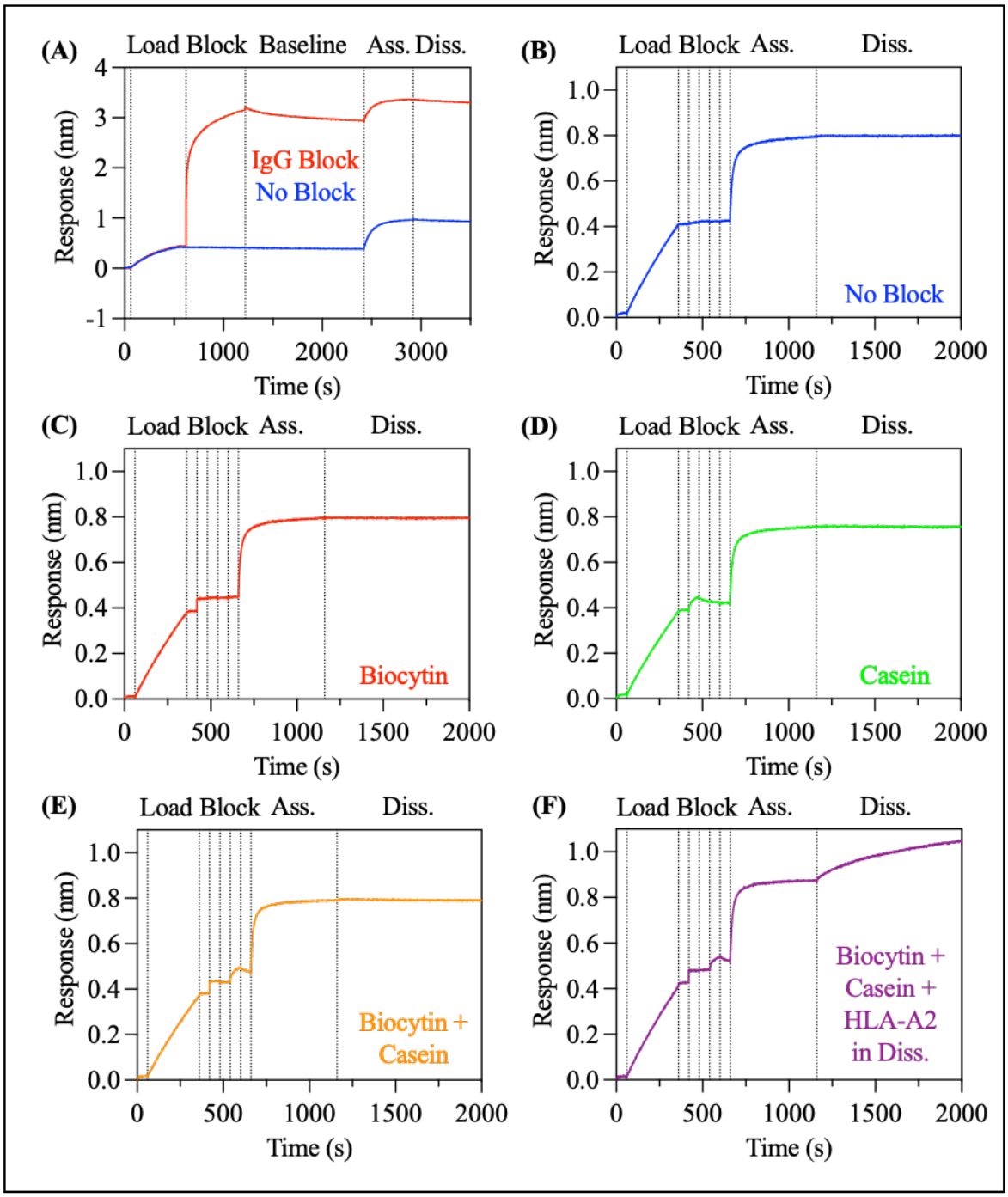

Figure 3.14. BLI sensor blocking does not improve BLI data quality. Sensorgrams yielded from the incubation of BLI sensors with various blocking agents post-ligand immobilisation. (A) The effect of blocking antibody capture sensors was assessed by incubating W6/32-loaded AMC sensors with either BLI buffer alone (blue), or by blocking with IgG isotype control (red) prior to assessment of the W6/32-A*02:01 interaction. Blocking of SA sensors was assessed by incubating HLA-loaded SA sensors with either PBS (B), 10 µg/ml biocytin (C), 10 µg/ml casein (D), or both 10 µg/ml biocytin and 10 µg/ml casein, prior to W6/32-A*02:01 interaction analysis. In all cases, blocking steps did not show any improvement to sensorgram quality nor the subsequent data analysis (not shown). Adding biotinylated A*02:01 to AMC sensors after W6/32-A*02:01 complex formation to aid in antibody dissociation resulted in further immobilisation of HLA-A*02:01 to the sensor. Ass. = Association, Diss. = dissociation.

3.2.3. Quantifying the Kinetics of Alloantibody-HLA Interactions

Now an optimised method for quantification of HLA-alloantibody interaction kinetics had been established, the next step was to assess the interactions selected during the screening process for more accurate, in-depth kinetic analysis. Monoclonal antibodies immobilised onto parallel AHC sensors were exposed to their interacting HLA molecules in a 2-fold dilution series, where the rates of complex formation and ligand dissociation were measured to yield quantifiable sensorgrams. Sensorgram data was fitted using global fitting and a 1:1 stoichiometry model to reveal a wide range of measured interaction affinities, ranging from 3.0 nM with B*58:01-SN230G6 to 5.0 μM with A*02:01-WIM8E5 (Figure 3.15, Table. 3.2, Appendix 4). Whilst most interactions yielded significant responses in which kinetic analysis was reliable, weaker interactions consistently generated lower responses in which interaction kinetics were more difficult to ascertain and the calculated values should be examined with caution (e.g., A*24:02-WIM8E5, A*02:01-WIM8E5, A*01:01-GV5D1, A*23:01-GV5D1, A*24:02-GV5D1 and B*08:01-BVK1F9).

Each antibody demonstrated a varying ability to bind its reactive antigens, represented by differences in the measured K_D (Figure 3.15.A). In most cases, the priming antigen of each antibody could also be identified as the HLA that bound with the strongest affinity (Table 3.2, grey shading). WIM8E5 was observed to have the largest range of affinities against its reactive antigens, each with significantly distinct K_Ds spanning from 18 nM with its sensitising antigen HLA-A*11:01, to over a 250-fold weaker value of 5 μM against HLA-A*02:01. WK1D12 and OUW4F11 interactions were noticeably less variable than WIM8E5, with measured K_D values covering approximately 4- and 10-fold ranges respectively. Whilst WK1D12 was measured to form relatively strong interactions with its reactive antigens in the 10^{-8} M range (17-61 nM), OUW4F11 formed significantly weaker interactions ranging from 410 nM to 4.5 μM. GV5D1 and BVK1F9 antibodies also measured to have relatively weaker affinities against their reactive antigens, with K_Ds consistently measuring within the hundreds of nanomolar to micromolar range.

Whilst comparing the measured affinities between interactions involving the same antibody enabled HLAs to be ranked based on binding strength, similar observations could also be made when comparing interactions involving multiple antibodies that react with the same antigen (Figure 3.15.B). Antibodies SN230G6 and SN607D8 were measured to bind HLA-A*02:01 with comparable affinities of 7.4 nM and 1.2 nM, respectively, despite being observed to have

slightly different reactivity patterns. WIM8E5's >1000-fold weaker affinity interaction with A*02:01 suggests a considerably different binding event may be occurring than that with SN230G6 or SN607D8. Similar observations were also made when comparing antibodies against A*68:01 (SN607D8; 12 nM and WIM8E5; 890 nM), B*40:01 (WK1D12; 26 nM and OUW4F11; 3.2 μM) and B*40:02 (WK1D12; 29 nM and OUW4F11; 4.4 μM), where the two antibodies found to interact with the antigen in question bind with largely disparate affinities, differing by greater than one order of magnitude. In contrast, the sets of antibodies which interacted with A*01:01 (WIM8E5; 200 nM and GV5D1; 710 nM), A*24:02 (WIM8E5; 2.7 μM and GV5D1; 4.0 μM) or B*08:01 (OUW4F11; 410 nM and BVK1F9; 820 nM), were observed to have much more comparable affinities that underpin their interactions, measuring within the same order of magnitude.

In summary, optimisation of the BLI method has enabled reliable and accurate quantification of the kinetics underpinning HLA-Alloantibody interactions. Whilst comparison of the K_D values enables interactions to be ranked by strength, the highest affinity interactions can be found to occur with the antigen that the antibody is primed against. Despite these observations, the role that interaction strength has on defining its immunological significance still needs to be explored.

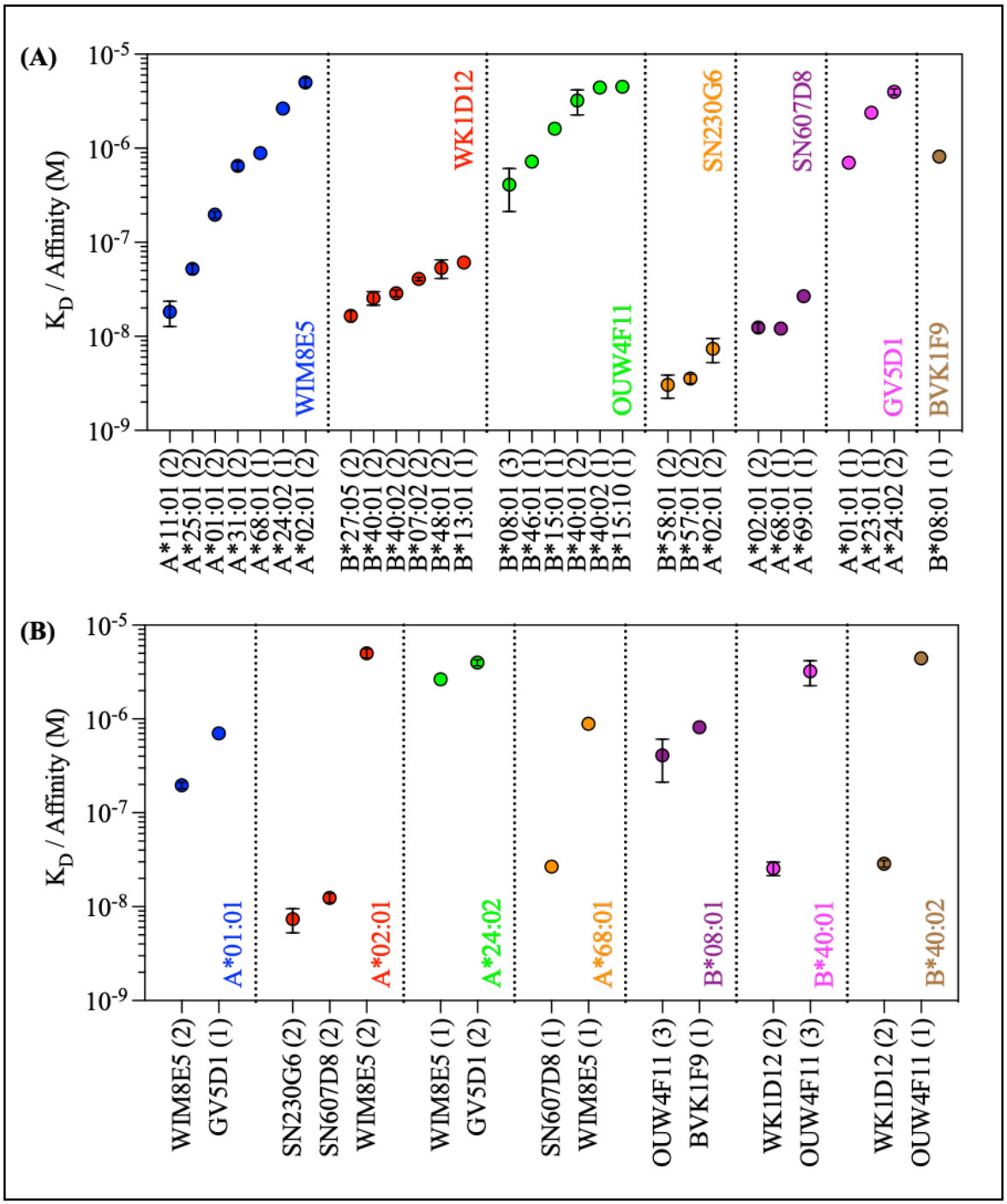

Figure 3.15. Alloantibody-HLA interaction affinity measurements. The mean measured affinities (K_D) calculated for each alloantibody-HLA interaction assessed using biolayer interferometry. K_D values were calculated as a function of k_{off}/k_{on} from sensorgram data fitted using global fitting and a 1:1 stoichiometry model. Interactions grouped by a common interacting mAb are represented in (A). Interactions grouped by a common interacting HLA are shown in (B). Where HLA reagents were available in sufficient quantities, interactions were repeated, where the values in brackets represent the number of replicates for each interaction. Symbols represent the mean affinity values for each interaction and error bars represent the mean ±SD of the measurements.

Table 3.2. Alloantibody-HLA interaction affinity measurements. The mean affinity values (K_D) of all the interactions assessed against each mAb using BLI. ±SD represents the standard deviation for the mean values. n represents the number of replicates for that interaction. K_D values were calculated as a function of k_{off}/k_{on} from sensorgram data fitted using global fitting and a 1:1 stoichiometry model. Grey filling represents the sesnitising HLAs for that mAb. * represents interactions which showed a low response using high ligand concentrations and so calculated affinities may be less reliable. See Appendix 4 for individual replicate values.

mAb	HLA	Mean K_D (M)	±SD (n)
WIM8E5	A*11:01	1.8×10^{-8}	5.4×10^{-9} (2)
	A*25:01	5.2×10^{-8}	6.5×10^{-9} (2)
	A*01:01	2.0×10^{-7}	1.5×10^{-8} (2)
	A*31:01	6.5×10^{-7}	7.4×10^{-8} (2)
	A*68:01	8.9×10^{-7}	N/A (1)
	A*24:02*	2.7×10^{-6}	N/A (1)
	A*02:01*	5.0×10^{-6}	5.8×10^{-7} (2)
WK1D12	B*27:05	1.7×10^{-8}	2.2×10^{-9} (2)
	B*40:01	2.6×10^{-8}	4.2×10^{-9} (2)
	B*40:02	2.9×10^{-8}	2.3×10^{-9} (2)
	B*07:02	4.1×10^{-8}	1.8×10^{-9} (2)
	B*48:01	5.3×10^{-8}	1.2×10^{-8} (2)
	B*13:01	6.1×10^{-8}	N/A (1)
OUW4F11	B*08:01	4.1×10^{-7}	2.0×10^{-7} (3)
	B*46:01	7.2×10^{-7}	N/A (1)
	B*15:01	1.6×10^{-6}	N/A (1)
	B*40:01	3.2×10^{-6}	9.5×10^{-7} (2)
	B*40:02	4.4×10^{-6}	N/A (1)
	B*15:10	4.5×10^{-6}	N/A (1)
SN230G6	B*58:01	3.0×10^{-9}	8.3×10^{-10} (2)
	B*57:01	3.9×10^{-9}	4.0×10^{-10} (2)
	A*02:01	7.4×10^{-9}	2.1×10^{-9} (2)
SN607D8	A*02:01	1.2×10^{-8}	1.4×10^{-9} (2)
	A*68:01	1.2×10^{-8}	N/A (1)
	A*69:01	2.7×10^{-8}	N/A (1)
GV5D1	A*01:01*	7.1×10^{-7}	N/A (1)
	A*23:01*	2.4×10^{-6}	N/A (1)
	A*24:02*	4.0×10^{-6}	2.9×10^{-7} (2)
BVK1F9	B*08:01*	8.2×10^{-7}	N/A (1)

3.2.4. Characterising Human Monoclonal Antibody Reactivity using Assays Employed in Clinic

The immunological risk associated with a particular alloantibody-HLA interaction is conventionally assessed in clinic based on the results of Luminex SAB, FC and CDC assays. Since the immunological relevance of the output from these immunoassays is often difficult to interpret, the notion that the affinity of antibody binding to an HLA target may provide a better understanding of the immunoassay output was hypothesised. To test this hypothesis, selected alloantibody-HLA interactions previously quantified using BLI were examined via Luminex SABs, Luminex C1qScreen, CDC and FC assays using mAb concentrations of 10 μg/ml, 3 μg/ml, 1 μg/ml, 0.1 μg/ml, and 0.3 μg/ml (64.5 nM, 19.4 nM, 6.45 nM, 1.94 nM, 0.65 nM) to evaluate the antibody's true immunological significance. Due to the broad specificity and varying affinity of interactions involving WIM8E5 against its HLA targets, this antibody was selected as a model to be examined in more detail to help understand the effects of varying affinity on immunoassay output.

3.2.4.1. Luminex Single Antigen Bead Assays

One of the principal objectives of this study was to provide a functional assessment of the Luminex single antigen bead (SAB) assay output. To do this, Luminex class I SAB binding profiles needed to be obtained for the mAbs of interest to observe how Luminex output differed upon antibody titration (Figure 3.16, Appendix 5). SAB MFI was observed to decrease upon antibody titration, highlighting the concentration dependence of this assay. Whilst many of the interactions characterised via BLI were found to have affinities in the nM range, incubation of beads with antibody concentrations below the measured affinity concentration still yielded positive signals, thought to be due to the avidity-dependent effects of solid-phase assays.

Luminex SAB analysis of WIM8E5 against its reactive antigens (Figure 3.16.A) showed that the three strongest affinity targets (HLA-A*11:01; 18.0 nM, -A*25:01; 52.0 nM, and -A*01:01; 200 nM) all gave very comparable MFI patterns upon antibody titration. These interactions maintained saturating MFI levels down to 0.3 μg/ml mAb and could not be distinguished from one another based on Luminex output alone despite the interactions differing in affinity by at least one order of magnitude. In contrast, WIM8E5's interactions with weaker affinity cross-reactive antigens (HLA-A*31:01; 650 nM, -A*24:02; 2.7 μM, and -A*02:01; 5.0 μM) were seen to output lower MFI signals when using the same antibody

concentrations. Here, the MFI outputs of these weaker interactions enabled them to be distinguished from one another due to the lesser ability of WIM8E5 to bind the HLA-bound SABs, which was concurrent with their lower affinities.

The observations made for WIM8E5 were also in agreement with the data obtained using other mAbs. Whilst WK1D12's interactions were measured to be of very similar, higher affinity (ranging from 17-61 nM), they also gave comparable SAB outputs which were observed to be at saturating MFIs down to 1.0 μg/ml (Figure 3.16.B). In contrast to WIM8E5 and WK1D12, OUW4F11's sensitising antigen (B*08:01) could be discerned from the weaker affinity, cross-reactive interactions as it was able to generate significantly larger MFIs across all assessed antibody concentrations (Figure 3.16.C). The high affinity interactions measured using antibodies SN230G6 and SN607D8 (all <30 nM) against their reactive antigens were further validated by producing saturating MFI values across all mAb concentrations using Luminex SABs (Figure 3.16.D-E, respectively). Conversely, GV5D1's weaker affinity interactions (all >700 nM) produced gradually declining MFI signals upon antibody dilution, concurrent with previous observations involving interactions that have higher K_Ds (Figure 3.16.F).

Comparing the outputs of interactions involving different antibodies that bind the same HLAs also substantiated the role of affinity in Luminex MFI output (Figure 3.17, Appendix 6). Whilst HLA-A*02:01 was observed to be recognised by WIM8E5, SN230G6 and SN607D8 (5.0 μM, 7.4 nM and 12.0 nM, respectively), it was only the latter two stronger affinities interactions that were able to generated elevated MFI signals across all used mAb concentrations (Figure 3.17.A). This same observation could also be made for interactions involving HLA-B*40:01-expressing SABs, where the differing affinities of WK1D12 (26.0 nM) and OUW4F11 (3.2 μM) may justify their varying MFI outputs (Figure 3.17.B); notably a very weak interaction such as B*40:01-OUW4F11 still resulted in relatively high MFI values on the SAB assay. Furthermore, HLA-A*24:02's relatively weak interactions against GV5D1 (4.0 μM) and WIM8E5 (2.7 μM) gave similar, decreasing MFI patterns upon antibody titration (Figure 3.17.C). Finally, by grouping interactions quantified using BLI to have similar affinities within a 10-fold range (10-100 nM and 500-5000 nM), it was possible to separate each of these groups based on their MFI patterns upon antibody dilution (Figure 3.17.D).

Taken together, these results suggest that both interaction affinity and antibody concentration are able to influence the MFI output of Luminex SAB assays, however the output/titre value alone is not sufficient to determine the interaction strength (affinity) with accuracy.

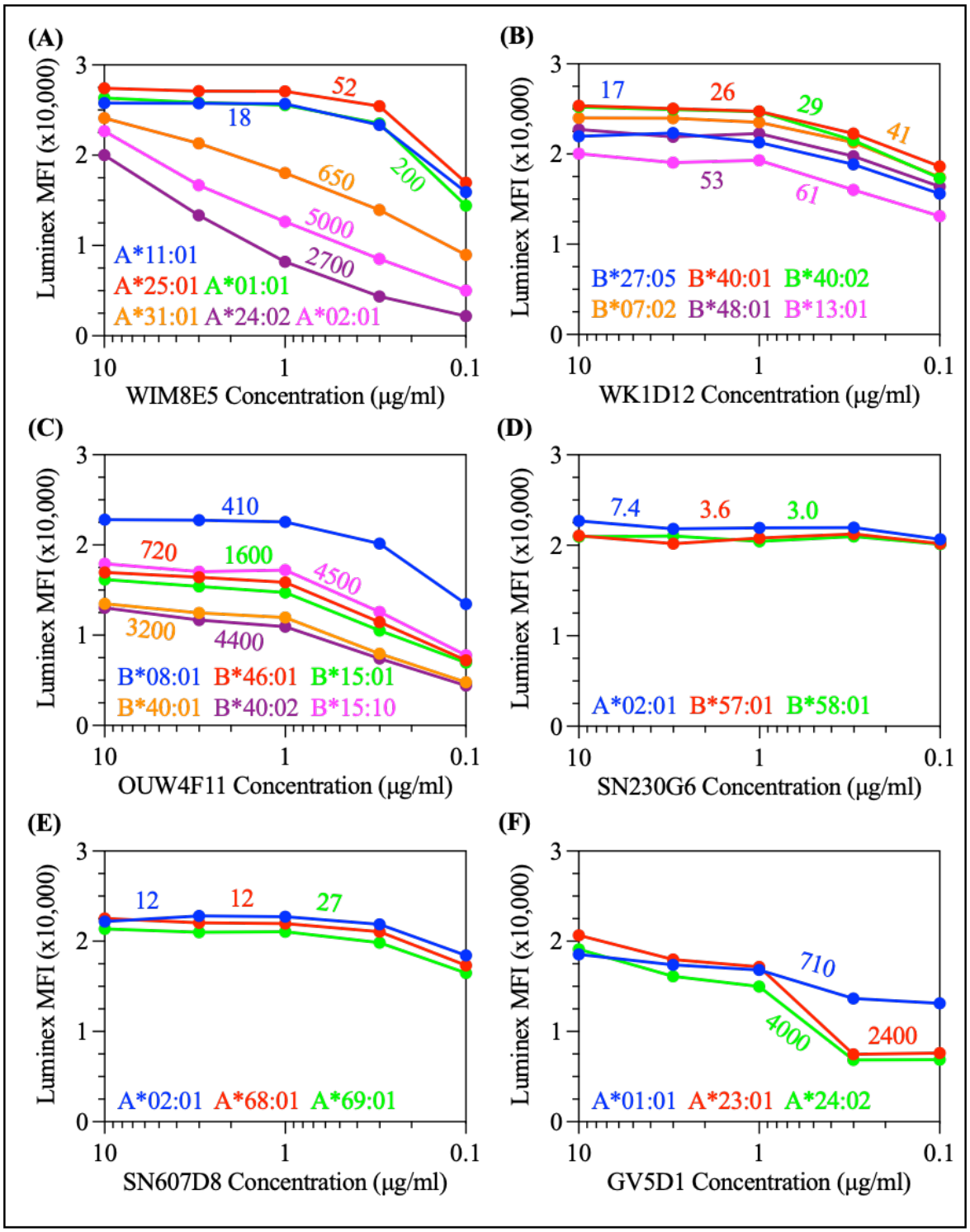

Figure 3.16. Luminex class I single antigen bead assessment of human monoclonal antibodies: comparing individual antibodies. Antibodies showed a varying ability to recognise their reactive antigens on SABs which was dependent on affinity of the interaction and antibody concentration. Luminex SABs were used to visualise a monoclonal antibody's pattern of reactivity against its reactive antigens upon antibody dilution. WIM8E5 (A), WK1D12 (B), OUW4F11 (C), SN230G6 (D), SN607D8 (E) and GV5D1 (F) were incubated with SABs at concentrations of 10 µg/ml (64.5 nM), 3 µg/ml (19.4 nM), 1 µg/ml (6.45 nM), 0.3 µg/ml (1.94 nM), and 0.1 µg/ml (0.65 nM) prior to secondary detection. Each point represents the mean fluorescence intensity taken from >100 beads in one experiment. Numerical values along each line represent the mean BLI-measured affinity (K_D, nM) for that specific interaction.

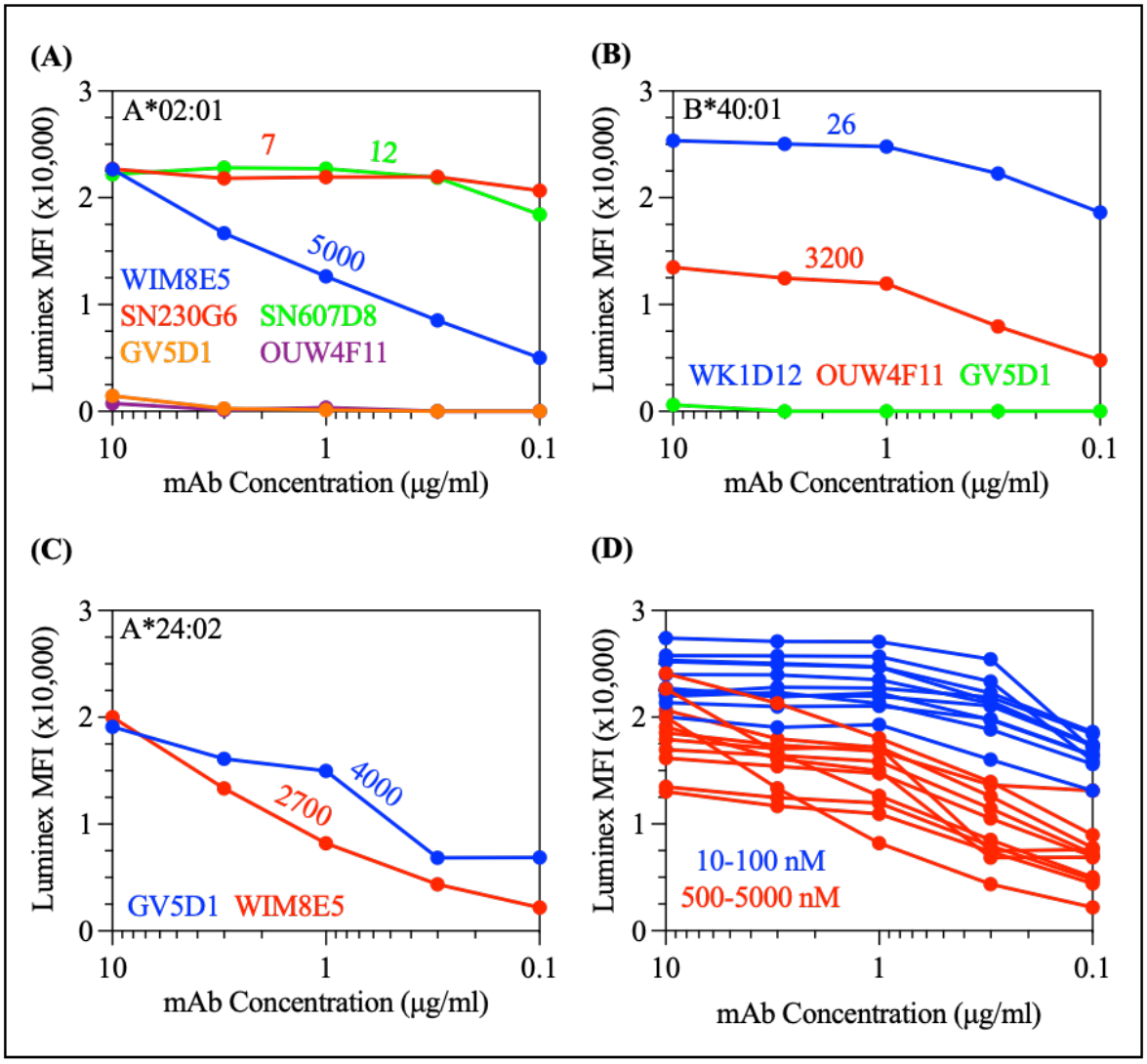

Figure 3.17. Luminex class I single antigen bead assessment of human monoclonal antibodies: comparing individual antigens. Different antibodies which recognise the same antigen expressed on SABs show an affinity-dependent ability to generate higher MFI signals. Luminex SABs were used to visualise the pattern of reactivity that different monoclonal antibodies have against the same bead-expressed antigen. HLA-A*02:01 (A), -B*40:01 (B) and -A*24:02 (C) were incubated with monoclonal antibodies at concentrations of 10 µg/ml (64.5 nM), 3 µg/ml (19.4 nM), 1 µg/ml (6.45 nM), 0.3 µg/ml (1.94 nM), and 0.1 µg/ml (0.65 nM) prior to secondary detection. Each point represents the mean fluorescence intensity taken from >100 beads in one experiment. Numerical values along each line represent the mean BLI-measured affinity (K_D, nM) for that specific interaction. (D) shows interactions can be grouped based on their affinities; between 10-100 nM (blue) and 0.5-5.0 µM (red), where interactions with affinities within one order of magnitude of each other show similar, decreasing MFI patterns upon antibody titration.

3.2.4.2. Luminex C1q-Binding Assays

It has previously been suggested that the capacity of antibodies to fix C1q on the Luminex SAB platform is a better indicator of the clinical significance of HLA-specific antibodies compared to the standard SAB assay [229-232]. To test this using the monoclonal antibodies in this setting, the ability of the antibodies to engage complement upon HLA binding, as determined by C1q detection on Luminex SAB using the C1qScreen assay, was examined (Figure 3.18, Appendix 7). The comparison of MFI patterns upon antibody titre showed that like the conventional SAB assay, outputs of the C1q SAB assay were antibody concentration dependent. Weak interactions (of micromolar affinity) were found to generate positive MFI values at high antibody concentrations, which went on to produce low MFI signals or became C1q negative at low antibody concentrations. Nevertheless, the C1q assay was observed to be less sensitive than the standard SAB assay, where loss of positive signal was more abrupt, reaching lower MFIs at higher antibody concentrations than in the standard SAB assay. Interestingly, C1q-positive interactions were associated with MFIs >10,000 on the respective conventional SAB assay as previously documented in the literature [217].

Consistent with alloantibody reactivity assessment using the standard SAB assay, analysis of C1q binding based on MFI values at specific antibody concentrations did not allow discrimination of cognate versus other higher-affinity cross-reactive HLA, however it could differentiate lower affinity interactions involving the same antibody (Figure 3.18.A-D). Furthermore, interactions involving different antibodies that recognise the same antigen with similar binding strengths, such as HLA-A*24:02 against GV5D1 or WIM8E5 (Figure 3.18.E), were found to generate comparable outputs as seen in the standard SAB assay. Conversely, those antibodies that recognise the same antigen with varying affinities, such as HLA-A*02:01 against WIM8E5 or SN230G6 (Figure 3.18.F), could be distinguished from one another based on MFI output, where higher affinity interactions generated consistently greater MFI signals.

Overall, this data demonstrates that the C1qScreen assay output is concentration and affinity dependent, where its reduced sensitivity may only provide a limited insight into the clinical significance of alloantibodies over that obtainable using the standard SAB assay in this setting.

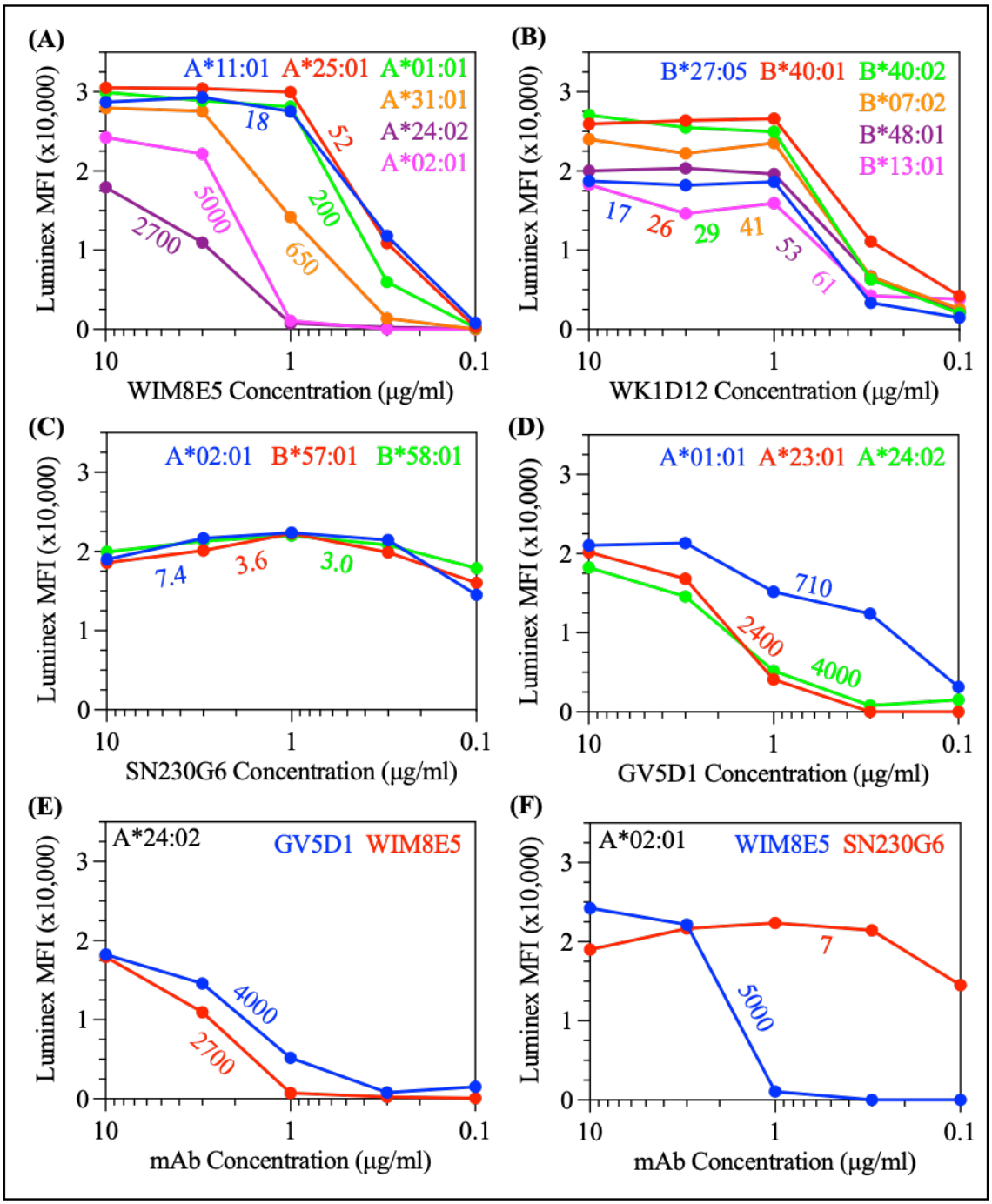

Figure 3.18. Luminex C1q-binding assessment of human monoclonal antibodies. The ability of an alloantibody-HLA interaction to bind C1q is dependent on interaction affinity and antibody concentration. The Luminex C1qScreen assay was used to observe the complement engaging abilities of interactions established with varying dilutions of monoclonal antibodies on Luminex SABs. WIM8E5 (A), WK1D12 (B), SN230G6 (C), and GV5D1 (D) were incubated with SABs at concentrations of 10 µg/ml (64.5 nM), 3 µg/ml (19.4 nM), 1 µg/ml (6.45 nM), 0.3 µg/ml (1.94 nM), and 0.1 µg/ml (0.65 nM). Antibody-bead mixtures were further incubated with C1q prior to secondary detection. (E) and (F) show the contrasting C1q-binding abilities of different antibodies that can recognise the same A*24:02 and A*02:01-expressing beads, respectively. Each point represents the mean fluorescence intensity taken from >100 beads in one experiment. Numerical values along each line represent the mean BLI-measured affinity (K_D, nM) for that specific interaction.

3.2.4.3. Flow Cytometry Assays

Next, the ability of mAbs to bind cellularly expressed HLA was assessed. Here, mAbs were incubated with molecularly typed, heterozygous donor T lymphocytes (Table 2.3, Appendix 8) prior to analysis by FC. To ensure the measured outputs were exclusively determined by the interaction of interest, cell samples were selected based on their ability to express only one antibody-specific target. The reactivities of each mAb as determined by the Luminex assays were confirmed using FC, where a decrease in signal was also observed upon antibody titration (Figure 3.19, Appendix 9). However, unlike Luminex assays in which low affinity interactions were able to produce high MFI values, these interactions could only generate weakly positive MFI fold changes at high antibody concentrations, if at all (e.g., A*02:01-WIM8E5 and A*24:02-WIM8E5).

Consistent with the SAB and BLI data for interactions involving the WIM8E5 antibody, stronger interactions with HLA-A*11:01, -A*25:01 and -A*01:01 were positive across all antibody titres, whilst the weaker-interacting HLA-A*31:01- and -A*02:01-expressing cells became negative upon antibody dilutions below 1 μg/ml and 3 μg/ml, respectively (Figure 3.19.A). FC data for WK1D12 also corroborated the Luminex and BLI experiments, where interactions were observed to output comparable MFI values across all antibody concentrations, all of which decreased analogously upon antibody titration (Figure 3.19.B). Comparing the effects of incubating the same HLA-A*02:01-expressing cell sample with either WIM8E5, SN230G6, or SN607D8 revealed that the higher affinity A*02:01-SN230G6/-SN607D8 interactions could generate greater MFI fold change values across all antibody concentrations when compared to the weaker A*02:01-WIM8E5 interaction (Figure 3.19.C).

Since each analysed antibody involved the use of a different heterozygous cell line to assess the ability to bind each of their cellularly-expressed targets, the effect of variable cellular HLA expression on the output of FC assays was evaluated. To do this, the A*01:01-WIM8E5 and B*07:02-WK1D12 interactions were assessed using three separate mono-reactive HLA-expressing cell samples each (Figure 3.19.D). Whilst WIM8E5 was able to bind T-cell samples 2 and 3 with similar effect, incubation with sample 1 yielded 30 % lower MFI levels across all antibody concentrations, suggesting this cell samples expresses surface HLA-A*01:01 to a lesser extent. Similarly, WK1D12's interaction with HLA-B*07:02 expressing-cells were found to yield variable MFI patterns across all cell samples, further corroborating the contribution of HLA expression to FC output.

Lastly, to understand the effect that a polyclonal serum sample will have on the output of FC assays, two interactions that had been measured to have a similar, intermediate affinity, A*01:01-WIM8E5 (200 nM) and B*08:01-OUW4F11 (410 nM), were analysed against cells that express both HLA targets on their surface (Sample 15). Here, these Abs were spiked, either separately or together, into blank serum before their subsequent incubation with the HLA-A*01:01 and -B*08:01-expressing cells (Figure 3.19.E). The selected cell sample (sample 15) also expresses HLA-C*07:01, an antigen belonging to the same allelic group of which OUW4F11 was shown to generate a low positive Luminex SAB MFI signal against (HLA-C*07:02; MFI=9,254, Appendix 1). To control for the expression of this HLA molecule, two HLA-C*07:01-expressing cell samples were added to the experiment to observe any potential C*07:01-OUW4F11 complex formation that would contribute to the MFI signal from incubating OUW4F11 with cell sample 15. In the control tests, OUW4F11 was unable to generate MFI-positive data against cellularly-expressed HLA-C*07:01, providing evidence to ensure the MFI outputs measured using sample 15 were exclusively determined by the desired interactions. Consistent with previous statements relating affinity to FC output, both A*01:01-WIM8E5 and B*08:01-OUW4F11 interactions were able to maintain FC-positivity across all assessed antibody concentrations when assessed individually. Despite the A*01:01-WIM8E5 interaction being of stronger affinity than B*08:01-OUW4F11, the raw MFI values generated by incubation with WIM8E5 were an average of over 2.7-times less in MFI fold change value than with the incubation of OUW4F11 across all used mAb concentrations, suggesting a greater expression of HLA-B*08:01 than HLA-A*01:01 at the cell surface. When assessing the outputs of incubating both antibodies in combination, the resultant FC MFI fold changes were found to reflect an additive effect of each individual antibody output. This provides evidence to demonstrate that each interaction occurs independently, where the contribution of one interaction to the overall MFI signal on one cell is irrespective of any other distinct antibody-HLA interaction occurring at the cell surface.

Overall, the FC experiments suggest that although cell-surface HLA expression may influence the MFI outputs of FC assays, antibodies that recognise the same cellularly-expressed targets with stronger affinity will produce higher MFI signals than those of weaker affinity, where this output will also be dependent on the concentration of antibody used. Furthermore, alloantibody-HLA interactions of weak affinity capable of producing high MFI signals using solid-phase assays such as Luminex SABs may result in negative or very low positive FC signal even at high antibody concentrations. This suggests that under more physiological conditions,

such as in cell-based assays compared to solid-phase assays, weaker interactions are less likely to be of significance in that they may not result in sustained binding and/or induction of down-stream events. Consequently, this data indicates that Luminex SAB output should be interpreted with caution.

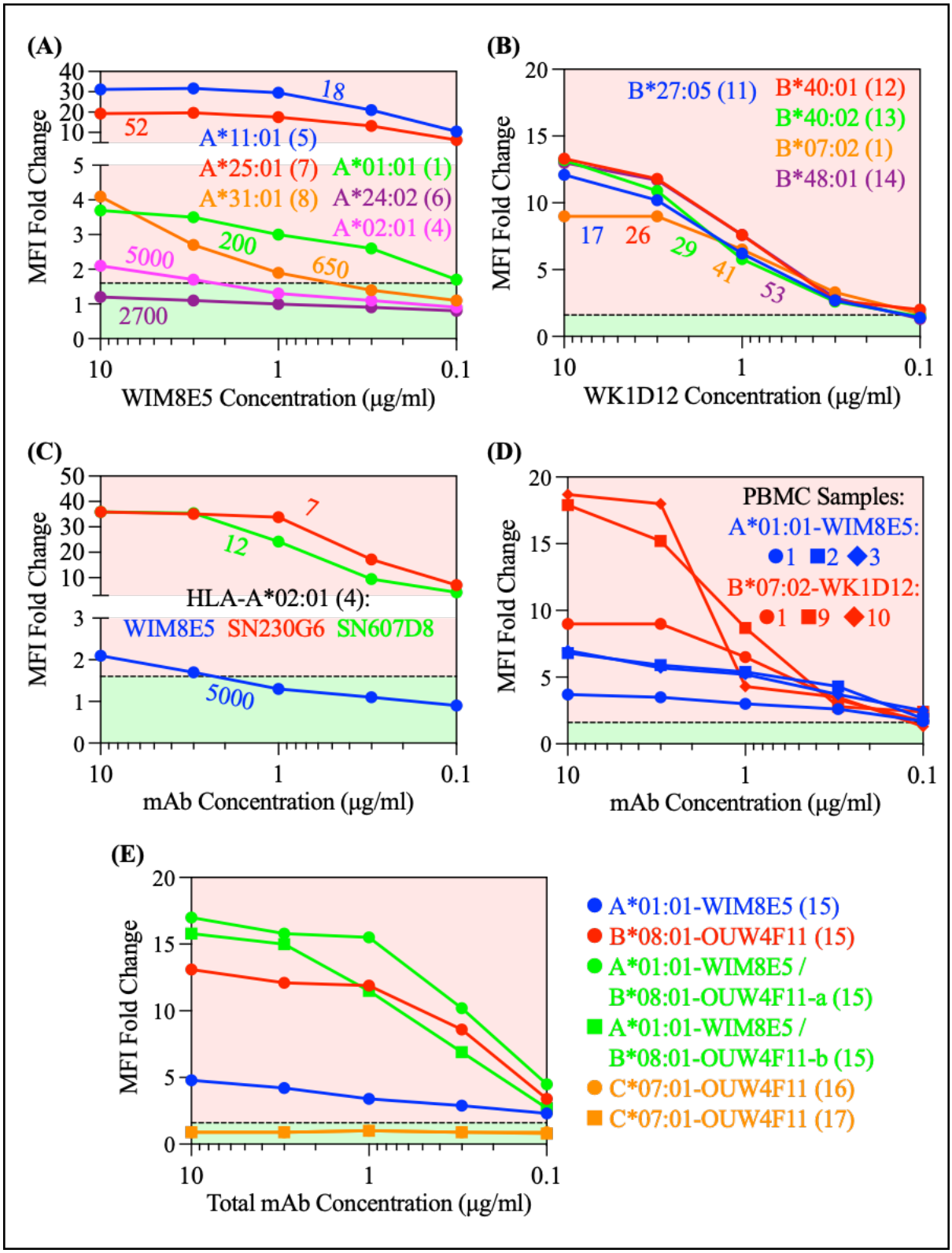

Figure 3.19. Human monoclonal antibodies show varying abilities to recognise HLA targets expressed on T-cells. Antibodies displayed varying ability to recognise T-cell expressed antigens as measured by FC, which was dependent on interaction affinity, antibody concentration, and cellular HLA expression. T-cell flow cytometry was used to visualise the pattern of reactivity a mAb has with its antigens upon antibody dilution. Abs were incubated at concentrations of 10 μg/ml (64.5 nM), 3 μg/ml (19.4 nM), 1 μg/ml (6.45 nM), 0.3 μg/ml (1.94 nM), and 0.1 μg/ml (0.65 nM) with PBMCs expressing a single HLA target of interest (see. Table 2.3). Secondary detection enabled MFI values to be measured, where MFI-fold change was calculated with reference to the control (symbols). Cell gating strategy is outlined in Appendix 8. Positive FC outputs are determined as an MFI fold change >1.6 (red shading). Brackets denote the cell sample used for that specific interaction. (A) and (B) represent the outputs of WIM8E5 or WK1D12 interactions, respectively, where stronger interactions resulted in higher MFI fold changes. (C) represents the comparative outputs of WIM8E5, SN230G6 or SN607D8 incubation against PBMC sample 4 (HLA-A*02:01), confirming the affinity-dependence of the output. (D) shows the comparative outputs of three separate HLA-A*01:01 (blue), or -B*07:02 (red) -expressing cell samples against WIM8E5 or WK1D12, respectively. The ability of the same interaction to generate differing MFIs on separate cells shows that the assay is dependent on cellular HLA expression. (E) shows the effect of multiple antibodies in one sera, where WIM8E5 and/or OUW4F11 spiked into blank serum was targeted against HLA-A*01:01 and/or –B*08:01 expressed on the same cell sample (15). The contribution of both interactions is an additive effect of each distinct interaction. In E, -a represents where each mAb was used at the concentration stated, while -b represents where each mAb was used at equal concentrations to make up the total mAb concentration stated. Each point represents the MFI fold change taken from >2,000 cells in one experiment. Numerical values along each line represent the mean BLI-measured affinity (K_D, nM) for that specific interaction.

3.2.4.4. Complement-Dependent Cytotoxicity Assays

Complement dependent cytotoxicity (CDC) is a favourable technique used in clinical laboratories to determine the immunological risk associated with a donor graft. This assay provides information on the capacity of an antibody to activate the classical complement pathway *in vitro*, where an antibody-HLA T-cell crossmatch that yields a positive result would be a veto to transplantation. In this regard, CDC assays offer a functional output that reflects the capacity of the antibody to carry out its effector function. Using the same mAb-PBMC combinations as used in FC assays, it was possible to measure the ability of these already characterised alloantibody-HLA binding events to fix complement and initiate complement-dependent cytotoxic cell death.

Consistent with the other assay assessments, CDC followed a decreasing pattern in output upon Ab titration. Across all interactions tested, no cytotoxic death was yielded using the lowest Ab concentrations, highlighting the limited sensitivity of the assay (Figure 3.20, Appendix 10). In

contrast to Luminex assays, CDC was able to distinguish the higher WIM8E5 affinity interactions from one another based on their ability to induce cytotoxic death. WIM8E5's priming antigen (HLA-A*11:01) could be distinguished as the interaction that produced the highest CDC output, whilst other stronger interactions were able to induce more death at concentrations at or above 1.0 μg/ml (Figure 3.20.A). Interestingly, A*02:01-WIM8E5 and A*24:02-WIM8E5 interactions were observed to be CDC negative, even at high antibody concentrations that produced elevated MFI outputs using Luminex SABs. Furthermore, analysis of CDC output when the three HLA-A*02:01-reactive antibodies were incubated with the same A*02:01-expressing cell sample showed that the higher affinity interactions resulted in a greater degree of CDC, consistent with FC assays (Figure 3.20.B).

When assessing the effect of a polyclonal spiked-serum model sample (WIM8E5/OUW4F11 against HLA-A*01:01/B*08:01-expressing PBMC sample 15) on CDC output, the effect of incubating both antibodies led to an additive output of each interaction in line with what was previously seen in FC assays (Figure 3.20.C). Although the lone B*08:01-OUW4F11 interaction gave consistently positive MFI outputs on FC assays, this interaction remained negative throughout the experiment, only reaching a very weakly positive signal (22 % kill) at the highest used antibody concentrations of 10 μg/ml. In contrast, the A*01:01-WIM8E5 interaction was able to generate slightly greater magnitudes of cell death, reaching positive levels of cytotoxic cell death at lower mAb concentrations of 3 μg/ml despite the FC MFIs being consistently lower than that of B*08:01-OUW4F11. This data suggests that while cellular HLA expression may bias the interpretation of FC assays, the output from CDC assays may be defined by the strength of the antibody-HLA interaction that occurs, along with antibody concentration, and not the levels of HLA on the cell surface (assuming the encoded HLA is expressed at a level that is recognisable by the antibody). This observation was further supported by experiments which aimed to discern the effects of cell variability on the CDC assay, where three separate cell lines expressing HLA-A*01:01 as a lone target generated similar outputs against WIM8E5 across all used concentrations despite FC outputs suggesting there was a variability in cellular HLA expression (Figure 3.20.D).

The data presented here collectively shows how CDC assays can provide a functional assessment of an alloantibody's ability to induce cytotoxic cell lysis through complement engagement, where the magnitude of cell death is positively correlated with the concentration of antibody in a sample as well as the strength at which it recognises its antigen, irrespective

of relative HLA expression. Furthermore, while antibodies within a polyclonal serum that recognise different HLA targets on the same cell may form complexes independently of each other, the contribution of both interactions may increase the overall immunological risk when compared to that of each constituent antibody individually.

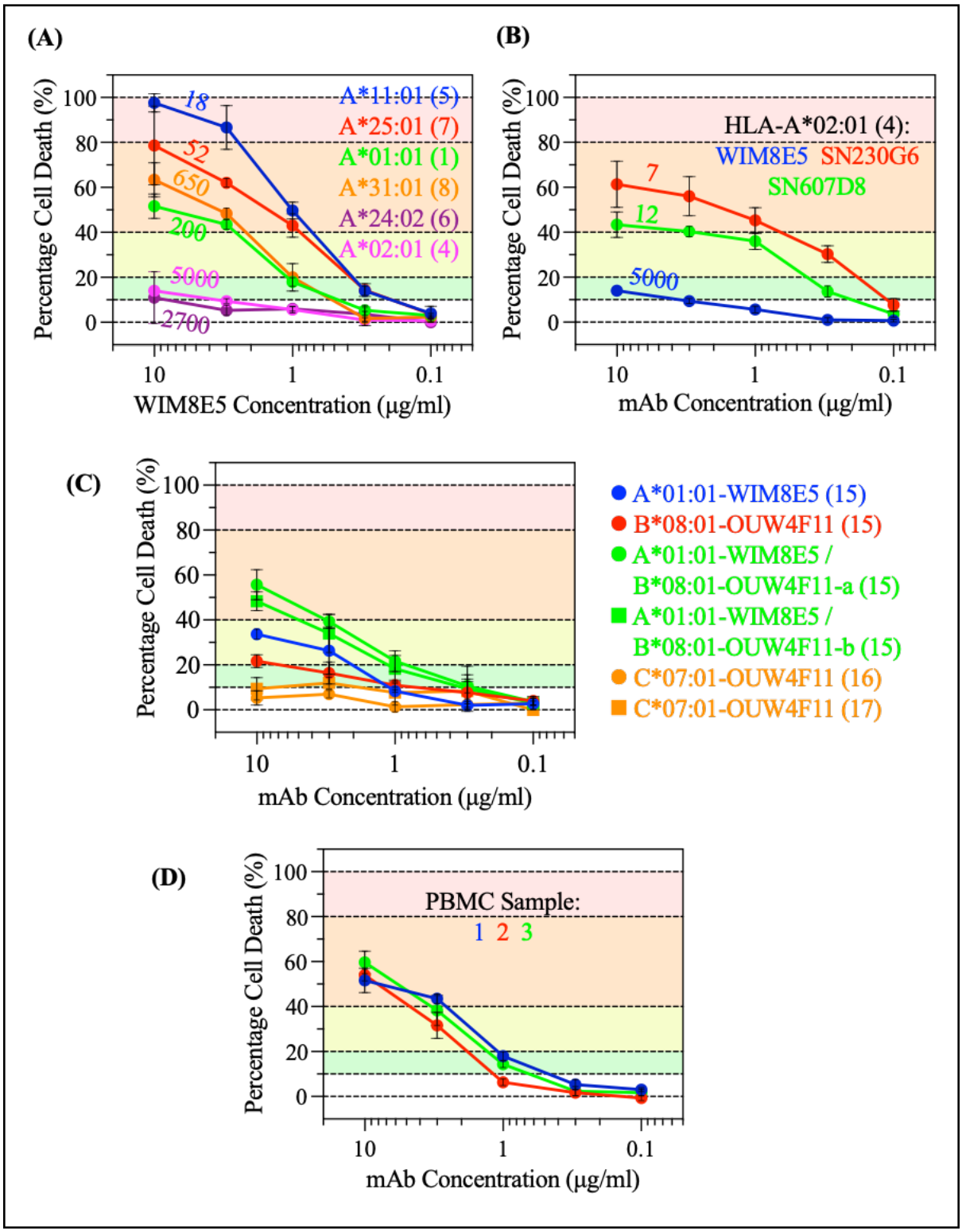

Figure 3.20. Alloantibody-HLA interactions show varying ability to elicit cytotoxic death. Antibodies displayed a varying ability to bind PBMC-expressed antigens and cause cytotoxic cell death through complement engagement, which was dependent on interaction affinity, antibody concentration, and independent of cellular HLA expression. CDC assays were used to visualise the pattern of cytotoxic kill an antibody can cause upon antibody dilution. Abs were incubated at concentrations of 10 µg/ml (64.5 nM), 3 µg/ml (19.4 nM), 1 µg/ml (6.45 nM), 0.3µg/ml (1.94 nM), and 0.1 µg/ml (0.65 nM) with PBMCs expressing a single HLA target of interest (see. Table 2.3). Incubation with complement proteins enabled complement pathway initiation, where the amount of induced cell death could be measured. CDC scoring is represented by coloured shading; 0-10 % kill / score of 1 = negative (white), 10-20 % kill / score of 2 = likely negative (green), 20-40 % kill / score of 4 = weakly positive (yellow), 40- 80 % kill / score of 6 = positive (orange), 80-100 % kill / score of 8 = strongly positive (red). Brackets denote the cell sample used for that specific interaction. (A) shows the varying ability of WIM8E5's interactions to cause cell death, where stronger interactions have a higher cytotoxic capacity, but all interactions cause no death at low mAb concentrations. (B) represents the comparative outputs of WIM8E5, SN230G6 or SN607D8 incubation with PBMC sample 4, confirming the affinity-dependence of the CDC output. (C) shows the effect of multiple antibodies in one sera, where WIM8E5 and/or OUW4F11 spiked into blank serum was targeted against HLA-A*01:01 and/or –B*08:01 expressed on the same cell sample (15). Consistent with FC assays, the contribution of both interactions is an additive effect of each distinct interaction. (D) shows the comparative outputs of three HLA-A*01:01 expressing cell samples when incubated with WIM8E5. Whilst this interaction generated variable outputs on different cells in FC assays, the CDC assay output was consistent across samples, displaying that CDC may not be dependent on cellular HLA expression. In C, -a represents where each mAb was used at the concentration stated, while -b represents where each mAb was used at equal concentrations to make up the total mAb concentration stated. Each point represents the % CDC kill taken from an average of 3 experimental replicates, where error bars represent the ±SD. Numerical values along each line represent the mean BLI-measured affinity (K_D, nM) for that specific interaction.

3.2.4.5. Potential Clinical Interpretation of Kinetically Characterised WIM8E5 Interactions

Relating interaction kinetics measured for WIM8E5 to the outputs of the clinical immunoassays measured at a concentration of 1 μg/ml enabled significant correlations to be observed between the measured affinities and the outputs Luminex SABs, FC and CDC assays (Figure 3.21.A). Pooling this WIM8E5 data makes it possible to weigh up the hypothetical immunological risk that each interaction may have in the transplant setting (Figure 3.21.B). Interactions of higher affinity, in the 10^{-8} M range (HLA-A*11:01 and -A*25:01), gave consistently larger, more positive results across all tests, suggesting they might represent a higher immunological risk. Weaker interactions in the 10^{-6} M affinity range (HLA-A*02:01 and -A*24:02) were negative in cell-based assays, despite reaching high MFI values using the more sensitive Luminex assays (albeit at very high antibody concentrations). Accordingly, it is likely that the interactions in the micromolar range are unlikely to be clinically relevant, although this would need confirmation in the clinical transplant setting.

The interpretation and clinical relevance of interactions at an 'intermediate' affinity level might be more difficult to ascertain as the output of clinical assays will be strongly dependent on the antibody concentration in the sample tested. WIM8E5 interactions with HLA-A*01:01 and -A*31:01 had affinities against WIM8E5 in the 10^{-7} M range, and while being positive in Luminex and FC assays at they were also measured to be CDC negative using the same antibody concentrations. Whether such cross-reactive interactions might represent a low or intermediate immunological risk (that might be easier to overcome with immunosuppression) also needs validation in the clinical setting. Overall, these observations highlight the complexity of current immunological risk assessment based on Luminex SAB output alone and suggests that kinetic analysis of antibody-HLA binding may provide additional insights to inform clinical decision making.

(A)

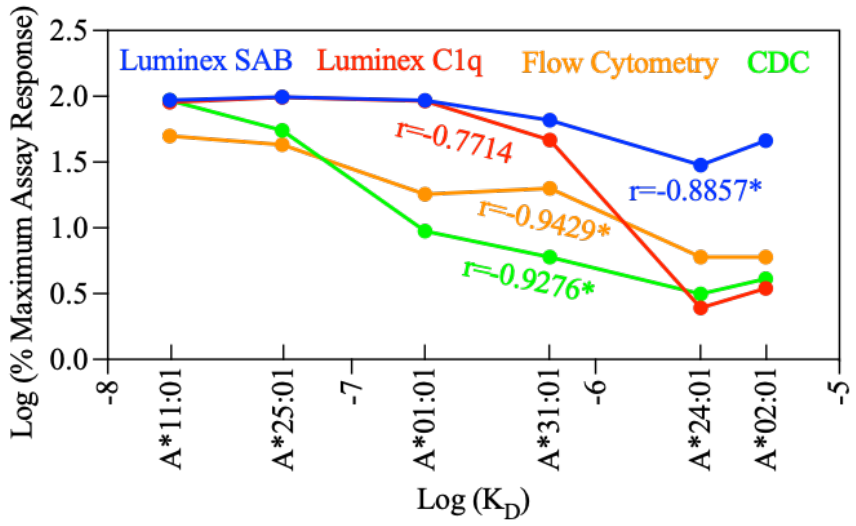

(B)

HLA	Luminex SAB MFI (A.U.)	Luminex C1qScreen MFI (A.U.)	FC (MFI fold-change)	CDC (% kill)	Affinity, K_D (M)	Risk Category
A*11:01	25706	27540	Positive	Positive	1.8×10^{-8}	High
A*25:01	27068	29977	Positive	Positive	5.2×10^{-8}	High
A*01:01	25563	28114	Positive	Negative	2.0×10^{-7}	Inter.
A*31:01	18047	14180	Positive	Weak	6.5×10^{-7}	Inter.
A*24:02	8220	754	Negative	Negative	2.7×10^{-6}	Low.
A*02:01	12629	1061	Negative	Negative	5.0×10^{-6}	Low.

Figure 3.21. Clinical immunoassay summary of WIM8E5 interactions. A) Outputs of the immunoassays using 1 µg/ml WIM8E5 enabled significant correlations between interaction affinity and the outputs of Luminex SAB (p=0.0333), FC (p=0.0167) and CDC assays (p=0.0222) to be observed. Y values represent the log of the percentage response normalised to the maximum output measured using 10µg/ml WIM8E5 against HLA-A*11:01. B) It was possible to determine the potential immunological risk associated with each of WIM8E5's interactions by comparing the positivity of the assay outputs. A*11:01 and A*25:01 possess the highest risk against WIM8E5 due to their high positivity throughout all assays and their strongest measured affinities. A*24:02 and A*02:01 possess the lowest risk to WIM8E5 due to low affinity and consistently negative cell-based assay outputs, despite being Luminex SAB positive. A*01:01 and A*31:01 may offer an intermediate risk to a WIM8E5 due to their variable ability to produce positive outputs on immunoassays and mid-level affinities. FC interpretation is given as positive (red) or negative (green), where the mean fold change in MFI when normalised to negative control is >1.6 or ≤1.6, respectively. CDC interpretation is represented by; green = negative (0-20 % Kill) , orange = weakly positive (20-40 % kill), or red = positive (40-100 % kill). Statistical analysis was carried out by Spearman's rank correlation (r). P-values are two-tailed and represented by *=<0.05.

3.3. Discussion

3.3.1. Chapter Overview

The binding strength between an alloantibody and its HLA target has been heavily implicated in its ability to carry out its effector function [233-235]. Despite studies attempting to correlate the binding strength, or affinity (K_D), of an antibody to semi-quantitative outputs of immunoassays [236, 237], its immunological significance remains poorly understood. The main aim of this study was to understand the role of binding affinity in determining an antibody's pathogenicity whilst also exploring the potential use of additional antibody-HLA binding parameter information to help interpret the outputs of assays used for immunological risk assessment. In this chapter, the establishment of an optimised biolayer interferometry method enabled real-time, quantitative kinetic assessment of interactions between purified monoclonal alloantibodies and soluble, recombinant HLA. In addition, ranking these interactions based on their measured binding affinities allowed the identification of the antibody's priming antigen as the interaction with the highest affinity. Furthermore, assessment of the same interactions using the current immunoassays for clinical alloantibody assessment showed a strong correlation between the strength of interaction and the outputs of CDC assays, FC assays, and to a lesser extent Luminex assays. Each assay also showed a dependence on antibody concentration, where the differential ability of an antibody to generate a positive response between assays highlighted the discrepancies in assay sensitivity. Overall, measurement of an interaction affinity may offer a promising approach to assessing an antibody's Fab-determined pathogenicity.

3.3.2. Biophysical Characterisation of Alloantibody Interactions

The data presented here documents the first time BLI has been applied to enable reliable assessment of alloantibody-HLA interactions. By optimising the parameters needed for accurate and reliable equilibrium rate constant (K_D) determination, the biophysical properties of 29 interactions were calculated using 6 separate monoclonal antibodies, marking the most in-depth study of cross-reactive antibody-HLA interactions to date. The measured K_D values varied significantly, spanning three orders of magnitude from the low nanomolar to mid-

micromolar range and are comparable to those measured subsequently by other groups using alternative methods [238,239].

Differing antibody binding capacities were evident when comparing interactions that involve a common binding partner, both for one antibody that binds multiple antigens, as well as different antibodies that bind the same antigen. This variability was expected based on the polymorphic nature of HLAs and the variety of antibody repertoires that can be produced by different individuals [240]. Remarkably, the strongest affinity interaction for each antibody was measured with its priming antigen, an observation that could provide insights into the state of immunological memory based on serum sample analysis [241]. SN230G6 was measured to form an interaction with cross-reactive antigen B*58:01 (3.0 nM) that was almost identical in the measured affinity to that of the sensitising antigen, B*57:01 (3.6 nM). HLA-B57 and -B58 antigens belong to the HLA-B17 broad antigen serotype and have a high degree of similarity [242], therefore the highly comparable K_Ds may suggest a high degree of priming epitope conservation. This rational may also be applied to SN607D8, where its affinity for its cross-reactive antigen, HLA-A*68:01, was identical to that of its priming antigen, HLA-A*02:01 (12 nM). In contrast, each of WIM8E5's interactions were observed to have distinctly unique affinities, suggesting a variable degree of epitope conservation between the antigens. These observations show the potential for antibody affinity assessment when measured against priming and cross-reactive antigens to assist in the determination of common HLA antibody epitopes [243]. Interestingly, both SN230G6 and SN607D8 were produced from the same individual after sequential sensitisation events (multiple pregnancies). Whilst both antibodies have high affinity against HLA-A*02:01, they both show distinct reactivity patterns with significant affinities for their cross-reactive antigens. Although it is unknown whether the antibody formed from the second priming event occurred through germinal centre re-entry or an altogether unique sensitising event [244], this scenario exemplifies the variability of developed mature immune responses in individuals and offers insights into the complexities of HLA epitope prediction [245-247].

3.3.3. The Contrasting Outputs of Clinical Immunoassays

The present study offers an in-depth examination of immunoassays currently used for antibody-related immunological risk assessment to understand how the variable parameters of anti-HLA antibodies may influence the assay output. Here, it was possible to show that the outputs of these assays are dependent on both the affinity of the interaction and the concentration of

antibodies within the sample, where the limitations of each assay may also allow for potential misinterpretation of the antibody's immunological significance. For decades, CDC and FC have been used to detect HLA-specific antibodies and provide an insight into their pathogenicity [248, 249], however the ability to distinguish a true positive and true negative result has often come with difficulty [206, 250]. In line with previous studies [206, 251, 252], this data demonstrates the contrasting sensitivities between these two cell-based assays, where positive outputs in FC assays do not always result in cytotoxic cell death in CDC assays. This is believed to be due to the need for stabilisation of the HLA-Ab-C1q complex through Antibody-C1q hexamerisation to enable classical complement cascade initiation in CDC assays [117], whilst FC assays only measure an antibody's capacity to bind HLA irrespective of its complement fixing abilities.

With the development of solid-phase assays, their higher sensitivity, higher throughput, and multiplexing abilities have resulted in their establishment as the main method for identification of recipient DSA and determination of their HLA specificity. Whilst this elevated sensitivity may enable detection of antibodies that otherwise may not have been picked up in cell-based assays, the true immunological significance of the MFI output is still uncertain [253]. Data presented here provides evidence to support the concerns surrounding the Luminex MFI outputs [214, 254], in that they may not directly reflect the pathogenic functionality of an antibody against a particular HLA target. This is evidenced in the case of HLA-A*02:01-WIM8E5, a clinically insignificant antibody incapable of engaging complement as measured by CDC but may generate a highly positive MFI output on Luminex. This is believed to be due to the high density of HLA on the SABs [254] which enable the interaction to be maintained at a divalent stoichiometry due to the interaction avidity, whereas in a more physiologically environment this may not be possible. In contrast, analysis of a highly pathogenic antibody capable of complement engagement (e.g., A*02:01-SN230G6) at lower antibody concentrations may still yield a negative result via CDC assessment due to the limited assay sensitivity, despite generating saturating Luminex MFIs. Other studies assessing the validity of Luminex assay outputs also reported the potential for false negative and false positive results due to the prozone effect in high antibody-containing sera, or the antibody recognition of non-native epitopes on denatured HLAs, respectively [255, 256]. In agreement with other concerns regarding the interpretation of these clinical assays [257-259], these results also convincingly highlight that immunoassay output is dependent on alloantibody concentration, and therefore would be contingent on the timing of serum-sampling in clinic. These statements highlight the

primary issue, in that there is the capacity for both pathogenic and non-pathogenic DSAs to be misinterpreted based on their ability to generate a positive response in these immunoassays. In a clinical setting, perceiving a high specificity, clinically relevant interaction as negative due to a low concentration of antibody at the time of sampling could possibly result in a high-risk transplant [260]. A case such as this may result in induction an anamnestic response upon re-exposure to antigen, resulting antibody mediated rejection. Conversely, a non-pathogenic interaction that yields positive outputs on more sensitive assays may be given clinical significance, especially if the cross-reactive antibody is at high concentration, thus limiting a recipient's access to suitable donor organs [261].

Recently, studies have suggested that using the combined MFI ('sum MFI') of DSAs may offer a better prognostic tool for prediction of ABMR or graft failure [262, 263]. Using a fabricated polyclonal antibody sample, we showed that the net CDC and FC outputs of multiple antibodies binding to the same cell sample may result in an additive effect of each separate interaction. This suggests combining the MFI output as measured Luminex to form a 'sum MFI' may be used as a valid way to assess the serum's immunological risk. However, this statement may only be applicable when antibodies have specificities against non-related antigens and where the interactions occur independently of one another in a non-competitive manner. Further experimentation would be needed to determine the significance of the total sum MFI in an environment when there is competition for antigen epitopes.

The cases presented here highlight the hiatus in sensitivity between different solid-phase and cell-based assays and present cases of how outputs from one assay may be misconstrued and not give a complete insight into the true characteristics of the assessed interaction.

3.3.4. The Influence of Antibody Affinity on Immunoassay Output

This chapter provides the first documented evidence that the ability of an alloantibody to produce positive outputs in Luminex SAB, CDC and FC assays is related to the absolute, quantified affinity at which it binds its reactive HLA molecules. Whilst previous studies have used these assays to define 'strong' and 'weak' antibodies [233-237], the semi-quantitative values gained from them often do not allow the pathogenicity of an antibody to be clearly defined. This issue is most prominent when determining the clinical significance of cross-reactive antibodies that may generate 'intermediate' responses in these assays. By using purified monoclonal antibodies which were the same antibody subclass (IgG1), standardisation

of antibody concentration enabled the Fab-dependent determinant (affinity) to be scrutinised in isolation. In agreement with the hypothesis and the surrounding literature [234, 236], the ability of antibodies to generate higher positive immunoassay outputs at any given concentration was contingent with the K_D at which the interaction is established. Furthermore, the highest outputs at each antibody concentration were generated for those interactions with the strongest measured affinities across all assays.

Five of the six cross-reactive antibodies displayed similar abilities to bind each of their reactive antigens as determined by the K_D, which was corroborated by their comparable immunoassay outputs. Contrastingly, WIM8E5 bound its cross-reactive HLA targets with variable K_Ds, where higher affinity interactions were able to generate elevated immunoassay responses. This was most prevalent in cell-based assays, where the antibody's ability to bind to cell-expressed HLA in FC assays, and induce cytotoxic death in CDC assays, could be directly associated to the antibody's affinity against its the HLA target. Whilst Luminex assays enabled WIM8E5's weaker affinity interactions (>200 nM) to be distinguished from one another based on the pattern of decreasing MFI upon antibody dilution, Luminex MFI outputs alone were unable to discriminate interactions of stronger affinity despite displaying different complement-fixing capabilities in CDC assays. The above observations were also consistent when assessing interactions involving different antibodies which recognise the same antigenic target. Here, antibodies which exhibited similar affinities against the same HLA output gave comparable values on immunoassays. Furthermore, outputs were higher for stronger antibodies in comparison to weaker antibodies which recognised the same HLA (e.g., SN230G6 and WIM8E5 binding A*02:01). Notably, interactions with micromolar K_Ds did not show the capacity to engage complement in CDC assays, despite generating positive responses using the Luminex methods at higher antibody concentrations. This point once again highlights the issue with detection of DSA with highly sensitive Luminex assays and suggests that interactions with micromolar affinity may be clinically irrelevant. Nevertheless, establishing a true K_D cut-off value defining an antibody's immunological significance would require significant justification and a lot more exploration, especially given the complexity of achieving this with other assays [253, 264, 265] and the known multitude of factors that contribute to an antibody's pathogenicity [84, 86, 91,94].

3.3.5. Moving Forward with Interaction Affinity Assessments in Serum

Biosensor-employing techniques such as BLI and SPR have become the current gold standard for biophysical characterisation of protein-protein interactions as they offer real-time, label free measurement of interaction kinetics. Whilst data presented here was carried out using purified samples, the ability to measure these interactions in clinical patients would necessitate the direct use of serum samples as antibody sources. Human serum contains many Ig molecules with countless specificities, and not knowing the ratio of antigen-specific antibody to non-antigenic antibodies within a sample would make it difficult to control the amount of relevant antibody immobilisation. Furthermore, the unknown active concentration of antibody within the serum would be an issue when using serum as an analyte as this property is mandatory for rate constant calculation [266, 267]. Using these methods to quantify protein-protein interactions in serum often leads to non-specific binding, making accurate kinetic measurements difficult to ascertain [268]. Whilst in pure buffer the amount of non-specific binding may be controlled through optimisation of the buffer pH, salt concentration, and/or the addition of surfactants or protein blockers, such as Tween or BSA, respectively, these factors may not be controllable using serum samples.

Detailed throughout this chapter was also the option to reverse the orientation of the interaction on the sensor, immobilising HLA and using antibodies as the analyte (section 3.2.2.3). Although other studies have used purified alloantibodies as analytes in solid-phase biophysical assays [238], their multivalent nature means that the contribution of an immunoglobulin molecule's avidity cannot be ruled out. Furthermore, cases in which the analyte molecule contains multiple high affinity antigen binding sites may need further, individualised optimisation due to the lack of analyte dissociation, such as the example seen with A*02:01-SN230G6 in Figure 3.11. This is believed to occur when a newly detached antibody Fab region at the surface of a sensor can re-bind before the dissociation of the Ig's second Fab region, a phenomenon known as 'walking' [269]. Although immobilisation of HLA to a sensor surface may not enable definitive determination of all IgG Fab domain interaction affinities, there is still scope for this orientation to offer an effective method of assessing an alloantibody's avidity for its antigen. Since these studies were carried out, Visentin et al published two SPR-based methods for measuring the active antibody concentration serum and sequentially calculating the kinetics of these interactions which overcome the non-specific binding issue [266, 270].

While this offers a promising option for studying kinetics in the research environment, the labour-intensive processes needed for this would not be suitable for clinical translation.

Overall, biophysical methods that require surface immobilisation offer great opportunities to assess kinetics of alloantibody-HLA interactions in a pure buffer setting. However, if this assessment is to be made clinically available then a novel method which enables quantification in human serum without the need for surface immobilisation would be imperative.

3.3.6. Conclusion

Throughout this chapter, substantial evidence has been provided to suggest that an alloantibody's capability to specifically bind HLA molecules with differing affinities will determine its effector function. Additionally, Luminex, FC and CDC assays used in clinic for antibody-related immunological risk assessment will be contingent on both the affinity an antibody for its antigen and its abundance within the serum sample. Furthermore, quantification of alloantibody-HLA binding kinetics enables further insight into the Fab-dependent effector function of HLA-specific antibodies that is not currently obtainable using the existing methods of clinical antibody assessment. This data supports use of alloantibody-HLA interaction affinity assessments to offer more detailed, fully quantified information about a binding event that may be used to elucidate an antibody's clinical significance.

Chapter Four

Intracellular Signalling in Response to Antibody-HLA Ligation

4.1. Introduction

Anchored to the cell membrane, HLAs play a major role in adaptive immunity by presenting a variety of exogenous and endogenous peptides to T-cells to aid in immune surveillance and pathogen clearance. If someone has been exposed to foreign HLAs, such as in transplantation, this molecule may become a target of the adaptive immune response resulting in the development of humoral immunity against this antigen. The recognition of foreign HLA by antibodies and other components of the humoral compartment can trigger a variety of pathways that may lead to destruction and/or injury of tissue through secondary extracellular effectors (see sections 1.3.3 and 1.4). Over the past ten years, the establishment of HLA-antibody complexes involving class I molecules has been linked to the occurrence of intracellular signalling events that promote a wide variety of cellular responses. Some of these responses have been show to promote growth, proliferation, and survival of the individual cell [271-274], whereas many of them have also been linked to the occurrence of allograft vasculopathy (AV) and chronic allograft nephropathy (CAN), which are major causes of late graft dysfunction [275-277]. Besides pathways involving stress-induced matrix metalloproteases and sphingolipid signalling which have been documented to promote proliferation upon antibody binding to HLA class I [278, 279], the formation of an alloantibody-HLA complex alone does not permit the transmission of an intracellular signal since HLAs lack a signalling motif. For HLA class-I signal propagation to occur, the complex must form molecular associations with

secondary proteins. Within endothelial cells, HLA class I molecules have been shown to colocalise with the hemidesmosomal laminin receptor integrin β4, which trigger various signalling events through its signalling domain [280-282].

Central to HLA signalling regulation, Rho kinase (ROK) and the Rho family of GTPases (Rho-GTP) have been documented to be some of the first proteins that become activated upon antibody ligation to HLA, where both signalling molecules mediate various other targets for signal transmission [283]. Src is a cytosolic non-receptor protein tyrosine kinase shown to be phosphorylated at tyrosine 527 during this process which triggers the initiation of the phosphoinositide 3-kinase (PI3K)/protein kinase B (Akt) signal transduction pathway [284, 285]. This pathway cross-links various mitogen-activated protein kinase (MAPK) cascades and has implications in many different cellular processes including proliferation and cell survival. Upon activation of the PI3K/Akt pathway, phosphorylation of mammalian target of rapamycin (mTOR) at serine 2448 has been widely observed, where it is able to associate with other proteins to form one of two mTOR-containing complexes [286-288]. mTORC1 is composed of mTOR, regulatory-associated protein of mTOR (raptor) and mTOR-associated protein LST8 Homolog (mLST8) and promotes cell proliferation and protein synthesis through S6 kinase (S6K), S6 ribosomal protein (S6RP) or eukaryotic translation initiation factor 4A1 (eIF4A1) [273, 287, 289-291]. mTORC2 is composed of mTOR, rapamycin-insensitive companion of mammalian target of rapamycin (rictor), mLST8 and MAPK associated protein 1 (MAPKAP1/Sin1) [273, 291, 292]. This complex promotes cell survival and migration through regulation of Akt and coordinates cytoskeleton remodelling through F-actin stress fibre formation alongside HLA-activated myosin light chain kinase (MLCK) and extracellular signal-regulated kinases (ERKs) [293-294]. Focal adhesion kinase (FAK) and paxillin are two other proteins found to be involved with cytoskeletal remodelling post-antibody ligation, where upon phosphorylation, FAK localises to paxillin-resident areas of the cell that form cell-to-cell contacts through their extracellular matrix, called focal adhesions. Here these focal adhesions stabilise which is essential for many other cellular processes to take place [295-297]. Endothelial cells have also been shown to increase the production and release of various growth factors in response to antibody ligation to HLA, such as vascular endothelial cell growth factor (VEGF), basic fibroblast growth factor (bFGF), insulin-like growth factor 1 (IGF-1) and platelet-derived growth factor (PDGF) [298, 299]. Along with the targeted upregulation of the receptors of these ligands, the number of proliferative signals received by these cells from the microenvironment increases in both autocrine and paracrine manners [300].

Endothelial cells contain intrinsic storage granules known as Weibel-Palade bodies which contain two major membrane-bound components: von Willebrand factor (vWF) and P-selectin [301]. Upon immunoglobulin ligation to HLA, these vesicles are mobilised and exocytosed, where vWF and P-selectin remain anchored to the cell surface membrane and exposed to the extracellular space where they act as cell anchors to aid in monocyte recruitment [302-306]. Additionally, these cells also increase the number of cell adhesion molecules found on the cell surface through transcriptional regulation of vascular cell adhesion molecule -I (VCAM-I) and intercellular adhesion molecule -I (ICAM-I) [307-310], whilst also increasing production and release of inflammatory chemokine attractants in a CREB/PKA-dependent manner [311, 312]. Although antibody-HLA ligation has most commonly been associated with rejection and/or graft dysfunction, there have also been several *in vitro* studies carried out that show the role of alloantibodies in promoting transplant accommodation [313-316]. While high concentrations of antibody have been shown to initiate death through complement engagement, low concentrations of antibody have been shown to activate protein kinase A (PKA) in a cyclic adenosine monophosphate (cAMP)- and PI3K/Akt-dependent manner [274]. This signalling causes upregulation of the anti-apoptotic genes such as B-cell lymphoma extra-large (Bcl-xL), B-cell lymphoma 2 (Bcl-2), and haem oxygenase I (HO-1), whilst also providing protection against complement-induced death through upregulation of cryoprotective genes [285, 316].

Although the establishment of HLA-Ab interactions have been heavily implicated in the processes summarised, the magnitude to which antibodies can activate these signalling cascades remains unexplored. In attempt to address the effect of affinity on the ability of AlloAbs to activate specific signalling pathways, this chapter aims to disseminate these individual signalling cascades *in vitro* with hopes to help further determine the clinical significance of alloantibodies. Through establishment of primary endothelial cell cultures as a model, exposing these cells to thoroughly characterised mAbs may permit the intracellular phosphorylation events and changes in the cell surface adhesion molecule levels to be mapped, enabling the mechanistic action that is downstream of Ab-HLA complex formation to be visualised. By then comparing the magnitude of the signalling response induced by mAbs of varying affinity, I then aimed to determine whether the ligation of expressed HLAs to antibodies of varying affinities would affect the overall response. I hypothesised that antibodies which bind their HLA targets with greater affinity will trigger an elevated intracellular signalling response than those that bind with a lower affinity.

4.2. Results

4.2.1. Primary Aortic Endothelial Cell Isolation

To investigate the downstream cellular effects of Ab ligation to cell-surface HLA, human aortic endothelial cells (HAoECs) were chosen as a relevant cellular model as these cells have been heavily documented to become activated upon HLA recognition (see section 4.1). In attempt to obtain a self-sufficient supply of HAoECs for these *in vitro* studies, establishment of a reliable protocol for isolation of these cells from donor tissues was needed. To initially develop the isolation protocol, porcine renal arteries were used as a source of cells. Here, AoECs were successfully and reproducibly isolated, where they could be cultured for up to six passages whilst maintaining their endothelial characteristics (Figure 4.1.A).

This protocol was then translated into human tissue using aortic rings from deceased human donors (Figure 4.1.C). Cell patches were observed to form 24 hours after isolation, where they were observed to have the emblematic "cobble-stone" like morphology (Figure 4.1.B). These cells were found to express CD31 via flow cytometry, confirming their endothelial nature (Figure 4.1.D, Appendix 11). Whilst culturing the cell patches over the next three days, the cells struggled to proliferate and transitioned to a more "spindle-like" morphology. After one week of continuous culture, these cells were seen to have lost their CD31 marker (not shown) and failed to restore any of their endothelial characteristics. The ability to yield significant quantities of primary cells from these samples was limited by the availability, quantity, and quality of donor tissues, where only two of the twelve donor samples yielded significant isolated endothelial cell patches. The general health and age of the donor prior to death often limited the ability to isolate HAoECs, where calcification of the aortic tissue was prominent in older donors and those with underlying health conditions which prevented efficient isolation. Despite attempting to optimise the isolation procedure in which the sample tissue source, storage buffers, culturing conditions and growth media components were altered according to other published methods [326-332], establishing healthy, proliferating cell cultures which maintained their endothelial characteristics was unsuccessful. To continue with the study and enable assessment of an antibody's capability to induce downstream cellular responses in this cell type, commercial primary HAoECs were purchased (Table 2.4.).

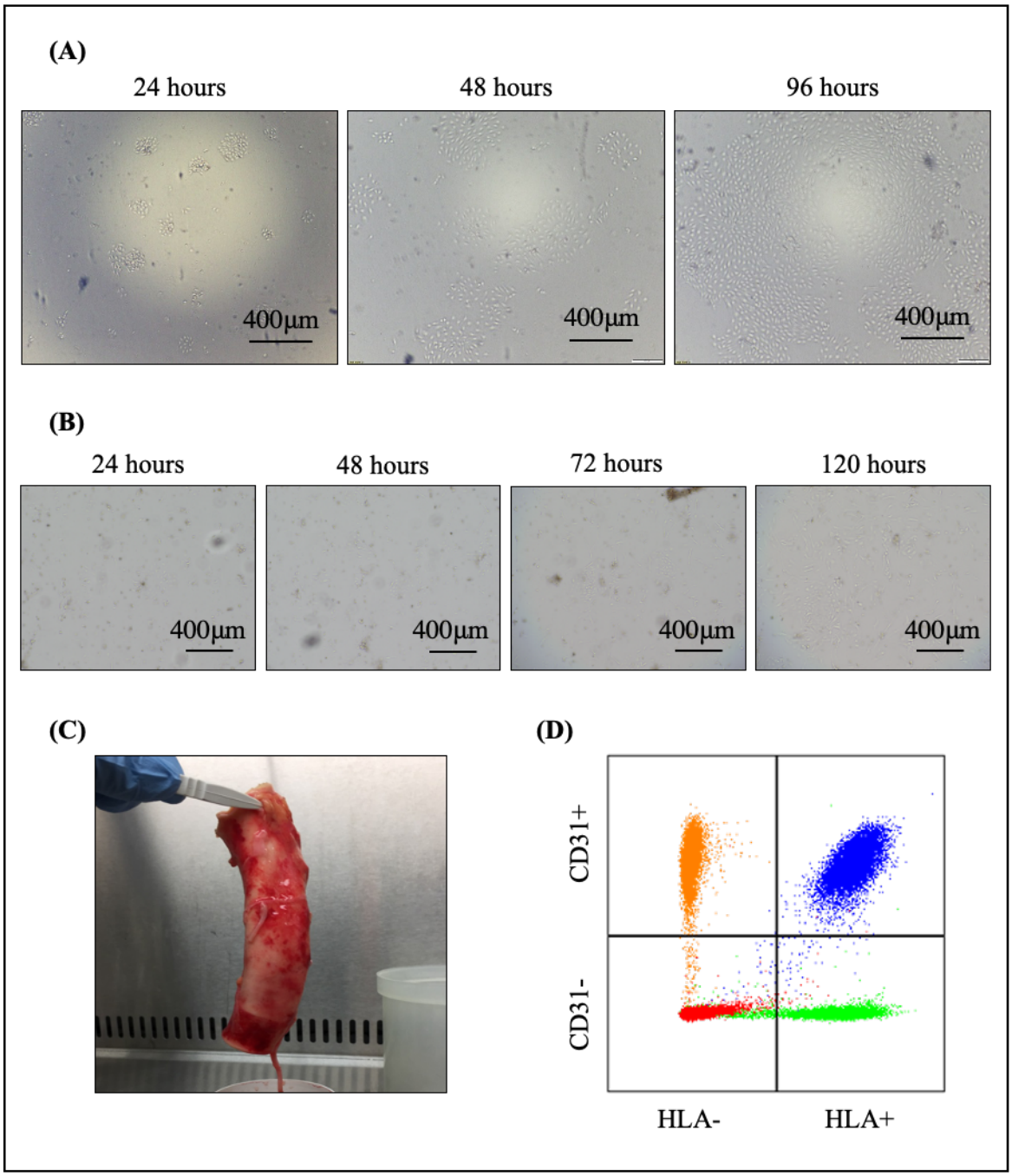

Figure 4.1. Isolation of aortic endothelial cells. Endothelial cells isolated from porcine renal artery tissue formed patches in cell culture where they proliferated to confluency over the first 96 hours and maintained the endothelial cobble-stone morphology (A). Cells isolated from human aortic rings (B-C) formed small endothelial cell patches after 24 hours of culture and were found to express both HLA (W6/32 primary, STAR70 secondary) and CD31 (anti-CD31-biotin primary, streptavidin-APC secondary) (D). Over a 5-day period the cells became more spindle-like in morphology, where the expression of CD31 was gradually lost (not shown). The cells did not return to an endothelial phenotype. Orange and green populations in (D) represent the single stain controls, red population represents unstained control cells and blue population represents double-stained cells. Gated HAoEC populations include >12,000 cells per sample. Gating strategy can be seen in Appendix 11.

4.2.2. Assessing the Capacity of mAbs to Bind Cell-Surface HLA Targets

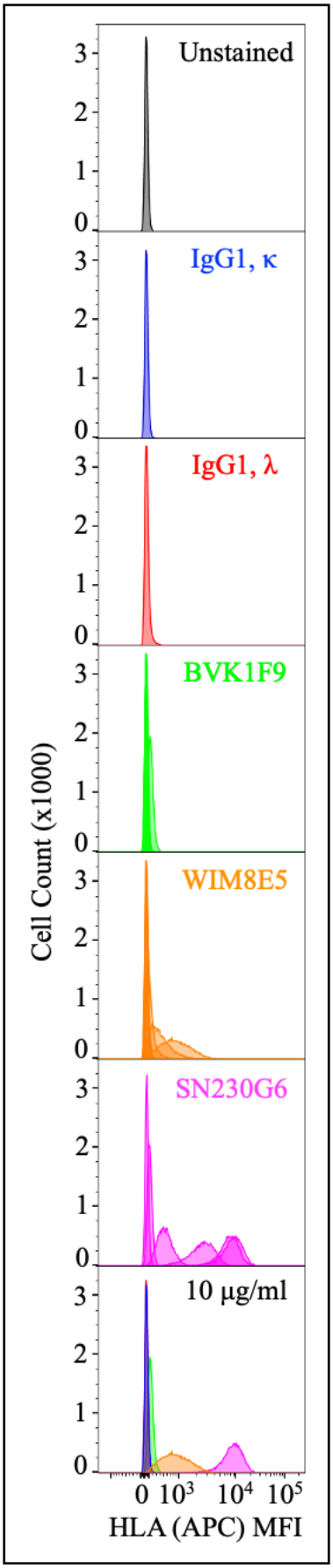

Antibodies previously measured to bind HLA-A*02:01 with differing affinities (see section 3.2.3) were assessed for their capacity to recognise HLA expressed on commercially-sourced primary HAoECs. Cells expressing A*02:01 as a lone antibody target were incubated with isotype control or one concentration of a ten-fold mAb dilution from 10 µg/ml (64.5 nM) to 100 pg/ml (0.65 pM), prior to analysis by FC (Figure 4.2, Appendix 11). BVK1F9 only bound to these cells minimally at the highest antibody concentrations, potentially due to its very low specificity for HLA-A2 as previously confirmed by Luminex (Appendix 5). WIM8E5, previously shown to have a relatively low affinity against A*02:01 of 5.0 µM, was able to demonstrate a weak capacity to bind cellularly-expressed HLA-A*02:01, observed as a slight increases in the fluorescence intensity of cells when incubated at mAb concentrations >100 ng/ml. Incubating these cells with the high affinity SN230G6 mAb (7.4 nM) enabled a further shift in the fluorescence intensity signals to be observed, where as little as 1 ng/ml mAb was enough to observe antibody binding. This supported the previous data in Chapter 3 that demonstrated SN230G6 to be more effective at binding HLA-A*02:01 than WIM8E5.

Figure 4.2. Human monoclonal antibodies show differing abilities to bind HLA-A*02:01-expressing HAoECs. Histograms displaying SN230G6's increased ability to bind HLA-A*02:01 expressed on HAoECs (lot #422Z038) when compared to the weaker WIM8E5 antibody. HAoECs (lot #422Z038) were incubated with 10 µg/ml isotype control IgG (blue and red), or 10 µg/ml, 1 µg/ml, 100 ng/ml, 10 ng/ml, 1 ng/ml or 100 pg/ml BVK1F9 (green), WIM8E5 (orange) or SN230G6 (pink) prior to anti-human IgG-biotin secondary antibody incubation. Samples were further incubated with Streptavidin-APC* and assessed via flow cytometry using the gating strategy outlined in appendix 11 to reveal the mAb-binding-determined fluorescence intensities. The bottom panel shows a comparative overlay of all the histograms using 10 µg/ml of each mAb, and the unstained control (black).

4.2.3. Measuring the Effect of Alloantibody-HLA Ligation on Downstream Cell Signalling Events

Although many molecules have been implicated in signalling downstream of HLA recognition, two well-studied proteins have been heavily documented throughout the literature; protein kinase B (Akt) and extracellular signal-related kinases 1 and 2 (ERK1/2) [270, 285, 316]. To initially determine the time course of signal transduction after the ligation of antibody to HLA, healthy, starved HLA-A*02:01-expressing cells were incubated with cell culture medium containing either 1 μg/ml of SN230G6 or control IgG, for a period of up to sixty minutes before their cell lysates were analysed via western blot (Figure 4.3). Both Akt and ERK1/2 were observed to show increases in activating phosphorylation status above the serum-starved baseline between ten and thirty minutes, peaking at twenty minutes. Despite this, a similar pattern was also observed when cells were incubated with isotype control IgG (not shown). In attempt to investigate whether there was an antibody concentration dependence to these signalling responses and whether this was more prevalent with addition of higher concentrations of alloantibody in comparison to isotype control, cells were incubated with ten-fold dilutions of anti-pan HLA class I antibody (W6/32), from 100 μg/ml (645 nM) to 100 pg/ml (0.65 pM), for a total of twenty minutes (Figure 4.4). This was carried out over a series of three repeated experiments, where the effect of three different alloantibodies and their isotype controls (SN230G6 and WIM8E5 not shown) were examined. It was noted that in all three experiments there were no significant differences between the signals arising from each antibody, whether control or HLA-specific, or between their variable concentrations.

Despite previous studies by other groups showing that the addition of antibody directly into the media of cultured endothelial cells is sufficient for signal transduction [272], the experiments to this point suggested otherwise. To investigate whether cross-linking of cell-bound mAb was crucial for phosphorylation signal transduction, an experiment was designed which intended to mimic the action of the immune response which occurs *in vivo*, by cross-linking the antibody though incubation of alloantibody-bound cells with either an anti-human IgG Fc secondary antibody, or through lymphocyte recruitment by addition of isolated PBMCs. The addition of PBMCs was observed to cause an increase in phosphorylation status of Akt and ERK, however this was seen in both experimental and isotype control groups, suggesting that this signal was caused by something independent of HLA-specific antibody ligation (Figure 4.5). Since the inability to observe significant changes in phosphorylation of Akt and

ERK above the negative controls had been consistently shown across various treatment conditions, a phospho-array was performed to examine whether there were any changes in the phosphorylation status of 41 other major membrane-related kinases upon addition of mAbs (Figure 4.6). Consistent with previous findings, there were no clear differences in the phosphorylation status of any of the kinases between each treatment group. This suggests that the protein phosphorylation events seen at 20 minutes post-treatment were not due to the formation of the mAb-HLA complex, but another aspect of the experimental procedure.

In attempt to account for cell sample variability and to ensure that what was being observed is not cell sample-specific, these experiments were repeated using three different lot numbers of commercial HAoECs (Figure 4.7). Consistent with previous results, these cells also showed no difference in pAkt or pERK upon alloantibody treatment. This experiment did however demonstrate that further activation of Akt and ERK is possible, where the unavoidable addition of small quantities of FCS in the OUW4F11 condition (OUW4F11 stock contains FCS) was able to induce further kinase phosphorylation in all cell samples. At this point it was decided that these experiments would be repeated using two alternative primary cell types; human umbilical vein endothelial cells (HUVECs) and human aortic smooth muscle cells (HAoSMCs). Upon alloantibody exposure, both cell types displayed similar activation patterns to what was seen in HAoECs (Figure 4.8). In attempt to further understand what factors were causing the observed phosphorylation of Akt and ERK in negative control tests, experiments which explored various starve conditions, cell passage number, cell confluency and volume of added treatment addition were attempted, all of which yielded similar results to what had previously been reported (data not shown). Throughout all attempts to examine the transduction of signal through phosphorylation of specific kinases, no alloantibody condition yielded results which displayed enhancement of the Akt or ERK phosphorylation signal above what was observed upon addition isotype control IgG. After many experiments attempting to determine the reason for the increase in phosphorylation signal from the baseline at time 0, an experiment was proposed which tested various physical conditions which the cells are exposed to throughout the treatment process. In this experiment it was uncovered that the physical act of moving the cells from the 37 °C incubator and leaving them at room temperature for 2 minutes (average time needed for addition of treatment condition), before replacing them back in the 37 °C incubator was sufficient to induce the phosphorylation events seen at 20 minutes post-treatment. This suggests that the changing temperature endured by the cells throughout the treatment process was sufficient to activate these cells (Figure 4.9).

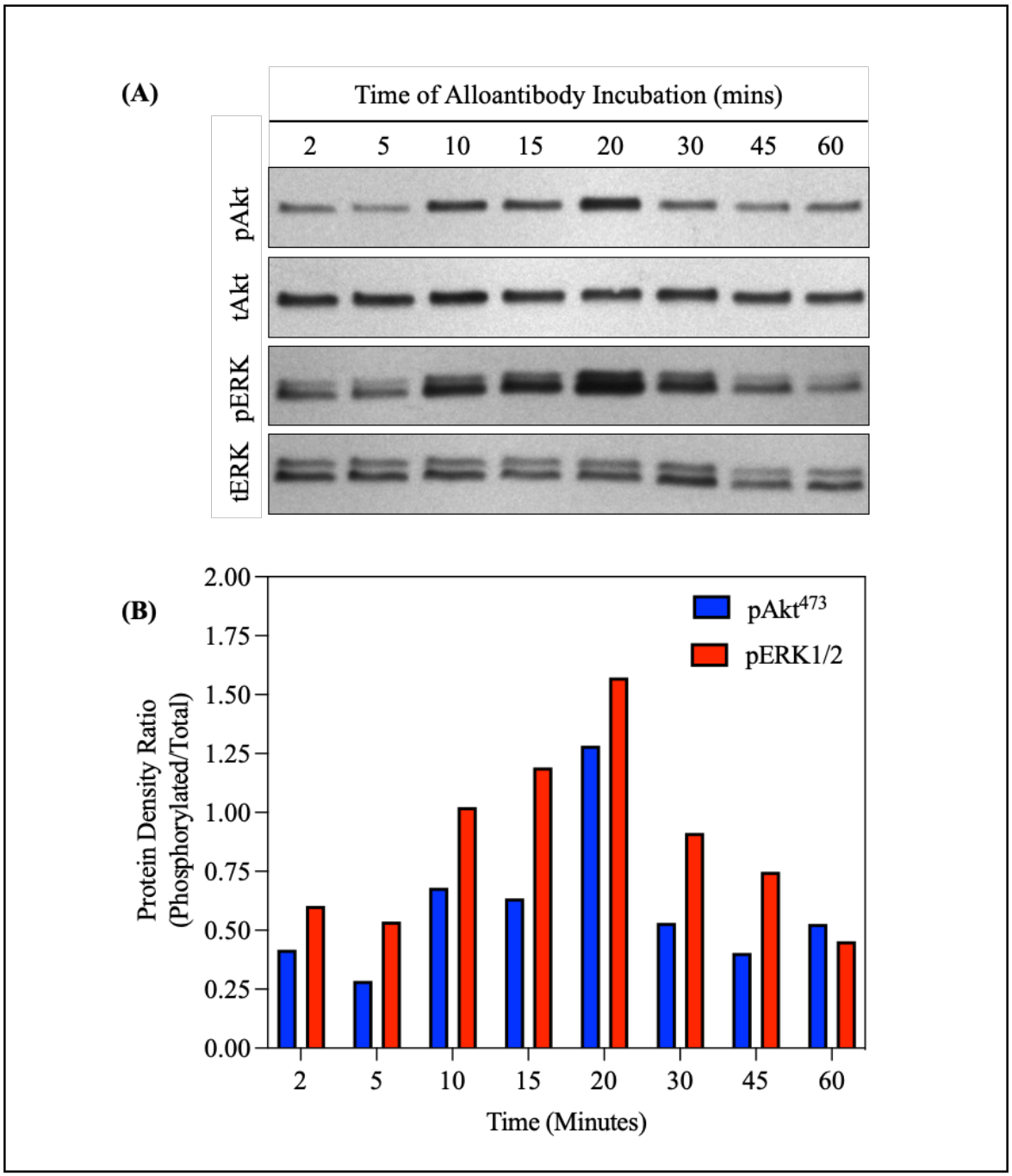

Figure 4.3. Measuring the time dependence of Akt and ERK 1/2 phosphorylation upon alloantibody binding. A one-hour time course of Akt and ERK phosphorylation within HAoECs following antibody ligation to HLA shows peak phosphorylation at 20 minutes. HAoECs (lot #422Z038) were treated with 1 µg/ml alloantibody (SN230G6) or isotype control, then harvested and lysed at various timepoints over a 60-minute period. The total expression and phosphorylation status of Akt and ERK1/2 within the cell lysate was assessed via western blot (A), where densitometry analysis of each band was carried out using ImageJ software, normalised to total target protein expression (B). The data displayed shows one experiment displaying the effects of SN230G6 ligation but is a fair representation of over ten individual experiments repeated using various alloantibodies and cell samples, where the displayed phosphorylation patterns were consistent in both experimental and control groups (not shown).

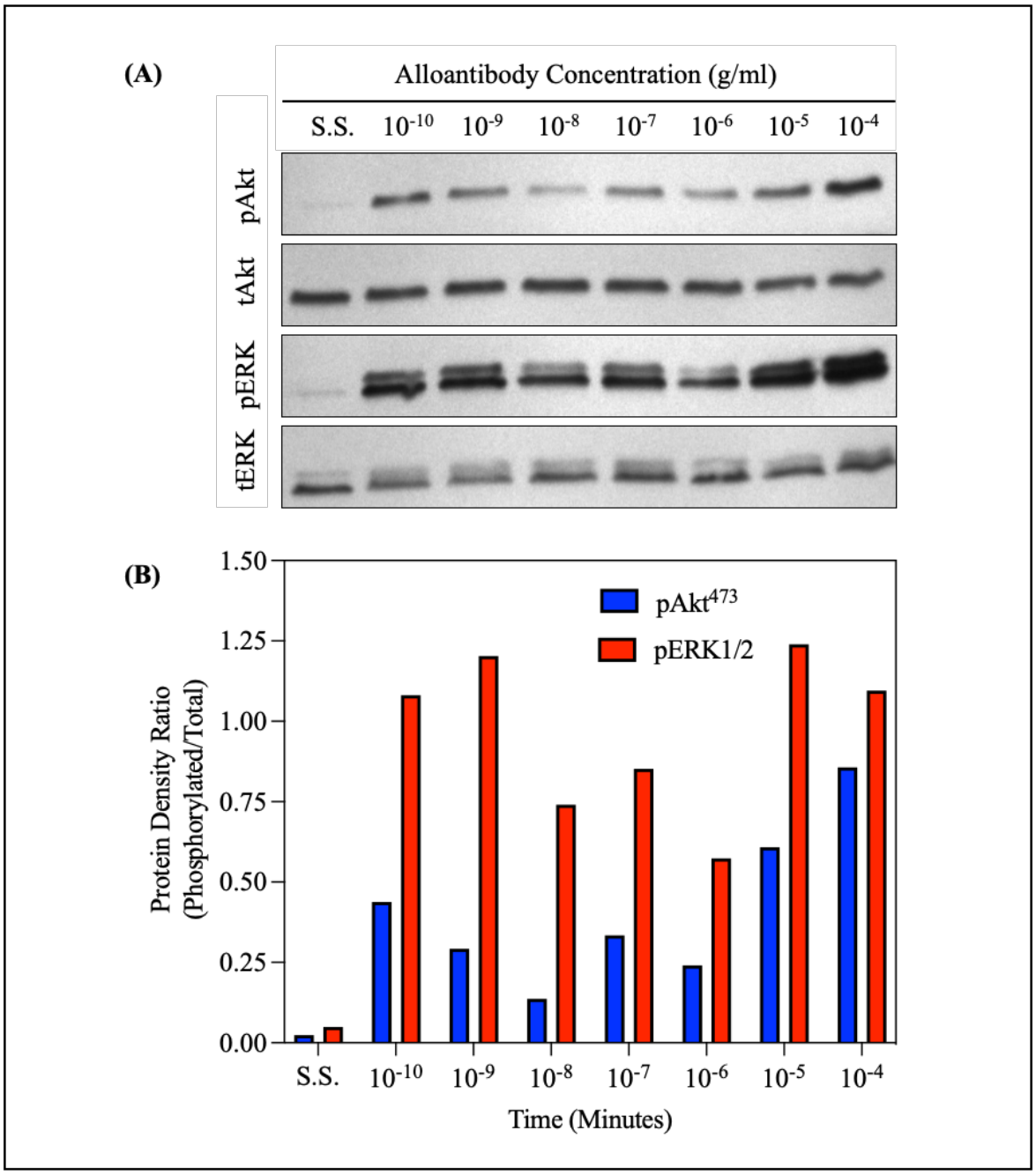

Figure 4.4. Measuring the antibody concentration dependence of Akt and ERK 1/2 phosphorylation. No difference in the phosphorylation status of Akt and ERK was observed within HAoECs following incubation with antibody at various concentrations. Serum-starved HAoECs (lot #415Z025) were treated with either 100 pg/ml, 1 ng/ml, 10 ng/ml, 100 ng/ml 1 µg/ml, 10 µg/ml or 100 µg/ml W6/32 or isotype control for 20 minutes prior to harvesting and lysis. Cell lysates were assessed for total expression and phosphorylation status of Akt and ERK1/2 via western blot (A), where densitometry analysis of each band was carried out using ImageJ software, normalised to total target protein expression (B). Displayed data only shows results of incubation with W6/32 but is a fair representation of results from both test and negative control conditions. This experiment was repeated using an alternative cell sample and/or anti-HLA antibody where consistent phosphorylation patterns were seen in both the experimental and negative control groups across all experiments (not shown). S.S. represents basal levels of expression/phosphorylation after 16 hours of serum starvation, which were harvested directly before treatment of the other cell samples.

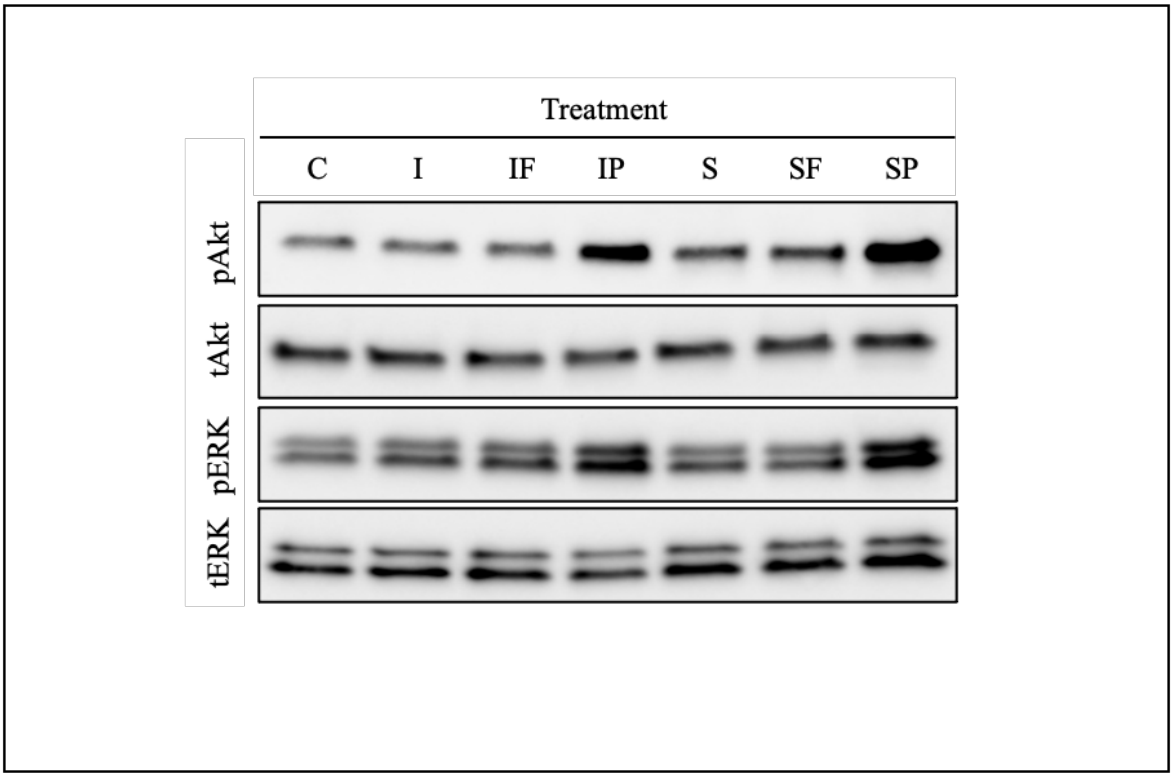

Figure 4.5. Cross-linking HLA-bound antibodies does not increase the magnitude of signaling cascades. Addition of an antibody cross-linking agent does not lead to Akt or ERK phosphorylation. Serum starved HAoECs (lot #422Z038) were incubated for 20 minutes with one of the following conditions: a change in media alone (C) , 1 μg/ml human isotype control IgG1 (I), 1 μg/ml human isotype control IgG1 + 1 μg/ml anti-human IgG Fc (IF), 1 μg/ml human isotype control IgG1 + 10^6 PBMCs (IP), 1 μg/ml SN230G6 (S), 1 μg/ml SN230G6 IgG1 + 1 μg/ml anti-human IgG Fc (SF), or 1 μg/ml SN230G6 + 10^6 PBMCs (SP), prior to harvesting and lysis. Cell lysates were assessed for total expression and phosphorylation status of Akt and ERK1/2 via western blot yielding the bands displayed. Incubation of PBMCs saw an increase in ERK and Akt phosphorylation, however this was not caused by alloantibody interactions (not shown). Densitometry analysis yielded no significant differences between the control and any of the experimental conditions (not shown).

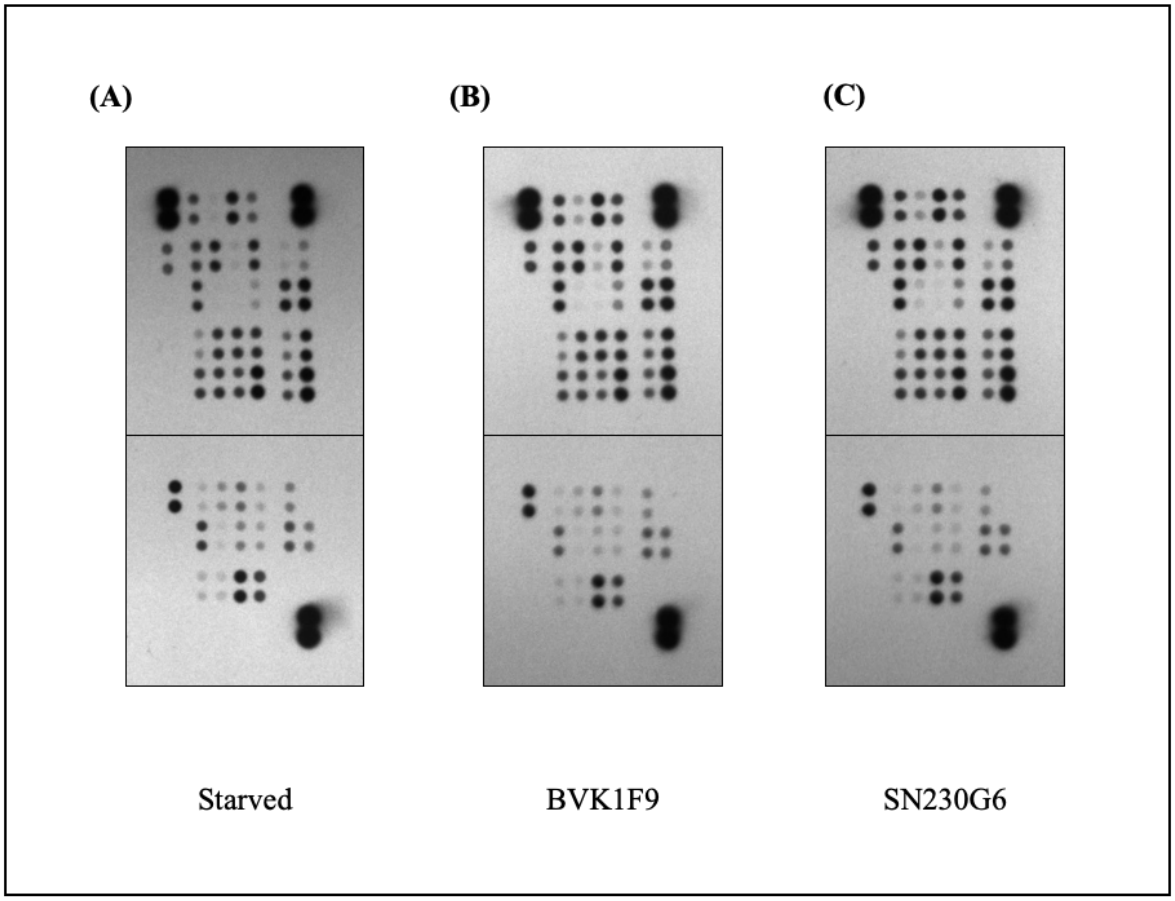

Figure 4.6. Phosphoarray analysis of endothelial cell lysates post-antibody incubation. Phospho-array analysis displaying the phosphorylation status of 43 different membrane-related human kinases after treatment of cells with binding and non-binding alloantibodies. Serum starved HAoECs (lot #422Z038) were harvested and lysed at time 0 (A, starved) or 20 minutes post-treatment with 1 µg/ml BVK1F9 (B, negative control) or 1 µg/ml SN230G6 (C, experimental). Cell lysates were assessed via phosphokinase array (Phosphokinase array kit; #ARY003B) to observe the alloantibody-reduced phosphorylation responses. Densitometry analysis of each spot was carried out using ImageJ and found to be consistent across all treatments. This experiment was repeated using cell lot #415Z025 using an additional treatment condition of 1 µg/ml W6/32, however similar results were yielded (not shown).

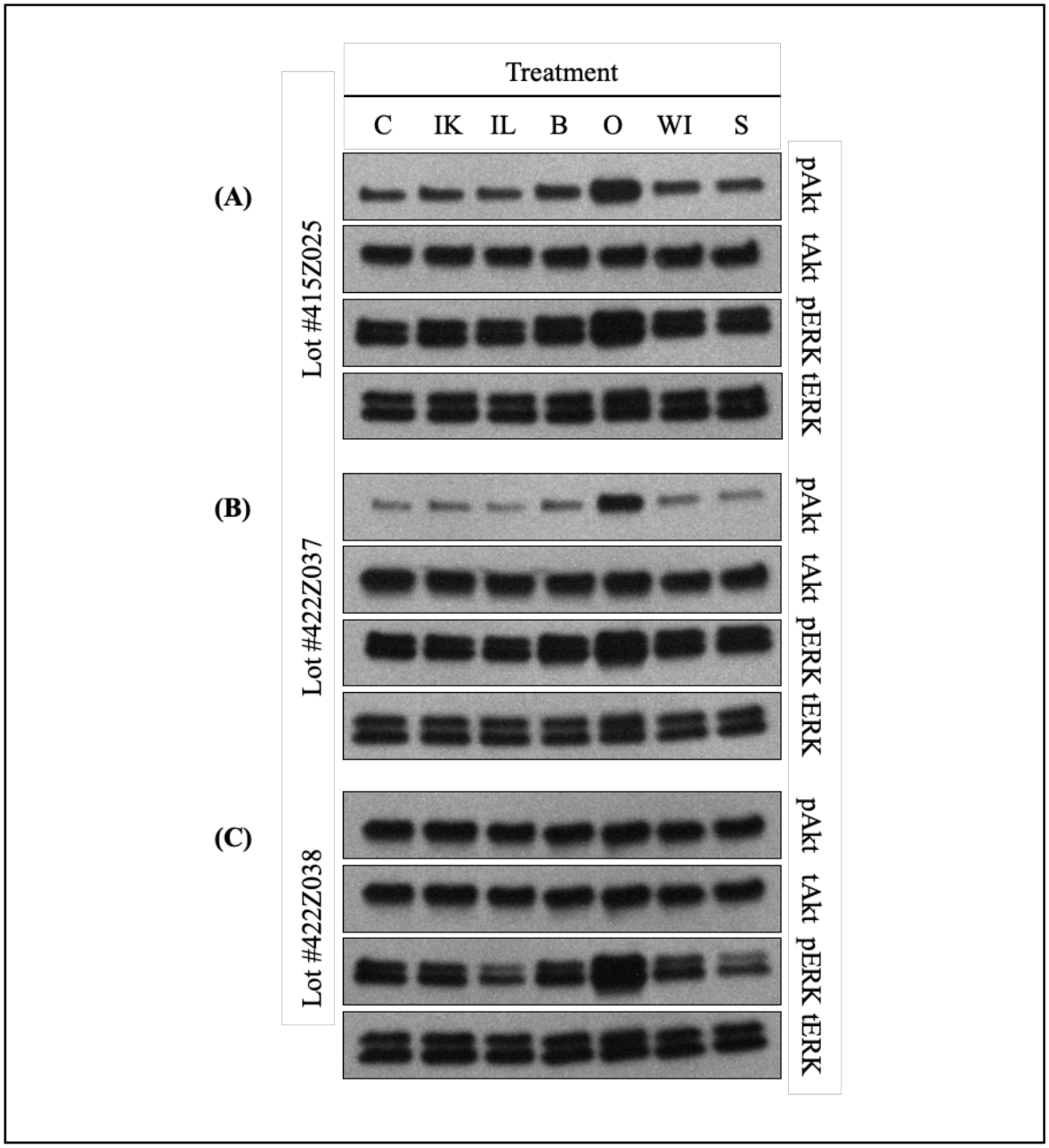

Figure 4.7. Testing the intracellular signaling response of different endothelial cell lot numbers. Three separate HAoEC cell samples from the same company yielded similar patterns of Akt or ERK phosphorylation after incubation with various alloantibodies. Serum-starved HAoECs from three different lots; (A) 415Z025, (B) 422Z037, and (C) 422Z038, were treated with either: a change of media (C), 1 µg/ml isotype control IgG1κ (IK), 1 µg/ml isotype control IgG1λ (IL), 1 µg/ml BVK1F9 (B), 1 µg/ml OUW4F11 (O, includes addition of 0.078 % FCS), 1 µg/ml WIM8E5 (WI), or 1 µg/ml SN230G6 (S), respectively, for 20 minutes prior to harvesting and lysis. Cell lysates were assessed for total expression and phosphorylation status of Akt and ERK1/2 via western blot. An increase in ERK and Akt phosphorylation was observed with addition of OUW4F11 due to the simultaneous addition of FCS. No increase in phosphorylation status of Akt or ERK was observed for any other condition as determined via densitometry analysis using ImageJ (not shown).

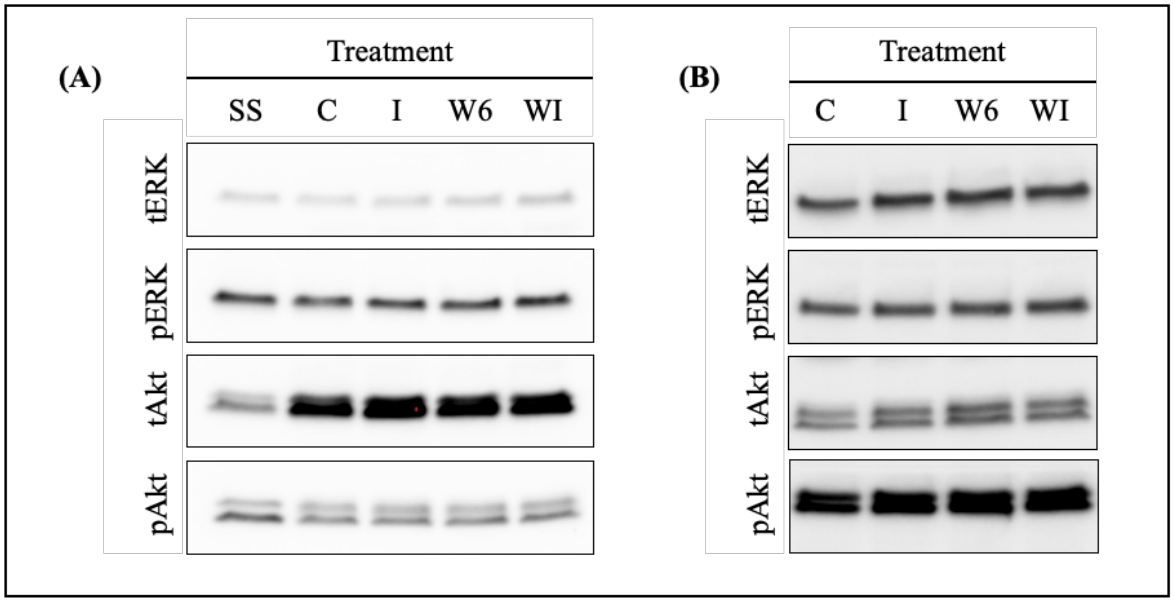

Figure 4.8. Testing the intracellular signaling response of different cell types. No differences in the in the phosphorylation status of Akt or ERK was observed within HUVEC (A) and HAoSMC (B) cells upon addition of alloantibody compared to control conditions. Serum-starved (SS) HUVECs or HAoSMCs were treated with either: a change of media (C), 1 µg/ml human isotype control IgG1 (I), 1 µg/ml W6/32 (W6) or 1 µg/ml WIM8E5 (WI), for 20 minutes prior to harvesting and lysis. Cell lysates were assessed for total expression and phosphorylation status of Akt and ERK1/2 via western blot. An increase in Akt and ERK phosphorylation was observed between starvation and treated cells, however there were no significant differences in phosphorylation status between control and experimental conditions within these treated cell groups.

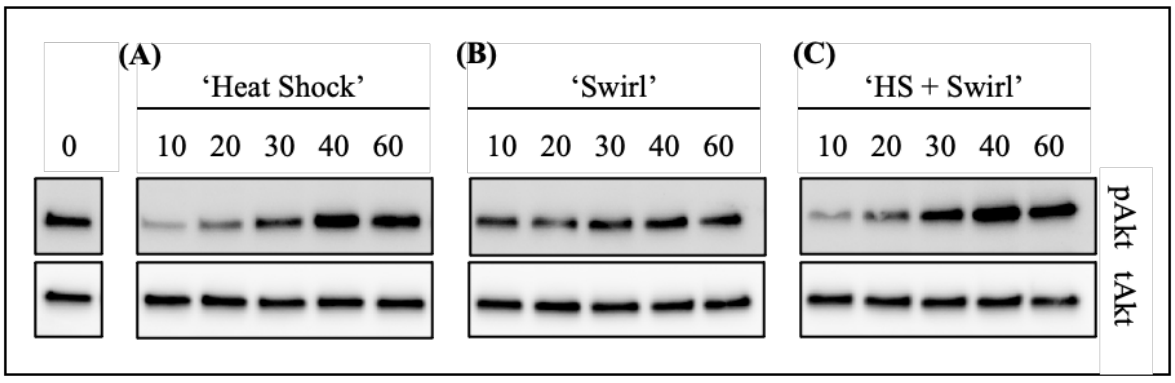

Figure 4.9. HAoECs are sensitive to changes in temperature. Removal of HAoECs from the incubator alone caused activation of the Akt pathway. To test why an increase in Akt phosphorylation was occurring in cell samples treated with a negative control, HAoECs (lot #422Z038) were starved for 6 hours and then exposed to three different physical conditions; relocation of cell dishes from the 37°C incubator to the biosafety cabinet for 2 minutes before returning to the incubator (A; 'heat shock'), swirling of media on cells within the incubator (B; swirl), or relocation of cells for 2 minutes and then swirling of media (C; 'HS'+Swirl), prior to cell harvesting and lysis. Cell lysates were assessed for total and phosphorylated Akt via western blot, where the phosphorylation status of Akt was seen to be consistently upregulated in those samples that had been removed from the incubator.

4.2.4. Assessing the Change in Cell Adhesion Markers on the Cell Surface Upon Alloantibody Binding

It was unclear whether the inability to observe activation of signalling cascades upon ligation of mAbs to cell-surface HLA was due to the technical issues of the experiment preventing the detection of subcellular activation, or whether a cellular response had not been induced. Nevertheless, in attempt to determine whether alloantibody ligation could activate alternate downstream pathways that lead to monocyte recruitment, changes in the expression of cell adhesion markers at the cell surface was selected as a valid way to assess this response [302, 304, 307, 310]. Here, HAoEC samples were assessed after treatment with alloantibodies or controls for either their total adhesion molecule protein expression in whole cell lysates via western blot, or through direct detection of cell surface molecules using FC or cell-based-ELISA. Incubation with alloantibody did not result in increased expression of P-selectin at the cell surface despite antibody ligation being confirmed via FC assays (Figure 4.10.A). This result was confirmed using cell-based ELISA, where P-selectin was detected within the internal compartments of permeabilised cells but remained unchanged from the control in treated, non-permeabilised cells (Figure 4.10.B). To investigate whether alloantibody ligation could affect the expression of cellular adhesion markers at a translational level, the total cellular expression of ICAM-I and VCAM-I was assessed over a 48-hour period post-treatment. Consistent with prior experiments, incubation with alloantibody was unable to cause a change in the cellular expression of these two cell adhesion molecules, despite upregulation of both ICAM-I and VCAM-I being attainable upon the addition of TNFα (Figure 4.11).

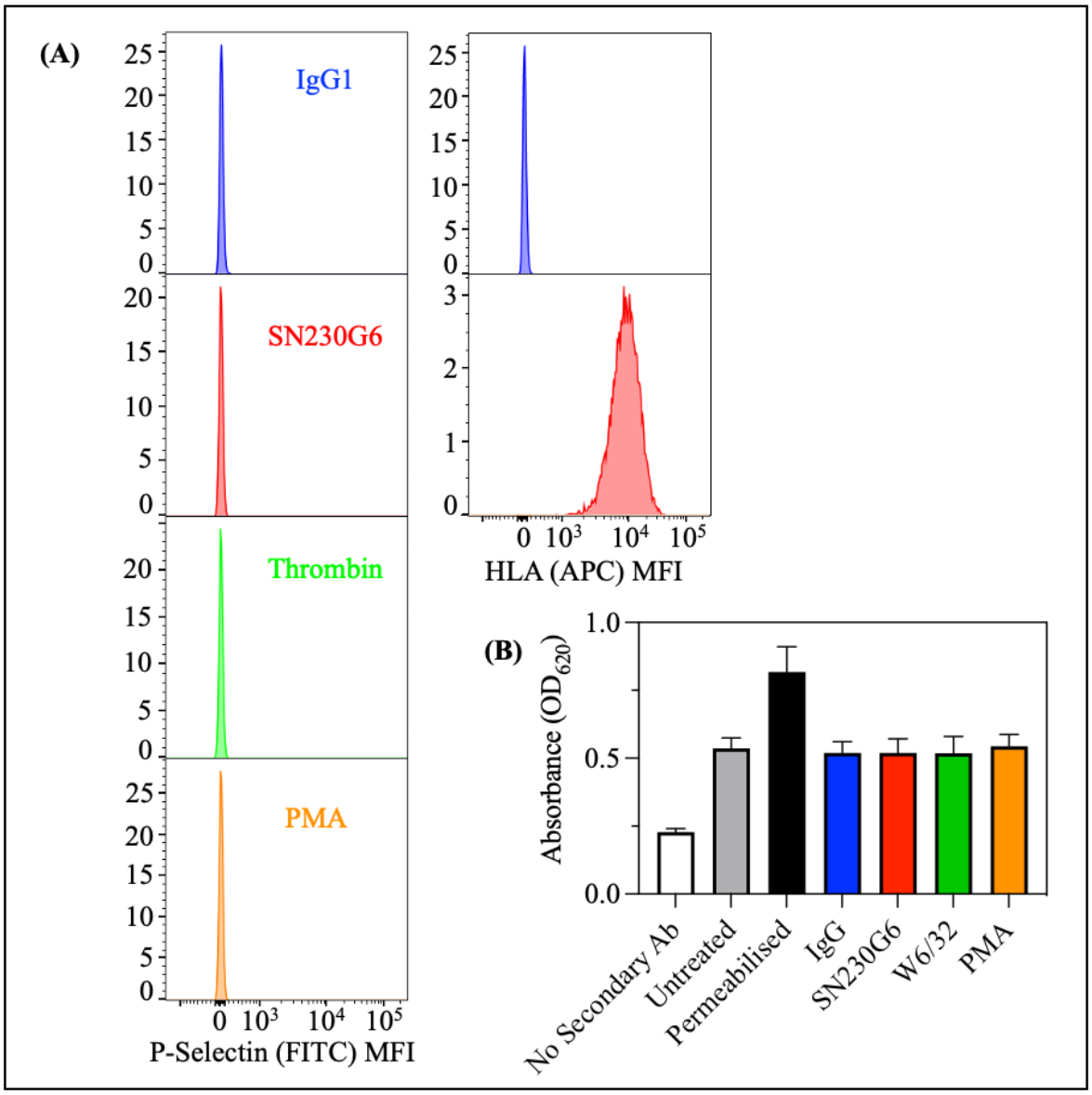

Figure 4.10. Alloantibody recognition of HLA does not affect cell surface P-selectin expression in HAoECs. Binding of alloantibody to HLA expressed on HAoECs did not induce a change in expression of P-selectin at the cell surface. A) HAoECs suspended in PBS were treated with either 1 µg/ml IgG isotype control antibody for 30 minutes (blue), 1 µg/ml SN230G6 for 30 minutes (red), 10 U/ml thrombin for 10 minutes (green), or 200 nM PMA for 20 minutes (orange) before analysis of cell surface P-selectin (anti-CD62P primary, STAR70) and cell-bound alloantibody (anti-human IgG-biotin secondary, Streptavidin-APC* detection) via flow cytometry using a similar gating strategy as outlined in appendix 11. No treatment condition, whether test or control, was seen to cause detectible P-selectin upregulation at the cell surface. B) HAoECs adhered to wells of a 96-well cell culture plate were exposed to similar conditions as in A, replacing the thrombin positive control with addition of 1 µg/ml W6/32 treatment for 30 minutes. All cells were fixed using paraformaldehyde after treatment, where cells in wells to be used for internal P-selectin quantification were then permeabilised with the addition of triton-X. P-selectin levels were assessed via cell-based sandwich ELISA (anti-CD62P primary, anti-mouse IgG-HRP secondary), where relative P-selectin levels were measured as an end-point absorbance at OD_{620} in triplicate wells. Internal P-selectin was measured in permeabilised cells, whilst no treatment condition caused upregulation to detectible levels at the cell-surface. Data presented in this figure represents over eight experiments for each assay, repeated using various cells, alloantibodies, treatment times and alternate treatment/detection antibody concentrations, all of which yielded similar results.

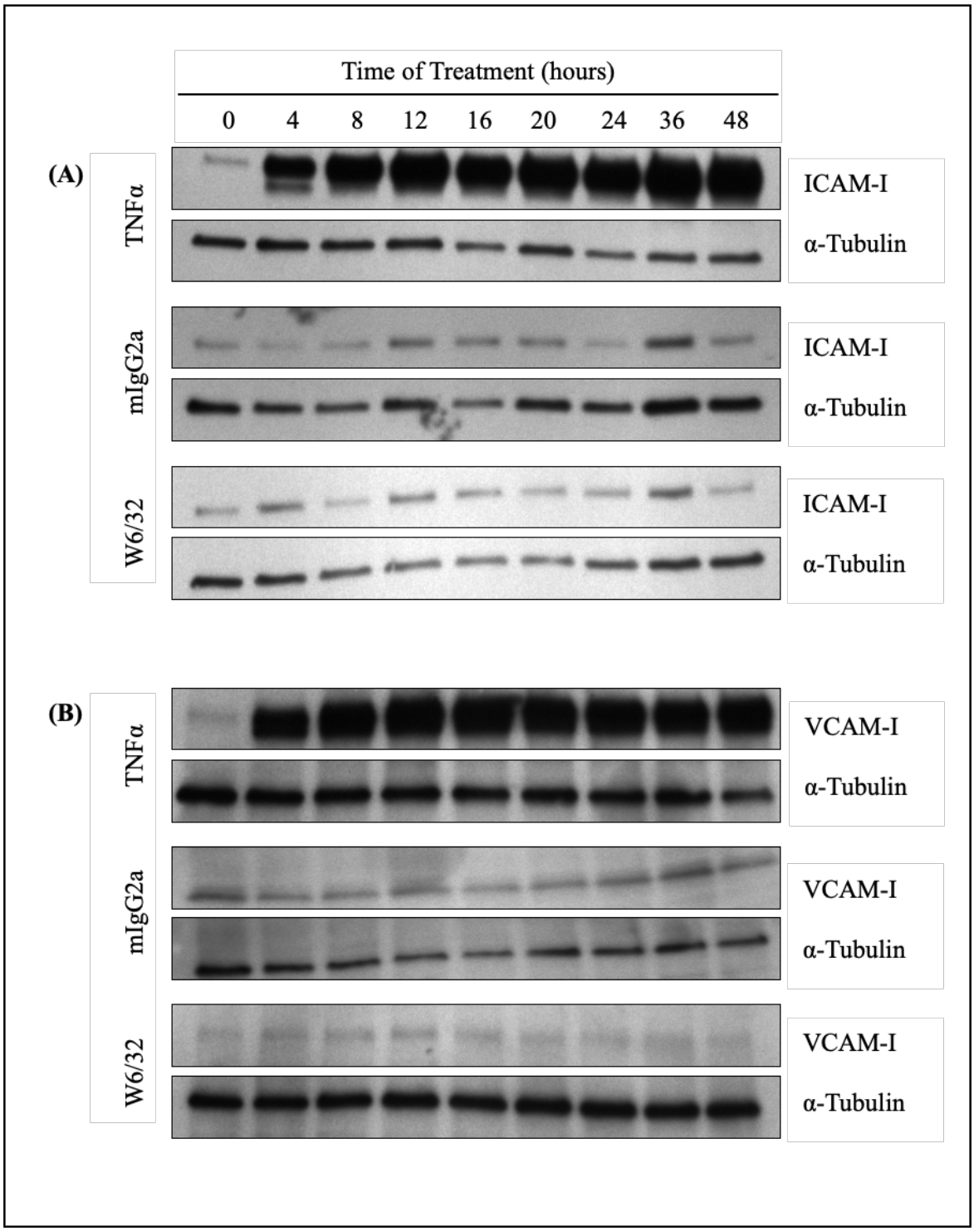

Figure 4.11. Alloantibody recognition of HLA does not affect ICAM-I/VCAM-I expression in HAoECs. There was no change in the total cellular expression of ICAM-I (A) or VCAM-I (B) within HAoECs after incubation with alloantibodies. Serum-starved HAoECs (lot #415Z025) were treated with either 10 µg/ml mouse IgG isotype control, 10 µg/ml W6/32 or 10 ng/ml TNFα (positive control), where they were harvested and lysed at various timepoints over a 48-hour period. Cell lysates were assessed via western blot for the total expression of ICAM-I, VCAM-I and α-Tubulin. TNFα was observed to upregulate ICAM-I and VCAM-I expression, however no change in adhesion marker expression was observed upon incubation with W6/32 or isotype control Abs.

4.3. Discussion

4.3.1. Chapter Overview

Endothelial cells (ECs) located on the intima of blood vessels lie at the interface between the bloodstream and smooth muscle cells of the vessel wall where they act as a selectively permeable barrier that organises the growth and development of the surrounding connective tissues [317]. Here they also function as the "first responder" to environmental stimuli within the blood, where their activation may be integral to activation of the innate immune system [318-319]. The aims of this chapter explore the capability of alloantibodies to induce various sub-cellular responses, and to understand how the antibody's affinity may affect the magnitude of the response generated. Throughout this chapter, the use of primary human aortic endothelial cells (HAoECs) as a model to map the cellular response upon AlloAb-HLA interaction formation was unsuccessful. Despite efficiently being able to isolate vascular endothelial cells originating from porcine tissue, achieving this with human aortic tissue proved to be problematic. Using HAoECs acquired commercially, it was possible to demonstrate the ability of mAbs to recognise HLAs on the surface of these cells, however the capacity of this interaction to activate subcellular phosphorylation signalling pathways under a range of conditions was non-evidential. Further to this, the ability of this interaction to alter the expression of cell adhesion molecules at the cell surface was also lacking, despite positive controls clearly demonstrating cellular upregulation. Upon further experimentation it was uncovered that a variety of these commercial cells were extremely sensitive to environmental conditions, where unavoidable changes in temperature that occurred during general cell culture procedures were enough to induce Akt/ERK phosphorylation, irrespective of Ab-HLA ligation. Overall, despite significant effort to address the subjects in the main aims, the inability to acquire a suitable cell model for these experiments prevented the aims from being achieved.

4.3.2. Selection of Cells to Model Alloantibody-HLA Interactions

Endothelial cells are widely used as a tool in biomaterial research due to their natural physical location at the interface of tissue and biological fluids [320]. In the context of immunology, vascular endothelial cells are a useful model to evaluate immune responses as they bridge the

gap between innate and adaptive arms of the immune system by acting as sensors that respond to pathogens and molecular damage signals, whilst also being able to act as APCs in an inflammatory setting [319, 321]. The use of HAoECs as a model was selected based previous studies carried out by Reed et al., who have heavily documented these cells to become activated upon antibody ligation, resulting in proliferation, migration, activation of downstream signalling events as well as many other cellular responses [282]. The use of primary cells for these studies was essential due to the caveats surrounding loss of endothelial cell characteristics following multiple passages [322, 323]. When choosing a cell sample to model a specific alloantibody-HLA interaction, it is important to select cells carefully to prevent any unwanted signals from off-target interactions. To do this it needs to be ensured that the HLA target is the only expressed antigen that can be recognised by the antibody under investigation. One limitation with this study is the inability to select the donor tissue type, meaning the isolation of donor cells expressing a target of interest comes down to a matter of chance. Within these studies, cells which express HLA-A*02:01 were selected as a model. Since HLA-A*02:01 is the most commonly expressed HLA-A allele within the donor population [324, 325], the ability to acquire donor tissue and/or commercially isolated cells which expressed HLA-A*02:01 was relatively easy. However, this may become an issue when modelling antibody interactions with rarer HLA molecules as cells expressing these antigens may be harder to acquire. Given the cross-reactive nature of antibodies and the variable expression of HLA per individual, the ability to characterise an isolated alloantibody-HLA interaction may require a primary donor cell library from which the specific cells can be selection from. Considering the rate of donor tissue acquisition throughout these studies, establishing such a library may take a long time, but if obtainable would provide a very useful possession that may open many pathways to research and further collaboration.

4.3.3. Primary Endothelial Cell Isolation

Using published methods for primary EC isolation as a reference [284, 321, 323, 326-332], the possibility of establishing a reliable method to acquire these cells was explored. Endothelial cells were successfully isolated from porcine renal arteries and maintained in cell culture. Isolated ECs had the characteristic squamous, cobblestone morphology and formed single layer sheets which could be propagated over multiple passages [330]. This method proved to be challenging when translating into tissues of deceased human origin, where only two of the twelve donor tissue samples used within these studies were found to yield isolated cells that

were displayed the endothelial CD31-expressing phenotype. Many of these samples were from donors of old age, where the tissue samples provided were observed to contain vast regions of vascular calcification and atherosclerotic plaques. Nevertheless, these successfully isolated cells were minimal in number and were observed to rapidly lose their characteristic endothelial traits in the days following isolation. Besides donor sample quality, prolonged ischaemic times (up to 12 hours) between harvesting and isolation may have contributed to low cell yield, as ischaemia has been related to autophagy, endothelial permeability, and dysfunction [333, 334].

The EC microenvironment generated by their location, intracellular signalling and intercellular cross-talking with other cell types has been shown define EC phenotypic and genetic characteristics, which also plays a major role in disease pathogenesis [335-338]. Cells isolated within this study could only be obtained at low seeding density, where the inability of these cells to establish cell-to-cell contacts and produce the chemical environment necessary for endothelium to thrive may have prevented them from maintaining their endothelial characteristics, despite the addition of many growth factors that intended to provide these signals. This loss of endothelial morphology may also be due to the cells undertaking a mesenchymal morphology through endothelial-to-mesenchymal transition (EndMT), a process which has been implicated in various wound healing responses and angiogenesis [339-342]. To determine whether EndMT was a factor that influenced this change in morphology, further phenotypic characterisation of these differentiated cells would need to be carried out. Endothelial cell differentiation may also be induced *in vitro* by exposure to fibroblast-derived soluble factors in endothelial cell and fibroblast co-cultures, where the ECs can be observed adopt an elongated spindle-shaped morphology [343]. Since the methods used to isolate endothelial cells in this chapter do not include any positive or negative cell selection steps, the contamination of cultures with fibroblast cells cannot be ruled out.

4.3.4. Commercial Endothelial Cell Activation

Throughout this study, commercially acquired cells were received at passage 2 and cultured to passage 4 using the recommended protocols prior to experimentation. Upon treatment, these cells were consistently shown to become activated, where a similar degree of kinase activation could be observed in both experimental and control conditions. This was discovered to be a result of the change in physical conditions during the treatment process, where the act of transferring cells from a 37 °C incubator to the biosafety cabinet at room temperature (roughly 20°C) and then back to the incubator enabled an increase in phospho-ERK and phospho-Akt

to be observed. Besides initiating immune responses, endothelial cells also play an important role in vascular tone. Here they are known to activate various pathways to release numerous vasoactive factors in response to changes in internal body temperatures that may result in vasodilation and vasoconstriction of the vessels [344], respectively, to regulate blood flow within the body to maintain an optimal 37 °C. One reason for not observing the response to antibody ligation could be that the magnitude of kinase phosphorylation caused by changes in temperature may have surmounted the signalling effect of mAb binding, preventing the antibody-induced response from being detected.

In the experiments presented here, it is difficult to ascertain whether kinase phosphorylation is caused by the cooling of cells when kept at room temperature or by the subsequent re-warming of them once returned to the heated incubator. *In vitro*, endothelial cells have been shown to be sensitive to hypothermia, where decreases in temperature have been shown to activate various cryoprotective genes and prevent the activation of extrinsic and intrinsic apoptotic pathways [345]. Other studies also show that cooling of cells may lead to injury if the temperature falls below that of the membrane-phase transition temperature [346]. Junctional-Adhesion-Molecule-A (JAM-A) expression has been shown to be modulated upon cooling and re-warming, where upregulation can be observed in the re-warming phase [347]. Contrary to my findings, JAM-A has also been implicated with inhibition of Akt signalling [348], however this may also offer a potential reason as to why this Akt phosphorylation signal was not observed upon antibody ligation. Furthermore, post-hypothermic re-warming has been demonstrated to activate the NF-κB pathway in response to ROS production [349]. Studies carried out my Valenzuela et al. have shown the ability of HAoECs to elicit exocytosis upon alloantibody ligation which results in the upregulation of P-selectin to aid in monocyte recruitment [304]. This data could not be reproduced in my studies, where the ability of antibody ligation to upregulate cell surface adhesion molecules ICAM-I and VCAM-I was also not observed. Whilst hypothermic conditions may have prevented the antibody-ligation related phosphorylation events from being measured, exposure of endothelial cells to low temperatures has been shown to induce ICAM-I and VCAM-I expression [349]. The inability of these HAoECs to regulate cell surface adhesion molecules upon decreasing temperatures may suggest an alternative reason that may explain the lack of response to alloantibody ligation, such as endothelial dysfunction [350, 351].

Although the use of commercial HAoECs has been documented throughout the literature, detailed information regarding the specific procedures used to isolate these cells is scarce. Furthermore, the inability to understand the reason for this lack of response to alloantibody ligation raises questions with regards to the reproducibility of experiments involving these cells. The experiments carried out on commercially bought cells in this chapter involve cells sourced primarily from one supplier, PromoCell GmbH. Although HAoECs from this supplier have been used to map various signalling pathways [352, 353], the use of these cells to model the effect of mAb binding on cellular responses has not been documented and so it is unknown whether this specific supplier provides cells that are a good model for these studies. Since cellular activation in response to changes in temperature was also observed in other cell types purchased from this vendor, there are questions surrounding the methods used in their isolation procedures and how this may affect the sensitivity of the cells. One more caveat to using commercially bought cells to study alloantibody-HLA interactions is that the cells are generally not HLA-typed, further emphasising the issues raised in the section 4.3.3. Overall, the commercial cells purchased to observe effects downstream of antibody-HLA ligation were inapt. Should these cells be used for further studies then the cause and effects of temperature sensitivity would need to be investigated.

4.3.5. Conclusion

In conclusion, this chapter highlights many of the issues that may be faced when trying to establish a relevant primary cellular model for *in vitro* studies. Although purchasing cells may avoid the limitations that come with isolating cells manually, the unknown methods used in commercial procedures may limit the understanding of the cell status. To continue with this study, a different source of endothelial cells would need to be found and/or an efficient, reproducible protocol for isolation of endothelial cells would need to be established.

Chapter Five

Microfluidic Antibody Affinity Profiling – Developing a Novel Assay for In-Solution Characterisation of Alloantibody-HLA Interactions in Serum

5.1. Introduction

The development of clinical methods designed to characterise antibodies, including ways to detect, visualise and quantify interactions, have assisted in developing our understanding about the many roles and specialised functions of antibodies in both health and disease. Having information on a patient's antibody repertoire ready and available at the point of patient assessment may be useful to clinicians to help inform them on a patient's molecular traits, to aid in clinical diagnosis, whilst also helping to improve the clinical decision-making process. In the transplant setting, characterisation of a recipients DSAs is currently done through several semi-quantitative methods which do not allow for absolute quantification of the antibody's parameters, which brings about discrepancies when interpreting the output data [204, 209]. The work described in chapter 3 of this thesis gives evidence to suggest that the affinity of an alloantibody-HLA interaction may relate to the antibody's pathogenic potential, and so may be informative in conjunction with current immunoassay outputs.

Biophysical methods such as surface plasmon resonance, biolayer interferometry, isothermal titration calorimetry etc. [354], have been developed to enable the kinetic assessment of protein-protein interactions (PPIs), however many of these methods come with caveats that limit the ability to quantify interactions in the presence of human serum. The contribution of non-specific binding, availability of epitopes (in terms of methods that rely on immobilisation), and lack of information with regards to the concentration of target-specific Abs within a serum sample, prevent the reliable quantification of serum antibody-antigen interaction kinetics without the need for sample preparation which can consume vast amounts of time, money, and reagents. To enable this information to be made readily available in clinical practice, a novel method to quantify Ab-HLA interactions in serum without the need for extensive antibody sample preparation needed to be established.

To explore whether such a method could be developed, firstly a platform needed to be selected in which the assay could be designed around. The use of microfluidics has revolutionised the field of science, where it has been incorporated into many research technologies to enable the accurate measurement of various sample properties using micro-scale volumes. Using the principles of microfluidic streams, Einstein relation, and Stokes Law, a novel platform called microfluidic diffusional sizing (MDS) was developed by Prof. Tuomas Knowles' group within the University of Cambridge Department of Chemistry, for the sensitive and accurate measurement of a protein's hydrodynamic radius (R_H) under native solution conditions [355]. This method exploits the fact that the rate of molecular diffusion in a defined volume correlates with the size of the molecule of interest. This size is dependent on the molecular weight, secondary structure, tertiary structure, aggregation, and the formation of interactions with other species. The original research suggested that MDS can be used to probe highly heterogeneous protein complexes and to characterise protein-protein interactions [355]. This novel technology was then implemented into a commercially developed instrument (Fluidic Analytics Ltd, Cambridge, UK) to enable rapid characterisation of specific biomolecular interactions in a quantitative manner without the need for purification or immobilisation of protein to a surface [356].

In comparison to flow-induced dispersion analysis (FIDA), which measures the axial spreading of bulk molecules due to both diffusive and convective aspects of Taylor-Aris's dispersion [357], MDS observes the ability of individual labelled molecules to diffuse across the axis between a sample stream and into a parallel auxiliary stream under controlled, steady-state

laminar flow (Figure 5.1). After allowing for diffusion of molecules to occur between the two streams, each stream is then split from the other where their fluorescence intensities are then measured and used to calculate the ratio of diffused versus non-diffused molecules. Larger molecules are expected to diffuse less than smaller molecules and so would yield a lower diffusion ratio. Using this diffusion ratio, it is then possible to decipher the average hydrodynamic radius (R_H) of the fluorescently labelled molecules according to Stokes-Einstein and Einstein-Smoluchowski equations (Appendix 12). In terms of PPI kinetics, this method also enables non-covalent interaction affinities to be calculated through quantification of the change in a labelled protein's R_H upon gradual titration of an unlabelled interaction partner [358]. The K_D of this interaction can then be measured as the concentration of unlabelled protein which yields a size increase of fifty percent response between the measured size of the labelled protein and the size of the protein in complex with its partner. Since this method of interaction affinity determination uses the read-out from a fluorescent label in solution, this eliminates many of the current limitations concerned with ligand immobilisation that prevent the quantification of PPIs in complex buffers such as serum, opening the door for the application of this technology for the clinical assessment of antibodies.

This chapter provides an exploration into how the principles of the MDS method may offer an alternative, quantitative approach to characterising alloantibodies that are present in human sera. An investigation into how MDS can be used to detect the presence of Ab-Ag binding and quantify the interaction strength was performed using several extensively characterised AlloAb-HLA interactions. Since the active concentration of antibody within a serum sample is needed for quantification of antibodies in patient serum samples, I then examined how MDS analysis can be used to develop an original, innovative method for absolute quantification of antibody parameters within non-purified antibody samples, these being the affinity the antibody has for its antigen and the concentration at which the antibody is present. To validate this method and to provide preliminary information on its applicability in the clinical setting, the assay was used to characterise a selection of patient serum samples that have previously been determined to have reactivity against HLA class I and II antigens. Finally, a brief proof-of-principle study was carried out to assess the potential of this method to provide useful information about a patient's HLA-specific antibodies that may be used in clinical decision making.

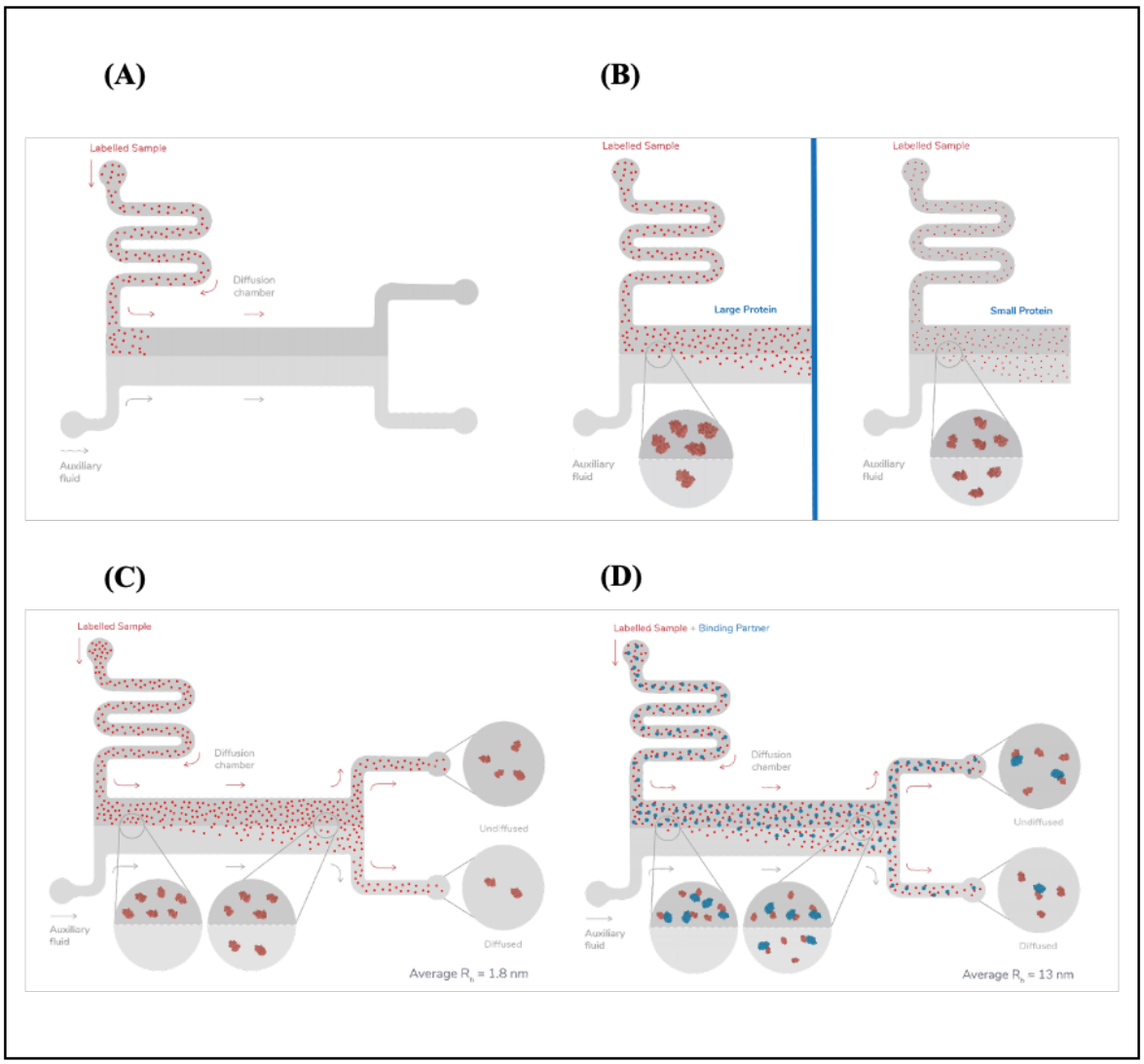

Figure 5.1. Principles of microfluidic diffusional sizing. (A) Two streams are introduced into the diffusion chamber under laminar flow: one containing the fluorescently labelled protein and an auxiliary stream. (B) Streams flow in parallel with no convective mixing. This allows for diffusion of the fluorescent molecules from the sample stream across into the auxiliary stream, where smaller molecules diffuse more than larger molecules. (C) At the end of the diffusion chamber the streams are split, where the amount of protein in each chamber is quantified using fluorescence readouts. These fluorescence readings are used to calculate the rate of diffusion, which is then used to calculate the fluorescent protein's hydrodynamic radius. D) By introducing a binding partner to the fluorescently labelled protein sample, the degree of binding can be calculated by measuring the change in rate of diffusion/size. Titrating the binding partner in consecutive measurements can be used to calculate the interaction affinity. Reproduced from: Fluidic Analytics. What is Microfluidic Diffusional Sizing (MDS)? 2019 [Available from: https://www.fluidic.com/resources/what-is-microfluidic-diffusional-sizing/.]

5.2. Results

5.2.1. Fluorophore Labelling and Purification of Recombinant HLA Molecules

MDS tracks the change in R_H of HLA upon antibody binding in the presence of human serum. To carry out measurements of R_H using the MDS platform, the protein of interest needed to be fluorescently tagged for optical detection. Alexa Fluor 647 (AF647) was selected as the fluorophore of choice since the autofluorescent signal of human serum was measured to be minimal within the far-red region of the visible light spectrum (Appendix 13). Using amine-reactive crosslinker chemistry (Figure 5.2.A), it was possible to successfully create a stable amide-bond that crosslinked the amine-reactive N-hydroxysuccinimide (NHS) ester group on a AF647 dye to the primary amines within HLA molecules. This reaction yielded two distinct peaks following gel filtration representing the labelled protein and excess dye, respectively (Figure 5.2.B). The molecular labelling ratio for labelled proteins was between 0.82-1.42 dye per HLA protein (excluding HLA-A*03:01) (Appendix 14).

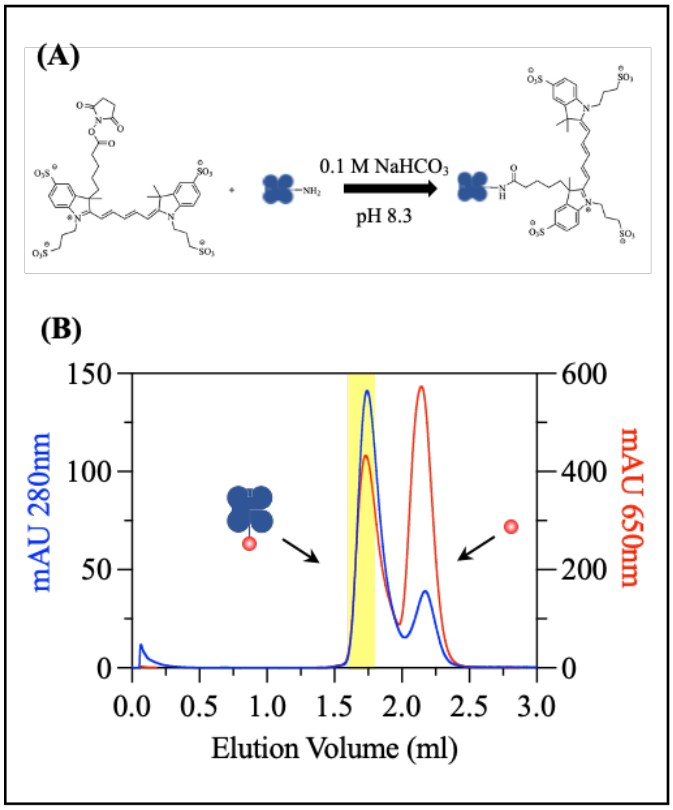

Figure 5.2. NHS ester chemistry enables successful labelling of HLA proteins. (A) The reaction scheme detailing the process of HLA labelling. The addition of an N-hydroxysuccinimide (NHS) ester group-containing fluorophore to HLA in 200 mM sodium bicarbonate buffer, pH 8.3 results in carbodiimide-activation of carboxylate molecules. This produces an amide bond between the ester group on primary amines via nucleophilic substitution. (B) After incubation, the labelling reaction was purified using size exclusion chromatography, yielding two distinct peaks representing the AF647-labelled HLA (first peak) and unbound free label (second peak). The displayed chromatogram is HLA-A*11:01, where yellow shading represents pooled fractions used for further experiments.

5.2.2. Assessing the Sensitivity of the MDS Method

Selecting a suitable concentration of labelled protein to be used in an experiment is based on two criteria: A) The expected affinity of the interaction, and B) the fluorescent signal of a protein at any chosen concentration. Since the total fluorescent signal emitted from a sample is correlated to the concentration of protein within that sample (Appendix 15), which is in turn determined by the degree to which the protein is labelled, it is important to ensure that the protein concentration selected gives a signal that can yield reliable R_H outputs. By measuring the size of HLA at various concentrations it was evident that class I HLA proteins consistently measured at ∽3.2 nm down to 1 nM (Figure 5.3), in agreement with what is expected for a natively folded ∽55 kDa protein [359, 360].

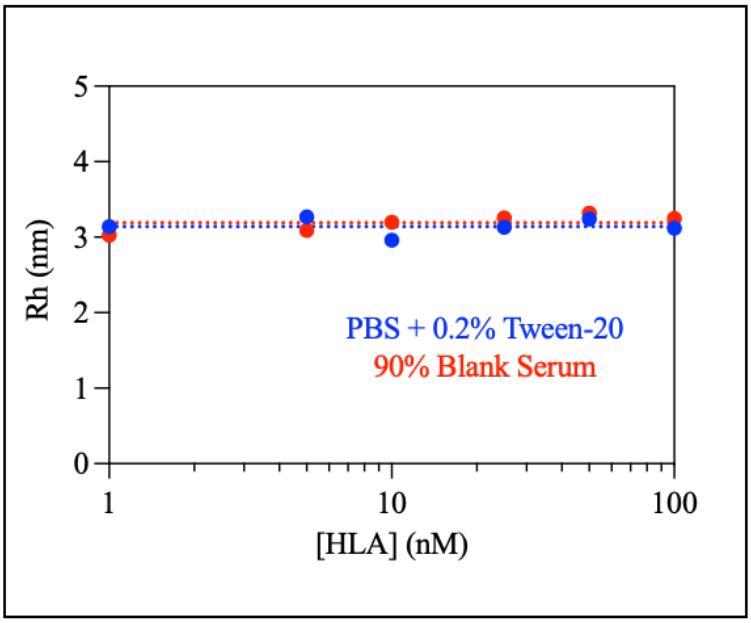

Figure 5.3. HLA-A*11:01 sizes similarly in blank buffer and in the presence of serum via microfluidic diffusional sizing. Taking MDS measurements of AF647-labelled HLA-A*11:01 at concentrations between 1 nM and 100 nM yields similar R_H measurements in the presence of PBS + 0.2% tween-20 or 90% blank human serum from a non-sensitised male. Symbols signify individual MDS measurements taken for each point. Dotted lines represent the mean R_H across all HLA concentrations measured within each buffer.

5.2.3. Sizing Alloantibody-HLA Complexes

The occurrence of a protein-protein interaction can be detected using MDS by observing a significant effective increase in R_H of a labelled protein upon ligand addition. To validate whether AlloAb-HLA interactions are suitable for this method of detection, the ability to observe the binding of the mAb WIM8E5 to its native priming antigen HLA-A*11:01 was investigated (Figure 5.4). The measured effective R_H of HLA-A*11:01 upon addition of 1 µM WIM8E5 IgG was found to double from 3.2 nm to around 6.4 nm, suggesting formation of the A*11:01-WIM8E5 IgG complex. When incubated with WIM8E5 Fab portions, the measured effective size increase of A*11:01 by 1.1 nm, up to 4.3 nm, was significantly less than that of IgG due to the smaller molecular weight of Fab molecules. When examining the pattern of rising R_H upon increasing ligand concentration, in both cases over 80 % of the effective size change can be observed with addition of 1 nM and 100 nM ligand. This suggests that the affinity of both interactions may fall between these two concentrations.

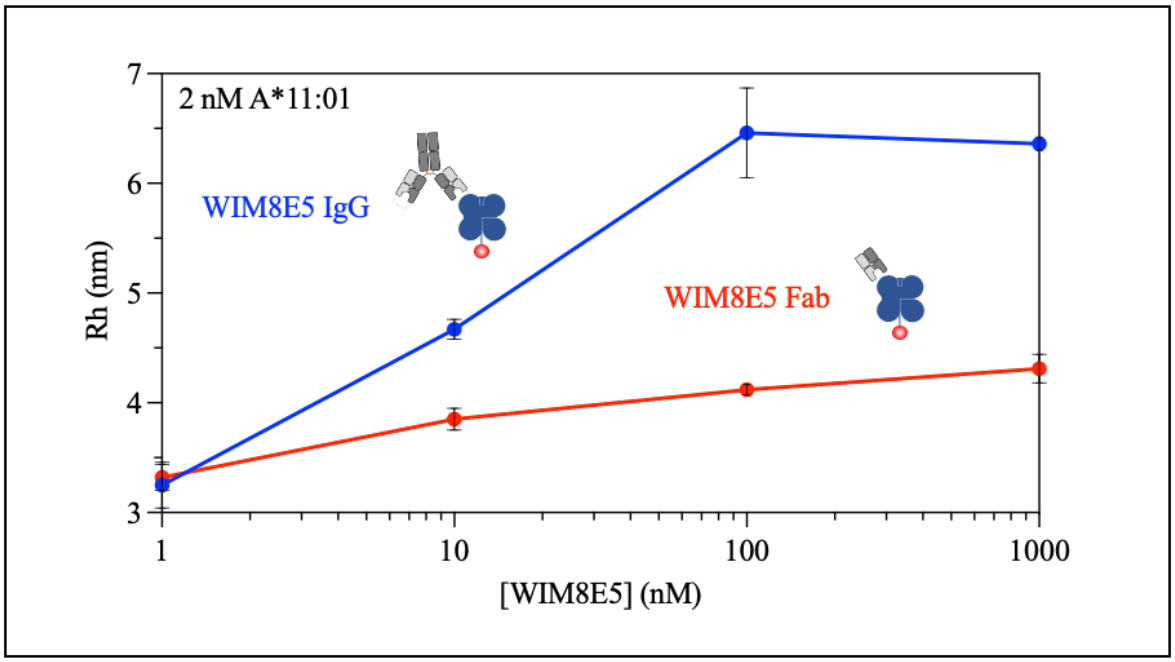

Figure 5.4. Binding of WIM8E5 IgG and WIM8E5 Fab to HLA-A*11:01 can be detected by microfluidic diffusional sizing. Incubation of 2nM fluorophore-labelled HLA-A*11:01 with WIM8E5 IgG (blue) or WIM8E5 Fab (red) causes an effective increase in the hydrodynamic radius of A*11:01 as measured by microfluidic diffusional sizing. Both WIM8E5 species bind in a concentration-dependent manner, where the measured R_H of the A11-IgG complex is significantly larger than that of A11-Fab, consistent with the differing sizes of each WIM8E5 molecule. Symbols represent the mean of triplicate MDS measurements for each point, where error bars represent the ±SD.

5.2.4. Determination of Interaction Affinity, Stoichiometry and Cooperativity via MDS

To explore the extent to which an AlloAb-HLA interaction could be characterised using this method, the interaction of HLA-A*11:01 with WIM8E5 was assessed using an equilibrium binding curve in PBS buffer (Figure 5.5.A, blue). Titrating WIM8E5 IgG against 2 nM HLA-A*11:01 enabled an affinity of 9.0 (± 5.6) nM to be measured. To verify the 1 to 2 (Ab to Ag) binding ratio as a result of immunoglobulin's two antigen binding sites, saturation binding curves were produced by using HLA-A*11:01 at >10-times the calculated K_D concentration [361] (Figure 5.5.C). As expected, the concentration of WIM8E5 IgGs needed to saturate 100 nM HLA-A*11:01 binding sites was ∽50% (58 nM), confirming the 2:1 stoichiometry and bivalent nature of WIM8E5 IgG. When measuring the affinity of multivalent interactions, it is also important to establish the cooperativity of the relationship between the interactions that occur at each binding site. Assessing the binding data via Hill plot yielded a Hill coefficient of ∽1 (0.8231-1.574 95% C.I.; Figure 5.5.B.), suggesting that interactions established at each IgG Fab arm occur independently of one another and show no cooperative relationship, where the affinity of each interaction that forms at either binding site should be equal.

To validate these findings, the WIM8E5-A*11:01 interaction was analysed using BLI, where the affinity of WIM8E5 IgG to non-labelled HLA-A*11:01 was measured within a similar range to that of the MDS method, at 19.2 (± 0.2) nM (Figure 5.5.E). To further corroborate this evidence, binding and saturation curves were produced by replacing whole IgG WIM8E5 with WIM8E5 Fab portions. The interaction was measured to have an affinity of 5.4 (± 1.4) nM via MDS (Figure 5.5.A, red), where 100 nM HLA-A*11:01 required around equal quantities (92 nM) of Fab to reach the saturation point (Figure 5.5.D), confirming the expected 1:1 stoichiometry of HLA to monovalent Fab. Measuring the interaction of WIM8E5 Fab with HLA-A*11:01 via BLI also confirmed the affinity measurements obtained using MDS, where it was measured to have a comparable K_D of 7.4 (± 0.07) nM (Figure 5.5.F). Finally, to ensure that these affinity measurements could be acquired for other alloantibody-HLA interactions, binding curves were successfully produced for a further four interactions involving different antibodies against their reactive AF647-labelled HLAs (Figure 5.6). The measured affinities of these interactions ranged from 5.2-125.1 nM and also agreed with the affinities as measured by BLI (not shown). This validation gives further evidence to verify the application of the MDS method for AlloAb-HLA interaction affinity determination.

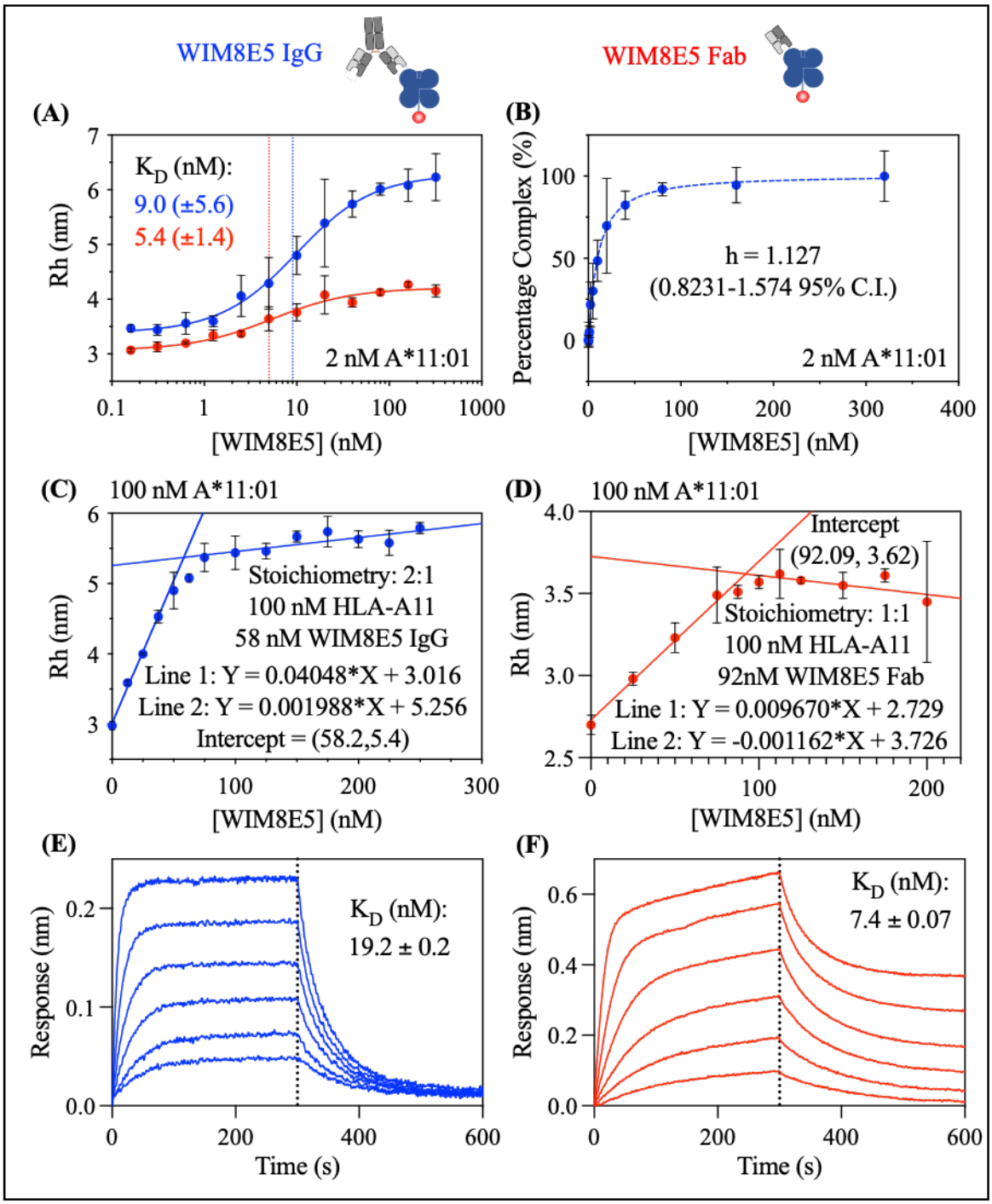

Figure 5.5. Microfluidic diffusional sizing enables the fundamental properties of alloantibody-HLA interactions to be measured. The application of MDS measurements to biophysical analyses permitted the affinity, stoichiometry and cooperativity of A*11:01-WIM8E5 binding to be determined in PBS-T buffer. AF647-HLA-A*11:01 was assessed via MDS in the presence of of a two-fold dilution series of WIM8E5 IgG (blue) or Fab (red) to quantify their interaction affinities (A) and binding stoichiometries (C, D). Both interactions were found to have comparable affinities of 9.0 (±5.6) and 5.4 (±1.4) nM, respectively. WIM8E5 IgG and Fab bound HLA-A*11:01 with stoichiometries of 2:1 and 1:1, respectively. WIM8E5 IgG showed no cooperative between the binding events at its distinct Fab regions against HLA-A*11:01, meaning the binding event at each Fab region occurs independently of one another (B). The affinities measured by MDS were validated using biolayer interferometry, where global fitting was applied to the sensorgrams produced in E-F using a 1:1 stoichiometry model to calculate the interaction K_D as a function of k_{off}/k_{on}. Symbols in A-D represent the mean of triplicate MDS measurements for each point, where error bars represent the ±SD.

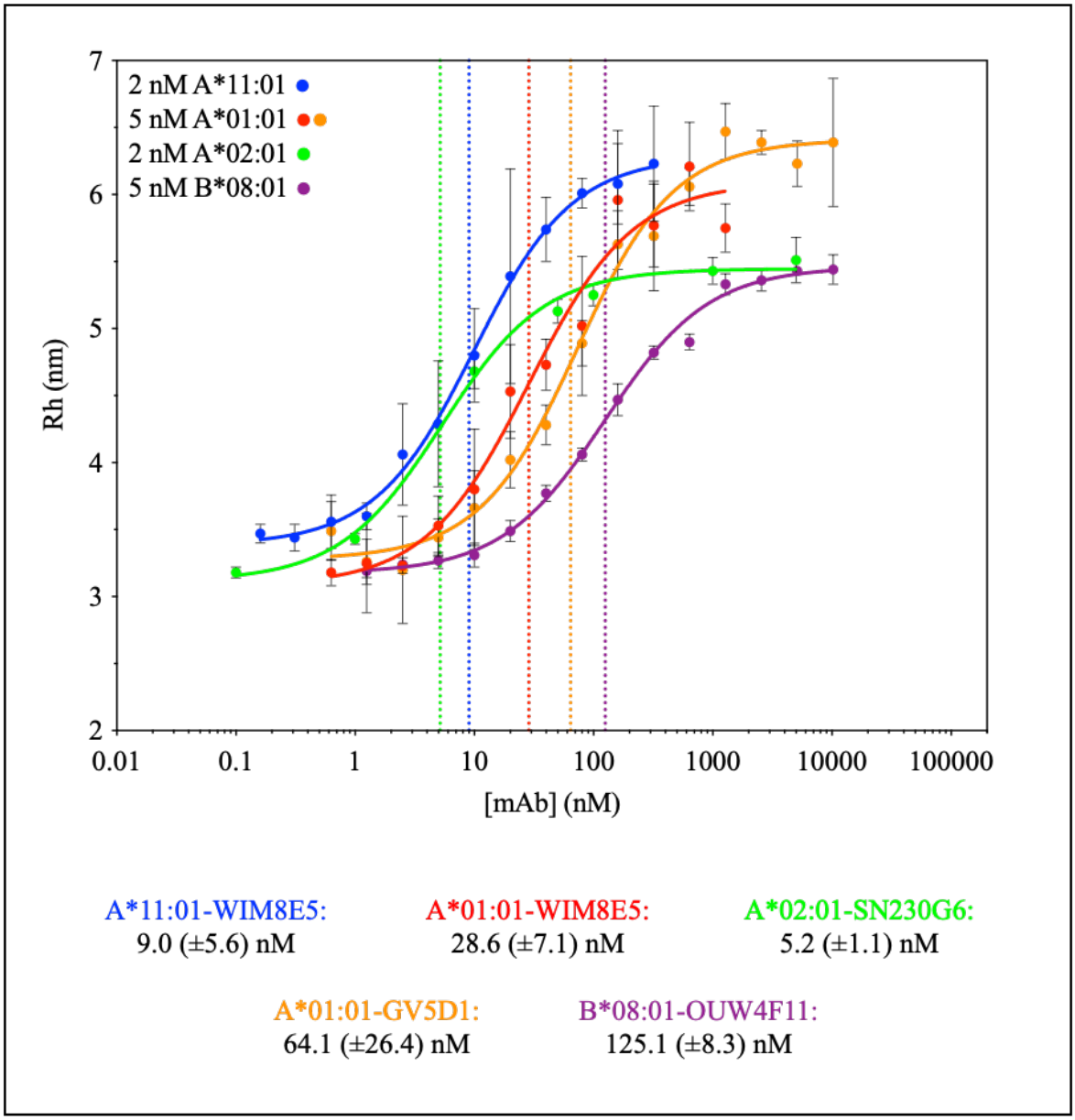

Figure 5.6. Measuring the affinities of various alloantibody-HLA interactions via microfluidic diffusional sizing. AF647-labelled HLA-A and HLA-B antigens were assessed via equilibrium binding curve using various HLA-specific monoclonal antibodies to determine the interaction binding affinities. HLA molecules were incubated with two-fold dilutions of monoclonal antibodies in PBS + 0.2% Tween-20 and were analysed via MDS. The affinities (K_D) of each interaction could be determined as the concentration of mAb which yielded 50% of the maximum response. Calculated K_Ds spanned 5-125 nM, displaying the possible range of interaction affinities that could be determined using MDS. Symbols represent the mean of triplicate MDS measurements for each point, where error bars represent the ±SD.

5.2.5. Affinity Measurements in Serum Require Background Fluorescence Signal Subtraction

Selecting the concentration of labelled protein to use when assessing an interaction is particularly important when incorporating complex media such as human serum into samples, as natural aromatic compounds that can be stabilised by the presence of serum albumin, such as bilirubin, may produce a natural fluorescent signal [362, 363]. Any autofluorescence given off by the media that is not accounted for may become integrated into the raw fluorescence measurements which may influence the output R_H measurements due to an apparent alteration of the diffusion ratio.

MDS measurements of HLA in the presence of 90% serum caused an apparent decrease in the size of HLA when compared the R_H as measured in PBS (Figure 5.7, blue and black, respectively). This discrepancy is caused by the inclusion of background serum fluorescence in MDS measurements, where this effect is enhanced at lower protein concentrations due to a decreased signal/noise ratio. To account for this unwanted background fluorescence, a subtraction step was added to the workflow. Here, prior to any experiment in which serum was used, MDS measurements were taken of raw serum at concentrations of 25%, 50% and 100%. The raw fluorescence intensity (FI) values measured within the diffused and non-diffused chambers of the microfluidic chip were then plotted on a graph of serum concentration vs fluorescence intensity to establish a standard curve (Appendix 16). From this point on, when using MDS to measuring the R_H of an experimental sample containing X concentration of AF647-labelled HLA in the presence of serum at concentration Y ($FI_{Total} = FI_X + FI_Y$), the background fluorescent signal (FI_Y) could be extrapolated from the standard curve using the known serum concentration. These background fluorescent values were then deducted from the total fluorescence (FI_{Total}) measured within each microfluidic chamber to yield the desired fluorescent signal produced by the AF647-labelled protein (FI_X). These background-deducted fluorescent values were then used to calculate the corrected diffusion ratio of the HLA molecules without the contribution of serum autofluorescence, from which the corrected R_H could be determined. As seen in Figure 5.7, The addition of this background subtraction step was found to correct for any measured deviations brought about by the inclusion of human serum autofluorescence, where background-subtracted R_H values at all concentrations were measured to be consistent with the values determined in PBS (Figure 5.7, red). From this point on all MDS measurements taken in the presence of serum included this subtraction step.

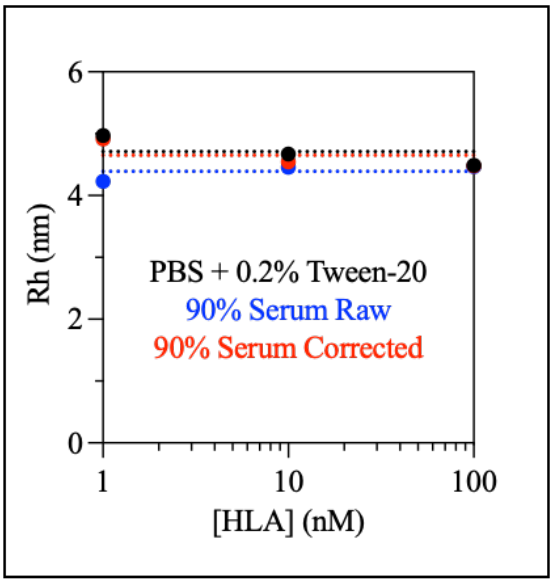

Figure 5.7 . Background fluorescence subtraction corrects for differences in HLA size observed due to serum effect. Taking MDS measurements of HLA-DRB1*07:01 in the presence of serum (blue) caused an apparent decrease in the measured R_H at lower antigen concentrations when compared to measurements taken in PBS (black). Subtraction of the autofluorescent serum background signal was able to ameliorate this effect, where the background-corrected sizes measured in serum (red) were consistent with the sizes measured in PBS down to 1 nM. Symbols represent single MDS measurements for each sample and dotted lines represent the mean R_H for each dataset.

To determine the possibility of using the MDS method to quantify alloantibody-HLA interactions in the presence of human serum, I re-assessed the WIM8E5-A*11:01 interaction using full equilibrium binding curves in the presence of a fixed 90 % concentration of blank human serum from a healthy, non-sensitised male (Figure 5.8, red). Since analysis of antibodies within patient samples would necessitate the dilution of sera with PBS (and therefore of the antibody within), this interaction was also analysed using serial dilutions of a stock sample consisting of purified WIM8E5 antibody spiked into 75 % serum to final concentrations of 320 nM (Figure 5.8, green). The respective measured K_Ds of 12.3 (± 2.9) nM and 6.6 (± 2.9) nM are both comparable with the value measured in pure buffer (9.0 ± 5.6 nM: Figure 5.8, blue). Overall, this data demonstrates the feasibility of MDS measurements in the presence of human sera, whereby inclusion of a background fluorescence subtraction step ensures a change in measured radius is solely dependent on the formation of the desired interaction alone. This provides evidence that MDS can be used as a platform for molecular-level characterisation of protein-protein interactions using complex media such as human sera without the need for analyte purification steps.

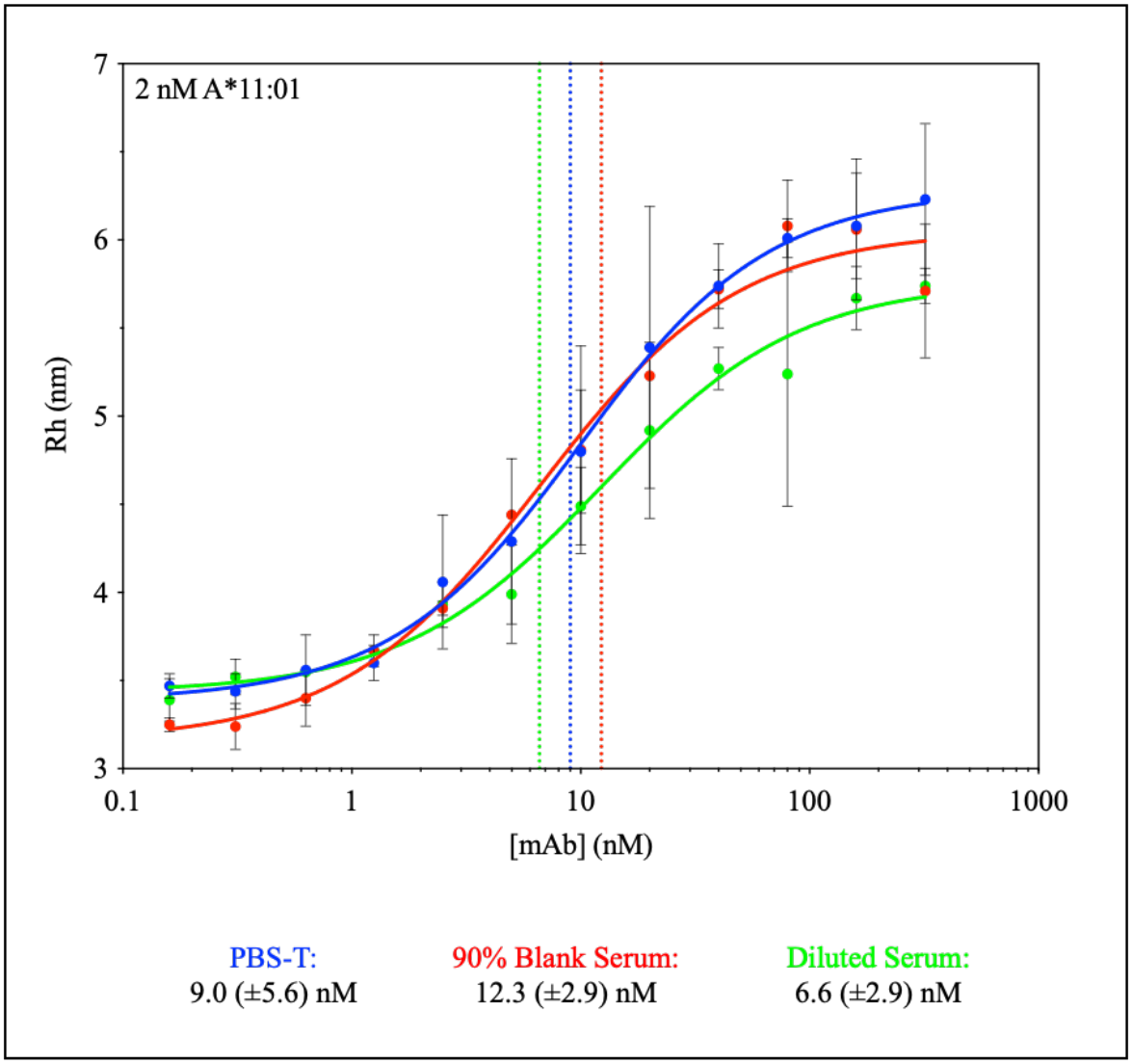

Figure 5.8. The affinities of alloantibody-HLA interactions can be measured reliably in both blank buffer and human serum. The affinity of the A*11:01-WIM8E5 interaction is consistently measured in PBS, serum and in diluted serum. 2nM HLA-A*11:01 was incubated with 2-fold dilutions of WIM8E5 in PBS +0.2% tween-20 (blue), a constant concentration of 90% blank human serum from a non-sensitised individual (red) or using a starting stock solution containing 320nM in 75% serum, where the serum would be linearly diluted with antibody dilution (green). The affinities (K_D) of each interaction could be determined as the concentration of mAb which yielded 50% of the maximum response. All experiments gave comparable affinity measurements with overlapping margins of error. Symbols represent the mean of triplicate MDS measurements for each point where error bars represent the ±SD. Values in brackets represent the standard error for the K_D values.

5.2.6. Introducing Microfluidic Antibody-Affinity Profiling

When characterising a specific population of antibodies present within patient serum, there are two unknown parameters to consider: the affinity against the antigen and the concentration of antibody molecules within the sample. Whilst full binding curves can elucidate the affinity of interactions where the concentrations of both species are known, it would not be possible to deduce the K_D value of an AlloAb-HLA interaction using simple titration binding curves when the HLA-specific Ab concentration is undetermined, such as in patient serum samples. Furthermore, when generating a binding curve, it is important to ensure that the antibody concentration present within the sample is adequate to saturate all the available HLA binding sites so that the maximum bound R_H can be reached, from which the K_D will be determined as the Ab concentration that elicits 50 % maximum response. When assessing a patient serum sample, the concentration of antigen-specific Ab within it will be dependent on the amount of time that has elapsed since the most recent immunological response. This means that in many cases, the concentration of antibodies within the serum at the time of sampling may not be sufficient to saturate all HLA binding sites to reach maximum R_H, therefore preventing K_D determination.

To address these the issues, Microfluidic Antibody-Affinity Profiling (MAAP) was developed (Figure 5.9). MAAP uses a series of MDS sample measurements taken at various concentrations of both labelled (HLA) and unlabelled (Ab) species to constrain the probability distribution of interaction affinity and antibody binding site concentration simultaneously and effectively, as demonstrated by Bayesian inference analysis. An application to patent this method internationally has been submitted through University of Cambridge enterprise (PCT international application number PCT/GB2021/051244 filed on 21/05/2021, See Appendix 17 for patent abstract). Placing MAAP into a workflow, the steps taken to constrain the most likely values for the antibody concentration and affinity within a sample are as follows: 1) The fluorescence of the antibody-containing sample is assessed in the absence of protein to establish a background fluorescence curve (Appendix 16); 2) HLA is sized in the absence of sample to establish the baseline R_H; 3) The first three test MDS measurements are taken using 40% antibody sample in the presence of 100 nM, 10nM and 2nM HLA to screen the interaction and assess the degree of binding; 4) The background fluorescence is subtracted from the total fluorescence in each MDS measurement using the previously calculated standard curve (see section 5.2.5); 5) Background-corrected MDS data is uploaded into the Bayesian analysis

which simultaneously constrains the interaction affinity and antibody concentration based on the data points provided thus far. If the lower and upper 95% confidence intervals of the calculated -logK_D and -log[Ab] values are constrained to within 0.5 of each other, then the interaction is said to be quantified. If the interaction parameters are outside of this 0.5 -log value threshold, then the analysis will suggest additional measurements to be taken at specific HLA concentrations and antibody sample percentages which are expected to provide the most optimal information to further constrain the interaction parameters. These measurements will then be taken and processed as described in workflow step 4-5 until the interaction parameters are constrained within the threshold limits.

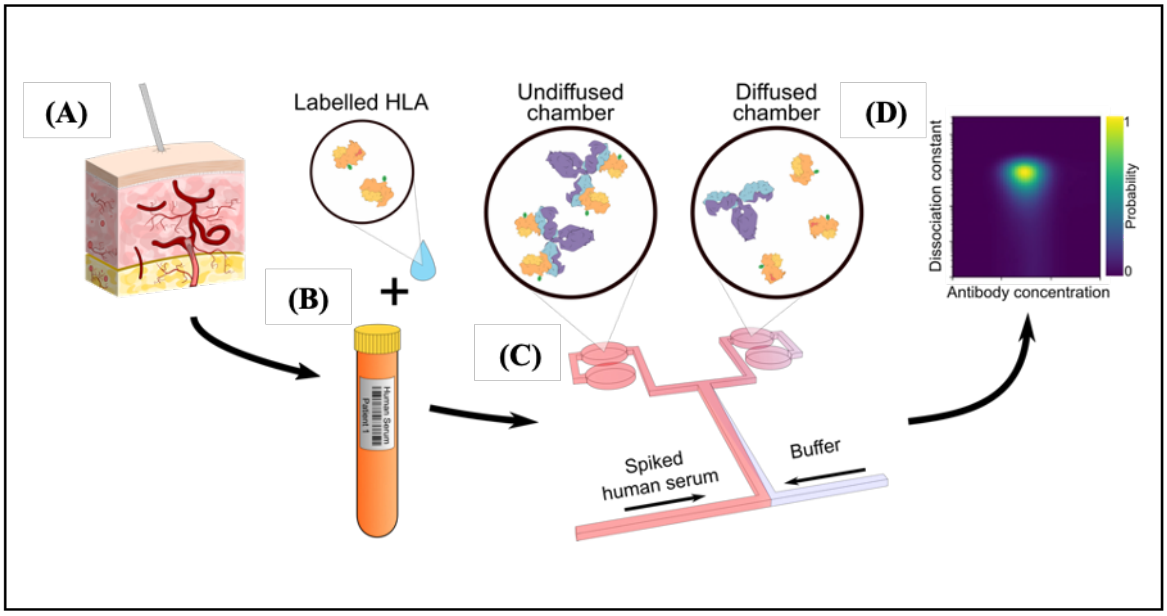

Figure 5.9. An overview of microfluidic antibody-affinity profiling. Schematical summary of the four main steps in determining the affinity and concentration of antibodies against a specific target within a serum sample via MAAP. (A) Blood is sampled from the patient in question from which serum is prepared. (B) Varying concentrations of AF647-labelled HLA and patient sample are incubated for one hour to reach equilibrium. (C) The samples are analysed via microfluidic diffusional sizing to calculate the average effective size of the HLA complex within each mixture. (D) Bayesian statistical analysis uses sequential MDS measurements to calculate the equilibrium dissociation constant (K_D) and antibody binding site concentration in parallel. The output is a distribution plot displaying the probability of each parameter being found at the respective values, where in this case blue represents low probability and yellow represents high probability.

To initially test this method, the ability of MAAP to correctly determine the concentration and affinity of WIM8E5 within a sample was assessed. To do this, WIM8E5 was diluted to a concentration of 30 nM in PBS-T, the specific molar concentration of which was left blinded to the subsequent Bayesian analysis. Assessing this via sample via MAAP against AF647-HLA-A*11:01 enabled the individual antibody parameters of WIM8E5 to be correctly and efficiently constrained (Figure 5.10). By taking MDS measurements of samples containing several concentrations of AF647-HLA-A*11:01 and various percentages of total antibody sample, MAAP was able to effectively constrain the interaction K_D to 16.4 (9.8-26.1 95% C.I.) nM, in line with previous value determined via full binding curve (Figure 5.5, see section 5.2.4). The was antibody binding site concentration within the sample was simultaneously constrained to 59.4 (39.2-78.4) nM, which implies a whole antibody concentration of 29.7 (19.6-39.2 95% C.I.) nM based on a 2:1 interaction stoichiometry. In summary, the ability of MAAP to correctly constrain these parameters of this WIM8E5 sample provided initial validation for the use of MAAP within PBS-based samples.

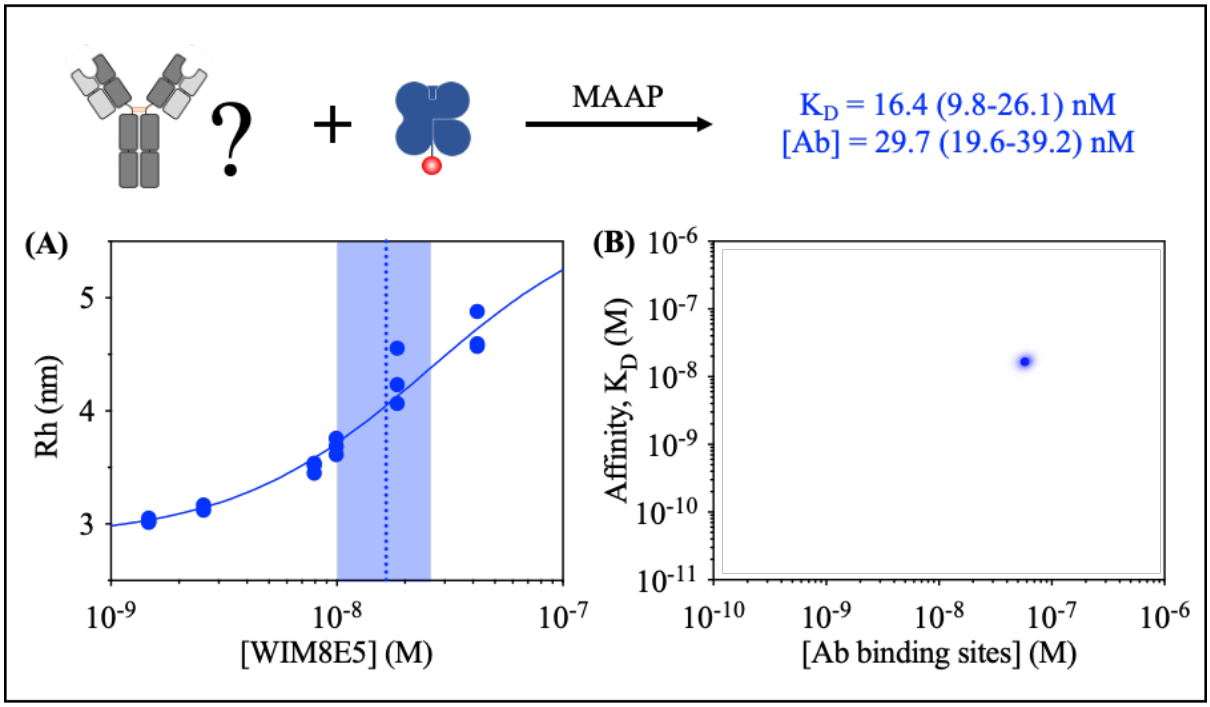

Figure 5.10. MAAP can correctly predict the fundamental parameters underpinning the WIM8E5-A*11:01 interaction. MAAP enabled the concentration and affinity of a WIM8E5 IgG-containing PBS-T sample to be correctly constrained when assessed against AF647-A*11:01, without providing any prior knowledge of these antibody parameters to the analysis. A sample containing WIM8E5 diluted to a concentration of 30 nM (concentration unknown to the analysis) in PBS-T buffer was assessed using microfluidic antibody affinity profiling against HLA-A*11:01. (A) MAAP was able to resolve this interaction's parameters whereby the affinity was predicted to be around 16.4 (9.8-26.1) nM, comparable to what has previously been determined using other methods (see Fig. 5.5). Symbols represent individual MDS measurements. Dotted line represents the probability best fit K_D value, where shading represents 95% confidence intervals. (B) The antibody concentration was simultaneously measured to be around 29.7 nM (19.6-39.2 nM) based on a 2:1 (HLA:Ab) stoichiometry. Darker shading represents higher probability of parameters being that value and the circle represents the probability best fit value. Brackets represent the 95% confidence intervals.

To examine the robustness of this assay and its application to assessment of serum samples, this 'blinded' experiment was repeated to test the ability of MAAP to quantify the antibodies within four fabricated serum samples. The samples were produced by spiking the HLA-A*02:01-reactive mAb SN230G6 into blank serum from a non-sensitised male donor (blank serum A) at concentrations of 100 nM, 30 nM, 10 nM, or 3 nM. Once again, these concentrations remained unknown to the Bayesian analysis. Assessing each of these samples separately via MAAP using AF647-HLA-A*02:01 enabled the effective K_D and the A*02:01-specific Ab concentrations to be effectively constrained, where tighter constraints were obtained for those samples containing a higher antibody concentration (Figure 5.11). Here, the 95% confidence intervals of each sample's measured antibody concentrations agreed with the known spiked concentrations chosen during experimental design. Furthermore, the output K_D 95% confidence intervals were consistently measured to overlap with the 5 nM value that had previously been determined for the interaction via equilibrium binding curve (Figure 5.6), further validating the use of the MAAP method in human serum samples.

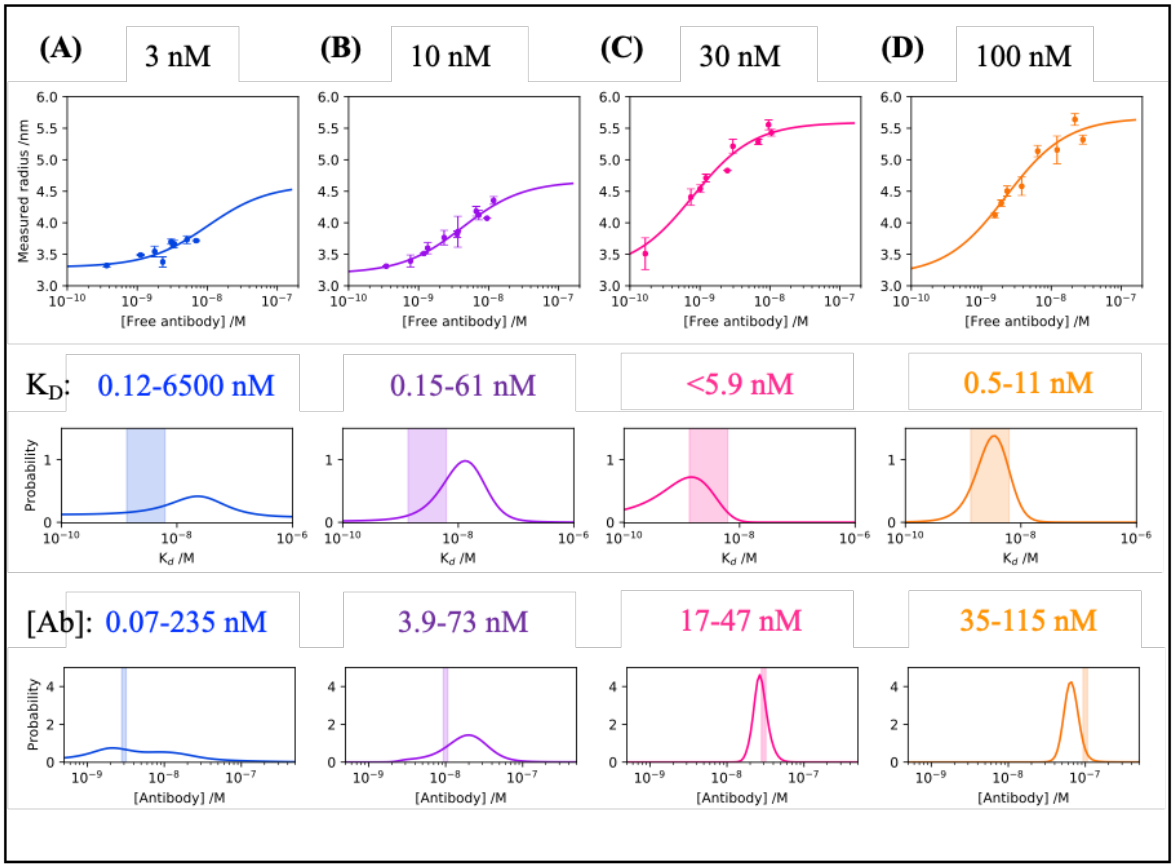

Figure 5.11. MAAP can reliably quantify antibodies in human serum samples. MAAP enabled the fundamental parameters of the A*02:01-SN230G6 interaction to be correctly constrained in the presence of serum. The monoclonal antibody SN230G6 was spiked into four individual samples of blank human serum from a non-sensitised individual at concentrations of (A) 3 nM, (B) 10 nM, (C) 30 nM and (D) 100 nM. Each sample was assessed via MAAP to quantify the concentration and affinity of antibodies in each sample against AF647-A*02:01, where the analyses assumed both parameters were unknown. MAAP analysis yielded the calculated binding curve (top) and the probability distribution of both interaction affinity (K_D, middle) and antibody binding site concentration ([Ab], bottom) for each sample. All samples were measured to have overlapping affinities, consistent with both the value measured via equilibrium binding curve (Figure 5.6) and the 95% confidence intervals when analysis was carried out when all datasets were combined (shaded region, middle row). Measured antibody concentrations agreed with the known antibody concentrations chosen on sample preparation (shaded region, bottom row) assuming a 2:1 binding stoichiometry, without providing this information to the analyses. Symbols in binding curves represent the mean of triplicate MDS measurements for each point and error bars represent the ±SD. Values stated represent the 95% confidence intervals of the analysis.

5.2.7. MAAP – Patient Sample Testing

Following the establishment and validation of MAAP in a controlled setting, the next step was to investigate the ability of the assay to quantify unknown HLA-specific Abs within the historic serum sample of a kidney transplant recipient. Patient A was identified as a suitable transplant recipient whose serum showed a high reactivity profile against HLA-A*11:01 (>20,000 MFI) across multiple samples as measured via Luminex SABs (Figure 5.12.A). To ensure detection of anti-A*11:01 antibodies within the serum was possible, MDS of AF647-HLA-A*11:01 was carried out in the presence of 20-80 % of the patient's serum (23,060 MFI) or blank serum A. Incubation with patient serum led to large increases in the measured R_H, whereas the addition of blank serum yielded no significant change (Figure 5.12.B). This effective increase in HLA-A*11:01 size signified complex formation, confirming the presence of HLA-A*11:01-specific Abs within the patient's serum and their ability to be detected via MDS. Using MAAP, it was then possible to quantify these antibodies against AF647-A*11:01, where the A*11:01-specific antibody binding site concentration could be tightly constrained to 113.6 (94.4-130.4) nM with an affinity against the antigen of 2.6 (1.8-3.7 95% C.I.) nM. This means the whole antibody concentration is said to be 56.8 (47.2-65.2 95% C.I.) nM assuming a stoichiometry of two HLAs to one Ab (Figure 5.12.C-D). This data displays the capability of MAAP to simultaneously deconvolute the fundamental biophysical parameters of the humoral response, these being antibody K_D and concentration, in a patient serum sample.

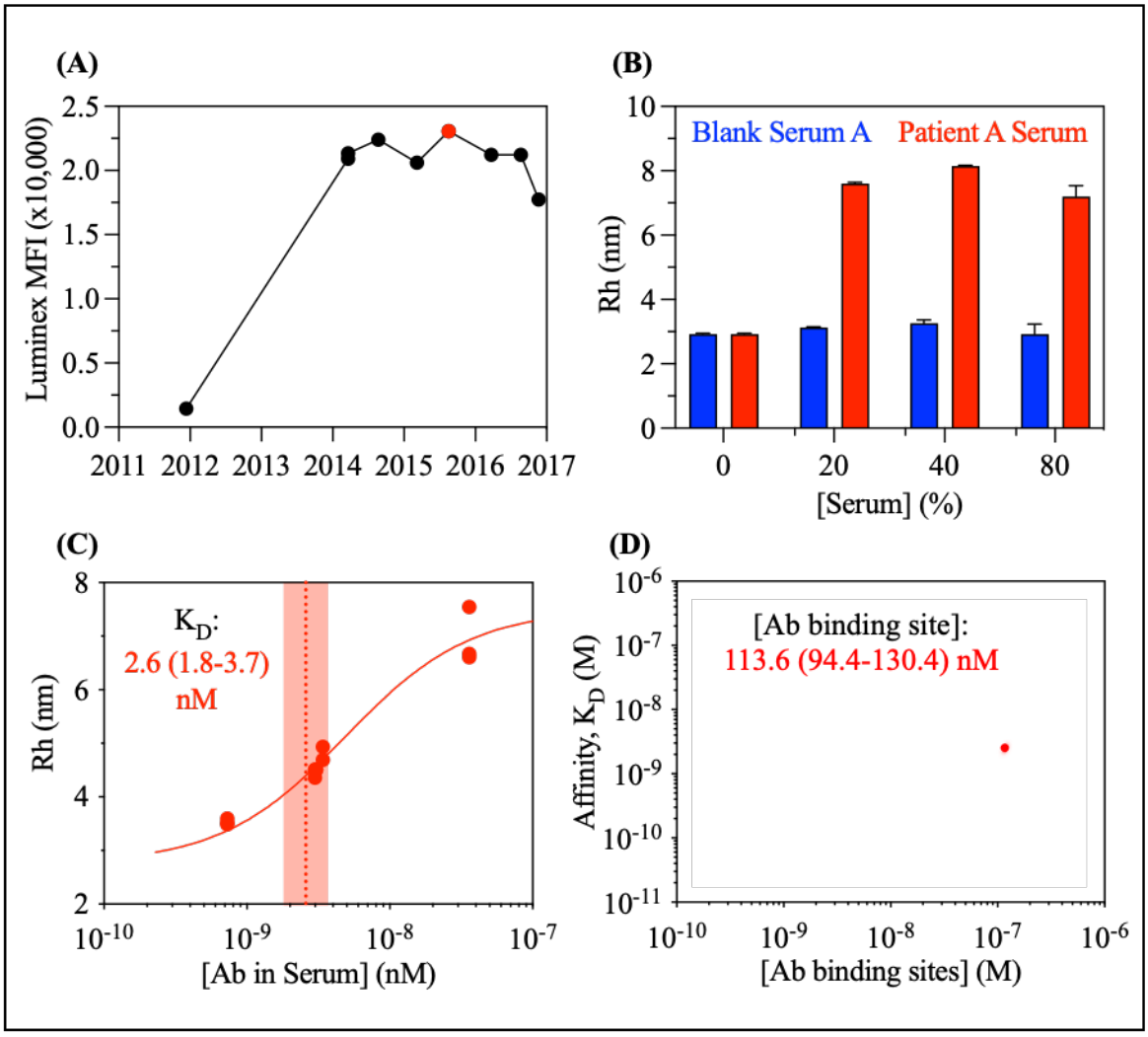

Figure 5.12. Quantification of alloantibodies in historic patient serum samples using MAAP. MAAP enabled the fundamental parameters of a natural humoral response against HLA-A*11:01, these being antibody concentration and affinity, to be simultaneously measured for the first time using a patient serum. (A) Patient A has a history of high DSA levels against HLA-A*11:01 as measured by Luminex single antigen bead assay. Black symbols signify the Luminex SAB MFI output from routine serum screening and the red symbol signifies the serum sample selected to be further analysed. (B) Incubation of 5 nM HLA-A*11:01 with the serum sample at concentrations of 20 %, 40 % and 80 % yielded increases in the effective hydrodynamic radius of A*11:01 as measured by MDS, signifying complex formation. Columns represent the mean measured R_H taken from triplicate measurements of each sample, where errors bars represent the ±SD. (C) MAAP analysis of this sample enabled a binding curve to be generated with a predicted interaction affinity of 2.6 (1.8-3.7) nM. The antibody concentration was measured at 56.8 (47.2-65.2) nM based on a 2:1 stoichiometry (D). In panel C, symbols represent individual MDS measurements, and the dotted line represents the probability best fit K_D value, where shading represents K_D 95% confidence intervals. Darker shading in panel D represents higher probability of parameters being that value, whilst the circle represents the probability best fit value. Values in brackets represent the 95% confidence intervals.

5.2.8. Translating the MAAP Assay for Use with Class II HLA Molecules

Although mismatching at HLA class I has been linked to the occurrence of graft rejection, it is now well documented that HLA class II mismatches are particularly important both in relation to their immunogenicity (most *de novo* DSAs occurring after transplantation are against HLA class II mismatches) and their relative contribution to the incidence of antibody-mediated rejection [364-367]. For MAAP to become available as a tool in the clinical setting, the MDS method needed to be applied and verified for use with class II HLA molecules. Successful labelling of HLA-DRB1*07:01 yielded an average ratio of 1.21 AF647 molecules per HLA, giving a measured free protein R_H at around 4.3 nm (Figure 5.13.A-B, Appendix 14). Incubation of 10 nM AF647-HLA-DRB1*07:01 with 1 μM concentrations of three separate anti-HLA-DR Abs (DR7 Ab 1, 2 and 3) previously shown to specifically bind epitopes on HLA-DRB1*07:01 [368] induced an increase in measured R_H due to Ab-HLA complex formation (Figure 5.13.C). Upon equilibrium binding curve analysis via MDS in PBS-T buffer (Figure 5.13.D), DR7 Ab 1 and 2 were found to bind DRB1*07:01 with affinities of 31.2 (± 6.1) nM (blue) and 5.0 (± 1.2) nM (red), respectively. The absolute K_D value of DR7 Ab 3 was unobtainable due to the current limit of assay sensitivity, however it was determined that this was to be in the sub-nM range (green). Assessing these interactions using MAAP, where unlike the blinded assays carried out in section 5.2.6 the known antibody concentrations were fed into the analysis, the K_Ds of DR7 Ab 1 and 2 were constrained to 18.5 (6.5-46.6 95% C.I.) nM and 10.4 (6.9-29.3 95% C.I.) nM, respectively. These confidence intervals overlapped with the values measured via equilibrium binding curve, supporting the data. Although an absolute value of the interaction affinity between DR7 Ab 3 and AF647-DRB1*07:01 could not be obtained using MAAP, it was possible to gain an 95% C.I. upper bound constraint on the interaction affinity of <0.36 nM, suggesting the true K_D of this interaction is somewhere below this value. Validation of these microfluidic affinity measurements was carried out using BLI (Figure 5.13.F), where the respective K_D outputs of 19 (± 1.2) nM, 12 (± 0.8) nM, 0.3 (± 0.2) nM against DR7 Ab 1, 2 and 3, were almost identical the values measured via MAAP. Collectively, this data provides evidence to validate the use of MAAP with class II HLA molecules in a pure buffer setting.

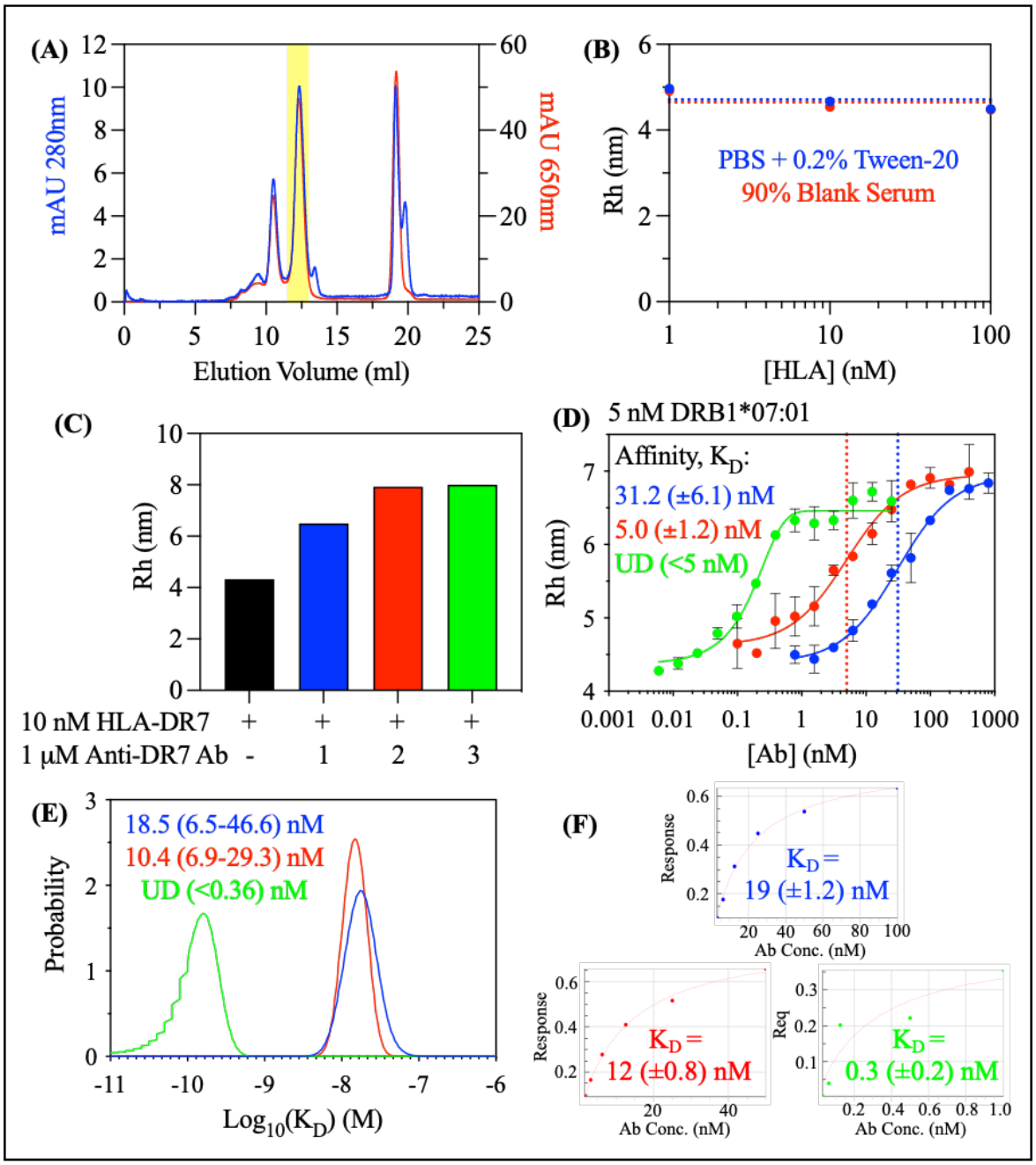

Figure 5.13. Validation of microfluidic diffusional sizing using HLA class II molecules. The use of MDS to quantify HLA-alloantibody interaction affinities could be translated into HLA class II molecules. (A) HLA-DRB1*07:01 was labelled and purified as outlined in Figure. 5.2 where yellow shading represents fractions which were pooled and taken further. (B) AF647-DRB1*07:01 sizes similarly in both blank buffer and human serum via MDS. Symbols represent single MDS measurements and dotted lines represent the mean size of all measurements taken in each buffer. (C) Incubation of 10 nM labelled HLA-DRB1*07:01 with purified monoclonal anti-DR7 mAbs causes an increase in measured radius by MDS (n=1). (D) Equilibrium binding curves using each of the 3 mAbs against 5 nM DR7 enables their differing affinities to be measured, where the absolute K_Ds of only DR7 Ab 1 and 2 could accurately be determined (31.2 nM and 5.0 nM, respectively). DR7 Ab 3 yielded a saturation curve suggesting the affinity is below the antigen concentration. Symbols are an average of three measurements. These interaction affinities were re-measured via MAAP (E) and biolayer interferometry (F), yielding comparable results which validate the MDS method. Brackets in panels D and F represent the ±std. error, in panel E they represent the 95% confidence intervals. BLI affinities were determined by steady state analysis. Throughout panels C-F, blue = DR7 Ab 1, red = DR7 Ab 2 and green = DR7 Ab 3.

To examine whether this HLA-DRB1*07:01 molecule could be used in MAAP assays to quantify DR7-specific Abs in patient sera, two patients, B and C, were identified as transplant recipients whose sera showed positive but variable reactivity against HLA-DRB1*07:01 as measured by Luminex SABs (Figure 5.14.A; Patient B = 13,288, Patient C = 24,048). Incubation of AF647-DRB1*07:01 with each patient sera prompted a measured increase in the effective R_H of HLA-DRB1*07:01 (Figure 5.14.B). Analysing these two sera via MAAP against HLA-DRB1*07:01 enabled the fundamental parameters of these interactions to be measured, demonstrating the functionality of this assay when using class II HLAs as the detected protein (Figure 5.14.C-D). Patient B's serum was found to contain 68.3 (41.1-345.3 95% C.I.) nM Abs with an affinity against HLA-DRB1*07:01 of 98.9 (15.5-176.3 95% C.I.) nM. Patient C's serum was found to contain a relatively similar concentration of 59.5 (20.5-82.2 95% C.I.) nM Abs, however these had over a 10-fold stronger affinity against DRB1*07:01, with a K_D measured at 8.7 (1.9-27.7 95% C.I.) nM. By relating the outputs of MAAP to the data yielded by Luminex, I was able to demonstrate how the enhanced DRB1*07:01 Luminex MFI signal generated with Patient C's serum with respect to Patient B's serum, may be due to the presence of higher affinity antibodies in Patient C's serum and not related to the concentration at which the antibodies are present. This conclusive observation could not have been made without the data generated from MAAP analysis. These cases provide model examples of how the semi-quantitative MFIs provided by Luminex may only enable a limited insight into the antibody's functionality to be obtained, whilst MAAP can provide a more informative and fully quantified antibody assessment that may be used to inform these Luminex outputs which may provide an understanding with regards to the antibody's clinical significance.

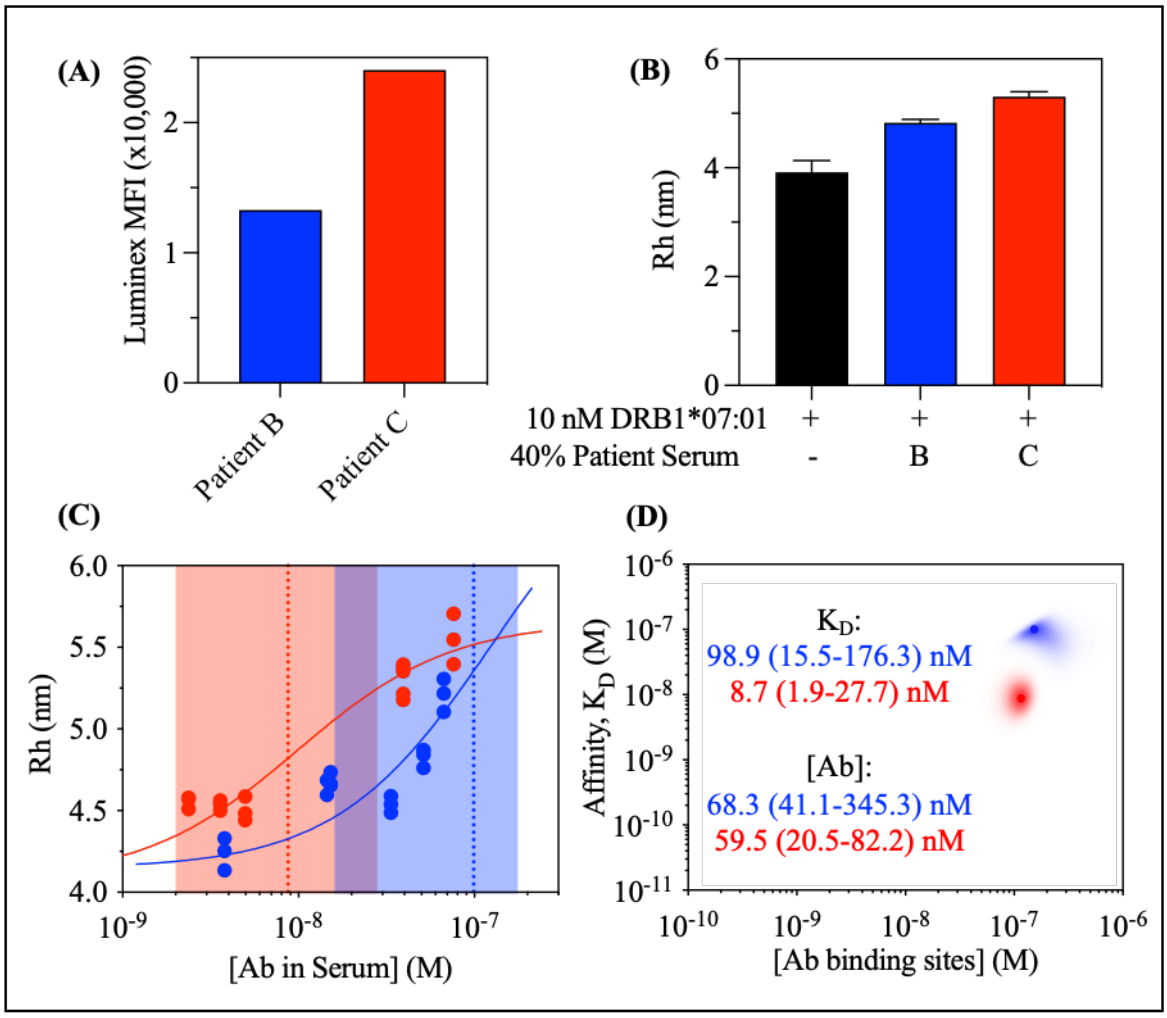

Figure 5.14. Quantification of anti-class II alloantibodies in historic patient serum samples using MAAP. The differing Luminex MFI signals measured using sera from two separate patients (B, blue and C, red) who had generated immune responses against DRB1*07:01 were shown to be caused by a difference in the serum antibody affinity as measured by MAAP. (A) Patients B and C have historic serum samples which contained DSAs that exhibit varying ability to bind HLA-DRB1*07:01 as measured by Luminex class II single antigen bead assay. Columns represent single Luminex SAB MFI measurements from routine serum screening. (B) Incubation of 10 nM HLA-DRB1*07:01 with 40% of each serum yielded increases in its hydrodynamic radius as measured by MDS, suggesting Ab-Ag complex formation. Columns represent the mean of two measurements where error bars represent the ±SD. (C-D) MAAP analysis of patient samples B and C against HLA-DRB1*07:01 generated binding curves with predicted interaction affinities of 98.9 (15.5-176.3) nM and 8.7 (1.9-27.7) nM, respectively. Patient B's sample was measured to contain 68.3 (41.1-345.3) nM antibodies and patient C's sample contained 59.5 (20.5-82.2) nM antibodies, assuming a 2:1 interaction stoichiometry. Since the sera contained similar antibody concentrations, this suggests difference in Luminex outputs may be caused by the 10-fold difference in antibody affinity between the samples. Symbols in panel C represent the individual MDS measurements, where the dotted line represents the probability best fit K_D value and shading represents 95% confidence intervals. Darker shading in panel D represents higher probability of parameters being that value and the circles represent the probability best fit values. All brackets represent the calculated 95% confidence intervals.

5.2.9. Clinical Translation of MAAP

Having shown that MAAP can be used for efficient quantification of HLA-specific Abs in patient serum samples, the next step was to investigate whether MAAP could provide additional, currently unobtainable information that may improve our understanding of the clinical significance of a patient's DSAs. To investigate the potential application of MAAP in the clinical setting, two separate clinical cases were retrospectively analysed. In these cases, two patients were identified who had historic DSA to similar levels prior to transplant as measured via Luminex SABs. These patients then went on to receive a kidney transplantation and but had differing clinical outcomes (Patient D and Patient E). The aim of this study was to assess the sera of these patients taken pre- and post-kidney transplantation to examine whether the data collected from MAAP analysis could provide information about the patient's DSAs further than what is obtainable using the currently used clinical methods.

5.2.9.1. Increasing Recipient Access to Donor Organs

Patient D was the recipient of an HLA-A*03:01-expressing deceased donor kidney allograft, who three years prior to transplantation exhibited serum MFI values of 8,289 against HLA-A*03:01, detected by Luminex SAB as part of routine testing (Figure 5.15.A). The patient's DSA levels were found to have dissipated (MFI = 903) at the time of transplant and no further alloantibody analysis was carried out at this time. During the early period after transplantation, anti-A*03:01 DSAs were observed at relatively high levels (MFI = 11,740) although there were no signs of antibody-mediated rejection and the patient had excellent graft function. DSA levels were observed to gradually diminish over a six-month period following transplantation where the graft maintained good function.

MAAP analysis of the 8,289 MFI pre-transplant serum (sample 1) against HLA-A*03:01 revealed no significant quantifiable binding of antibodies within the serum (Figure 5.15.B). MAAP analysis of the post-transplant sera at the peak of DSA levels confirmed this finding, where absolute quantification of the anti-HLA-A*03:01 Abs was unobtainable (Figure 5.15.C-D). The inability to quantify these antibodies was due to the interaction falling outside the upper sensitivity limit of the assay, where large confidence intervals were yielded that spanned a range of almost 2 magnitudes for both K_D and Ab concentration. Despite the inability to effectively constrain these values, posterior plots (Figure 5.15.D) indicate that these Abs are expected to be of weak affinity (high K_D) but at a high enough concentration which was able to induce a small increase in the effective hydrodynamic radii (Figure 5.14.C), corroborating the pre-transplant sera data. The data obtained via MAAP would suggest that the signal detected by Luminex may be due to a non-clinically relevant interaction.

This data illustrates how in an alternative setting there is the potential for non-clinically relevant DSAs within patient sera to be perceived as pathogenic due to positive output in the Luminex SAB assay. Although the transplant procedure in this case went ahead and had successful outcomes, in another scenario this may lead to wrongly listing the antigens as unacceptable mismatches, thus reducing a patient's access to available organ donors. For this case, MAAP was able to inform this positive Luminex data, providing evidence to show that Luminex positivity occurred due to an antibody of very weak affinity and therefore is likely to be clinically irrelevant. This case exemplifies the potential of MAAP to inform clinical decision making, although this would need to be confirmed in further studies.

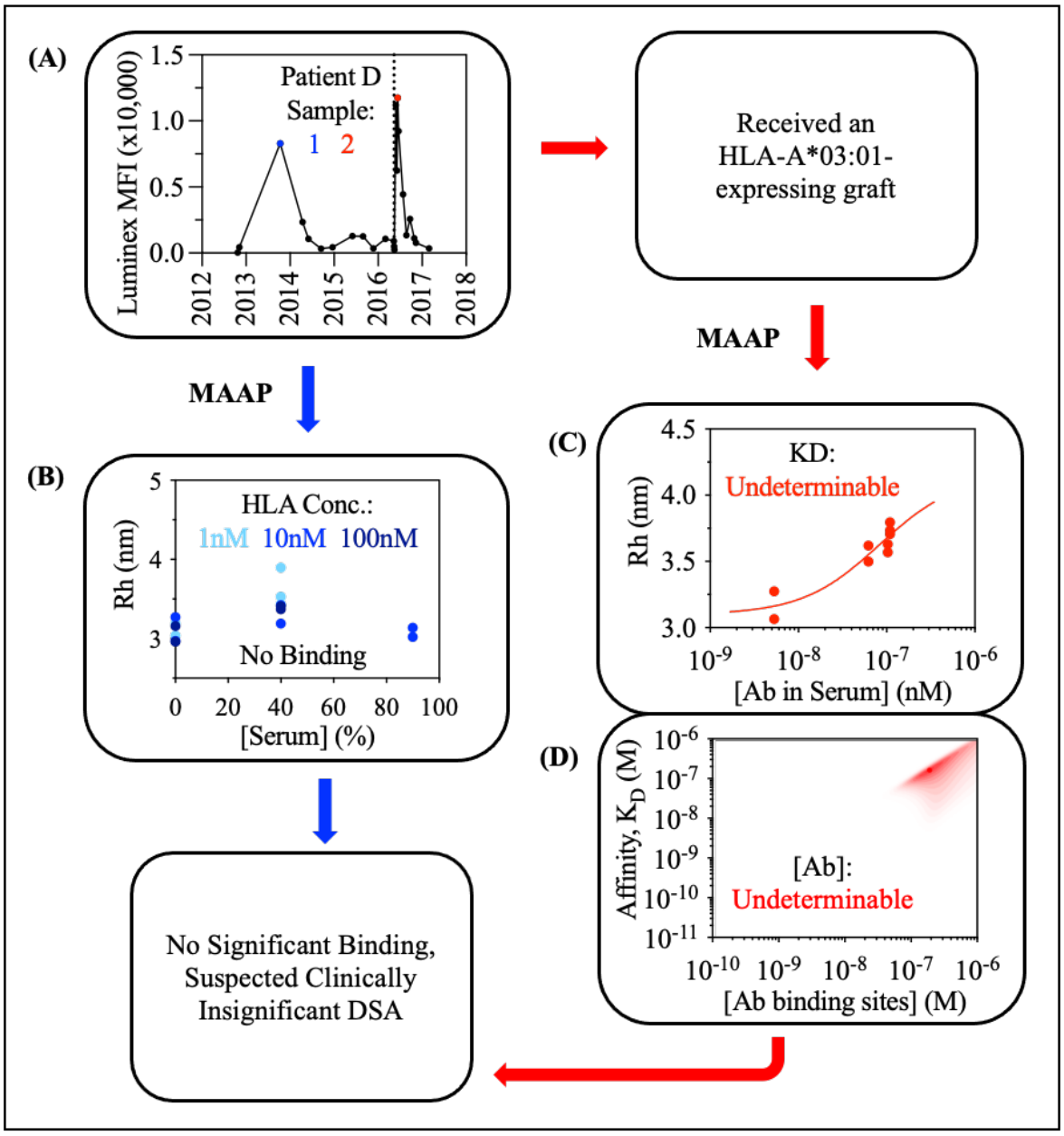

Figure 5.15. Information from MAAP may increase a recipient's access to donor organs. MAAP enabled an informative assessment of HLA-A*03:01 DSAs in Luminex-positive pre- and post-transplant sera to determine their minimal risk to transplant. (A) Patient D's Luminex SAB profile showed a history of DSA against A*03:01 which was seen to elevate following surgery in 2016 (dotted line). The patient was observed to tolerate these antibodies without any detected graft damage being induced. Black symbols signify the Luminex SAB MFI output from routine serum screening, whereas blue and red symbols signify the pre- and post-transplant serum samples selected to be further analysed, respectively. (B) MAAP analysis of the 8,289 MFI pre-transplant sera against A*03:01 found no significant binding against AF647-A*03:01. (C-D) MAAP analysis of the 11,740 MFI post-transplant serum sample against AF647-A*03:01 did detect binding of antibody but was unable to determine absolute quantified parameters of the anti-HLA-A*03:01 antibodies. This analysis did predict the antibodies to be of low affinity (high K_D) and present at high concentrations, suggesting they are clinically insignificant and may pose low risk to transplantation with an A*03:01-expressing graft. Symbols in panels B and C represent individual MDS measurements. Darker shading in panel D represents higher probability of parameters being that value.

5.2.9.2. Detection of Clinically Relevant DSA at Low Concentrations

Patient E was a highly sensitised female with an extensive sensitisation history, including two previous transplants, one pregnancy, and a blood transfusion. Analysis of the historic clinical Luminex data revealed the presence of pre-transplant DSA against HLA-A*11:01, peaking six years prior to transplantation with an MFI of 9,428. At the point of transplant, anti-A*11:01 DSA MFI levels had fallen to <2,500 (2,350) which was deemed acceptable upon the offer of an A*11:01-expressing DCD kidney. Within weeks following transplantation, anti-A*11:01 DSA levels were observed to spike (peak MFI = 20,117) (Figure 5.16.A). Biopsy analysis at day seventeen post-transplantation showed positive C4d deposition in the presence of DSA, however there was no overt signs of AMR. This was possibly due to ongoing intervention with thymoglobulin (ATG) and Eculizumab, where the graft went on to show good function.

Analysis of the 9,428 Luminex MFI pre-transplant serum (sample 1) via MAAP using AF647-HLA-A*11:01 revealed antibodies with sub-nanomolar (0.01-0.91 nM) level affinity against A*11:01 (Figure 5.16, blue). MAAP analysis of two post-transplantation serum samples, taken at day 6 (sample 2, MFI = 9,599) and day 13 (sample 3, MFI = 20,117), confirmed the pre-transplant serum findings, where the detected DSAs exhibited a high affinity for HLA-A*11:01. The 95% confidence intervals of the measured DSA K_D values in both post-transplant sera overlapped with that of the pre-transplant serum assessment (Figure 5.15, red = D6; 0.04-3.1 nM, green = D13; 0.19-4.6nM).

In contrast to patient D's DSAs (see section 5.2.9.1), Patient E's antibodies bound their target with strong affinity, despite the sera from both patients generating similar pre-transplant Luminex MFI values. Antibody-antigen interactions of high strength imply an affinity-matured response associated with immunological memory. This was confirmed with the rapid increase in DSA MFI observed post-transplant, suggesting an anamnestic response. It is well known that a response such as this due to pre-existing B-cell memory can often be detrimental and may lead to graft loss, however the effect of this response was fortunately mitigated with strong immunosuppression and the use of a novel complement-specific monoclonal antibody. MAAP analysis of pre-transplant sera on this occasion would suggest the presence of a clinically relevant HLA-specific antibody with high affinity to HLA-A*11:01, that in the transplant setting might best be avoided. In summary, the above example demonstrates how the MAAP immunoassay may provide clinically relevant information in both pre- and post-transplant assessment to provide insights into the significance of a patient's detected DSAs.

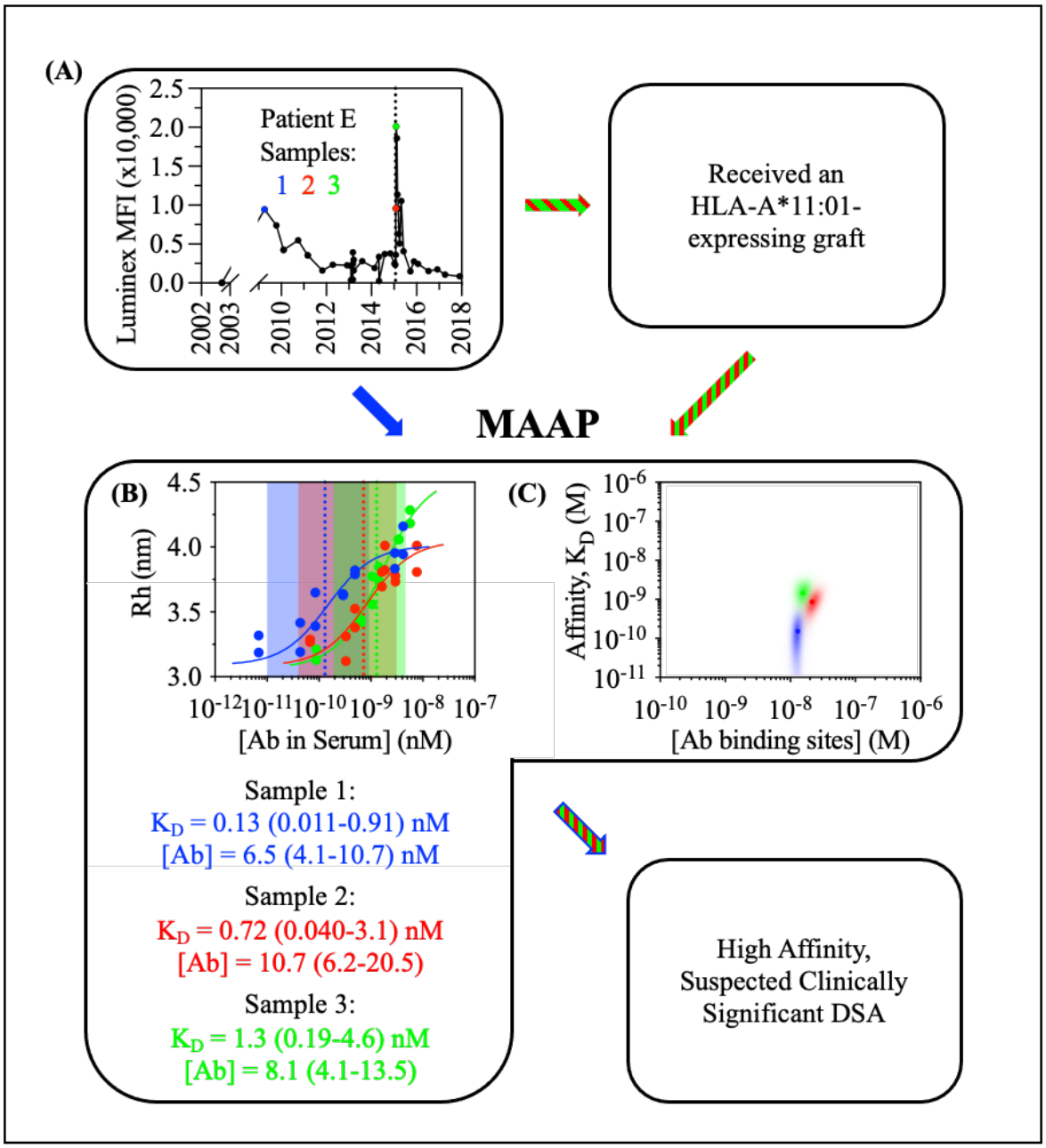

Figure 5.16. MAAP may detect clinically relevant antibodies at low concentrations. Assessment of a patient's Luminex-positive serum samples via MAAP enabled detection of DSAs with high specificity to HLA-A*11:01. (A) Patient E's HLA-A*11:01 Luminex single antigen bead profile showed a history of DSA against A*11:01. DSA levels were seen to elevate at two weeks following transplantation in 2015 (dotted line), where biopsies showed signs of C4d deposition (although Eculizumab and thymoglobulin induction may have prevented AMR). Black symbols signify the Luminex SAB MFI output from routine serum screening, whereas blue, red and green circles signify the serum samples that were assessed via MAAP. (B-C) MAAP analysis of each selected serum against HLA-A*11:01 enabled the antibodies in all samples to be measured of similar, high affinity (all K_Ds measured < 2 nM), suggesting they may be clinically relevant and offer a high risk to transplantation. Symbols in panel B represent the individual MDS measurements for each serum, where the dotted lines represent the probability best fit K_D values and shaded regions represent K_D 95% confidence intervals. Darker shading in panel C represents a higher probability of the parameters being that value and the circles represent the probability best fit values. All brackets represent the calculated 95% confidence intervals.

5.3. Discussion

5.3.1. Chapter Overview

The ability of an antibody to bind to cellular HLA and exert its pathogenic potential is dependent on two fundamental parameters, namely the affinity that the antibody has for its antigen and the concentration of the antibodies within the sample (see chapter 3). Although techniques have been developed in attempt to quantify these two parameters independently [269, 265, 266, 369, 370], the need for sample purification, protein immobilisation and methodological expertise when using these methods limits their capacity to be used in a wider clinical setting. The aims of this chapter were to investigate the use of microfluidic diffusional sizing (MDS) to measure alloantibody-HLA interaction binding affinity in-solution and to develop a novel method which would enable absolute quantification of HLA-specific antibodies within patient serum samples. Using AlexaFluor 647-labeled HLA it was possible to quantify the affinity and stoichiometry of alloantibody-HLA interactions using purified samples. A background subtraction step was introduced to MDS measurements to correct for any autofluorescence that may contribute to the signal when using complex samples such as serum. To determine alloantibody-HLA interaction affinities using human serum samples where the active antibody concentration is unknown, Microfluidic Antibody Affinity Profiling (MAAP) was developed. MAAP was initially validated by successfully quantifying several well-characterised interactions, both in PBS and blank serum. This method was then used to quantify the biophysical properties of antibodies within HLA-incompatible transplant sera, where the K_D and [Ab] values obtained showed the potential to be used as a tool for interpreting Luminex outputs and/or determining the antibody's immunological significance.

5.3.2. Development of Microfluidic Antibody Affinity Profiling and Quantifying the Humoral Response

Microfluidic diffusional sizing was developed to measure the molecular size of a labelled protein and the complexes they form under native solution conditions [355, 356, 358]. Labelling of HLA molecules with AlexaFluor 647 enabled the R_H of HLA class I and class II molecules to be measured via MDS, where the measured sizes of each HLA were in good agreement with the expected R_H of natively folded globular proteins with their respective

number of residues [359, 360]. Incubation of AlexaFluor 647-labelled HLA with a dilution series of purified HLA-specific mAbs permitted reliable determination of the interaction affinity and stoichiometry [371]. A total of nine interactions were quantified via equilibrium binding curve using purified samples, where the K_D values extrapolated from these curves ranged from 10^{-10} to 10^{-7} molar range, consistent with previously measured values [238]. With incorporation of a background subtraction step which accounted for the autofluorescent serum signal [372], MDS enabled quantification of interactions in the presence of human serum, thus avoiding the non-specific binding effects that are seen with other methods that require ligand immobilisation [269]. These results showed that the measured interaction is solely based on specific interaction of labelled HLA with HLA-specific antibody and is not influenced by non-specific protein species that may be present within the serum [373].

Despite MDS offering an alternative measurement to assess interaction affinity in the presence of complex media, the unknown active antibody concentration within human serum samples remained an issue. To address this, Microfluidic Antibody Affinity Profiling was developed. MAAP is a novel assay which uses Bayesian inference analysis and a series of MDS measurements taken at various antigen and antibody sample concentrations to simultaneously calculate the antibody affinity and active antibody concentration in-solution [374]. Using MAAP it was possible to quantify the antibodies in eight patient sera, documenting the first time that one assessment of patient sera has enabled simultaneous deconvolution of the fundamental biophysical parameters underpinning the humoral response (i.e., K_D and [Ab] concentration). By assessing the antibodies in serum of two patients who had developed responses against HLA-DRB1*07:01 (patients B and C), the measured affinity and concentration values gained from MAAP could also be used to explain their differing Luminex DR7 SAB MFI output. Here it could be determined that the difference in Luminex MFI was not caused by a difference in antibody concentration within the sera, but due to patient B's antibodies being of weaker affinity than those in patient C's sample, potentially offering insights into their cross-reactive disposition [375]. Additionally, MAAP was able to provide a retrospective assessment of sera from two clinical cases, which if available at the time of transplant may have provided further information to aid in clinical decision making. Here, MAAP of Luminex positive pre-transplant sera calculated serum antibodies to be of low affinity against the expressed HLA target, offering a possible explanation as to why these antibodies were tolerated and the graft was accommodated [376]. In contrast, MAAP was able to measure high affinity antibodies within the pre-transplant sera of a different transplant

recipient which generated similarly positive MFIs via Luminex pre-transplant, however the C4d depositions on the graft shortly following transplant substantiated this measured antibody strength, where this graft may have rejected without necessary interventions [377-378]. Collectively, these cases provide examples of how fully quantitative affinity analyses acquired from MAAP can be used to assist in interpretation of clinical immunoassay output, outlining a path towards in-depth profiling of antibody responses in patient sera.

5.3.3. Considerations of Microfluidic Diffusional Sizing and Microfluidic Antibody Affinity Profiling

Compared to the widely utilised surface-based methods, MAAP offers many advantages such as: in-solution analysis which nullifies the limitations involved with ligand immobilisation, the need for only small amounts/volumes of sample, the ability to measure interaction stoichiometry and sample concentration, and the ability to use Bayesian analysis to guide optimal subsequent measurements so that maximum information is obtained efficiently with the least possible points [374]. As highlighted in section 5.2.6, MAAP can be used to constrain the antibody parameters without requiring the saturation of all antigen binding sites that is needed when for interaction affinity determination via equilibrium binding curve. Despite this, the ability to constrain the antibody parameters will still be dependent on the antibody concentration with respect to the interaction affinity ($[Ab]/K_D$). Antibody binding site concentrations at or below the K_D may limit accurate parameter determination due to inadequate complex formation and change in the measured R_H. Although an $[Ab]/K_D$ threshold of >1 should theoretically enable distinction of the two parameters [379-381], the practicality of this cut-off in the experimental setting still needs to be explored. Whilst MAAP was developed for quantification of anti-HLA antibodies in the transplant setting, this method may provide a useful tool for diagnostic testing beyond histocompatibility where it could be utilised for immune profiling in various fields, such as autoimmunity, infectious disease, and biomarker detection, as well as many other disciplines in which Ab-Ag interactions are implicated [379-382].

The requirement of protein labelling for MDS means that the ability for the interaction to occur will be dependent on the positioning of the label and maintenance of the antibody epitope [383]. The sensitivity of the assay is also dependent on the ability of the instrument to detect the fluorescent molecules within each microfluidic stream. Although the inclusion of background subtraction could account for unwanted noise due to serum autofluorescence, using samples

with high levels of background may lead to an elevated signal-to-noise ratio which may mask the fluorescent protein signal even at higher antigen concentrations, preventing the sample from being accurately measured. Additionally, the brightness of a fluorophore is dependent on the properties of its buffer environment [384], where the properties of different sera may vary quite radically from one sample to the next. To understand whether variability between serum samples may become an issue, further assessment into the effects of variable serum background conditions on the measurements taken from MDS and MAAP should be investigated. With the current equipment specifications, this allows labelled protein to be detected in the nanomolar range in pure buffers such as PBS. This detection level enables interactions with nanomolar K_Ds or higher to be fully quantified, however interactions of stronger affinity may only be quantified as sub-nM, where determination of their absolute K_Ds would require a more sensitive level of detection. MDS measurements are determined by the rate of molecular diffusion across streams under laminar flow. To detect the binding of a molecule to the labelled protein, it needs to be ensured that the difference in the diffusive capacity between the complex and protein alone is significant enough to induce a measurable change in the R_H. Whilst the Fluidity One-W is capable of sizing globular proteins between 0.5-20 nm (1-1,400 kDa) across three separate flow rates, the inability to detect small changes in molecular size means that studies such as those aiming to quantify the binding affinity of small drug molecules to a large globular protein, where the small molecule cannot be labelled, may not be suitable for this method [385]. There is however the scope to assess the competitive behaviour of proteins via MDS by assessing the ability of these small molecules to disrupt protein complexes [382]. This may also be useful in understanding the competitive behaviour of cross-reactive alloantibodies when two HLA targets are present and/or multiple antibodies against the same target.

5.3.4. Conclusion

There is currently no available technique that can determine the abundance of antibody within an unquantified serum sample and the affinity it has for its antigen without the need for antibody purification steps. Outlined in this chapter are the details that have led to the successful development of MAAP for the absolute quantification of the biophysical parameters that underline antibody interactions using non-purified samples. MAAP offers an alternative in-solution approach to quantification of antibody affinity and concentration within crude samples, where it shows the potential to be used as a tool in clinic to improve transplant-related decision-making processes.

Chapter 6

General Discussion

6.1. Thesis Overview - Revisiting the Aims

Donor HLA recognition and development of HLA-specific antibodies present a major immunological risk in solid organ transplantation. Whilst the development of methods to detect and assess the pathogenic potential of DSAs have significantly helped decrease the incidence of acute antibody mediated rejection, chronic AMR continues to be a major cause of tissue injury and graft loss [386,387]. This thesis investigated the current methods used to identify and characterise alloantibody-HLA interactions in clinic, whilst also delving into the antibody parameters that govern the outputs of these assays, these being antibody affinity and concentration. With this information, alternative approaches to assess antibody-antigen interactions were explored which led to the development a novel method of antibody quantification using serum samples, Microfluidic Antibody Affinity Profiling (MAAP). Assessment of patient serum samples using MAAP enabled additional antibody information to be gathered which is not currently obtainable using the conventional immunoassays. By doing so, this analysis provided examples of how this information may be relevant in the clinical setting to assist with immunological risk evaluation. This chapter summarises the findings of this body of work, discusses limitations, and outlines further studies needed to enable clinical translation.

Aim 1: Investigation into the potential of alloantibody-HLA kinetic analysis to inform the interpretation of currently used assays for detection and characterisation of human HLA-specific antibodies.

Currently employed clinical immunoassays for HLA-specific antibody assessment and immunological risk stratification include single antigen bead assays such as Luminex and cell-based assays such as flow cytometry and complement-dependent cytotoxicity [28, 206, 209]. Biophysical quantification of alloantibody-HLA interactions that were also characterised using these clinical immunoassays revealed that assay output is dependent on two fundamental antibody properties; their concentration within a sample and affinity for their antigenic target. Measuring the affinity of each antibody interaction also enabled the priming HLA to be differentiated from cross-reactive antigens, where interaction affinity closely correlated with cytotoxic capacity. Additionally, interactions measured to have a comparable K_Ds displayed similar cytotoxic potential. Solid phase assays were observed to have high sensitivity [195] but were unable to differentiate antibody interactions against priming versus cross-reactive HLA molecules. Importantly, interactions of both high and low affinity could generate positive MFI signals in Luminex assays whilst also producing negative results in CDC assays, highlighting the issues with regards to assay interpretation and the use of these outputs to define antibody pathogenicity [218]. Finally, the ability of a polyclonal serum to enhance the pathogenic capacity of the humoral response was explored, demonstrating that two antibodies that target different HLA on the same cell surface may have an additive cytotoxic effect. Overall, this work provides evidence in support of the hypothesis, demonstrating that antibody affinity is an important immunological parameter, where being able to quantify the strength an antibody has against donor-expressed HLA may provide important clinical insights to enable a more accurate assessment of antibody-related immunological risk.

Aim 2: Examining the relationship between alloantibody-HLA interaction affinity and the activation of intracellular signalling pathways that lead to endothelial cell activation.

Intracellular signalling events are an important aspect of the humoral immune response, where the initiation of signalling cascades upon antibody ligation to HLA expressed on primary isolated human aortic endothelial cells *in vitro* has previously been shown to result in a variety of cellular responses [270-312]. Endothelial cells could be successfully isolation and cultured from tissues of porcine origin, however issues surrounding donor sample quality and the inability to control endothelial cell differentiation prevented this from being achieved using

human aortic ring tissues. Upon procurement of commercially isolated endothelial cells to continue with the study, results from these experiments suggest that these cells were not a suitable model due to their susceptibility to activation upon minor, unavoidable changes in environmental conditions. The inability to establish a viable model for this study prevented the main aims from being addressed. If this aim were to be pursued further, optimisation of the method for isolation and culture of primary human aortic endothelial cells would need to be performed and/or alternative sources of these primary cells would need to be obtained.

Aim 3: Development of a novel method for HLA-specific antibody affinity and concentration quantification in patient sera to improve immunological risk assessment.

To be able to measure the affinity (KD) and concentration ([Ab]) of antibodies present in human-serum sample, a novel method called Microfluidic Antibody Affinity Profiling (MAAP) was developed. This method uses the principles of Microfluidic Diffusional Sizing (MDS) and Bayesian inference analysis to constrain both [Ab] and K_D parameters simultaneously without the need for antibody purification steps. MAAP demonstrated the capability to quantify anti-HLA antibodies spiked into PBS and blank serum. After method validation, MAAP was successfully applied to quantify the fundamental properties of alloantibodies in transplant recipient sera, offering a more in-depth quantitative assessment of the patient's humoral response that would otherwise be unattainable using the current immunoassays. This marked the first time these antibody properties could be obtained from clinical serum samples. In an exploratory study, an initial investigation was performed to assess the potential application of MAAP into the clinical setting. This preliminary data showed that the outputs of MAAP provided details about the affinity of recipient DSAs that was able to inform the interpretation of Luminex assays and offer data that may be used to determine antibody clinical significance. Overall, aim three of this thesis was achieved through the development of MAAP, where this method shows the potential to provide information that may enable better clinical decision-making during pre-transplant antibody-related immunological risk assessment and post-transplant immune monitoring.

6.2. Antibody Titre versus Affinity Assessment

The most common way that transplant patients are assessed for the presence of DSA is via Luminex single antigen bead assay, which is commercialised by two main companies, OneLambda and Immucor [388]. During routine clinical assessment, patient sera is incubated with these antigen-expressing beads, where the MFI output is said to represent the amount of antibody that is bound to HLA to each bead [214]. Despite this, the ability to visualise the true effect of antibody binding to these beads may be limited by several factors, including the interference of naturally occurring molecules, such as complement, causing the prozone effect [254, 389] or underrepresentation of HLA-specific antibody on the beads when many of the multiplexed antigens are recognised by the antibody [390], to name a few. The effect of this is particularly prevalent in highly sensitised patients, where one study showed up to 70% of assessed sera demonstrate inhibition of DSA detection [235]. To avoid these issues, some laboratories use serial dilutions of patient sera to get a broader picture of their DSA profiles [254, 391, 392]. By titrating the sera, the antibody strength is assigned by the last dilution of antibody that can generate a 'positive' output. The logic behind this methodology is that stronger interactions are expected to sustain for greater dilutions than weaker interactions if they were to measure the same starting MFI. Although carrying out antibody titrations in these studies has enabled separation of interactions with similar, 'lower' MFI outputs than when measured at neat [391], many questions still arise when it comes to evaluating these antibody titres. Firstly, consistent with multiple published studies and the experimental data presented in this thesis, titration does not enable interactions that are measured with higher MFIs, or higher affinities, to be distinguished from one another [233, 391]. Secondly, although titration aims to identify those stronger interaction which can sustain at a greater dilution, this output will still be heavily dependent on the initial antibody concentration within the serum. Furthermore, the threshold which defines a positive and negative interaction is often determined quite arbitrarily, meaning that the ability of an interaction to appear 'positive' will depend on where this threshold is manually set. Studies carried out to understand the significance of antibody titre in the clinical setting remain inconclusive, where the ability for antibody titre to offer a better indicator of graft loss or AMR than MFI is unclear [393]. From a more economic viewpoint, with the number of patients on the transplant list and the high cost

of commercial single antigen beads, the ability to assess the DSA titres of every patient is also not feasible.

In terms of cell-based immunoassays, carrying out titration studies does not necessarily mean that any further useful information will be provided than what can be gathered from doing the assessment at neat serum concentrations. Whilst assessing interactions using antibody dilutions in FC crossmatch assays may give a better insight into the strength of antibodies against HLA targets, this MFI output is also semi-quantitative and will be dependent on not only the initial antibody concentration within the sample but also the variable HLA expression on the donor cells, which is also inducible in a physiological setting [59]. The purpose of assessment via CDC assays is to gain an insight into the antibody's cytotoxic capacity to help understand its clinical significance. As documented in this study, the ability of an antibody to induce its cytotoxic effects is related to the affinity it has for its antigen. When carrying out CDC assays, if the antibody yields a positive result at any dilution then that is an automatic veto to transplant [394], regardless of what dilution this interaction would become negative. Besides, the limited sensitivity of CDC assays means that diluting the sera would only weaken the signal, opening the interaction up to misinterpretation which may prevent the true pathogenicity of the antibody from being obtained [259]. As documented throughout this thesis, the ability to measure the affinity that an antibody possesses for its antigen may not only enable you to gain a better insight into its ability to ligate with cell-expressed HLA, but it may also provide an insight into its fab-dependent complement fixing abilities. In contrast to carrying out titrations studies in immunoassays which only provide a limited insight into the strength of serum antibodies, assessments such as MAAP enables fully quantified determination of both antibody concentration and affinity in one experiment. Whilst higher outputs from the currently used immunoassays may be sufficient to assess the immunological risk associated with that specific DSA, it is the intermediate responses that are usually difficult to ascertain. In these scenarios it may be possible to use MAAP to quantify the affinity of the DSAs within the sample to provide additional information for immunological risk stratification.

Overall, the ability to titrate serum in assays may provide a slightly improved insight into the antibody load [233], however little evidence is given to suggest this offers an improved assessment of DSAs over MFI alone. Using affinity analysis, it may be possible to quantify the parameters of detected antibodies, which may be used to gain a more informed interpretation of their clinical significance.

6.3. Limitations and Future Directions

6.3.1. MDS and MAAP Assay Sensitivity

In terms of MAAP, the current sensitivity limits of this assay are governed by the ability of the Fluidity One-W instrument to detect the fluorescent antigenic tag as well as the fluorescent background within the serum being assessed. Being able to detect fluorophore-labelled antigen at lower concentrations is crucial to enable efficient quantification of high affinity interactions. Due to the current instrument specifications, the minimal detectible fluorophore-labelled HLA concentration is generally in the single nanomolar range (Appendix 15), making it difficult to accurately quantify interactions of sub-nanomolar affinity. Additionally, the ability to detect a fluorescent protein becomes even more complex in the presence of human serum due to its natural autofluorescence which may interfere with the fluorescent signal of the detection protein [362, 363]. Although optimal selection of the AF647 fluorescent molecule as well as the inclusion of a background subtraction step may have ameliorated many of these background issues, samples that have a naturally higher background fluorescence will increase the signal to noise ratio, further limiting the degree of labelled protein detection. Whilst serum cleaning steps have been incorporated into many other serum analysis techniques to reduce the amount of background signal, being able to reduce this noise in samples with higher autofluorescence may be critical for their accurate analysis. Potential ways to improve on the sensitivity of MAAP would be to alter the fluorescent label to one which gives a brighter signal, or to increase the antigen labelling ratio so that there are more fluorescent molecules per protein (although this may hinder epitope accessibility). Although these approaches may improve the ability to detect signals to a small extent, the need for drastic sensitivity enhancement may require the need for an alternative method which can detect picomolar concentrations of fluorophore-labelled molecules and/or single molecule-level detection [395].

6.3.2. Affinity vs Avidity Assessment

Interaction affinity is defined by the strength of a single protein-protein interaction that occurs between an antigen's epitope and the antibody's paratope, which is determined by the overall thermodynamic and electrochemical forces that occur at the binding interface [396]. In cases where proteins interact at multiple binding sites, the overall binding strength between the

molecules will be determined by three factors: the individual affinities of each binding site, the number of binding sites involved in the interaction (valency), and the accessibility of the binding sites due to each protein's overall structure. This is known as the functional affinity, or avidity [397]. Physiologically speaking, this work provides evidence to suggest that the ability of an Ig molecule to form contacts with cell-surface HLA will depend on the concentration of antibodies circulating within the blood, the affinity these antibodies have for their HLA antigen(s), and the extent of antibody-reactive HLA expression at the cell-surface. Upon interaction establishment, this HLA-ligated antibody is then able to carry out its pathogenic function which will also be dependent on antibody class/subclass identity, effector cell properties etc [84, 86, 94]. Whilst affinity is known to be associated with the ability of an antibody to form an interaction with its HLA antigen, the physiological relevance of an antibody's avidity against its target remains unexplored. By investigating the role of avidity in establishing/maintaining an alloantibody-HLA interaction and how this may also relate to the antibody's effector function may also provide further insights into an antibody's mechanism of action.

6.3.3. Heterogenous Samples in MAAP: Binding Competition and Subtype Determination

During development of the MAAP method, many of the assessed alloantibody-HLA interactions were carried out under controlled conditions in pure buffer, where the response observed was known to be exclusively due to the establishment of the interaction of interest. Whilst many other immunoassays use a secondary reporter to positively select for a target-ligated antibody [198, 201, 218], MAAP does not incorporate this secondary selection and therefore assumes that any signal increase is due to the binding of the desired interaction. When using crude samples such as human serum, the complete repertoire of components that make up each sample is unknown and therefore there is the potential for any unwanted antigen-reactive proteins present within a sample to interact with the target, which may be interpreted as positive binding. Additionally, the ability to detect and individually quantify each of the target-specific antibodies in heterogenous samples is not possible. At lower antigen concentrations, competition of antigen binding sites will conform to that of the strongest antibodies present [379]. Increasing the antigen concentration may result in saturation of these stronger antibodies, causing any free antigen binding sites to become occupied by weaker

binders. Quantification of such samples will result in measurements of affinity and antibody concentration that are convoluted outputs of both interacting species [379].

One potential avenue for further development of the MAAP assay is the ability to provide more information that reflects the pathogenic functionality of a detected antibody an HLA target. Whilst the current outputs of MAAP do not currently provide information on the Fc function of the detected antibodies [94, 117-138], there is scope to expand on this method so that this information can be obtainable. One way to do so would be to introduce a secondary analysis that can confirm the identity of the binding molecule and/or categorise the reactive antibody by its class/subclass, such as in the adapted Luminex assay [226, 398]. Exploiting this avenue may enable further information regarding the antibody effector function to become available, offering more in-depth profiling of antibodies which may help further understand their clinical significance.

6.3.4. The Clinical Translation of MAAP

In chapter six, two scenarios were presented that demonstrated how MAAP may provide further information that can be used to inform the currently employed immunoassays to improve clinical decision making. Although these cases provide good examples of how MAAP may be used in clinic, further studies would need to be carried out to truly understand the full potential of this method. Firstly, MAAP should be used to assess patients who have generated antibodies against HLA class II molecules. Recently, the occurrence of alloantibodies against HLA-DQ molecules has been linked to poor graft outcome after kidney transplantation [399, 400]. Although this thesis provides a series of proof-of-principle experiments for the effective use of MAAP with class II molecules, whether data generated using these class II HLAs has any clinical validity is yet to be explored. One limitation to this investigation is that monomeric, recombinant class II HLA molecules, particularly HLA-DP and -DQ molecules, are notoriously difficult to produce [401]. The limited availability of HLA reagents would restrict the analysis that can be carried out to those patients who have developed antibodies against HLA antigens that are available in purified form. An alternative approach is to establish a method for production of recombinant HLA molecules in-house. Another avenue to be explored is the potential for data generated from MAAP to provide information with regards to an antibody's priming event. The ability of an antibody to recognise non-priming HLA is dependent on the conservation of the priming epitope across different antigen species and/or the diversification of epitope specificity through B-cell "epitope spreading" [402-404]. Being

able to decipher whether a detected interaction is due to the recognition of a priming or cross-reactive antigen epitope may provide further understanding with regards to immunological memory and/or the clinical significance of an interaction. This is especially important in cases that involve highly sensitised patients that have a broad sensitisation profile [205, 405, 406], where being able to differentiate clinically irrelevant interactions from those that have clinical significance may have a considerable impact on the highly sensitised individual's capacity to access suitable donor organs.

In terms of assessing the validity of MAAP data in the clinical setting, broader studies need to be carried out to investigate which stages of clinical assessment may benefit from having the antibody information provided by MAAP. To assess whether the information obtainable by MAAP can be useful at the time of transplant, a larger cohort of past transplant recipients who had a history of DSA prior to transplantation could be examined retrospectively. Observing whether the outputs of MAAP could've been used to inform the clinical decision made at the point of transplant and/or whether the output data can explain the observed clinical outcomes would offer a good insight into MAAP's application. Another point at which data obtained from MAAP may be deemed clinically useful is during post-transplant immune monitoring. Being able to quantify the affinity and concentration of antibodies produced in response to graft introduction may offer a pre-requisite for antibody-mediated rejection diagnosis [407] and/or aid in the process of selecting suitable immunosuppression/therapeutics [408].

6.4. Final Remarks

This body of work highlights the influence of antibody concentration and interaction affinity when characterising HLA-specific antibodies in transplantation. By having this information available at the point of assessment, I have shown how this data may better the ability to interpret the outputs of immunoassays currently used for antibody assessment in clinic, enabling an improved understanding of antibody-related immunological risk to be attained. Through the development of MAAP, I have been able to introduce a novel method for the absolute quantification of these antibody parameters in human serum samples for the first time. I have also provided preliminary evidence of the ability to quantify these antibodies in real patient samples using this method, where the data acquired shows the potential to provide useful information further than what is currently obtainable, which may be used to make more informed clinical decisions. Overall, this thesis provides the groundwork for the molecular assessment of clinically relevant antibody-HLA interactions, whilst opening new avenues to seek explanations for the unanswered questions surrounding alloantibody significance and how clinical practice can be improved for maximal patient benefit.

References

[1] Wolfe RA, Ashby VB, Milford EL, Ojo AO, Ettenger RE, Agodoa LYC, et al. Comparison of Mortality in All Patients on Dialysis, Patients on Dialysis Awaiting Transplantation, and Recipients of a First Cadaveric Transplant. *New England Journal of Medicine*, 341(23):1725-1730, 1999.

[2] Ang GC. History of skin transplantation. *Clin Dermatol*, 23(4):320-324, 2005.

[3] Ullman E. Tissue and Organ Transplantation. *Ann Surg*, 60(2):195-219, 1914.

[4] Dörfler J. Uber die Naht von Arterienwunden 261. *Chir*, 22:1113, 1895.

[5] Jaboulay M, Briau E. Recherches expérimentales sur la suture et la greffe artérielles. *Lyon méd*, 81:97-99, 1896.

[6] Jaboulay M. Kidney grafts in the antecubital fossa by arterial and venous anastomosis. *Lyon méd*, 107:575-592, 1906.

[7] Unger E. Kidney transplantation. *Wien Klin Wochenschr*, 47:573, 1910.

[8] Voronoy U. Blocking the reticuloendothelial system in man in some forms of mercuric chloride intoxication and the transplantation of the cadaver kidney as a method of treatment for the anuria resulting from the intoxication. *Siglo Med*, 97:296, 1937.

[9] Merrill JP, Murray JE, Harrison JH, Guild WR. Successful homotransplantation of the human kidney between identical twins. *J Am Med Assoc*, 160(4):277-282, 1956.

[10] Brown JB. Homo grafting of skin: with report of success in identical twins. *Surgery*, 1(4):558-563, 1937.

[11] Converse JM, Duchet G. Successful homologous skin grafting in a war burn using an identical twin as donor. *Plast Reconstr Surg (1946)*, 2(4):342-344, 1947.

[12] Murray JE, Merrill JP, Dammin GJ, Dealy JB, Jr., Alexandre GW, Harrison JH. Kidney transplantation in modified recipients. *Ann Surg*, 156:337-355, 1962.

[13] Schöne G. Die heteroplastische und homöoplastische Transplantation: Springer; 1912.

[14] Gibson T, Medawar PB. The fate of skin homografts in man. *J Anat*, 77(Pt 4):299-310 294, 1943.

[15] Lindsten J, Ringertz N. The Nobel Prize in physiology or medicine, 1901-2000. *The*

Nobel prize: the first, 100:111-137, 2001.

[16] Silverstein AM. The lymphocyte in immunology: from James B. Murphy to James L. Gowans. *Nat Immunol*, 2(7):569-571, 2001.

[17] Auchincloss H, Jr., Winn HJ. Clarence Cook Little (1888-1971): the genetic basis of transplant immunology. *Am J Transplant*, 4(2):155-159, 2004.

[18] Gorer PA. The detection of a hereditary antigenic difference in the blood of mice by means of human group a serum. *Journal of Genetics*, 32(1):17, 1936.

[19] Gorer PA. The Detection of Antigenic Differences in Mouse Erythrocytes by the Employment of Immune Sera. *British Journal of Experimental Pathology*, 17(1):42-50, 1936.

[20] Gorer PA. The genetic and antigenic basis of tumour transplantation. *The Journal of Pathology and Bacteriology*, 44(3):691-697, 1937.

[21] Gorer PA, Lyman S, Snell GD. Studies on the Genetic and Antigenic Basis of Tumour Transplantation. Linkage between a Histocompatibility Gene and 'Fused' in Mice. *Proceedings of the Royal Society of London Series B*, 135:499, 1948.

[22] Dausset J. Iso-leuco-anticorps. *Acta haematologica*, 20(1-4):156-166, 1958.

[23] Van Rood J, Eernisse J, Van Leeuwen A. Leucocyte antibodies in sera from pregnant women. *Nature*, 181(4625):1735-1736, 1958.

[24] Payne R. Leukocyte agglutinins in human sera: correlation between blood transfusions and their development. *AMA archives of internal medicine*, 99(4):587-606, 1957.

[25] Van Rood JJ, Van Leeuwen A. LEUKOCYTE GROUPING. A METHOD AND ITS APPLICATION. *J Clin Invest*, 42(9):1382-1390, 1963.

[26] Payne R, Tripp M, Weigle J, Bodmer W, Bodmer J. A New Leukocyte Isoantigen System in Man. *Cold Spring Harb Symp Quant Biol*, 29:285-295, 1964.

[27] Thorsby E. A short history of HLA. *Tissue Antigens*, 74(2):101-116, 2009.

[28] Terasaki PI, McClelland JD. MICRODROPLET ASSAY OF HUMAN SERUM CYTOTOXINS. *Nature*, 204:998-1000, 1964.

[29] Kissmeyer-Nielsen F, Svejgaard A, Hauge M. Genetics of the human HL-A transplantation system. *Nature*, 219(5159):1116-1119, 1968.

[30] Thorsby E, Sandberg L, Lindholm A, Kissmeyer-Nielsen F. The HL-A system: evidence of a third sub-locus. *Scand J Haematol*, 7(3):195-200, 1970.

[31] Bach F, Hirschhorn K. Lymphocyte Interaction: A Potential Histocompatibility Test in Vitro. *Science*, 143(3608):813-814, 1964.

[32] Bain B, Vas MR, Lowenstein L. The Development of Large Immature Mononuclear Cells in Mixed Leukocyte Cultures. *Blood*, 23:108-116, 1964.

[33] Bach FH, Amos DB. Hu-1: Major histocompatibility locus in man. *Science*, 156(3781):1506-1508, 1967.

[34] Bach FH, Widmer MB, Bach ML, Klein J. Serologically defined and lymphocyte-defined components of the major histocompatibility complex in the mouse. *J Exp Med*, 136(6):1430-1444, 1972.

[35] Sheehy MJ, Sondel PM, Bach ML, Wank R, Bach FH. HL-A LD (lymphocyte defined) typing: a rapid assay with primed lymphocytes. *Science*, 188(4195):1308-1310, 1975.

[36] Albert E, Balner H, Cohen N, Collins N, David C, Dorf M, et al. The major histocompatibility system in man and animals: Springer Science & Business Media; 2012.

[37] Horton R, Wilming L, Rand V, Lovering RC, Bruford EA, Khodiyar VK, et al. Gene map of the extended human MHC. *Nat Rev Genet*, 5(12):889-899, 2004.

[38] Monos DS, Winchester RJ. The major histocompatibility complex. Clinical Immunology: Elsevier; 2019. p. 79-92. e71.

[39] Braud VM, Allan DSJ, McMichael AJ. Functions of nonclassical MHC and non-MHC-encoded class I molecules. *Current Opinion in Immunology*, 11(1):100-108, 1999.

[40] Allen RL. Non-classical immunology. *Genome Biology*, 2(2):reports4004.4001, 2001.

[41] Neefjes J, Jongsma MLM, Paul P, Bakke O. Towards a systems understanding of MHC class I and MHC class II antigen presentation. *Nature Reviews Immunology*, 11(12):823-836, 2011.

[42] Ayala Garcia MA, Gonzalez Yebra B, Lopez Flores AL, Guani Guerra E. The major histocompatibility complex in transplantation. *J Transplant*, 2012:842141, 2012.

[43] Cruz-Tapias P, Castiblanco J, Anaya J-M. Major histocompatibility complex: antigen processing and presentation. Autoimmunity: From Bench to Bedside [Internet]: El Rosario University Press; 2013.

[44] Bjorkman PJ, Saper MA, Samraoui B, Bennett WS, Strominger JL, Wiley DC. Structure of the human class I histocompatibility antigen, HLA-A2. *Nature*, 329(6139):506-512, 1987.

[45] Walter P, Johnson AE. Signal sequence recognition and protein targeting to the endoplasmic reticulum membrane. *Annu Rev Cell Biol*, 10:87-119, 1994.

[46] Song W, Raden D, Mandon EC, Gilmore R. Role of Sec61alpha in the regulated transfer of the ribosome-nascent chain complex from the signal recognition particle to the translocation channel. *Cell*, 100(3):333-343, 2000.

[47] Bacher G, Pool M, Dobberstein B. The ribosome regulates the GTPase of the beta-subunit of the signal recognition particle receptor. *J Cell Biol*, 146(4):723-730, 1999.

[48] Lemberg MK, Bland FA, Weihofen A, Braud VM, Martoglio B. Intramembrane proteolysis of signal peptides: an essential step in the generation of HLA-E epitopes. *J Immunol*, 167(11):6441-6446, 2001.

[49] Blobel G. Intracellular protein topogenesis. *Proc Natl Acad Sci U S A*, 77(3):1496-1500, 1980.

[50] Cresswell P, Ackerman AL, Giodini A, Peaper DR, Wearsch PA. Mechanisms of MHC class I-restricted antigen processing and cross-presentation. *Immunol Rev*, 207:145-157, 2005.

[51] Dick TB. Assembly of MHC class I peptide complexes from the perspective of disulfide bond formation. *Cell Mol Life Sci*, 61(5):547-556, 2004.

[52] Serwold T, Gonzalez F, Kim J, Jacob R, Shastri N. ERAAP customizes peptides for MHC class I molecules in the endoplasmic reticulum. *Nature*, 419(6906):480-483, 2002.

[53] Reits E, Griekspoor A, Neijssen J, Groothuis T, Jalink K, Van Veelen P, et al. Peptide diffusion, protection, and degradation in nuclear and cytoplasmic compartments before antigen presentation by MHC class I. *Immunity*, 18(1):97-108, 2003.

[54] Wearsch PA, Cresswell P. The quality control of MHC class I peptide loading. *Curr Opin Cell Biol*, 20(6):624-631, 2008.

[55] Lamers M, Berlin I, Neefjes J. Antigen Presentation: Visualizing the MHC Class I Peptide-Loading Bottleneck. *Curr Biol*, 28(2):R83-R86, 2018.

[56] Dick TP, Bangia N, Peaper DR, Cresswell P. Disulfide bond isomerization and the assembly of MHC class I-peptide complexes. *Immunity*, 16(1):87-98, 2002.

[57] Ilca T, Boyle LH. The Ins and Outs of TAPBPR. *Curr Opin Immunol*, 64:146-151, 2020.

[58] Boyle LH, Hermann C, Boname JM, Porter KM, Patel PA, Burr ML, et al. Tapasin-related protein TAPBPR is an additional component of the MHC class I presentation pathway. *Proc Natl Acad Sci U S A*, 110(9):3465-3470, 2013.

[59] Steimle V, Siegrist CA, Mottet A, Lisowska-Grospierre B, Mach B. Regulation of MHC class II expression by interferon-gamma mediated by the transactivator gene CIITA. *Science*, 265(5168):106-109, 1994.

[60] Alfonso C, Karlsson L. Nonclassical MHC class II molecules. *Annu Rev Immunol*, 18:113-142, 2000.

[61] Brown JH, Jardetzky TS, Gorga JC, Stern LJ, Urban RG, Strominger JL, et al. Three-dimensional structure of the human class II histocompatibility antigen HLA-DR1. *Nature*, 364(6432):33-39, 1993.

[62] Chicz RM, Urban RG, Lane WS, Gorga JC, Stern LJ, Vignali DA, et al. Predominant naturally processed peptides bound to HLA-DR1 are derived from MHC-related molecules and are heterogeneous in size. *Nature*, 358(6389):764-768, 1992.

[63] Roche PA. Out damned CLIP! Out, I say! *Science*, 274(5287):526-527, 1996.

[64] Janeway Jr CA, Travers P, Walport M, Shlomchik MJ. Antigen recognition by T cells. Immunobiology: The Immune System in Health and Disease 5th edition: Garland

Science; 2001.

[65] Shiina T, Hosomichi K, Inoko H, Kulski JK. The HLA genomic loci map: expression, interaction, diversity and disease. *J Hum Genet*, 54(1):15-39, 2009.

[66] Behring Ev. Ueber das zustandekommen der diphtherie-immunität und der tetanus-immunität bei thieren. Drucke 19 Jh, 1890.

[67] Kaufmann SH. Emil von Behring: translational medicine at the dawn of immunology. *Nature Reviews Immunology*, 17(6):341-343, 2017.

[68] Cavaillon JM, Sansonetti P, Goldman M. 100th Anniversary of Jules Bordet's Nobel Prize: Tribute to a Founding Father of Immunology. *Front Immunol*, 10:2114, 2019.

[69] Ehrlich P. Die seitenkettentheorie und ihre gegner. *Münchner Med Wochenschr*, 52:2123-2124, 1901.

[70] Lemieux RU, Spohr U. How Emil Fischer was led to the lock and key concept for enzyme specificity. *Adv Carbohydr Chem Biochem*, 50:1-20, 1994.

[71] Marrack J. Nature of Antibodies. *Nature*, 133(3356):292-293, 1934.

[72] Goldberg RJ. A theory of antibody—antigen reactions. I. Theory for reactions of multivalent antigen with bivalent and univalent antibody2. *Journal of the American Chemical Society*, 74(22):5715-5725, 1952.

[73] Goldberg RJ. A Theory of Antibody—Antigen Reactions. II. Theory for Reactions of Multivalent Antigen with Multivalent Antibody. *Journal of the American Chemical Society*, 75(13):3127-3131, 1953.

[74] Fagraeus A. The plasma cellular reaction and its relation to the formation of antibodies in vitro. *J Immunol*, 58(1):1-13, 1948.

[75] Burnet FM. A modification of Jerne's theory of antibody production using the concept of clonal selection. *Australian Journal of Science*, 20(3):67-69, 1957.

[76] Edelman GM. Dissociation of γ-globulin. *Journal of the American Chemical Society*, 81(12):3155-3156, 1959.

[77] Porter RR. The hydrolysis of rabbit y-globulin and antibodies with crystalline papain.

Biochem J, 73(1):119-126, 1959.

[78] Poljak RJ, Amzel LM, Avey HP, Chen BL, Phizackerley RP, Saul F. Three-dimensional structure of the Fab' fragment of a human immunoglobulin at 2,8-A resolution. *Proc Natl Acad Sci U S A*, 70(12):3305-3310, 1973.

[79] Inbar D, Hochman J, Givol D. Localization of antibody-combining sites within the variable portions of heavy and light chains. *Proc Natl Acad Sci U S A*, 69(9):2659-2662, 1972.

[80] Kohler G, Milstein C. Continuous cultures of fused cells secreting antibody of predefined specificity. *Nature*, 256(5517):495-497, 1975.

[81] Porter RR. Separation and isolation of fractions of rabbit gamma-globulin containing the antibody and antigenic combining sites. *Nature*, 182(4636):670-671, 1958.

[82] Nisonoff A, Wissler FC, Lipman LN. Properties of the major component of a peptic digest of rabbit antibody. *Science*, 132(3441):1770-1771, 1960.

[83] Williams AF, Barclay AN. The immunoglobulin superfamily--domains for cell surface recognition. *Annu Rev Immunol*, 6:381-405, 1988.

[84] Schroeder HW, Cavacini L. Structure and function of immunoglobulins. *Journal of Allergy and Clinical Immunology*, 125(2, Supplement 2):S41-S52, 2010.

[85] Davies DR, Chacko S. Antibody structure. *Accounts of Chemical Research*, 26(8):421-427, 1993.

[86] Chiu ML, Goulet DR, Teplyakov A, Gilliland GL. Antibody Structure and Function: The Basis for Engineering Therapeutics. *Antibodies*, 8(4):55, 2019.

[87] North B, Lehmann A, Dunbrack RL. A New Clustering of Antibody CDR Loop Conformations. *Journal of Molecular Biology*, 406(2):228-256, 2011.

[88] Dörner T, Foster SJ, Farner NL, Lipsky PE. Somatic hypermutation of human immunoglobulin heavy chain genes: targeting of RGYW motifs on both DNA strands. *European journal of immunology*, 28(10):3384-3396, 1998.

[89] Rada C, Ehrenstein MR, Neuberger MS, Milstein C. Hot Spot Focusing of Somatic Hypermutation in MSH2-Deficient Mice Suggests Two Stages of Mutational Targeting.

Immunity, 9(1):135-141, 1998.

[90] Jennewein MF, Alter G. The Immunoregulatory Roles of Antibody Glycosylation. *Trends in Immunology*, 38(5):358-372, 2017.

[91] Arnold JN, Wormald MR, Sim RB, Rudd PM, Dwek RA. The impact of glycosylation on the biological function and structure of human immunoglobulins. *Annu Rev Immunol*, 25:21-50, 2007.

[92] Janeway Jr CA, Travers P, Walport M, Shlomchik MJ. Structural variation in immunoglobulin constant regions. Immunobiology: The Immune System in Health and Disease 5th edition: Garland Science; 2001.

[93] Cruse J, Lewis R. Atlas of immunology. ed. Boca Raton, Fla.: CRC. London: Taylor & Francis; 2010.

[94] Vidarsson G, Dekkers G, Rispens T. IgG subclasses and allotypes: from structure to effector functions. *Front Immunol*, 5:520, 2014.

[95] Hamilton RG. Human IgG subclass measurements in the clinical laboratory. *Clin Chem*, 33(10):1707-1725, 1987.

[96] Roux KH, Strelets L, Michaelsen TE. Flexibility of human IgG subclasses. *J Immunol*, 159(7):3372-3382, 1997.

[97] Redpath S, Michaelsen TE, Sandlie I, Clark MR. The influence of the hinge region length in binding of human IgG to human Fcγ receptors. *Human immunology*, 59(11):720-727, 1998.

[98] Nezlin R. CHAPTER 1 - General Characteristics of Immunoglobulin Molecules. In: Nezlin R, editor. The Immunoglobulins. New York: Academic Press; 1998. p. 3-73.

[99] Lightle S, Aykent S, Lacher N, Mitaksov V, Wells K, Zobel J, et al. Mutations within a human IgG2 antibody form distinct and homogeneous disulfide isomers but do not affect Fc gamma receptor or C1q binding. *Protein Science*, 19(4):753-762, 2010.

[100] Wypych J, Li M, Guo A, Zhang Z, Martinez T, Allen MJ, et al. Human IgG2 Antibodies Display Disulfide-mediated Structural Isoforms*. *Journal of Biological Chemistry*, 283(23):16194-16205, 2008.

[101] Aalberse RC, Schuurman J. IgG4 breaking the rules. *Immunology*, 105(1):9-19, 2002.

[102] Rispens T, Ooijevaar-de Heer P, Bende O, Aalberse RC. Mechanism of Immunoglobulin G4 Fab-arm Exchange. *Journal of the American Chemical Society*, 133(26):10302-10311, 2011.

[103] Woof JM, Russell MW. Structure and function relationships in IgA. *Mucosal Immunol*, 4(6):590-597, 2011.

[104] Zikan J, Novotny J, Trapane TL, Koshland ME, Urry DW, Bennett JC, et al. Secondary structure of the immunoglobulin J chain. *Proc Natl Acad Sci U S A*, 82(17):5905-5909, 1985.

[105] Collins C, Tsui FW, Shulman MJ. Differential activation of human and guinea pig complement by pentameric and hexameric IgM. *Eur J Immunol*, 32(6):1802-1810, 2002.

[106] Stone KD, Prussin C, Metcalfe DD. IgE, mast cells, basophils, and eosinophils. *Journal of Allergy and Clinical Immunology*, 125(2, Supplement 2):S73-S80, 2010.

[107] Watson CT, Breden F. The immunoglobulin heavy chain locus: genetic variation, missing data, and implications for human disease. *Genes Immun*, 13(5):363-373, 2012.

[108] Zachau H. Immunoglobulin genes. *Immunology today*, 10(8):S9-10, 1989.

[109] Kawasaki K, Minoshima S, Nakato E, Shibuya K, Shintani A, Schmeits JL, et al. One-megabase sequence analysis of the human immunoglobulin lambda gene locus. *Genome Res*, 7(3):250-261, 1997.

[110] Tallmadge RL, Tseng CT, Felippe MJB. Diversity of immunoglobulin lambda light chain gene usage over developmental stages in the horse. *Developmental & Comparative Immunology*, 46(2):171-179, 2014.

[111] Desjardins L, Liabeuf S, Lenglet A, Lemke H-D, Vanholder R, Choukroun G, et al. Association between Free Light Chain Levels, and Disease Progression and Mortality in Chronic Kidney Disease. *Toxins*, 5(11):2058-2073, 2013.

[112] Rafae A, Malik MN, Abu Zar M, Durer S, Durer C. An Overview of Light Chain Multiple Myeloma: Clinical Characteristics and Rarities, Management Strategies, and

Disease Monitoring. *Cureus*, 10(8):e3148, 2018.

[113] de Lange GG. Polymorphisms of human immunoglobulins: Gm, Am, Em and Km allotypes. *Exp Clin Immunogenet*, 6(1):7-17, 1989.

[114] Webster CI, Bryson CJ, Cloake EA, Jones TD, Austin MJ, Karle AC, et al. A comparison of the ability of the human IgG1 allotypes G1m3 and G1m1,17 to stimulate T-cell responses from allotype matched and mismatched donors. *mAbs*, 8(2):253-263, 2016.

[115] Fudenberg HH, Fudenberg BR. Antibody to Hereditary Human Gamma-Globulin (Gm) Factor Resulting from Maternal-Fetal Incompatibility. *Science*, 145(3628):170-171, 1964.

[116] Jefferis R, Lefranc M-P. Human immunoglobulin allotypes. *mAbs*, 1(4):332-338, 2009.

[117] Diebolder CA, Beurskens FJ, Jong RNd, Koning RI, Strumane K, Lindorfer MA, et al. Complement Is Activated by IgG Hexamers Assembled at the Cell Surface. *Science*, 343(6176):1260-1263, 2014.

[118] Gessner JE, Heiken H, Tamm A, Schmidt RE. The IgG Fc receptor family. *Ann Hematol*, 76(6):231-248, 1998.

[119] Koenderman L. Inside-Out Control of Fc-Receptors. *Front Immunol*, 10:544, 2019.

[120] Bruhns P, Iannascoli B, England P, Mancardi DA, Fernandez N, Jorieux S, et al. Specificity and affinity of human Fcγ receptors and their polymorphic variants for human IgG subclasses. *Blood*, 113(16):3716-3725, 2009.

[121] Powell MS, Hogarth PM. Fc receptors. *Adv Exp Med Biol*, 640:22-34, 2008.

[122] Getahun A, Cambier JC. Of ITIMs, ITAMs, and ITAMis: revisiting immunoglobulin Fc receptor signaling. *Immunol Rev*, 268(1):66-73, 2015.

[123] Ben Mkaddem S, Benhamou M, Monteiro RC. Understanding Fc Receptor Involvement in Inflammatory Diseases: From Mechanisms to New Therapeutic Tools. *Front Immunol*, 10:811, 2019.

[124] Boggon TJ, Eck MJ. Structure and regulation of Src family kinases. *Oncogene*, 23(48):7918-7927, 2004.

[125] Geissmann F, Launay P, Pasquier B, Lepelletier Y, Leborgne M, Lehuen A, et al. A subset of human dendritic cells expresses IgA Fc receptor (CD89), which mediates internalization and activation upon cross-linking by IgA complexes. *J Immunol*, 166(1):346-352, 2001.

[126] Morton HC, van Egmond M, van de Winkel JG. Structure and function of human IgA Fc receptors (Fc alpha R). *Crit Rev Immunol*, 16(4):423-440, 1996.

[127] Ishizaka T, Ishizaka K. Triggering of histamine release from rat mast cells by divalent antibodies against IgE-receptors. *The Journal of Immunology*, 120(3):800-805, 1978.

[128] Wakahara S, Fujii Y, Nakao T, Tsuritani K, Hara T, Saito H, et al. GENE EXPRESSION PROFILES FOR FcεRI, CYTOKINES AND CHEMOKINES UPON FcεRI ACTIVATION IN HUMAN CULTURED MAST CELLS DERIVED FROM PERIPHERAL BLOOD. *Cytokine*, 16(4):143-152, 2001.

[129] Ferguson DC, Blanco JG. Regulation of the Human Fc-Neonatal Receptor alpha-Chain Gene FCGRT by MicroRNA-3181. *Pharmaceutical Research*, 35(1):15, 2018.

[130] Liu X, Ye L, Bai Y, Mojidi H, Simister NE, Zhu X. Activation of the JAK/STAT-1 signaling pathway by IFN-gamma can down-regulate functional expression of the MHC class I-related neonatal Fc receptor for IgG. *J Immunol*, 181(1):449-463, 2008.

[131] Liu X, Ye L, Christianson GJ, Yang JQ, Roopenian DC, Zhu X. NF-kappaB signaling regulates functional expression of the MHC class I-related neonatal Fc receptor for IgG via intronic binding sequences. *J Immunol*, 179(5):2999-3011, 2007.

[132] Brambell FW. The transmission of immunity from mother to young and the catabolism of immunoglobulins. *Lancet*, 2(7473):1087-1093, 1966.

[133] Shah U, Dickinson BL, Blumberg RS, Simister NE, Lencer WI, Walker AW. Distribution of the IgG Fc receptor, FcRn, in the human fetal intestine. *Pediatric research*, 53(2):295-301, 2003.

[134] Schlachetzki F, Zhu C, Pardridge WM. Expression of the neonatal Fc receptor (FcRn) at the blood-brain barrier. *J Neurochem*, 81(1):203-206, 2002.

[135] Vaysburd M, Watkinson RE, Cooper H, Reed M, O'Connell K, Smith J, et al. Intracellular antibody receptor TRIM21 prevents fatal viral infection. *Proc Natl Acad*

Sci U S A, 110(30):12397-12401, 2013.

[136] Rakebrandt N, Lentes S, Neumann H, James LC, Neumann-Staubitz P. Antibody- and TRIM21-dependent intracellular restriction of Salmonella enterica. *Pathog Dis*, 72(2):131-137, 2014.

[137] Anthony RM, Kobayashi T, Wermeling F, Ravetch JV. Intravenous gammaglobulin suppresses inflammation through a novel T(H)2 pathway. *Nature*, 475(7354):110-113, 2011.

[138] Sidorin EV, Solov'eva TF. IgG-binding proteins of bacteria. *Biochemistry (Mosc)*, 76(3):295-308, 2011.

[139] Rogers NJ, Lechler RI. Allorecognition. *American Journal of Transplantation*, 1(2):97-102, 2001.

[140] Afzali B, Lombardi G, Lechler RI. Pathways of major histocompatibility complex allorecognition. *Curr Opin Organ Transplant*, 13(4):438-444, 2008.

[141] Siu JHY, Surendrakumar V, Richards JA, Pettigrew GJ. T cell Allorecognition Pathways in Solid Organ Transplantation. *Front Immunol*, 9:2548, 2018.

[142] Ali JM, Negus MC, Conlon TM, Harper IG, Qureshi MS, Motallebzadeh R, et al. Diversity of the CD4 T Cell Alloresponse: The Short and the Long of It. Cell Rep, 14(5):1232-1245, 2016.

[143] Warrens AN, Lombardi G, Lechler RI. Presentation and recognition of major and minor histocompatibility antigens. *Transplant Immunology*, 2(2):103-107, 1994.

[144] Shoskes DA, Wood KJ. Indirect presentation of MHC antigens in transplantation. *Immunol Today*, 15(1):32-38, 1994.

[145] Benichou G, Takizawa PA, Olson CA, McMillan M, Sercarz EE. Donor major histocompatibility complex (MHC) peptides are presented by recipient MHC molecules during graft rejection. *Journal of Experimental Medicine*, 175(1):305-308, 1992.

[146] Valujskikh A, Lantz O, Celli S, Matzinger P, Heeger PS. Cross-primed CD8+ T cells mediate graft rejection via a distinct effector pathway. *Nature Immunology*, 3(9):844-851, 2002.

[147] Harshyne LA, Watkins SC, Gambotto A, Barratt-Boyes SM. Dendritic Cells Acquire Antigens from Live Cells for Cross-Presentation to CTL. *The Journal of Immunology*, 166(6):3717-3723, 2001.

[148] Herrera OB, Golshayan D, Tibbott R, Ochoa FS, James MJ, Marelli-Berg FM, et al. A Novel Pathway of Alloantigen Presentation by Dendritic Cells. *The Journal of Immunology*, 173(8):4828-4837, 2004.

[149] Russo V, Zhou D, Sartirana C, Rovere P, Villa A, Rossini S, et al. Acquisition of intact allogeneic human leukocyte antigen molecules by human dendritic cells. *Blood*, 95(11):3473-3477, 2000.

[150] Mogensen TH. Pathogen Recognition and Inflammatory Signaling in Innate Immune Defenses. *Clinical Microbiology Reviews*, 22(2):240-273, 2009.

[151] Sharma SK, Naidu G. The role of danger-associated molecular patterns (DAMPs) in trauma and infections. J Thorac Dis, 8(7):1406-1409, 2016.

[152] Heeger PS. T-cell allorecognition and transplant rejection: a summary and update. *Am J Transplant*, 3(5):525-533, 2003.

[153] Zhang N, Bevan MJ. CD8(+) T cells: foot soldiers of the immune system. *Immunity*, 35(2):161-168, 2011.

[154] Barry M, Bleackley RC. Cytotoxic T lymphocytes: all roads lead to death. *Nat Rev Immunol*, 2(6):401-409, 2002.

[155] Luckheeram RV, Zhou R, Verma AD, Xia B. CD4(+)T cells: differentiation and functions. *Clin Dev Immunol*, 2012:925135, 2012.

[156] Rocha PN, Plumb TJ, Crowley SD, Coffman TM. Effector mechanisms in transplant rejection. *Immunological reviews*, 196(1):51-64, 2003.

[157] Tarlinton D, Lew A. Antigen to the Node: B Cells Go Native. *Immunity*, 26(4):388-390, 2007.

[158] Waldmann H, Munro A. B cell activation. *Immunological reviews*, 23(1):213-222, 1975.

[159] Tarlinton DM, Batista F, Smith KG. The B-cell response to protein antigens in

immunity and transplantation. *Transplantation*, 85(12):1698-1704, 2008.

[160] McHeyzer-Williams MG, McLean MJ, Lalor PA, Nossal GJ. Antigen-driven B cell differentiation in vivo. *J Exp Med*, 178(1):295-307, 1993.

[161] Zhang Y, Garcia-Ibanez L, Toellner KM. Regulation of germinal center B-cell differentiation. *Immunol Rev*, 270(1):8-19, 2016.

[162] Tarlinton DM, Smith KG. Dissecting affinity maturation: a model explaining selection of antibody-forming cells and memory B cells in the germinal centre. *Immunol Today*, 21(9):436-441, 2000.

[163] Stavnezer J, Jeroen E.J. Guikema, Schrader CE. Mechanism and Regulation of Class Switch Recombination. *Annual Review of Immunology*, 26(1):261-292, 2008.

[164] Shapiro-Shelef M, Calame K. Regulation of plasma-cell development. *Nat Rev Immunol*, 5(3):230-242, 2005.

[165] Román VRG, Murray JC, Weiner LM. Antibody-dependent cellular cytotoxicity (ADCC). Antibody Fc: Elsevier; 2014. p. 1-27.

[166] Haas P-J, van Strijp J. Anaphylatoxins. *Immunologic Research*, 37(3):161-175, 2007.

[167] Loupy A, Lefaucheur C, Vernerey D, Prugger C, Duong van Huyen JP, Mooney N, et al. Complement-binding anti-HLA antibodies and kidney-allograft survival. *N Engl J Med*, 369(13):1215-1226, 2013.

[168] Colvin RB, Smith RN. Antibody-mediated organ-allograft rejection. *Nature Reviews Immunology*, 5(10):807-817, 2005.

[169] Lubbers R, van Essen MF, van Kooten C, Trouw LA. Production of complement components by cells of the immune system. Clin Exp Immunol, 188(2):183-194, 2017.

[170] Worthington JE, Martin S, Al-Husseini DM, Dyer PA, Johnson RW. Posttransplantation production of donor HLA-specific antibodies as a predictor of renal transplant outcome1. *Transplantation*, 75(7):1034-1040, 2003.

[171] Williams GM, Hume DM, Hudson Jr RP, Morris PJ, Kano K, Milgrom F. Hyperacute renal-homograft rejection in man. *New England Journal of Medicine*, 279(12):611-618, 1968.

[172] Schinstock C, Stegall MD. Acute Antibody-Mediated Rejection in Renal Transplantation: Current Clinical Management. *Current Transplantation Reports*, 1(2):78-85, 2014.

[173] Libby P, Pober JS. Chronic rejection. *Immunity*, 14(4):387-397, 2001.

[174] Martinu T, Howell DN, Palmer SM. Acute cellular rejection and humoral sensitization in lung transplant recipients. *Semin Respir Crit Care Med*, 31(2):179-188, 2010.

[175] Li C, Yang CW. The pathogenesis and treatment of chronic allograft nephropathy. *Nature Reviews Nephrology*, 5(9):513-519, 2009.

[176] Sun Q, Yang Y. Late and chronic antibody-mediated rejection: main barrier to long term graft survival. *Clin Dev Immunol*, 2013:859761, 2013.

[177] Zachary AA, Leffell MS. HLA Mismatching Strategies for Solid Organ Transplantation - A Balancing Act. *Front Immunol*, 7:575, 2016.

[178] Persijn GG, Cohen B, Lansbergen Q, D'Amaro J, Selwood N, Wing A, et al. Effect of HLA-A and HLA-B matching on survival of grafts and recipients after renal transplantation. *N Engl J Med*, 307(15):905-908, 1982.

[179] Ting A, Morris PJ. POWERFUL EFFECT OF HL-DR MATCHING ON SURVIVAL OF CADAVERIC RENAL ALLOGRAFTS. *The Lancet*, 316(8189):282-285, 1980.

[180] Opelz G, Wujciak T. Cadaveric kidneys should be allocated according to the HLA match. *Transplant Proc*, 27(1):93-99, 1995.

[181] Kim JJ, Fuggle SV, Marks SD. Does HLA matching matter in the modern era of renal transplantation? *Pediatr Nephrol*, 36(1):31-40, 2021.

[182] Kloss K, Ismail S, Redeker S, van Hoogdalem L, Luchtenburg A, Busschbach JJ, et al. Factors influencing access to kidney transplantation: a research protocol of a qualitative study on stakeholders' perspectives. *BMJ open*, 9(9):e032694, 2019.

[183] Erlich HA, Opelz G, Hansen J. HLA DNA Typing and Transplantation. *Immunity*, 14(4):347-356, 2001.

[184] Taylor CJ, Dyer PA. Maximizing the benefits of HLA matching for renal transplantation: Alleles, specificities, CREGs, epitopes, or residues? *Transplantation*,

68(8):1093-1094, 1999.

[185] Pratschke J, Dragun D, Hauser IA, Horn S, Mueller TF, Schemmer P, et al. Immunological risk assessment: The key to individualized immunosuppression after kidney transplantation. *Transplantation Reviews*, 30(2):77-84, 2016.

[186] House AA, Chang PC, Luke PP, Leckie SH, Howson WT, Ball EJ, et al. Re-exposure to mismatched HLA class I is a significant risk factor for graft loss: multivariable analysis of 259 kidney retransplants. *Transplantation*, 84(6):722-728, 2007.

[187] Starzl T, Marchioro T, Terasaki P, Porter K, Faris T, Merrman T, et al. Chronic survival after human renal homotransplantation: Lymphocyte-antigen matching, pathology and influence of thymectomy. *Transplantation*, 4(3):350, 1966.

[188] Terasaki PI, Mickey MR, Singal DP, Mittal KK, Patel R. Serotyping for homotransplantation. XX. Selection of recipients for cadaver donor transplants. *N Engl J Med*, 279(20):1101-1103, 1968.

[189] Festenstein H, Doyle P, Holmes J. Long-term follow-up in London Transplant Group recipients of cadaver renal allografts. The influence of HLA matching on transplant outcome. *N Engl J Med*, 314(1):7-14, 1986.

[190] Wujciak T, Opelz G. EVALUATION OF HLA MATCHING FOR CREG ANTIGENS IN EUROPE1. *Transplantation*, 68(8):1097-1099, 1999.

[191] Crowe DO. The effect of cross-reactive epitope group matching on allocation and sensitization. *Clin Transplant*, 17 Suppl 9:13-16, 2003.

[192] Duquesnoy RJ, Askar M. HLAMatchmaker: A Molecularly Based Algorithm for Histocompatibility Determination. V. Eplet Matching for HLA-DR, HLA-DQ, and HLA-DP. *Human immunology*, 68(1):12-25, 2007.

[193] Lobashevsky AL, Senkbeil RW, Shoaf JL, Stephenson AK, Skelton SB, Burke RM, et al. The number of amino acid residues mismatches correlates with flow cytometry crossmatching results in high PRA renal patients. *Human immunology*, 63(5):364-374, 2002.

[194] Kosmoliaptsis V, Bradley JA, Sharples LD, Chaudhry A, Key T, Goodman RS, et al. Predicting the immunogenicity of human leukocyte antigen class I alloantigens using

structural epitope analysis determined by HLAMatchmaker. *Transplantation*, 85(12):1817-1825, 2008.

[195] Mallon DH, Kling C, Robb M, Ellinghaus E, Bradley JA, Taylor CJ, et al. Predicting Humoral Alloimmunity from Differences in Donor and Recipient HLA Surface Electrostatic Potential. *J Immunol*, 201(12):3780-3792, 2018.

[196] Mallon D, Kling C, Bradley JA, Taylor C, Kabelitz D, Kosmoliaptsis V. Computational scoring system to predict HLA immunogenicity. *The Lancet*, 387:S68, 2016.

[197] Sidney J, Peters B, Frahm N, Brander C, Sette A. HLA class I supertypes: a revised and updated classification. *BMC immunology*, 9(1):1-15, 2008.

[198] Picascia A, Infante T, Napoli C. Luminex and antibody detection in kidney transplantation. *Clin Exp Nephrol*, 16(3):373-381, 2012.

[199] Amico P, Honger G, Mayr M, Steiger J, Hopfer H, Schaub S. Clinical relevance of pretransplant donor-specific HLA antibodies detected by single-antigen flow-beads. *Transplantation*, 87(11):1681-1688, 2009.

[200] Schonemann C, Lachmann N, Kiesewetter H, Salama A. Flow cytometric detection of complement-activating HLA antibodies. *Cytometry B Clin Cytom*, 62(1):39-45, 2004.

[201] Chen G, Tyan DB. C1q assay for the detection of complement fixing antibody to HLA antigens. Transplantation Immunology: Springer; 2013. p. 305-311.

[202] Taylor RP, Lindorfer MA. Cytotoxic mechanisms of immunotherapy: Harnessing complement in the action of anti-tumor monoclonal antibodies. *Semin Immunol*, 28(3):309-316, 2016.

[203] Tait BD. Detection of HLA Antibodies in Organ Transplant Recipients - Triumphs and Challenges of the Solid Phase Bead Assay. *Front Immunol*, 7:570, 2016.

[204] Appel JZ, 3rd, Hartwig MG, Cantu E, 3rd, Palmer SM, Reinsmoen NL, Davis RD. Role of flow cytometry to define unacceptable HLA antigens in lung transplant recipients with HLA-specific antibodies. *Transplantation*, 81(7):1049-1057, 2006.

[205] Fuggle SV, Martin S. Tools for human leukocyte antigen antibody detection and their application to transplanting sensitized patients. *Transplantation*, 86(3):384-390, 2008.

[206] Graff RJ, Buchanan PM, Dzebisashvili N, Schnitzler MA, Tuttle-Newhall J, Xiao H, et al. The clinical importance of flow cytometry crossmatch in the context of CDC crossmatch results. *Transplant Proc*, 42(9):3471-3474, 2010.

[207] Cross DE, Greiner R, Whittier FC. Importance of the autocontrol crossmatch in human renal transplantation. *Transplantation*, 21(4):307-311, 1976.

[208] Kao K-J, Scornik JC, Small SJ. Enzyme-linked immunoassay for anti-HLA antibodies--an alternative to panel studies by lymphocytotoxicity. *Transplantation*, 55(1):192-196, 1993.

[209] Utzig MJ, Blümke M, Wolff-Vorbeck G, Lang H, Kirste G. Flow cytometry crossmatch: a method for predicting graft rejection. *Transplantation*, 63(4):551-554, 1997.

[210] Daniel V, Opelz G. Clinical Relevance of Immune Monitoring in Solid Organ Transplantation. *International Reviews of Immunology*, 28(3-4):155-184, 2009.

[211] Kerman RH, Katz SM, Van Buren CT, Ruth J, McKissick E, Rasmussen S, et al. Posttransplant immune monitoring of anti-HLA antibody. *Transplantation Proceedings*, 33(1):402, 2001.

[212] Salcido-Ochoa F, Allen Jr JC. Biomarkers and a tailored approach for immune monitoring in kidney transplantation. *World journal of transplantation*, 7(6):276, 2017.

[213] Guillaume N. Improved flow cytometry crossmatching in kidney transplantation. HLA, 92(6):375-383, 2018.

[214] Pei R, Lee J-h, Shih N-J, Chen M, Terasaki PI. Single human leukocyte antigen flow cytometry beads for accurate identification of human leukocyte antigen antibody specificities. *Transplantation*, 75(1):43-49, 2003.

[215] McCaughan J, Xu Q, Tinckam K. Detecting donor-specific antibodies: the importance of sorting the wheat from the chaff. *Hepatobiliary Surgery and Nutrition*, 8(1):37-52, 2019.

[216] Wehmeier C, Hönger G, Schaub S. Caveats of HLA antibody detection by solid-phase assays. *Transplant International*, 33(1):18-29, 2020.

[217] Taylor CJ, Kosmoliaptsis V, Martin J, Knighton G, Mallon D, Bradley JA, et al.

Technical limitations of the C1q single-antigen bead assay to detect complement binding HLA-specific antibodies. *Transplantation*, 101(6):1206, 2017.

[218] Tait BD, Susal C, Gebel HM, Nickerson PW, Zachary AA, Claas FH, et al. Consensus guidelines on the testing and clinical management issues associated with HLA and non-HLA antibodies in transplantation. *Transplantation*, 95(1):19-47, 2013.

[219] Taylor CJ, Kosmoliaptsis V, Summers DM, Bradley JA. Back to the future: application of contemporary technology to long-standing questions about the clinical relevance of human leukocyte antigen-specific alloantibodies in renal transplantation. *Human immunology*, 70(8):563-568, 2009.

[220] van den Berg-Loonen EM, Billen EV, Voorter CE, van Heurn LWE, Claas FH, van Hooff JP, et al. Clinical relevance of pretransplant donor-directed antibodies detected by single antigen beads in highly sensitized renal transplant patients. *Transplantation*, 85(8):1086-1090, 2008.

[221] Lefaucheur C, Loupy A, Hill GS, Andrade J, Nochy D, Antoine C, et al. Preexisting Donor-Specific HLA Antibodies Predict Outcome in Kidney Transplantation. *Journal of the American Society of Nephrology*, 21(8):1398-1406, 2010.

[222] Wu P, Everly MJ, Jin J, Mao Y, Chen J. Understanding the significance of low-level preformed donor-specific anti-HLA antibodies in renal transplant patients. *Clin Transpl*:365-368, 2011.

[223] Mazor Y, Yang C, Borrok MJ, Ayriss J, Aherne K, Wu H, et al. Enhancement of Immune Effector Functions by Modulating IgG's Intrinsic Affinity for Target Antigen. *PLoS One*, 11(6):e0157788, 2016.

[224] Tang Y, Lou J, Alpaugh RK, Robinson MK, Marks JD, Weiner LM. Regulation of Antibody-Dependent Cellular Cytotoxicity by IgG Intrinsic and Apparent Affinity for Target Antigen. *The Journal of Immunology*, 179(5):2815-2823, 2007.

[225] Garces JC, Giusti S, Staffeld-Coit C, Bohorquez H, Cohen AJ, Loss GE. Antibody-Mediated Rejection: A Review. *Ochsner J*, 17(1):46-55, 2017.

[226] Mohan S, Palanisamy A, Tsapepas D, Tanriover B, Crew RJ, Dube G, et al. Donor-Specific Antibodies Adversely Affect Kidney Allograft Outcomes. Journal of the

American Society of Nephrology, 23(12):2061-2071, 2012.

[227] Valenzuela NM, Hickey MJ, Reed EF. Antibody subclass repertoire and graft outcome following solid organ transplantation. *Frontiers in immunology*, 7:433, 2016.

[228] Concepcion J, Witte K, Wartchow C, Choo S, Yao D, Persson H, et al. Label-free detection of biomolecular interactions using BioLayer interferometry for kinetic characterization. *Combinatorial chemistry & high throughput screening*, 12(8):791-800, 2009.

[229] Chen G, Sequeira F, Tyan DB. Novel C1q assay reveals a clinically relevant subset of human leukocyte antigen antibodies independent of immunoglobulin G strength on single antigen beads. *Hum Immunol*, 72(10):849-858, 2011.

[230] Teo R, Goh A, Koh R, Ling LM, Gu Y, MacAry P, et al. C1q Assay to Determine Complement Fixing of Anti-Human Leukocyte Antigen Antibodies, but not Immunoglobulin Subclass Identification, Allows Better Prediction of Kidney Allograft Outcomes in an Asian Population. *Transplantation*, 102:S88, 2018.

[231] Brugiere O, Roux A, Le Pavec J, Sroussi D, Parquin F, Pradere P, et al. Role of C1q-binding anti-HLA antibodies as a predictor of lung allograft outcome. *Eur Respir J*, 52(2), 2018.

[232] Sutherland SM, Chen G, Sequeira FA, Lou CD, Alexander SR, Tyan DB. Complement-fixing donor-specific antibodies identified by a novel C1q assay are associated with allograft loss. *Pediatric transplantation*, 16(1):12-17, 2012.

[233] Birnbaum D, Kourilsky FM. Differences in the cell binding affinity of a cross-reactive monoclonal anti-Ia alloantibody in mice of different H-2 haplotypes. *Eur J Immunol*, 11(9):734-738, 1981.

[234] Mizutani K, Terasaki P, Hamdani E, Esquenazi V, Rosen A, Miller J, et al. The importance of anti-HLA-specific antibody strength in monitoring kidney transplant patients. *Am J Transplant*, 7(4):1027-1031, 2007.

[235] Duquesnoy RJ, Marrari M, Jelenik L, Zeevi A, Claas FH, Mulder A. Structural aspects of HLA class I epitopes reacting with human monoclonal antibodies in Ig-binding, C1q-binding and lymphocytotoxicity assays. *Hum Immunol*, 74(10):1271-1279, 2013.

[236] Tambur AR, Herrera ND, Haarberg KM, Cusick MF, Gordon RA, Leventhal JR, et al. Assessing Antibody Strength: Comparison of MFI, C1q, and Titer Information. *Am J Transplant*, 15(9):2421-2430, 2015.

[237] Marfo K, Ajaimy M, Colovai A, Kayler L, Greenstein S, Lubetzky M, et al. Pretransplant immunologic risk assessment of kidney transplant recipients with donor-specific anti-human leukocyte antigen antibodies. *Transplantation*, 98(10):1082-1088, 2014.

[238] Daga S, Moyse H, Briggs D, Lowe D, Evans N, Jones J, et al. Direct quantitative measurement of the kinetics of HLA-specific antibody interactions with isolated HLA proteins. *Human immunology*, 79(2):122-128, 2018.

[239] Visentin J, Leu DL, Mulder A, Jambon F, Badier L, Lee J-H, et al. Measuring anti-HLA antibody active concentration and affinity by surface plasmon resonance: Comparison with the luminex single antigen flow beads and T-cell flow cytometry crossmatch results. *Molecular Immunology*, 108:34-44, 2019.

[240] Williams TM. Human leukocyte antigen gene polymorphism and the histocompatibility laboratory. *J Mol Diagn*, 3(3):98-104, 2001.

[241] Farber DL, Netea MG, Radbruch A, Rajewsky K, Zinkernagel RM. Immunological memory: lessons from the past and a look to the future. *Nat Rev Immunol*, 16(2):124-128, 2016.

[242] Illing PT, Pymm P, Croft NP, Hilton HG, Jojic V, Han AS, et al. HLA-B57 micropolymorphism defines the sequence and conformational breadth of the immunopeptidome. *Nat Commun*, 9(1):4693, 2018.

[243] Cai J, Terasaki PI. Post-transplantation antibody monitoring and HLA antibody epitope identification. *Curr Opin Immunol*, 20(5):602-606, 2008.

[244] Palm AE, Henry C. Remembrance of Things Past: Long-Term B Cell Memory After Infection and Vaccination. *Front Immunol*, 10:1787, 2019.

[245] Sarkizova S, Klaeger S, Le PM, Li LW, Oliveira G, Keshishian H, et al. A large peptidome dataset improves HLA class I epitope prediction across most of the human population. *Nat Biotechnol*, 38(2):199-209, 2020.

[246] Duquesnoy RJ. Reflections on HLA Epitope-Based Matching for Transplantation. *Front Immunol*, 7:469, 2016.

[247] Geneugelijk K, Thus KA, Spierings E. Predicting alloreactivity in transplantation. *J Immunol Res*, 2014:159479, 2014.

[248] Garovoy, Rheinschmidt M, Bigos M, Perkins HA, Colombe BW, Feduska NJ, et al., editors. Flow cytometry analysis: A high technology cross-match technique facilitating transplantation,1983.

[249] Patel R, Terasaki PI. Significance of the positive crossmatch test in kidney transplantation. *N Engl J Med*, 280(14):735-739, 1969.

[250] Gebel HM, Bray RA, Nickerson P. Pre-transplant assessment of donor-reactive, HLA-specific antibodies in renal transplantation: contraindication vs. risk. *Am J Transplant*, 3(12):1488-1500, 2003.

[251] Katalinic N, Starcevic A, Mavrinac M, Balen S. Complement-dependent cytotoxicity and Luminex technology for human leucocyte antigen antibody detection in kidney transplant candidates exposed to different sensitizing events. *Clin Kidney J*, 10(6):852-858, 2017.

[252] Lachmann N, Todorova K, Schulze H, Schonemann C. Systematic comparison of four cell- and Luminex-based methods for assessment of complement-activating HLA antibodies. *Transplantation*, 95(5):694-700, 2013.

[253] Pande A, Pandey P, Kumar Devra A, Kumar Sinha V, Prasad Bhatt A. Significance of Luminex-based single antigen class II bead assay and its mean fluorescence intensity in renal transplant cases; a retrospective observation in 97 cases. *J Immunoassay Immunochem*, 41(3):322-336, 2020.

[254] Lachmann N, Todorova K, Schulze H, Schonemann C. Luminex((R)) and its applications for solid organ transplantation, hematopoietic stem cell transplantation, and transfusion. *Transfus Med Hemother*, 40(3):182-189, 2013.

[255] Weinstock C, Schnaidt M. The complement-mediated prozone effect in the Luminex single-antigen bead assay and its impact on HLA antibody determination in patient sera. *Int J Immunogenet*, 40(3):171-177, 2013.

[256] Jucaud V, Ravindranath MH, Terasaki PI. Conformational Variants of the Individual HLA-I Antigens on Luminex Single Antigen Beads Used in Monitoring HLA Antibodies: Problems and Solutions. *Transplantation*, 101(4):764-777, 2017.

[257] Kosmoliaptsis V, Bradley JA, Peacock S, Chaudhry AN, Taylor CJ. Detection of immunoglobulin G human leukocyte antigen-specific alloantibodies in renal transplant patients using single-antigen-beads is compromised by the presence of immunoglobulin M human leukocyte antigen-specific alloantibodies. *Transplantation*, 87(6):813-820, 2009.

[258] Vaidya S. Clinical importance of anti-human leukocyte antigen-specific antibody concentration in performing calculated panel reactive antibody and virtual crossmatches. *Transplantation*, 85(7):1046-1050, 2008.

[259] Rebibou JM, Chabod J, Bittencourt MC, Thevenin C, Chalopin JM, Herve P, et al. Flow-PRA evaluation for antibody screening in patients awaiting kidney transplantation. *Transpl Immunol*, 8(2):125-128, 2000.

[260] Zecher D, Bach C, Preiss A, Staudner C, Utpatel K, Evert M, et al. Analysis of Luminex-based Algorithms to Define Unacceptable HLA Antibodies in CDC-crossmatch Negative Kidney Transplant Recipients. *Transplantation*, 102(6):969-977, 2018.

[261] Huh KH, Kim MS, Kim HJ, Joo DJ, Kim BS, Ju MK, et al. Renal transplantation in sensitized recipients with positive luminex and negative CDC (complement-dependent cytotoxicity) crossmatches. *Transpl Int*, 25(11):1131-1137, 2012.

[262] Gjelaj C, Luke A, Paschenko A, Fletcher R, Borukhov E, Nnani D, et al. Sum Total MFI of Donor-Specific Antibody - A Prognostic Marker in Antibody-Mediated Rejection. *The Journal of Heart and Lung Transplantation*, 39(4, Supplement):S243, 2020.

[263] Roux A, Bendib Le Lan I, Holifanjaniaina S, Thomas KA, Picard C, Grenet D, et al. Characteristics of Donor-Specific Antibodies Associated With Antibody-Mediated Rejection in Lung Transplantation. *Front Med (Lausanne)*, 4:155, 2017.

[264] Baranwal AK, Bhat DK, Goswami S, Agarwal SK, Kaur G, Kaur J, et al. Comparative analysis of Luminex-based donor-specific antibody mean fluorescence intensity values

with complement-dependent cytotoxicity & flow crossmatch results in live donor renal transplantation. *Indian J Med Res*, 145(2):222-228, 2017.

[265] Moreno C, Burgos L, Perez-Robles C, Delgado JA, Mata JJ, Errasti P, et al. Predictive value of the Luminex single antigen panel for detecting flow cytometry cross-match positivity. *Hum Immunol*, 73(5):517-521, 2012.

[266] Visentin J, Minder L, Lee JH, Taupin JL, Di Primo C. Calibration free concentration analysis by surface plasmon resonance in a capture mode. *Talanta*, 148:478-485, 2016.

[267] Karlsson R, Fagerstam L, Nilshans H, Persson B. Analysis of active antibody concentration. Separation of affinity and concentration parameters. *J Immunol Methods*, 166(1):75-84, 1993.

[268] Wang C, Wu Y, Wang L, Hong B, Jin Y, Hu D, et al. Engineered Soluble Monomeric IgG1 Fc with Significantly Decreased Non-Specific Binding. *Front Immunol*, 8:1545, 2017.

[269] Schasfoort RBM. Handbook of surface plasmon resonance. 2nd ed. Cambridge: Royal Society of Chemistry; 2017.

[270] Visentin J, Couzi L, Dromer C, Neau-Cransac M, Guidicelli G, Veniard V, et al. Overcoming non-specific binding to measure the active concentration and kinetics of serum anti-HLA antibodies by surface plasmon resonance. *Biosens Bioelectron*, 117:191-200, 2018.

[271] Bian H, Reed EF. Anti-HLA antibodies transduce proliferative signals in endothelial cells and smooth muscle cells. *Transplant Proc*, 31(4):1924, 1999.

[272] Valenzuela NM, Reed EF. The link between major histocompatibility complex antibodies and cell proliferation. *Transplantation Reviews*, 25(4):154-166, 2011.

[273] Jin YP, Valenzuela NM, Zhang X, Rozengurt E, Reed EF. HLA Class II-Triggered Signaling Cascades Cause Endothelial Cell Proliferation and Migration: Relevance to Antibody-Mediated Transplant Rejection. *J Immunol*, 200(7):2372-2390, 2018.

[274] Jindra PT, Hsueh A, Hong L, Gjertson D, Shen XD, Gao F, et al. Anti-MHC class I antibody activation of proliferation and survival signaling in murine cardiac allografts. *J Immunol*, 180(4):2214-2224, 2008.

[275] Coupel S, Leboeuf F, Boulday G, Soulillou JP, Charreau B. RhoA activation mediates phosphatidylinositol 3-kinase-dependent proliferation of human vascular endothelial cells: an alloimmune mechanism of chronic allograft nephropathy. *J Am Soc Nephrol*, 15(9):2429-2439, 2004.

[276] Galvani S, Augé N, Calise D, Thiers JC, Canivet C, Kamar N, et al. HLA class I antibodies provoke graft arteriosclerosis in human arteries transplanted into SCID/beige mice. *Am J Transplant*, 9(11):2607-2614, 2009.

[277] Li F, Atz ME, Reed EF. Human leukocyte antigen antibodies in chronic transplant vasculopathy—mechanisms and pathways. *Current Opinion in Immunology*, 21(5):557-562, 2009.

[278] Galvani S, Trayssac M, Augé N, Thiers JC, Calise D, Krell HW, et al. A key role for matrix metalloproteinases and neutral sphingomyelinase-2 in transplant vasculopathy triggered by anti-HLA antibody. *Circulation*, 124(24):2725-2734, 2011.

[279] Newby AC. Matrix metalloproteinases regulate migration, proliferation, and death of vascular smooth muscle cells by degrading matrix and non-matrix substrates. *Cardiovasc Res*, 69(3):614-624, 2006.

[280] Zhang X, Reed EF. HLA Class I: An unexpected role in integrin β4 signaling in endothelial cells. *Human immunology*, 73(12):1239-1244, 2012.

[281] Zhang X, Rozengurt E, Reed EF. HLA class I molecules partner with integrin β4 to stimulate endothelial cell proliferation and migration. *Sci Signal*, 3(149):ra85, 2010.

[282] Sun C, Liu X, Qi L, Xu J, Zhao J, Zhang Y, et al. Modulation of vascular endothelial cell senescence by integrin β4. *J Cell Physiol*, 225(3):673-681, 2010.

[283] Lepin EJ, Jin Y-P, Barwe SP, Rozengurt E, Reed EF. HLA class I signal transduction is dependent on Rho GTPase and ROK. *Biochemical and Biophysical Research Communications*, 323(1):213-217, 2004.

[284] Anwar T, Sinnett-Smith J, Jin YP, Reed EF, Rozengurt E. Ligation of HLA Class I Molecules Induces YAP Activation through Src in Human Endothelial Cells. *J Immunol*, 205(7):1953-1961, 2020.

[285] Jin YP, Singh RP, Du ZY, Rajasekaran AK, Rozengurt E, Reed EF. Ligation of HLA

class I molecules on endothelial cells induces phosphorylation of Src, paxillin, and focal adhesion kinase in an actin-dependent manner. *J Immunol*, 168(11):5415-5423, 2002.

[286] Jin YP, Fishbein MC, Said JW, Jindra PT, Rajalingam R, Rozengurt E, et al. Anti-HLA class I antibody-mediated activation of the PI3K/Akt signaling pathway and induction of Bcl-2 and Bcl-xL expression in endothelial cells. *Hum Immunol*, 65(4):291-302, 2004.

[287] Jindra PT, Jin YP, Rozengurt E, Reed EF. HLA class I antibody-mediated endothelial cell proliferation via the mTOR pathway. *J Immunol*, 180(4):2357-2366, 2008.

[288] Jindra PT, Reed EF. 204: mTOR knockdown inhibits anti-HLA antibody induced MHC class I signaling. *The Journal of Heart and Lung Transplantation*, 26(2, Supplement):S133, 2007.

[289] Lepin EJ, Zhang Q, Zhang X, Jindra PT, Hong LS, Ayele P, et al. Phosphorylated S6 ribosomal protein: a novel biomarker of antibody-mediated rejection in heart allografts. *Am J Transplant*, 6(7):1560-1571, 2006.

[290] Li F, Wei J, Valenzuela NM, Lai C, Zhang Q, Gjertson D, et al. Phosphorylated S6 kinase and S6 ribosomal protein are diagnostic markers of antibody-mediated rejection in heart allografts. *The Journal of Heart and Lung Transplantation*, 34(4):580-587, 2015.

[291] Ziegler ME, Souda P, Jin YP, Whitelegge JP, Reed EF. Characterization of the endothelial cell cytoskeleton following HLA class I ligation. *PLoS One*, 7(1):e29472, 2012.

[292] Jindra PT, Jin Y-P, Jacamo R, Rozengurt E, Reed EF. MHC class I and integrin ligation induce ERK activation via an mTORC2-dependent pathway. *Biochemical and Biophysical Research Communications*, 369(2):781-787, 2008.

[293] Ziegler ME, Jin Y-P, Young SH, Rozengurt E, Reed EF. HLA class I-mediated stress fiber formation requires ERK1/2 activation in the absence of an increase in intracellular Ca2+ in human aortic endothelial cells. *American Journal of Physiology-Cell Physiology*, 303(8):C872-C882, 2012.

[294] Shen Q, Rigor RR, Pivetti CD, Wu MH, Yuan SY. Myosin light chain kinase in

microvascular endothelial barrier function. *Cardiovascular Research*, 87(2):272-280, 2010.

[295] Jin YP, Korin Y, Zhang X, Jindra PT, Rozengurt E, Reed EF. RNA interference elucidates the role of focal adhesion kinase in HLA class I-mediated focal adhesion complex formation and proliferation in human endothelial cells. *J Immunol*, 178(12):7911-7922, 2007.

[296] Abdel-Ghany M, Cheng HC, Elble RC, Pauli BU. Focal adhesion kinase activated by beta(4) integrin ligation to mCLCA1 mediates early metastatic growth. *J Biol Chem*, 277(37):34391-34400, 2002.

[297] Li F, Zhang X, Jin YP, Mulder A, Reed EF. Antibody ligation of human leukocyte antigen class I molecules stimulates migration and proliferation of smooth muscle cells in a focal adhesion kinase-dependent manner. *Hum Immunol*, 72(12):1150-1159, 2011.

[298] Bocelli-Tyndall C, Zajac P, Di Maggio N, Trella E, Benvenuto F, Iezzi G, et al. Fibroblast growth factor 2 and platelet-derived growth factor, but not platelet lysate, induce proliferation-dependent, functional class II major histocompatibility complex antigen in human mesenchymal stem cells. *Arthritis & Rheumatism*, 62(12):3815-3825, 2010.

[299] Jaramillo A, Smith CR, Maruyama T, Zhang L, Patterson GA, Mohanakumar T. Anti-HLA class I antibody binding to airway epithelial cells induces production of fibrogenic growth factors and apoptotic cell death: a possible mechanism for bronchiolitis obliterans syndrome. *Human immunology*, 64(5):521-529, 2003.

[300] Bian H, Harris PE, Reed EF. Ligation of HLA class I molecules on smooth muscle cells with anti-HLA antibodies induces tyrosine phosphorylation, fibroblast growth factor receptor expression and cell proliferation. *International immunology*, 10(9):1315-1323, 1998.

[301] Metcalf DJ, Nightingale TD, Zenner HL, Lui-Roberts WW, Cutler DF. Formation and function of Weibel-Palade bodies. *J Cell Sci*, 121(Pt 1):19-27, 2008.

[302] Yamakuchi M, Kirkiles-Smith NC, Ferlito M, Cameron SJ, Bao C, Fox-Talbot K, et al. Antibody to human leukocyte antigen triggers endothelial exocytosis. *Proc Natl Acad*

Sci U S A, 104(4):1301-1306, 2007.

[303] Hirohashi T, Chase CM, Della Pelle P, Sebastian D, Alessandrini A, Madsen JC, et al. A novel pathway of chronic allograft rejection mediated by NK cells and alloantibody. *Am J Transplant*, 12(2):313-321, 2012.

[304] Valenzuela NM, Mulder A, Reed EF. HLA Class I Antibodies Trigger Increased Adherence of Monocytes to Endothelial Cells by Eliciting an Increase in Endothelial P-Selectin and, Depending on Subclass, by Engaging FcγRs. *The Journal of Immunology*, 190(12):6635-6650, 2013.

[305] Valenzuela NM, Hong L, Shen X-D, Gao F, Young SH, Rozengurt E, et al. Blockade of P-Selectin Is Sufficient to Reduce MHC I Antibody-Elicited Monocyte Recruitment In Vitro and In Vivo. *American Journal of Transplantation*, 13(2):299-311, 2013.

[306] Hidalgo LG, Sis B, Sellares J, Campbell PM, Mengel M, Einecke G, et al. NK cell transcripts and NK cells in kidney biopsies from patients with donor-specific antibodies: evidence for NK cell involvement in antibody-mediated rejection. *Am J Transplant*, 10(8):1812-1822, 2010.

[307] Bian H, Reed EF. Anti-HLA class I antibodies transduce signals in endothelial cells resulting in FGF receptor translocation, down-regulation of ICAM-1 and cell proliferation. *Transplant Proc*, 33(1-2):311, 2001.

[308] Salehi S, Sosa RA, Jin YP, Kageyama S, Fishbein MC, Rozengurt E, et al. Outside-in HLA class I signaling regulates ICAM-1 clustering and endothelial cell-monocyte interactions via mTOR in transplant antibody-mediated rejection. *Am J Transplant*, 18(5):1096-1109, 2018.

[309] Valenzuela NM, Thomas KA, Mulder A, Parry GC, Panicker S, Reed EF. Complement-Mediated Enhancement of Monocyte Adhesion to Endothelial Cells by HLA Antibodies, and Blockade by a Specific Inhibitor of the Classical Complement Cascade, TNT003. *Transplantation*, 101(7):1559-1572, 2017.

[310] Dufour A, Corsini E, Gelati M, Ciusani E, Zaffaroni M, Giombini S, et al. Modulation of ICAM-1, VCAM-1 and HLA-DR by cytokines and steroids on HUVECs and human brain endothelial cells. *Journal of the Neurological Sciences*, 157(2):117-121, 1998.

[311] Moreno CS, Beresford GW, Louis-Plence P, Morris AC, Boss JM. CREB Regulates MHC Class II Expression in a CIITA-Dependent Manner. *Immunity*, 10(2):143-151, 1999.

[312] Naemi FM, Carter V, Kirby JA, Ali S. Anti-donor HLA class I antibodies: pathways to endothelial cell activation and cell-mediated allograft rejection. *Transplantation*, 96(3):258-266, 2013.

[313] Lynch RJ, Platt JL. Accommodation in organ transplantation. *Curr Opin Organ Transplant*, 13(2):165-170, 2008.

[314] Mohiuddin MM, Ogawa H, Yin DP, Shen J, Galili U. Antibody-mediated accommodation of heart grafts expressing an incompatible carbohydrate antigen. *Transplantation*, 75(3):258-262, 2003.

[315] Narayanan K, Jendrisak MD, Phelan DL, Mohanakumar T. HLA class I antibody mediated accommodation of endothelial cells via the activation of PI3K/cAMP dependent PKA pathway. *Transpl Immunol*, 15(3):187-197, 2006.

[316] Narayanan K, Jaramillo A, Phelan DL, Mohanakumar T. Pre-exposure to sub-saturating concentrations of HLA class I antibodies confers resistance to endothelial cells against antibody complement-mediated lysis by regulating Bad through the phosphatidylinositol 3-kinase/Akt pathway. *Eur J Immunol*, 34(8):2303-2312, 2004.

[317] Alberts B, Johnson A, Lewis J, et al. Molecular Biology of the Cell. 4th edition. New York: Garland Science; 2002. Blood Vessels and Endothelial Cells. Available from: https://www.ncbi.nlm.nih.gov/books/NBK26848/

[318] Barrett EJ, Liu Z. The endothelial cell: An “early responder” in the development of insulin resistance. *Reviews in Endocrine and Metabolic Disorders*, 14(1):21-27, 2013.

[319] Mai J, Virtue A, Shen J, Wang H, Yang XF. An evolving new paradigm: endothelial cells--conditional innate immune cells. *J Hematol Oncol*, 6:61, 2013.

[320] Hauser S, Jung F, Pietzsch J. Human Endothelial Cell Models in Biomaterial Research. *Trends Biotechnol*, 35(3):265-277, 2017.

[321] Danese S, Dejana E, Fiocchi C. Immune regulation by microvascular endothelial cells: directing innate and adaptive immunity, coagulation, and inflammation. *J Immunol*,

178(10):6017-6022, 2007.

[322] Liao H, He H, Chen Y, Zeng F, Huang J, Wu L, et al. Effects of long-term serial cell passaging on cell spreading, migration, and cell-surface ultrastructures of cultured vascular endothelial cells. *Cytotechnology*, 66(2):229-238, 2014.

[323] Maciag T, Hoover GA, Stemerman MB, Weinstein R. Serial propagation of human endothelial cells in vitro. *Journal of Cell Biology*, 91(2):420-426, 1981.

[324] Burt C, Cryer C, Fuggle S, Little A-M, Dyer P. HLA-A, -B, -DR allele group frequencies in 7007 kidney transplant list patients in 27 UK centres. International *Journal of Immunogenetics*, 40(3):209-215, 2013.

[325] Mack SJ, Tu B, Lazaro A, Yang R, Lancaster AK, Cao K, et al. HLA-A, -B, -C, and -DRB1 allele and haplotype frequencies distinguish Eastern European Americans from the general European American population. *Tissue Antigens*, 73(1):17-32, 2009.

[326] Jarrell B, Levine E, Shapiro S, Williams S, Carabasi RA, Mueller S, et al. Human adult endothelial cell growth in culture. *J Vasc Surg*, 1(6):757-764, 1984.

[327] Donnini D, Perrella G, Stel G, Ambesi-Impiombato FS, Curcio F. A new model of human aortic endothelial cells in vitro. *Biochimie,* 82(12):1107-1114, 2000.

[328] Marin V, Kaplanski G, Gres S, Farnarier C, Bongrand P. Endothelial cell culture: protocol to obtain and cultivate human umbilical endothelial cells. *J Immunol Methods*, 254(1-2):183-190, 2001.

[329] Leitinger N, Watson AD, Faull KF, Fogelman AM, Berliner JA. Monocyte binding to endothelial cells induced by oxidized phospholipids present in minimally oxidized low density lipoprotein is inhibited by a platelet activating factor receptor antagonist. Adv *Exp Med Biol*, 433:379-382, 1997.

[330] Carrillo A, Chamorro S, Rodriguez-Gago M, Alvarez B, Molina MJ, Rodriguez-Barbosa JI, et al. Isolation and characterization of immortalized porcine aortic endothelial cell lines. *Vet Immunol Immunopathol*, 89(1-2):91-98, 2002.

[331] Wang JM, Chen AF, Zhang K. Isolation and Primary Culture of Mouse Aortic Endothelial Cells. *J Vis Exp*, (118), 2016.

[332] Le Bas-Bernardet S, Hourmant M, Coupel S, Bignon JD, Soulillou JP, Charreau B. Non-HLA-type endothelial cell reactive alloantibodies in pre-transplant sera of kidney recipients trigger apoptosis. *Am J Transplant*, 3(2):167-177, 2003.

[333] Jeong I-H, Bae W-Y, Choi J-S, Jeong J-W. Ischemia induces autophagy of endothelial cells and stimulates angiogenic effects in a hindlimb ischemia mouse model. *Cell Death & Disease*, 11(8):624, 2020.

[334] Yang Q, He GW, Underwood MJ, Yu CM. Cellular and molecular mechanisms of endothelial ischemia/reperfusion injury: perspectives and implications for postischemic myocardial protection. *Am J Transl Res*, 8(2):765-777, 2016.

[335] Wang P, Luo R, Zhang M, Wang Y, Song T, Tao T, et al. A cross-talk between epithelium and endothelium mediates human alveolar–capillary injury during SARS-CoV-2 infection. *Cell Death & Disease*, 11(12):1042, 2020.

[336] Humbert M, Morrell NW, Archer SL, Stenmark KR, MacLean MR, Lang IM, et al. Cellular and molecular pathobiology of pulmonary arterial hypertension. *J Am Coll Cardiol*, 43(12 Suppl S):13S-24S, 2004.

[337] Humbert M, Montani D, Perros F, Dorfmüller P, Adnot S, Eddahibi S. Endothelial cell dysfunction and cross talk between endothelium and smooth muscle cells in pulmonary arterial hypertension. *Vascular Pharmacology*, 49(4):113-118, 2008.

[338] Zhang L, Yao J, Yao Y, Bostrom KI. Contributions of the Endothelium to Vascular Calcification. *Front Cell Dev Biol*, 9:620882, 2021.

[339] Gerwins P, Sköldenberg E, Claesson-Welsh L. Function of fibroblast growth factors and vascular endothelial growth factors and their receptors in angiogenesis. Critical *Reviews in Oncology/Hematology*, 34(3):185-194, 2000.

[340] Breier G, Albrecht U, Sterrer S, Risau W. Expression of vascular endothelial growth factor during embryonic angiogenesis and endothelial cell differentiation. *Development*, 114(2):521-532, 1992.

[341] Li Y, Lui KO, Zhou B. Reassessing endothelial-to-mesenchymal transition in cardiovascular diseases. *Nature Reviews Cardiology*, 15(8):445-456, 2018.

[342] Stone RC, Pastar I, Ojeh N, Chen V, Liu S, Garzon KI, et al. Epithelial-mesenchymal

transition in tissue repair and fibrosis. *Cell Tissue Res*, 365(3):495-506, 2016.

[343] Kuzuya M, Kinsella JL. Induction of endothelial cell differentiation in vitro by fibroblast-derived soluble factors. *Exp Cell Res*, 215(2):310-318, 1994.

[344] Sandoo A, van Zanten JJ, Metsios GS, Carroll D, Kitas GD. The endothelium and its role in regulating vascular tone. *Open Cardiovasc Med J*, 4:302-312, 2010.

[345] Yang D, Guo S, Zhang T, Li H. Hypothermia attenuates ischemia/reperfusion-induced endothelial cell apoptosis via alterations in apoptotic pathways and JNK signaling. *FEBS Lett*, 583(15):2500-2506, 2009.

[346] Hansen TN, Dawson PE, Brockbank KG. Effects of hypothermia upon endothelial cells: mechanisms and clinical importance. *Cryobiology*, 31(1):101-106, 1994.

[347] Bogert NV, Werner I, Kornberger A, Meybohm P, Moritz A, Keller T, et al. Influence of hypothermia and subsequent rewarming upon leukocyte-endothelial interactions and expression of Junctional-Adhesion-Molecules A and B. *Scientific Reports*, 6(1):21996, 2016.

[348] Nava P, Capaldo CT, Koch S, Kolegraff K, Rankin CR, Farkas AE, et al. JAM-A regulates epithelial proliferation through Akt/β-catenin signalling. EMBO reports, 12(4):314-320, 2011.

[349] Awad EM, Khan SY, Sokolikova B, Brunner PM, Olcaydu D, Wojta J, et al. Cold induces reactive oxygen species production and activation of the NF-kappa B response in endothelial cells and inflammation in vivo. *J Thromb Haemost*, 11(9):1716-1726, 2013.

[350] Mankad P, Slavik Z, Yacoub M. Endothelial dysfunction caused by University of Wisconsin preservation solution in the rat heart: The importance of temperature. The *Journal of Thoracic and Cardiovascular Surgery*, 104(6):1618-1624, 1992.

[351] Regueiro A, Freixa X, Heras M, Penela D, Fernandez-Rodriguez D, Brugaletta S, et al. Impact of therapeutic hypothermia on coronary flow. *Int J Cardiol*, 172(1):228-229, 2014.

[352] Chitalia V, Shivanna S, Martorell J, Meyer R, Edelman E, Rahimi N. c-Cbl, a Ubiquitin E3 Ligase That Targets Active β-Catenin: A NOVEL LAYER OF Wnt SIGNALING

REGULATION *. *Journal of Biological Chemistry*, 288(32):23505-23517, 2013.

[353] Holmes K, Chapman E, See V, Cross MJ. VEGF Stimulates RCAN1.4 Expression in Endothelial Cells via a Pathway Requiring Ca2+/Calcineurin and Protein Kinase C-δ. *PLoS One*, 5(7):e11435, 2010.

[354] Miura K. An overview of current methods to confirm protein-protein interactions. *Protein and peptide letters*, 25(8):728-733, 2018.

[355] Yates EV, Müller T, Rajah L, De Genst EJ, Arosio P, Linse S, et al. Latent analysis of unmodified biomolecules and their complexes in solution with attomole detection sensitivity. *Nature chemistry*, 7(10):802-809, 2015.

[356] Arosio P, Muller T, Rajah L, Yates EV, Aprile FA, Zhang Y, et al. Microfluidic Diffusion Analysis of the Sizes and Interactions of Proteins under Native Solution Conditions. *ACS Nano*, 10(1):333-341, 2016.

[357] Otzen DE, Buell AK, Jensen H. Microfluidics and the quantification of biomolecular interactions. *Current Opinion in Structural Biology*, 70:8-15, 2021.

[358] Herling TW, O'Connell DJ, Bauer MC, Persson J, Weininger U, Knowles TP, et al. A microfluidic platform for real-time detection and quantification of protein-ligand interactions. *Biophysical journal*, 110(9):1957-1966, 2016.

[359] Wilkins DK, Grimshaw SB, Receveur V, Dobson CM, Jones JA, Smith LJ. Hydrodynamic radii of native and denatured proteins measured by pulse field gradient NMR techniques. *Biochemistry*, 38(50):16424-16431, 1999.

[360] Zhang Y, Yates EV, Hong L, Saar KL, Meisl G, Dobson CM, et al. On-chip measurements of protein unfolding from direct observations of micron-scale diffusion. *Chemical science*, 9(14):3503-3507, 2018.

[361] Jarmoskaite I, AlSadhan I, Vaidyanathan PP, Herschlag D. How to measure and evaluate binding affinities. *Elife*, 9, 2020.

[362] Shrirao AB, Schloss RS, Fritz Z, Shrirao MV, Rosen R, Yarmush ML. Autofluorescence of blood and its application in biomedical and clinical research. *Biotechnology and Bioengineering*, 118(12):4550-4576, 2021.

[363] Lamola AA, Russo M. Fluorescence Excitation Spectrum of Bilirubin in Blood: A Model for the Action Spectrum for Phototherapy of Neonatal Jaundice. *Photochemistry and Photobiology*, 90(2):294-296, 2014.

[364] Opelz G, Döhler B. Effect of human leukocyte antigen compatibility on kidney graft survival: comparative analysis of two decades. *Transplantation*, 84(2):137-143, 2007.

[365] Süsal C, Opelz G. Current role of human leukocyte antigen matching in kidney transplantation. *Current opinion in organ transplantation*, 18(4):438-444, 2013.

[366] Lee P-C, Zhu L, Terasaki PI, Everly MJ. HLA-specific antibodies developed in the first year posttransplant are predictive of chronic rejection and renal graft loss. *Transplantation*, 88(4):568-574, 2009.

[367] Barten MJ, Schulz U, Beiras-Fernandez A, Berchtold-Herz M, Boeken U, Garbade J, et al. The clinical impact of donor-specific antibodies in heart transplantation. *Transplantation Reviews*, 32(4):207-217, 2018.

[368] Kramer CSM, Franke-van Dijk MEI, Bakker KH, Uyar-Mercankaya M, Karahan GE, Roelen DL, et al. Generation and reactivity analysis of human recombinant monoclonal antibodies directed against epitopes on HLA-DR. *American Journal of Transplantation*, 20(12):3341-3353, 2020.

[369] Beeg M, Nobili A, Orsini B, Rogai F, Gilardi D, Fiorino G, et al. A Surface Plasmon Resonance-based assay to measure serum concentrations of therapeutic antibodies and anti-drug antibodies. *Scientific Reports*, 9(1):2064, 2019.

[370] Abucayon EG, Whalen C, Torres OB, Duval AJ, Sulima A, Antoline JFG, et al. A Rapid Method for Direct Quantification of Antibody Binding-Site Concentration in Serum. *ACS Omega*, 7(30):26812-26823, 2022.

[371] Azouz M, Gonin M, Fiedler S, Faherty J, Decossas M, Cullin C, et al. Microfluidic diffusional sizing probes lipid nanodiscs formation. *Biochimica et Biophysica Acta (BBA) - Biomembranes*, 1862(6):183215, 2020.

[372] Wolfbeis OS, Leiner M. Mapping of the total fluorescence of human blood serum as a new method for its characterization. *Analytica Chimica Acta*, 167:203-215, 1985.

[373] DeVito-Haynes LD, Jankowska-Gan E, Meyer KC, Cornwell RD, Zeevi A, Griffith B,

et al. Soluble donor HLA class I and β2m-free heavy chain in serum of lung transplant recipients: steady-state levels and increases in patients with recurrent CMV infection, acute rejection episodes, and poor outcome. *Human immunology*, 61(12):1370-1382, 2000.

[374] Schneider MM, Scheidt T, Priddey AJ, Xu CK, Hu M, Devenish SRA, et al. Microfluidic Antibody Affinity Profiling for In-Solution Characterisation of Alloantibody - HLA Interactions in Human Serum. *bioRxiv*:2020.2009.2014.296442, 2020.

[375] Rodey GE, Revels K, Fuller TC. Epitope specificity of HLA class I alloantibodies: II. Stability of cross-reactive group antibody patterns over extended time periods. *Transplantation*, 63(6):885-893, 1997.

[376] Koch CA, Khalpey ZI, Platt JL. Accommodation: Preventing Injury in Transplantation and Disease. *The Journal of Immunology*, 172(9):5143, 2004.

[377] Herzenberg AM, Gill JS, Djurdjev O, Magil AB. C4d Deposition in Acute Rejection: An Independent Long-Term Prognostic Factor. *Journal of the American Society of Nephrology*, 13(1):234, 2002.

[378] Rotman S, Collins AB, Colvin RB. C4d deposition in allografts: current concepts and interpretation. *Transplantation Reviews*, 19(2):65-77, 2005.

[379] Schneider MM, Emmenegger M, Xu CK, Condado Morales I, Meisl G, Turelli P, et al. Microfluidic characterisation reveals broad range of SARS-CoV-2 antibody affinity in human plasma. *Life Science Alliance*, 5(2):e202101270, 2022.

[380] Denninger V, Xu CK, Meisl G, Morgunov AS, Fiedler S, Ilsley A, et al. Understanding the role of memory re-activation and cross-reactivity in the defense against SARS-CoV-2. *bioRxiv*:2021.2007.2023.453352, 2021.

[381] Fiedler S, Denninger V, Morgunov AS, Ilsley A, Worth R, Meisl G, et al. Mutations in two SARS-CoV-2 variants of concern reflect two distinct strategies of antibody escape. *bioRxiv*:2021.2007.2023.453327, 2021.

[382] Fiedler S, Piziorska MA, Denninger V, Morgunov AS, Ilsley A, Malik AY, et al. Antibody Affinity Governs the Inhibition of SARS-CoV-2 Spike/ACE2 Binding in

Patient Serum. *ACS Infectious Diseases*, 7(8):2362-2369, 2021.

[383] Zhang Y, Park K-Y, Suazo KF, Distefano MD. Recent progress in enzymatic protein labelling techniques and their applications. *Chemical Society Reviews*, 47(24):9106-9136, 2018.

[384] Lim YT, Kim S, Nakayama A, Stott NE, Bawendi MG, Frangioni JV. Selection of quantum dot wavelengths for biomedical assays and imaging. *Mol Imaging*, 2(1):50-64, 2003.

[385] Renaud J-P, Chung C-w, Danielson UH, Egner U, Hennig M, Hubbard RE, et al. Biophysics in drug discovery: impact, challenges and opportunities. *Nature Reviews Drug Discovery*, 15(10):679-698, 2016

[386] Halloran PF, Melk A, Barth C. Rethinking Chronic Allograft Nephropathy. *Journal of the American Society of Nephrology*, 10(1):167, 1999.

[387] Pascual M, Theruvath T, Kawai T, Tolkoff-Rubin N, Cosimi AB. Strategies to improve long-term outcomes after renal transplantation. *N Engl J Med*, 346(8):580-590, 2002.

[388] Clerkin KJ, See SB, Farr MA, Restaino SW, Serban G, Latif F, et al. Comparative Assessment of Anti-HLA Antibodies Using Two Commercially Available Luminex-Based Assays. *Transplantation Direct*, 3(11), 2017.

[389] Zachary AA, Lucas DP, Detrick B, Leffell MS. Naturally occurring interference in Luminex® assays for HLA–specific antibodies: Characteristics and resolution. *Human immunology*, 70(7):496-501, 2009.

[390] Konvalinka A, Tinckam K. Utility of HLA Antibody Testing in Kidney Transplantation. *Journal of the American Society of Nephrology*, 26(7):1489, 2015.

[391] Tambur AR, Wiebe C. HLA Diagnostics: Evaluating DSA Strength by Titration. *Transplantation*, 102(1S Suppl 1):S23-S30, 2018.

[392] Tambur AR, Glotz D, Herrera ND, Chatroop EN, Roitberg T, Friedewald JJ, et al. Can solid phase assays be better utilized to measure efficacy of antibody removal therapies? *Human immunology*, 77(8):624-630, 2016.

[393] Schinstock CA, Gandhi MJ, Stegall MD. Interpreting Anti-HLA Antibody Testing

Data: A Practical Guide for Physicians. *Transplantation*, 100(8), 2016.

[394] Althaf MM, El Kossi M, Jin JK, Sharma A, Halawa AM. Human leukocyte antigen typing and crossmatch: A comprehensive review. *World J Transplant*, 7(6):339-348, 2017.

[395] Ruggeri FS, Mannini B, Schmid R, Vendruscolo M, Knowles TPJ. Single molecule secondary structure determination of proteins through infrared absorption nanospectroscopy. *Nature Communications*, 11(1):2945, 2020.

[396] BoŽIČ B, ČUČNik S, Kveder T, Rozman B. 4 - AFFINITY AND AVIDITY OF AUTOANTIBODIES. In: Shoenfeld Y, Gershwin ME, Meroni PL, editors. Autoantibodies (Second Edition). Burlington: Elsevier; 2007. p. 21-28.

[397] Rudnick SI, Adams GP. Affinity and avidity in antibody-based tumor targeting. *Cancer Biother Radiopharm*, 24(2):155-161, 2009.

[398] Honger G, Hopfer H, Arnold ML, Spriewald BM, Schaub S, Amico P. Pretransplant IgG subclasses of donor-specific human leukocyte antigen antibodies and development of antibody-mediated rejection. *Transplantation*, 92(1):41-47, 2011.

[399] Tambur AR, Kosmoliaptsis V, Claas FHJ, Mannon RB, Nickerson P, Naesens M. Significance of HLA-DQ in kidney transplantation: time to reevaluate human leukocyte antigen–matching priorities to improve transplant outcomes? An expert review and recommendations. *Kidney International*, 100(5):1012-1022, 2021.

[400] DeVos JM, Gaber AO, Knight RJ, Land GA, Suki WN, Gaber LW, et al. Donor-specific HLA-DQ antibodies may contribute to poor graft outcome after renal transplantation. *Kidney International*, 82(5):598-604, 2012.

[401] Justesen S, Harndahl M, Lamberth K, Nielsen LL, Buus S. Functional recombinant MHC class II molecules and high-throughput peptide-binding assays. *Immunome Res*, 5:2, 2009.

[402] Vanderlugt CL, Miller SD. Epitope spreading in immune-mediated diseases: implications for immunotherapy. *Nature Reviews Immunology*, 2(2):85-95, 2002.

[403] Ciubotariu R, Liu Z, Colovai AI, Ho E, Itescu S, Ravalli S, et al. Persistent allopeptide reactivity and epitope spreading in chronic rejection of organ allografts. The Journal of *Clinical Investigation*, 101(2):398-405, 1998.

[404] Cornaby C, Gibbons L, Mayhew V, Sloan CS, Welling A, Poole BD. B cell epitope spreading: Mechanisms and contribution to autoimmune diseases. *Immunology Letters*, 163(1):56-68, 2015.

[405] Bray RA, Nickerson PW, Kerman RH, Gebel HM. Evolution of HLA antibody detection. *Immunologic Research*, 29(1):41-53, 2004.

[406] Braun WE. Laboratory and clinical management of the highly sensitized organ transplant recipient. *Human immunology*, 26(4):245-260, 1989.

[407] Morath C, Opelz G, Zeier M, Susal C. Clinical relevance of HLA antibody monitoring after kidney transplantation. *J Immunol Res*, 2014:845040, 2014.

[408] Schinstock CA, Mannon RB, Budde K, Chong AS, Haas M, Knechtle S, et al. Recommended Treatment for Antibody-mediated Rejection After Kidney Transplantation: The 2019 Expert Consensus from the Transplantion Society Working Group. *Transplantation*, 104(5):911-922, 2020.

[409] Takemoto SK. HLA amino acid residue matching. *Clin Transpl*:397-425, 1996.

[410] *Molecular Medicine©*. Copyright, Daniele Focosi 2001-2014. Available at: http://www.mm.interhealth.info. Accessed [01/09/2021].

Appendices

Appendix 1. Luminex single antigen bead screening of mAbs. Normalised MFI data from the screening of WIM8E5, WK1D12, OUW4F11, SN230G6, SN607D8, GV5D1 and BVK1F9 using Luminex Class I SABs at antibody concentrations of 1 µg/ml.

HLA Bead	SAB MFI
WIM8E5	
A*66:01	24589
A*11:02	24550
A*25:01	24318
A*26:01	23453
A*43:01	22832
A*11:01	22900
A*01:01	22700
A*34:02	21407
A*68:01	20594
A*29:02	19996
A*33:03	19235
A*34:01	17869
A*31:01	17126
A*33:01	16190
A*30:01	13597
A*29:01	13450
A*02:06	13307
A*66:02	13115
A*02:01	12609
A*02:03	12390
A*30:02	12088
A*23:01	11753
A*69:01	11372
A*36:01	10937
A*68:02	10760
A*24:02	9233
A*24:03	5458
C*03:03	5062
C*03:02	4940
C*03:04	4701
A*80:01	4617
B*15:13	2469
B*15:10	2252
B*15:02	1014
B*07:02	43
B*15:01	33
B*15:03	30
B*81:01	20
B*40:01	10
B*40:06	6

WK1D12	
B*40:01	21488
B*81:01	21336
B*07:02	20666
B*27:08	20654
B*40:02	20389
B*13:02	18517
B*40:06	18366
B*27:05	18282
B*48:01	17867
B*13:01	14802
B*47:01	10809
C*02:02	6386
B*73:01	2794
A*66:02	2170
A*11:01	189
A*25:01	129
A*66:01	123
A*68:01	121
A*01:01	113
A*33:01	74
A*26:01	71
A*34:02	66

GV5D1	
A*01:01	21559
A*24:02	16728
A*23:01	16016
B*15:12	7029
A*80:01	4776
A*68:01	114

OUW4F11	
B*08:01	24513
B*14:01	19813
B*15:10	19595
B*18:01	19232
B*15:02	18995
B*14:02	18452
B*78:01	17684
B*15:12	17593
B*39:01	17366
C*08:01	17164
B*15:03	17126
B*46:01	16339
C*03:04	15966
B*15:01	14901
B*35:01	14635
C*03:02	14366
B*40:01	13923
B*54:01	12980
C*12:03	11780
B*40:02	11542
B*15:11	11530
C*16:01	11101
B*56:01	10383
B*45:01	10272
B*55:01	9881
C*03:03	9848
B*48:01	9775
B*50:01	9448
C*07:02	9254
B*82:01	9108
B*40:06	9107
B*41:01	8862
B*81:01	8479
C*14:02	8464
C*01:02	7816
B*42:01	6818
B*07:02	6399
B*67:01	4399
B*27:08	2478
B*73:01	1084

SN230G6	
A*02:03	25872
A*02:01	25718
A*02:06	25218
B*57:03	25209
B*58:01	24550
B*57:01	24048
A*11:02	543
B*15:16	487
A*74:01	280
A*11:01	254
A*01:01	97
A*68:01	70
B*07:02	34
A*25:01	23
A*66:01	23
B*40:01	17
B*81:01	16
A*33:03	11
B*40:06	7

SN607D8	
A*02:06	25437
A*02:01	25433
A*02:03	25411
A*68:01	25194
A*68:02	25126
A*69:01	24864
B*57:03	2893
B*57:01	2816
B*58:01	2658

BVK1F9	
B*08:01	24653

Appendix 2. Assigned HLA cross-reactive groups. A list of the cross-reactive groups (CREGs) identified by various authors and institutions, and the HLA alleles that have been assigned to them [375, 409, 410].

Assigning Author(s)/ Institution(s)	CREG	HLA Antigens
Rodey (1994)	1C	A1, A3, A9(A23,A24), A11, A29, A30, A31, A36, A80
	2C	A2, A9(A23,A24), A28(A68,A69), B17(B57,B58)
	10C	A10(A25,A26,A34,A66), A11, A28(A68,A69), A32, A33, A43, A74
	5C	B5(B51,B52), B15(B62,B63,B75,B76,B77), B17(B57,B58), B18, B21(B49,B50), B35, B46, B53, B70(B71,B72) B73, B78
	7C	B7, B8, B13, B22(B54,B55,B56), B27, B40(B60,B61), B41, B42, B47, B48, B59, B67, B81, B82
	8C	B8, B14(B64,B65), B16(B38,B39), B18, B59, B67
	12C	B12(B44,B45), B13, B21(B49,B50), B37, B40(B60,B61) B41, B47
	Bw4	A23, A24, A25, A32, B13, B27, B37, B38, B44, B47, B49, B51, B52, B53, B57, B58, B59, B63, B77
	Bw6	B7, B8, B18, B35, B39, B41, B42, B45, B46, B48, B50, B54, B55, B56, B60, B61, B62, B64, B65, B67, B71, B72, B73, B75, B76, B78, B81, B82
McKenna and Takemoto (1996)	A1C	A1, A3, A11, A19(A29,A30,A31), A36, A80
	A2	A2, A9(A23,A24), A28(A68,A69), B17(B57,B58)
	A10C	A10(A25,A26,A34,A66), A32, A33, A43, A74
	B5C	B5(B51,B52), B18, B35, B53
	B5C2	B5(B51,B52), B15(B62,B63,B71, B72, B75,B76,B77), B17(B57,B58), B21(B49,B50), B35, B53, B73, B78
	B7C	B7, B8, B13, B27, B41, B42, B47, B48, B54, B55, B56, B60, B61, B81
	B8C	B8, B18, B38, B39, B64, B65
	B12C	B12(B44,B45), B13, B21(B49,B50), B37, B40(B60,B61), B41, B47
	Bw4	A9 (A23,A24), A25, A32, B13, B27, B37, B38, B44, B47, B49, B51, B52, B53, B57, B58, B59, B63, B77
	Bw6	B7, B8, B18, B35, B39, B40(B60,B61), B41, B42, B45, B46, B48, B50, B54, B55, B56, B62, B64, B65, B67, B71, B72, B73, B75, B76

Appendix 2. Continued...

LABScreen Analysis Software-2 (Japanese Red Cross Tokyo Blood Center)	1C1	A1, A3, A11, A36
	1C2	A1, A9, A11, A23, A24, A36
	1C3	A1, A11, A25, A26, A29, A34, A36, A66
	2C1	A2, A28, A68, A69
	2C2	A2, A9, A23, A24, A28, A68, A69
	28C	A11, A25, A26, A30, A31, A33, A34, A66, A68, A69
	B4	B13, B27, B37, B38, B44, B47, B49, B51, B52, B53, B57, B58, B59, B63, B77
	5C	B18, B35, B51, B52, B53, B57, B58, B62, B63, B71, B72, B75, B76, B77
	B6	B7, B8, B18, B35, B39, B41, B42, B45, B46, B50, B54, B55, B56, B57, B60, B61, B62, B64, B65, B71, B72, B75, B76
	INTL2	A9, A23, A24, A32, Bw4
	INTL3	A11, Bw6, Cw3
Other Private Proteins Sharing Public Epitopes	1C (A1)	A1, A3, A11, A36
	2C (A2)	A2, A28
	28C (A28)	A10, A11, A28, A30, A31, A33
	5C (B5)	B5, B15, B17, B18, B35, B53, B70
	7C (B7)	B7, B41, B42, B60
	8C (B8)	B8, B14, B18, B39, B38*, B51*
	12C (B12)	B12, B13, B21, B37*, B41, B47, B60, B61*
	21C (B21)	B5, B15, B21, B35
	22C (B22)	B7, B17*, B22, B27, B46*
	27C (B27)	B7, B13, B27, B40, B47
	Bw4	A9, A25, A32, B5, B13, B17, B27, B37, B38, B44, B49, B53, B59, B63, B77
	Bw6	All non-Bw4 HLA-B alleles
	Interlocus	A2, B17
	Interlocus	A9, A32, Bw4
	Interlocus	A11*, Bw6, Cw3

Appendix 3. Derivation of the equation for equilibrium binding curve fitting for K_D determination. B_f = Concentration of free substrate binding sites, L_f = concentration of free ligand, L_b = concentration of bound ligand, L_0 = total concentration of ligand, K_a/K_b = association constants, K_d = dissociation constant, B_0 = total concentration of substrate binding sites, n = number of binding sites, E_0 = total substrate concentration, Δr_s = difference in stokes radii, $\Delta r_{s,tot}$ = maximum difference in stokes radii, r_0 = strokes radii at no binding.

$$B_f + L_f \rightleftarrows L_b$$

Equation 1: $K_a = \frac{L_b}{B_f \cdot L_f}$ Equation 2: $B_0 = B_f + L_b = n \cdot E_0$ Equation 3: $L_f = L_0 - L_b$ Equation 4: $K_a = \frac{1}{K_d}$

Equation 2 in 1: $$K_a = \frac{L_b}{L_f \cdot (n \cdot E_0 - L_b)}$$

$$\frac{L_b}{L_f} = -K_a \cdot L_b + K_a \cdot n \cdot E_0$$

L_b and L_f are related to: $L_b = \frac{\Delta r_s \cdot B_0}{\Delta r_{s,tot}}$ L_f can be calculated from equation 3.

Equation 2 and 3 in Equation 1 is: $$K_a = \frac{L_b}{(L_0 - L_b) \cdot (n \cdot E_0 - L_b)} = \frac{L_b}{L_0 \cdot n \cdot E_0 - L_0 \cdot L_b - L_b \cdot n \cdot E_0 + L_b^2}$$

$$L_0 \cdot n \cdot E_0 - L_0 \cdot L_b - L_b \cdot n \cdot E_0 + L_b^2 = \frac{L_b}{K_a}$$

$$0 = L_0 \cdot n \cdot E_0 - L_0 \cdot L_b - L_b \cdot n \cdot E_0 + L_b^2 - \frac{L_b}{K_a}$$

$$0 = L_0 \cdot n \cdot E_0 - L_0 \cdot L_b - L_b \cdot n \cdot E_0 + L_b^2 - \frac{L_b}{K_a}$$

$$0 = L_b^2 - L_b\left(L_0 + n \cdot E_0 + \frac{1}{K_a}\right) + L_0 \cdot n \cdot E_0$$

(including equation 4) $$0 = L_b^2 - L_b(L_0 + n \cdot E_0 + K_d) + L_0 \cdot n \cdot E_0$$

$$L_{b1,2} = \frac{L_0 + n \cdot E_0 + K_d}{2} \pm \sqrt{\left(\frac{L_0 + n \cdot E_0 + K_d}{2}\right)^2 - L_0 \cdot n \cdot E_0}$$

$$\frac{\Delta r_s \cdot n \cdot E_0}{\Delta r_{s,tot}} = \frac{L_0 + n \cdot E_0 + K_d}{2} - \sqrt{\left(\frac{L_0 + n \cdot E_0 + K_d}{2}\right)^2 - L_0 \cdot n \cdot E_0}$$

$$\Delta r_s = \left(\frac{L_0 + n \cdot E_0 + K_d}{2} - \sqrt{\left(\frac{L_0 + n \cdot E_0 + K_d}{2}\right)^2 - L_0 \cdot n \cdot E_0}\right)\frac{\Delta r_{s,tot}}{n \cdot E_0}$$

$$\Delta r_s = r_{measured} - r_0$$

$$r_{measured} = \left(\left(\frac{L_0 + n \cdot E_0 + K_d}{2} - \sqrt{\left(\frac{L_0 + n \cdot E_0 + K_d}{2}\right)^2 - L_0 \cdot n \cdot E_0}\right)\frac{\Delta r_{s,tot}}{n \cdot E_0}\right) + r_0$$

Appendix 4. Interaction affinity measurements as determined by BLI – Individual replicates. The affinities (K_D) measured in individual experiments that assessed the kinetics of each alloantibody-HLA interaction using BLI. K_D values were calculated as a function of k_{off}/k_{on} from sensorgram data fitted using global fitting and a 1:1 stoichiometry model. * represents interactions which showed a low response using high ligand concentrations and so calculated affinities may be less reliable. Interactions where HLA was needed at a high concentrations to observe a quantifiable responses were not repeated.

mAb	HLA	K_D (M)				
		1	2	3	Mean	±SD (n)
WIM8E5	A*11:01	2.2×10^{-8}	1.4×10^{-8}	-	1.8×10^{-8}	5.4×10^{-9}
	A*25:01	4.8×10^{-8}	5.7×10^{-8}	-	5.2×10^{-8}	6.5×10^{-9}
	A*01:01	2.1×10^{-7}	1.9×10^{-7}	-	2.0×10^{-7}	1.5×10^{-8}
	A*31:01	7.0×10^{-7}	6.0×10^{-7}	-	6.5×10^{-7}	7.4×10^{-8}
	A*68:01	8.9×10^{-7}	-	-	8.9×10^{-7}	N/A
	A*24:02*	2.7×10^{-6}	-	-	2.7×10^{-6}	N/A
	A*02:01*	5.4×10^{-6}	4.6×10^{-6}	-	5.0×10^{-6}	5.8×10^{-7}
WK1D12	B*27:05	1.8×10^{-8}	1.5×10^{-8}	-	1.7×10^{-8}	2.2×10^{-9}
	B*40:01	2.9×10^{-8}	2.3×10^{-8}	-	2.6×10^{-8}	4.2×10^{-9}
	B*40:02	2.7×10^{-8}	3.0×10^{-8}	-	2.9×10^{-8}	2.3×10^{-9}
	B*07:02	3.9×10^{-8}	4.2×10^{-8}	-	4.1×10^{-8}	1.8×10^{-9}
	B*48:01	4.5×10^{-8}	6.2×10^{-8}	-	5.3×10^{-8}	1.2×10^{-8}
	B*13:01	6.1×10^{-8}	-	-	6.1×10^{-8}	N/A
OUW4F11	B*08:01	3.2×10^{-7}	6.4×10^{-7}	2.7×10^{-7}	4.1×10^{-7}	2.0×10^{-7}
	B*46:01	7.2×10^{-7}	-	-	7.2×10^{-7}	N/A
	B*15:01	1.6×10^{-6}	-	-	1.6×10^{-6}	N/A
	B*40:01	3.9×10^{-6}	2.5×10^{-6}	-	3.2×10^{-6}	9.5×10^{-7}
	B*40:02	4.4×10^{-6}	-	-	4.4×10^{-6}	N/A
	B*15:10	4.4×10^{-6}	-	-	4.5×10^{-6}	N/A
SN230G6	B*58:01	2.5×10^{-9}	3.6×10^{-9}	-	3.0×10^{-9}	8.3×10^{-10}
	B*57:01	3.3×10^{-9}	3.8×10^{-9}	-	3.6×10^{-9}	4.0×10^{-10}
	A*02:01	8.9×10^{-9}	5.9×10^{-9}	-	7.4×10^{-9}	2.1×10^{-9}
SN607D8	A*02:01	1.1×10^{-8}	1.3×10^{-8}	-	1.2×10^{-8}	1.4×10^{-9}
	A*68:01	1.2×10^{-8}	-	-	1.2×10^{-8}	N/A
	A*69:01	2.7×10^{-8}	-	-	2.7×10^{-8}	N/A
GV5D1	A*01:01*	7.1×10^{-7}	-	-	7.1×10^{-7}	N/A
	A*23:01*	2.4×10^{-6}	-	-	2.4×10^{-6}	N/A
	A*24:02*	4.2×10^{-6}	3.6×10^{-6}	-	4.0×10^{-6}	2.9×10^{-7}
BVK1F9	B*08:01*	8.2×10^{-7}	-	-	8.2×10^{-7}	N/A

Appendix 5. Luminex single antigen bead data - by mAb. The normalised MFI outputs from Luminex Class I SAB assays when assessing WIM8E5, WK1D12, OUW4F11, SN230G6, SN607D8, GV5D1 and BVK1F9 using concentrations of 10 µg/ml (64.5 nM), 3 µg/ml (19.4 nM), 1 µg/ml (6.45 nM), 0.3 µg/ml (1.94 nM), and 0.1 µg/ml (0.65 nM).

mAb	HLA	Luminex SAB Mean Fluorescence Intensity (MFI) at Specific mAb Conc. (µg/ml)				
		10.0	3.0	1.0	0.3	0.1
WIM8E5	A*01:01	26355	25840	25563	23523	14425
	A*02:01	22680	16673	12629	8530	5002
	A*11:01	25783	25762	25706	23360	15929
	A*24:02	20008	13336	8220	4377	2195
	A*25:01	27426	27114	27068	25429	16975
	A*31:01	24113	21304	18047	13929	8967
WK1D12	B*07:02	23987	23965	23530	21292	17442
	B*13:01	20049	19052	19302	16044	13118
	B*27:05	21966	22340	21272	18847	15615
	B*40:01	25351	25034	24792	22284	18632
	B*40:02	25216	24943	24707	21517	17324
	B*48:01	22719	21899	22264	19769	16395
OUW4F11	B*08:01	22822	22741	22543	20159	13462
	B*15:01	16185	15422	14731	10521	6952
	B*15:10	17913	17053	17223	12579	7786
	B*40:01	13477	12481	11977	7939	4799
	B*40:02	13041	11690	10949	7421	4428
	B*46:01	16960	16428	15869	11464	7231
SN230G6	A*02:01	22696	21830	21948	21957	20653
	B*57:01	21047	20177	20804	21254	20192
	B*58:01	20947	21030	20429	20966	20123
SN607D8	A*02:01	22198	22813	22729	21880	18420
	A*68:01	22519	22062	21970	21046	17333
	A*69:01	21381	21004	21072	19857	16472
GV5D1	A*01:01	18556	17388	16830	13669	13125
	A*23:01	20671	17990	17163	7469	7610
	A*24:02	19110	16108	14983	6861	6874
BVK1F9	B*08:01	22635	22901	22624	22521	21114
	A*02:01	254	0	0	0	0

Appendix 6. Luminex single antigen bead data – by HLA. The normalised MFI outputs from Luminex assays when assessing HLA-A*02:01, HLA-B*40:01, and HLA-A*24:01 single antigen beads with their reactive monoclonal antibodies at concentrations of 10 µg/ml (64.5 nM), 3 µg/ml (19.4 nM), 1 µg/ml (6.45 nM), 0.3 µg/ml (1.94 nM), and 0.1 µg/ml (0.65 nM).

HLA	mAb	Luminex SAB Mean Fluorescence Intensity (MFI) at Specific mAb Conc. (µg/ml)				
		10.0	3.0	1.0	0.3	0.1
A*02:01	SN230G6	22696	21830	21948	21957	20653
	SN607D8	22198	22813	22729	21880	18420
	WIM8E5	22680	16673	12629	8530	5002
	GV5D1	1453	271	122	0	0
	OUW4F11	752	113	359	0	0
B*40:01	WK1D12	25351	25035	24729	22284	18632
	OUW4F11	13477	12481	11977	7939	4799
	GV5D1	607	8	0	0	0
A*24:02	GV5D1	19110	16108	14983	6861	6874
	WIM8E5	20008	13336	8220	4377	2195

Appendix 7. Luminex C1qScreen data. (A) The normalised MFI outputs from Luminex C1qScreen assays when assessing WIM8E5, WK1D12, SN230G6, or GV5D1 at concentrations of 10 µg/ml (64.5 nM), 3 µg/ml (19.4 nM), 1 µg/ml (6.45 nM), 0.3 µg/ml (1.94 nM), and 0.1 µg/ml (0.65 nM). (B) The same MFI data displaying HLA-A*02:01 and HLA-A*24:02 single antigen beads against their reactive mAbs.

(A)

mAb	HLA	Luminex Mean Fluorescence Intensity (MFI) at Specific mAb Conc. (µg/ml)				
		10.0	3.0	1.0	0.3	0.1
WIM8E5	A*01:01	29943	28883	28114	5984	175
	A*02:01	24239	22171	1061	16	0
	A*11:01	28738	29326	27540	11809	823
	A*24:02	17939	10969	754	255	75
	A*25:01	30536	30437	29977	10893	240
	A*31:01	27953	27570	14180	1364	0
WK1D12	B*07:02	24005	22223	23542	6644	2579
	B*13:01	18261	14615	15944	4243	3808
	B*27:05	18727	18209	18642	3361	1457
	B*40:01	25959	26374	26597	11106	4209
	B*40:02	27079	25501	24975	6263	2038
	B*48:01	20006	20355	19622	6703	2163
SN230G6	A*02:01	19009	21661	22357	21451	14519
	B*57:01	18579	20124	22273	19884	16043
	B*58:01	19958	21321	21984	20796	17866
GV5D1	A*01:01	21048	21328	15180	12418	3156
	A*23:01	20187	16828	4109	0	0
	A*24:02	18245	14579	5178	819	1540

(B)

mAb	HLA	Luminex Mean Fluorescence Intensity (MFI) at Specific mAb Conc. (µg/ml)				
		10.0	3.0	1.0	0.3	0.1
A*02:01	SN230G6	19009	21661	22357	21451	14519
	WIM8E5	24239	22171	1061	16	0
A*24:02	GV5D1	18245	14579	5178	819	1540
	WIM8E5	17939	10969	754	255	75

Appendix 8. Gating strategy for T-cell flow cytometry. (A) P1 – The entire population of PBMCs were gated based on forward and side scatter area to remove unwanted signals from cell debris and other blood components. (B) P1 cells were stained with anti-CD3-PE and anti-CD19-APC, where they were further gated into T and B cells. Only T cells were analysed in this data due to low B cell count. (C) A representative histogram showing positive alloantibody detection on gated T-cells using anti-IgG-FITC secondary. Representative image is taken from incubation with 10 µg/ml GV5D1.

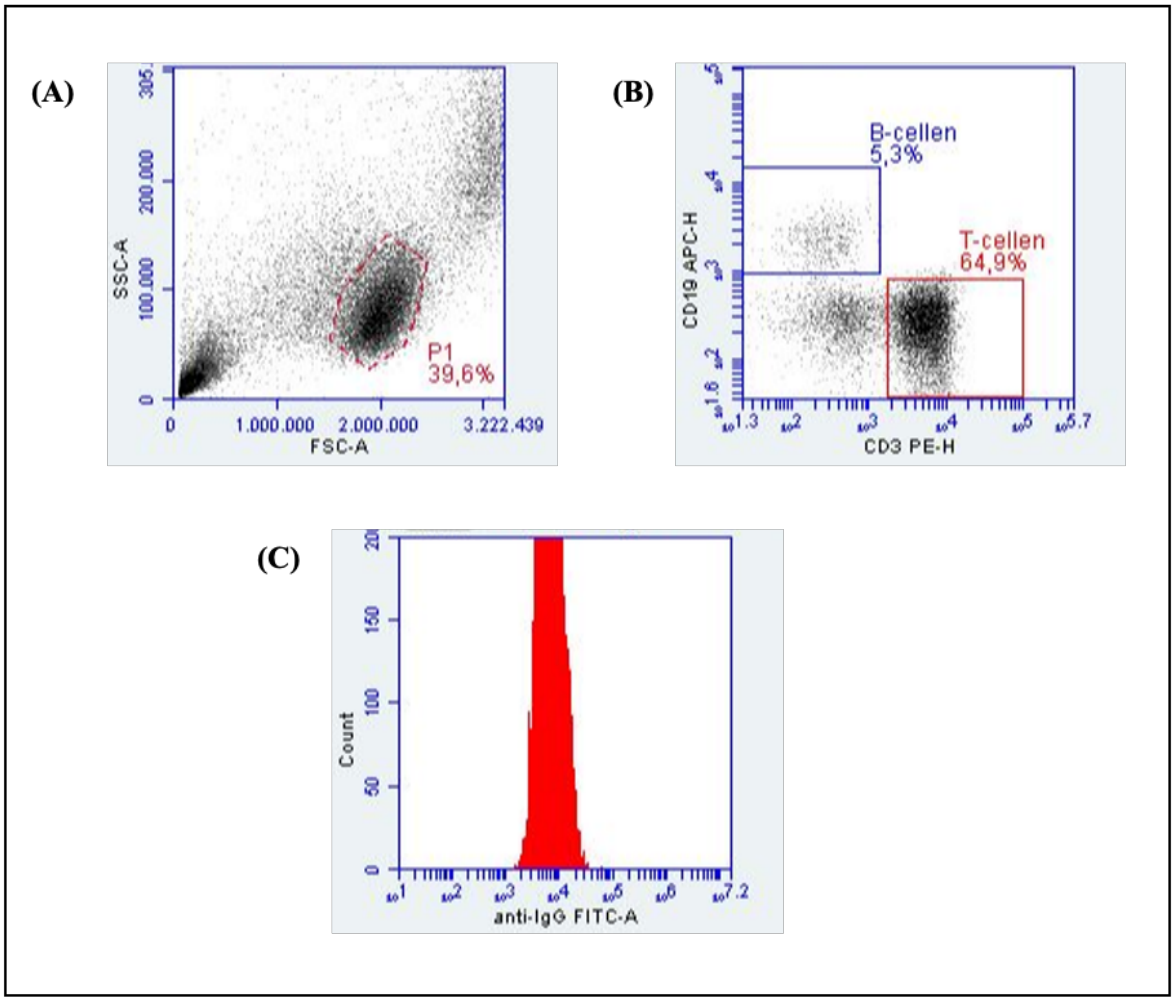

Appendix 9. T-cell flow cytometry data. The normalised fold change in MFI outputs from flow cytometry assays when WIM8E5, WK1D12, OUW4F11, SN230G6, SN607D8 and OUW4F11 were incubated with T-cells that expressing their respective antibody-reactive HLA targets (Table 2.3) at antibody concentrations of 10 µg/ml (64.5 nM), 3 µg/ml (19.4 nM), 1 µg/ml (6.45 nM), 0.3 µg/ml (1.94 nM), and 0.1 µg/ml (0.65 nM). Red = positive outputs where MFI-FC is >1.6. Green = negative outputs where MFI-FC is ≤1.6. * = where each mAb was used at equal concentrations to make up the total mAb concentration stated. MFI values are taken from >2000 cells.

mAb	HLA	PBMC Sample	+ve Con. MFI	-ve Con. MFI	Flow cytometry Mean Fluorescence Intensity fold-change measured at the stated mAb conc. (µg/ml)				
					10	3.0	1.0	0.3	0.1
WIM8E5	A*11:01	5	51572	1317	31.1	31.7	29.5	21	10.5
	A*25:01	7	52433	1254	19.3	19.6	17.5	13.2	6.3
	A*01:01	1	22210	1464	3.7	3.5	3.0	2.6	1.7
	A*31:01	8	45799	1315	4.1	2.7	1.9	1.4	1.1
	A*02:01	4	60576	1296	2.1	1.7	1.3	1.1	0.9
	A*24:02	6	54389	1935	1.2	1.1	1.0	0.9	0.8
	A*01:01	2	42656	1201	6.8	5.9	5.4	4.3	1.9
	A*01:01	3	40931	1333	7.0	5.7	5.2	3.7	2.5
	A*01:01	15	43789	1390	4.8	4.2	3.4	2.9	2.3
WK1D12	B*40:01	12	37620	1407	13.3	11.8	7.6	2.7	2.0
	B*40:02	13	51342	1429	13.2	10.9	5.8	2.6	1.5
	B*48:01	14	33794	1336	13.0	11.7	7.6	2.9	1.3
	B*27:05	11	39281	1334	12.1	10.2	6.2	2.7	1.4
	B*07:02	1	22210	1464	9.0	9.0	6.5	3.3	1.7
	B*07:02	9	26157	1481	17.9	15.2	8.7	2.8	2.4
	B*07:02	10	50902	1431	18.7	18.0	4.3	3.5	1.3
SN230G6	A*02:01	4	71503	1214•	35.9	35.1	33.8	17.2	7.1
SN607D8	A*02:01	4	54133	1214	35.9	35.4	24.2	9.5	4.2
OUW4F11	B*08:01	15	43789	1390	13.1	12.1	11.9	8.6	3.4
	C*07:02	16	42133	1319	0.9	0.9	1.0	0.9	0.9
	C*07:02	17	71116	1351	0.9	0.9	1.0	0.9	0.8
WIM8E5 + OUW4F11	A*01:01/ B*08:01	15	43789	1390	17.0 15.8*	15.8 15.0*	15.5 11.5*	10.2 6.9*	4.5 2.7*

Appendix 10. Complement-dependent cytotoxicity data. The normalised percentage kill from CDC assays when WIM8E5, SN230G6, SN607D8 and OUW4F11 were incubated with T-cells that express the respective antibody-reactive HLA targets (Table 2.3) at antibody concentrations of 10 µg/ml (64.5 nM), 3 µg/ml (19.4 nM), 1 µg/ml (6.45 nM), 0.3 µg/ml (1.94 nM), and 0.1 µg/ml (0.65 nM). Values are an average of triplicate measurements from three identical wells in one experiment. Pale green = 0-10 % kill / score of 1 = negative, darker green = 10-20 % kill / score of 2 = likely negative, yellow = 20-40 % kill / score of 4 = weakly positive, orange = 40- 80 % kill / score of 6 = positive, red = 80-100 % kill / score of 8 = strongly positive. * = where each mAb was used at equal concentrations to make up the total mAb concentration stated. Values are an average of triplicate measurements.

mAb	HLA	PBMC Sample	+ve con. % kill	-ve con. % kill	Cell Death via Complement Dependent Cytotoxicity (%) at stated mAb conc. (µg/ml)				
					10.0	3.0	1.0	0.3	0.1
WIM8E5	A*11:01	5	96	0	98	87	50	14	4
	A*25:01	7	97	0	79	62	43	14	4
	A*31:01	8	96	10	63	48	20	2	2
	A*01:01	1	94	2	52	44	18	5	3
	A*02:01	4	97	3	14	9	6	1	1
	A*24:02	6	96	4	11	5	6	4	0
	A*01:01	3	92	2	60	38	14	2	2
	A*01:01	2	75	6	54	32	6	2	0
	A*01:01	15	98	9	34	26	8	2	3
SN230G6	A*02:01	4	97	4	61	56	45	30	8
SN607D8	A*02:01	4	97	4	43	40	36	14	4
OUW4F11	B*08:01	15	92	6	22	16	11	8	4
	C*07:02	16	91	7	5	7	1	2	3
	C*07:02	17	96	11	9	12	8	8	0
WIM8E5 + OUW4F11	A*01:01/ B*08:01	15	94	6	56	39	22	11	4
			97*	13*	48*	34*	18*	9*	3*

Appendix 11. Gating strategy for characterisation of HAoECs via flow cytometry. (A) P1 – The entire population of whole cells were gated based on forward and side scatter area to remove unwanted signal from cell debris. (B) P2 – Cells were further gated by forward scatter width to ensure only single cells were being analysed. (C-F) The establishment of a negatively stained control cell population was established by incubating HAoECs with anti-human IgG Fc + streptavidin-APC* or STAR70 (FITC), respectively, without the addition of primary antibody. (E-F) Positive controls for APC* and FITC fluorescent signals were established by incubating HAoECs with the same secondary detection molecules after the addition of SN230G6 or W6/32, respectively. This strategy was also used for characterisation of cellular P-selectin, replacing STAR70 with anti-CD2P.

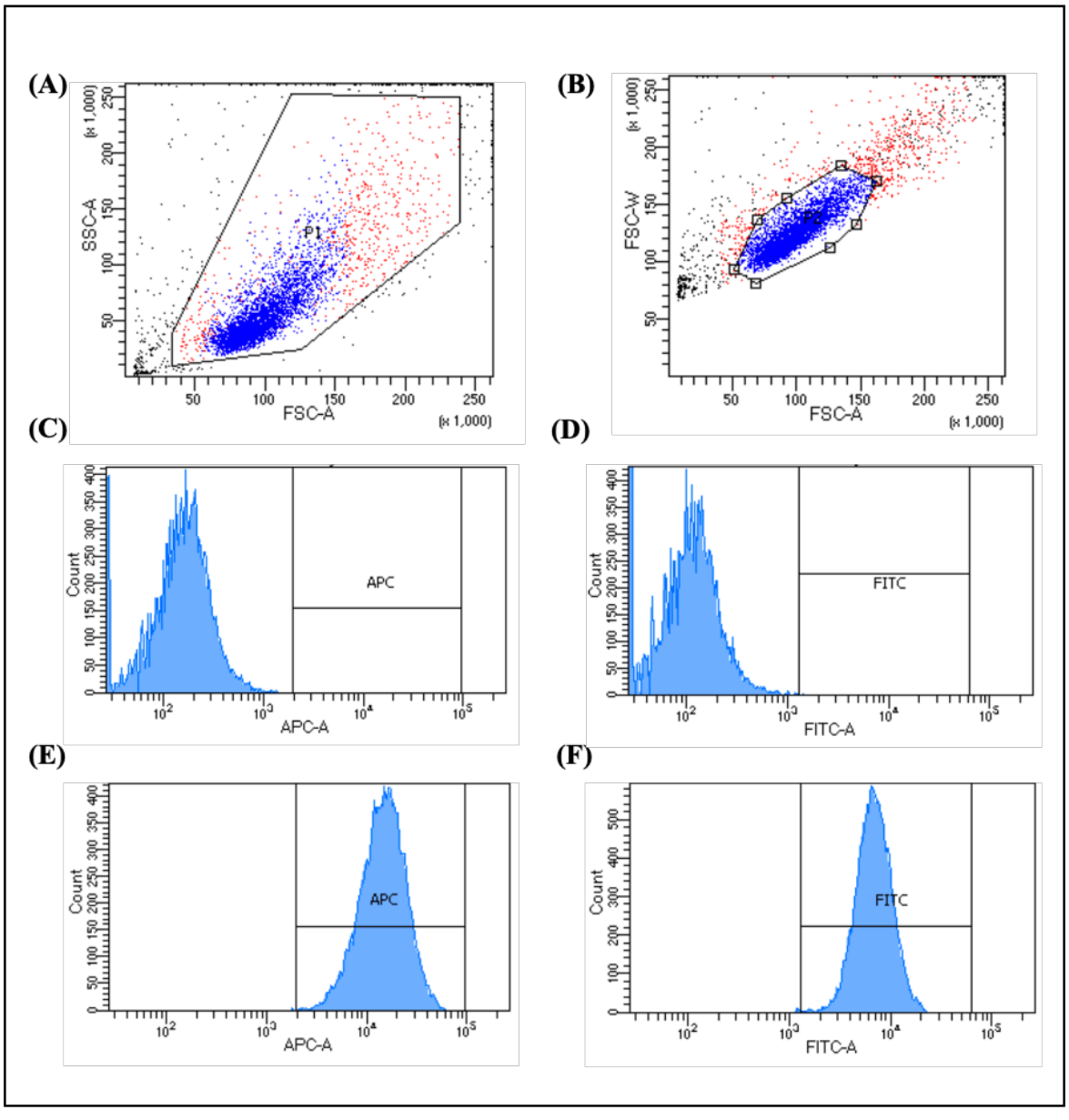

Appendix 12. Stokes-Einstein and Einstein-Smoluchowski equations. The scientific equations used to explain the relationship behind antibody size and the diffusion coefficient. (A) Stokes-Einstein equation where: D = diffusion coefficient, k_B = Boltzmann's constant, T = temperature (K), η = solvent viscosity, and R_H = hydrodynamic radius. (B) = Einstein-Smoluchowski equation, where: D = diffusion coefficient, λ = distance that a particle can jump when diffusing in a time, τ.

(A)

$$D = \frac{k_B T}{6 \pi \eta R_H}$$

(B)

$$D = \frac{\lambda^2}{2\tau}$$

Appendix 13. Examining the contribution of serum background autofluorescence to the absorbance and fluorescence signals of AlexaFluor 647 excited at wavelengths across the light spectrum. A minimal fluorescent background signal was detected at 650nm in serum, making AF647 a good choice for fluorescent protein detection within human serum samples. Alexa Fluor 647 was diluted 10-fold from 1 µM to 10 pM, where it was analysed for its absorbance and emission spectra across light wavelengths of 0-720 nm in the presence of PBS or human serum. (A) Absorbance spectra of AF647 in human serum. (B) Absorbance spectra of AF647 in PBS. (C) Fluorescence spectra of AF647 in human serum. (D) Fluorescence spectra of AF647 in PBS. (E) The natural fluorescent signal of human serum and PBS alone. (F) The signal to noise ratio of AF647 is slightly reduced in the presence of human serum compared to PBS.

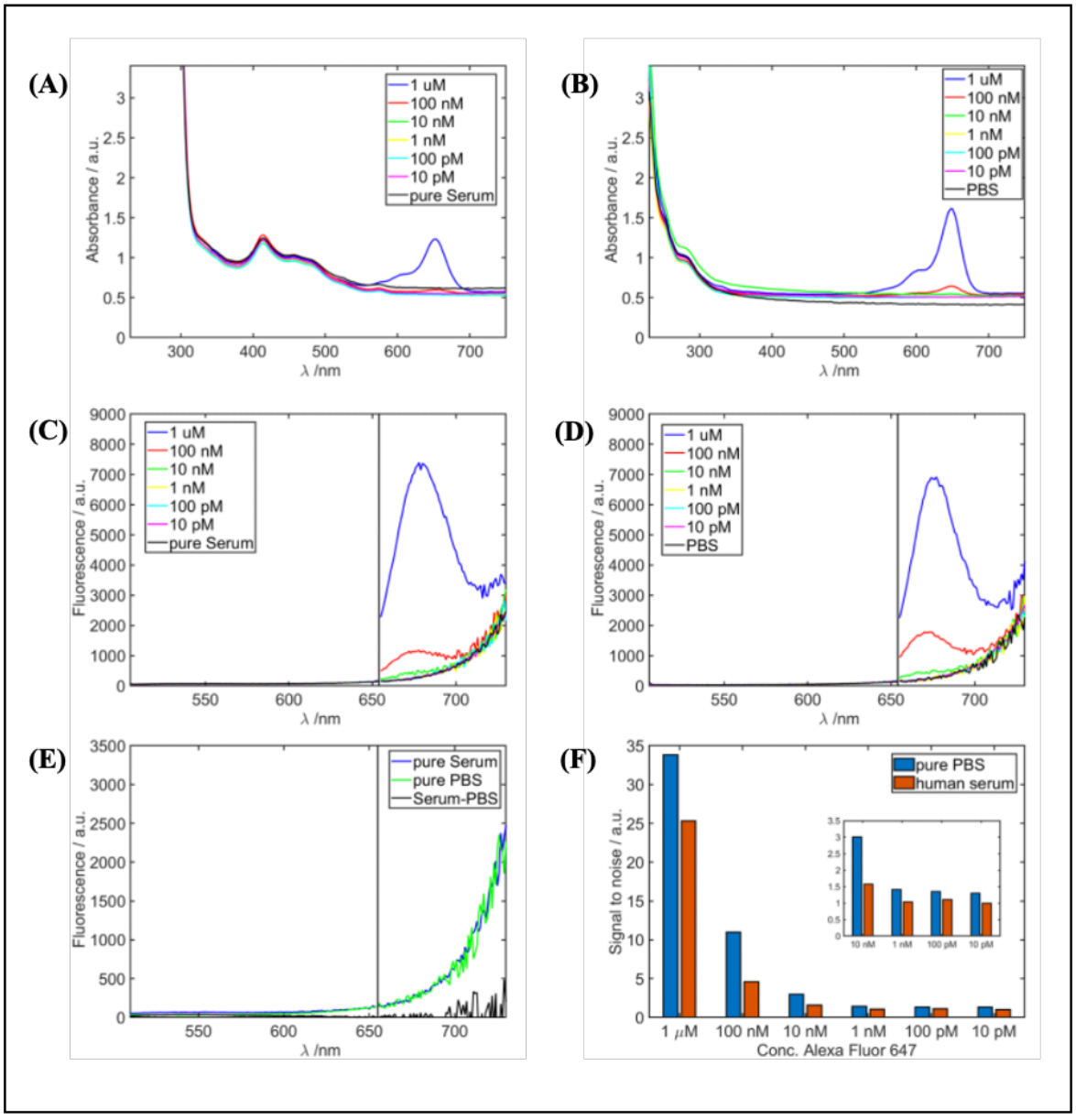

Appendix 14. Quantification of the HLA-Alexa Fluor 647 labelling ratio. HLA was labelled with Alexa Fluor 647 as documented in sections 2.4.2 and 5.2.1. The absorbance of the purified labelled protein was measured at 280 nm and 650 nm, from which the protein and fluorophore concentrations could be calculated using the Beer-Lambert law (Equation 1, see section 2.1.1).

HLA	Measured Concentration of HLA (M)	Measured Concentration of AF 647 (M)	Labeling ratio ([AF647]/[HLA])
A*01:01	2.56×10^{-6}	2.86×10^{-6}	1.12
A*02:01	8.05×10^{-7}	6.62×10^{-7}	0.82
A*03:01	7.04×10^{-6}	3.48×10^{-5}	4.94
A*11:01	1.88×10^{-6}	1.95×10^{-6}	1.04
B*08:01	1.05×10^{-6}	1.49×10^{-6}	1.42
DRB1*07:01	1.52×10^{-6}	1.84×10^{-6}	1.21

Appendix 15. Measured fluorescent signals of Alexa Fluor 647-labelled HLA molecules. HLA molecules labelled with AF647 were measured via MDS at concentrations of 100 nM, 10 nM and 1 nM (5 nM used for B*08:01 instead of 1 nM), where their fluorescence intensities were analysed to determine the lowest detectible signal for MDS/MAAP analysis.

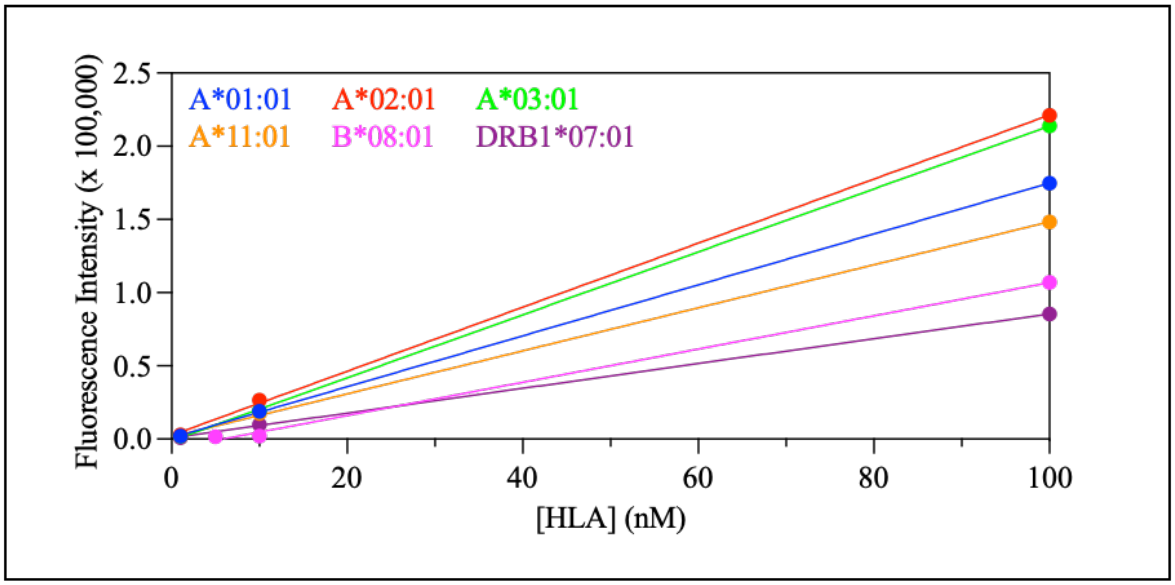

Appendix 16. Background fluorescent signals of human sera. Human sera selected for antibody assessment via MDS/MAAP were examined for their natural fluorescent signals. MDS measurements were taken at serum concentrations of 25%, 50% and 100% in the absence of fluorophore-labelled protein. This enabled a serum fluorescence curve to be produced which can be used as a standard to deduct background signal when taking MDS measurements of serum-containing samples (see sections 2.4.4 and 5.2.5). Where multiple samples were taken for one patient, the number in brackets represents the sample number.

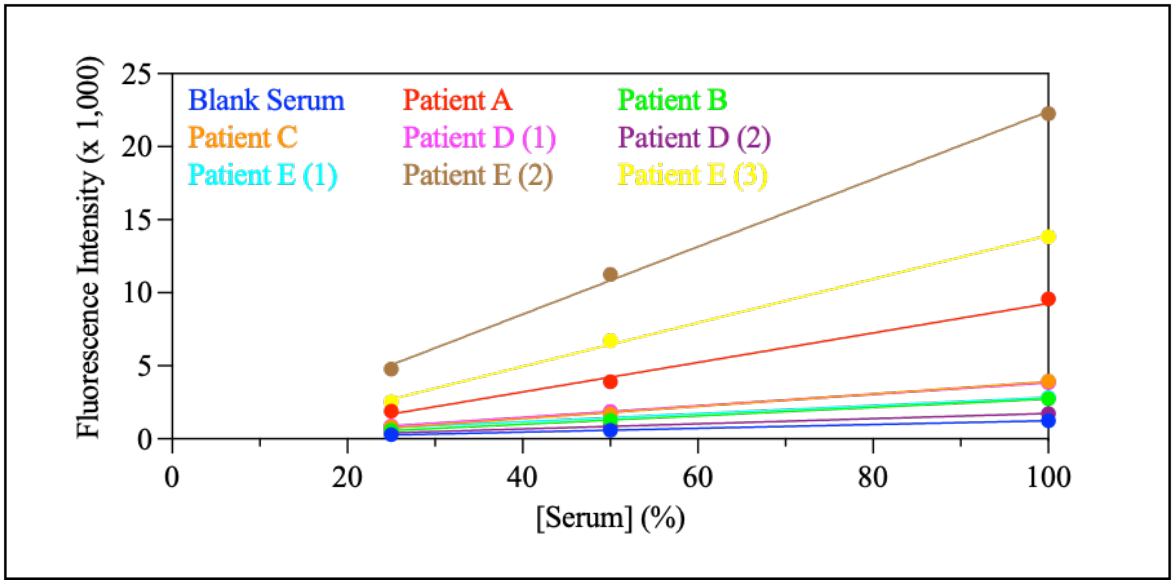

Appendix 17. Abstract for PCT international application number PCT/GB2021/051244. This patent was submitted on 21st May 2021 to protect the IP associated with the development and use of the Microfluidic Antibody Affinity Profiling method.

Abstract

An apparatus for characterising a biomolecule is provided. The apparatus comprising a sample inlet channel configured to introduce a sample fluid including the 5 biomolecule to the apparatus; an auxiliary inlet channel configured to introduce an auxiliary fluid to the apparatus; a distribution channel in fluid communication with the sample inlet channel and the auxiliary inlet channel; wherein the distribution channel is adapted to generate a distribution of biomolecules; a measurement module configured to detect a signature profile of the biomolecule to obtain a measured 10 dataset of the detected biomolecule; a storage location configured to store and maintain a stored dataset comprising a plurality of parameters that are associated with the measured dataset obtained from the measurement module; and an analysis module configured to receive the stored dataset from the storage location and correlate the stored dataset with the measured dataset from the measurement 15 module to provide a correlation value, wherein the analysis module is further configured to use the correlation value to determine at least two characteristics of the biomolecule simultaneously using Bayesian analysis. A method for characterising a biomolecule is also provided.

Microfluidic Antibody Affinity Profiling for In-Solution Characterisation of Alloantibody - HLA Interactions in Human Serum

Matthias M. Schneider[1,+], Tom Scheidt[1,+], Ashley J. Priddey[2,+], Catherine K. Xu[1,+], Mengsha Hu[1,+], Sean R. A. Devenish[3], Georg Meisl[1], Christopher M. Dobson[1,†], Vasilis Kosmoliaptsis[1,4,5,*], Tuomas P. J. Knowles[1,6,*]

[1] Centre for Misfolding Diseases, Department of Chemistry, University of Cambridge, Lensfield Road, Cambridge CB2 1EW, United Kingdom
[2]Department of Surgery, University of Cambridge, Addenbrooke's Hospital, Hills Road, Cambridge CB2 0QQ, UK
[3]Fluidic Analytics, Unit A, The Paddocks Business Centre, Cherry Hinton Rd, Cambridge CB1 8DH, UK
[4] NIHR Blood and Transplant Research Unit in Organ Donation and Transplantation, University of Cambridge, Hills Road, Cambridge CB2 0QQ, UK
[5] NIHR Cambridge Biomedical Research Centre, Hills Road, Cambridge CB2 0QQ, UK
[6] Cavendish Laboratory, Department of Physics, University of Cambridge, JJ Thomson Ave, Cambridge CB3 0HE, UK
[+] contributed equally
[†] Passed away September 2019
[*] corresponding to vk256@cam.ac.uk and tpjk2@cam.ac.uk

Abstract

The detection and characterisation of antibodies in human blood is a key for clinical diagnostics and risk assessment for autoimmunity, infectious diseases and transplantation. Antibody titre derived from immunoassays is a commonly used measure for antibody response, but this metric does not resolve readily the two fundamental properties of antibodies in solution, namely their affinity and concentration. This difficulty originates from the fact that the fundamental parameters describing the binding interaction, affinity and ligand concentration, are convoluted into the titre measurement; moreover, the difficulty of controlling the surface concentration and activity of the immobilised ligand can make it challenging to distinguish between avidity and affinity. To address these challenges, we developed microfluidic antibody affinity profiling, an assay which allows the simultaneous determination of both affinity and antibody concentration, directly in solution, without surface immobilisation or antibody purification. We demonstrate these measurements in the context of alloantibody characterisation in organ transplantation, using complex patient sera, and quantify the concentration and affinity of alloantibodies against donor Human Leukocyte Antigens (HLA), an extensively used clinical biomarker to access the risk of allograft rejection. These results outline a path towards detection and in depth profiling of antibody response in patient sera.

Introduction

Non-covalent protein-protein interactions underlie many biological and physiological processes, including protein self-assembly,[1–3] protein aggregation,[4–6] antibody-antigen recognition,[7–9] muscle contraction,[10] and cellular communication.[11] One fundamental application of measuring protein-protein interactions is based on immuno-assays for the detection of biomarkers in body fluids, primarily human serum, related to various diseases including cancer,[12–15] protein misfolding diseases,[16–21] auto-immune diseases,[22] and graft rejection.[23] In the latter, detection of antibodies against donor Human Leukocyte Antigens (HLA), termed alloantibodies, in patient serum serve as strong indicator for potential rejection of transplants. The analysis and characterisation of these biomarkers is essential for pre-transplant assessment and post-transplant immune monitoring.[24–27]

Current approaches for the detection and characterisation of antibodies, including alloantibodies, rely mostly on surface immobilisation of one of the binding partners, such as in enzyme-linked immunosorbant assays (ELISA),[28–30] bead-based multiplex assays,[31–34] and surface plasmon resonance (SPR) spectroscopy.[35–37] The requirement for protein immobilisation is associated with a number of challenges, such as non-specific interactions with the surface or suppressed accessibility due to alterations of substrate and ligand structures.[38–40] Furthermore, avidity effects caused by dense substrate occupation are hard to control in surface based measurements.[41] Additionally, the hook/prozone effect, most prevalent in sandwich immunoassays or complement interference, can result in false negative measurements.[42–44] More generally, for measurements on surfaces, the fundamental parameters of antibodies in solution, namely their affinity and concentration, are challenging to resolve due to the difficulty in controlling the concentration of the surface-bound species. For instance, the commonly used EC50 value obtained in surface measurements is only weakly dependent on the affinity of the interaction for strong antibody binding, as illustrated in Fig.1a.

To overcome the limitations of surface-based immunoassays, we demonstrate here an in-solution Microfluidic Antibody Affinity Profiling (MAAP) apporach, allowing quantitative measurement of biophysical parameters governing specific antibody-antigen interactions in unpurified human serum and its complex background with more than 10 million different proteins.[45] Unlike existing microfluidic immunoassays, many of which rely on surface immobilisation,[46,47] the approach described in this paper operates fully in solution. We use a strategy based on microfluidic diffusional sizing, which tracks the spatial and temporal evolution of a fluorescently labelled protein in a microfluidic channel under laminar flow conditions to determine its hydrodynamic radius, R_h (Fig. 1) and hence effective molecular weight. When an antigen molecule interacts with an antibody in solu-

tion, its effective molecular weight increases to that of the antibody-antigen complex and hence its diffusion coefficient decreases.

We focus here on humoral responses against HLA, also known as the human major histocompatibility complex (MHC), a biomolecule of key clinical significance. The extensive polymorphism of the HLA system, evolved to enable immune protection against an ever-changing environment of human pathogens, is a major barrier in organ and cell transplantation.[48] Exposure to donor HLA through pregnancy, transfusion and/or transplantation leads to development of alloantibodies, principal mediators of acute and chronic allograft loss.[23,49] Detection and characterisation of alloantibodies is essential for evaluation of donor-recipient compatibility and to facilitate post-transplant immune monitoring and provide individual therapeutic intervention.[50–52] In current clinical practice, this is mainly performed using solid phase assays which suffer from the aforementioned

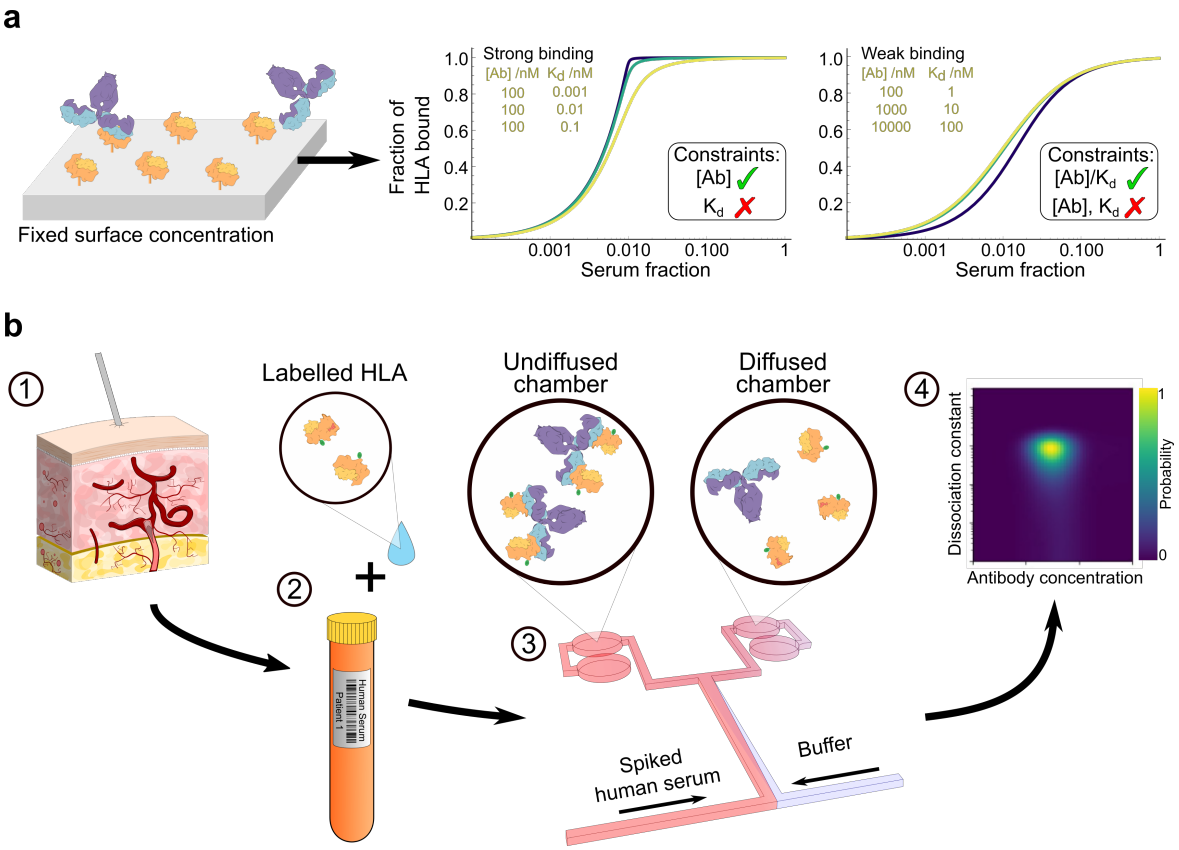

Figure 1: (**a**) Basic Principle of surface based antibody-binding measurements. In a strong binding regime, the antibody concentration can be determined, in a weak binding regime the ratio between antibody concentration and dissociation constant, K_d, can be determined only. (**b**) Basic principle of applying MDS for clinical samples. (1) Patient-derived human serum (2) is incubated with different concentrations of labelled HLA to allow binding. (3) The effective size of the complex is determined by microfluidic diffusional sizing, from which (4) the dissociation constant K_d and the antibody concentration $[Ab]$ are determined. As it is an in-solution approach, both K_d and antibody concentration become accessible. The posterior shows the probability distribution, whereby yellow stands for high, blue for low probability that the according parameters K_d and $[Ab]$ are found at the respective values.

disadvantages of surface-based techniques. Such semi-quantitative approaches do not allow the full characterisation of fundamental biophysical properties of the humoral alloresponse such as alloantibody levels (concentration) and the affinity of alloantibody-HLA interaction.[27,53–55] In the following, we show that MAAP is an advanced technique capable of quantifying an analyte in human serum under native solution conditions to yield physiologically relevant results and thus propose this platform as an additional procedure for immuno-profiling in human serum.

Results and Discussion

Binding Interactions of Covalently Labelled HLA

In order to detect alloantibodies in solution using HLA, a microfluidic diffusional sizing (MDS) platform was used that enables determination of binding parameters by measuring the hydrodynamic radius, R_h, of a fluorescently labelled protein, as previously described.[56–59] We used a reliable and stable labelling strategy for fluorescence detection, relying on NHS-Chemistry (Fig. S1a) for N-terminal labelling, which yields highly pure HLA with labelling stoichiometry of 0.33 to 1.55, depending on the variant (Fig. S1c-f). This allows control of the stoichiometry of the binding interaction more accurately than traditional strategies utilising biotin-streptavidin-HLA complexes which are highly heterogeneous (Fig. S1b). A fluorophore in the far-red spectral region was chosen ($\lambda_{\mathrm{em,\,max}} = 650$ nm), since serum autofluorescence is minimised in this spectral region (Fig. S2e).

Rapid and physiologically accurate investigation of antibodies in human samples is crucial for clinical evaluation. Therefore, immunoassays must be able to cope with untreated samples and not be influenced by non-specific binding to surfaces, by the hook/prozone-effect, and by surface-mediated avidity effects.[42–44] To validate the applicability of the assay for quantification of alloantibody-HLA interactions, the binding of the HLA variant A*03:01 to the mouse derived anti-human monoclonal antibody W6/32, which specifically recognises a monomorphic epitope on all HLA class I molecules that includes both the heavy chain and the β_2-microglobulin chain,[60] was investigated first in pure buffer. The hydrodynamic radius, R_h, of pure HLA A*03:01 was determined to be 3.47 ± 0.13 nm (Fig. 2a), which is consistent with the expected radius for a natively folded protein with a molecular weight of approximately 55 kDa (Fig. 2b). Upon addition of a 380-fold excess of antibody W6/32, a significant increase of the hydrodynamic radius to $R_h = 5.01 \pm 0.13$ nm was observed, indicating an interaction between both species. The hydrodynamic radius of 5.01 nm suggests that two antigens are bound per antibody,

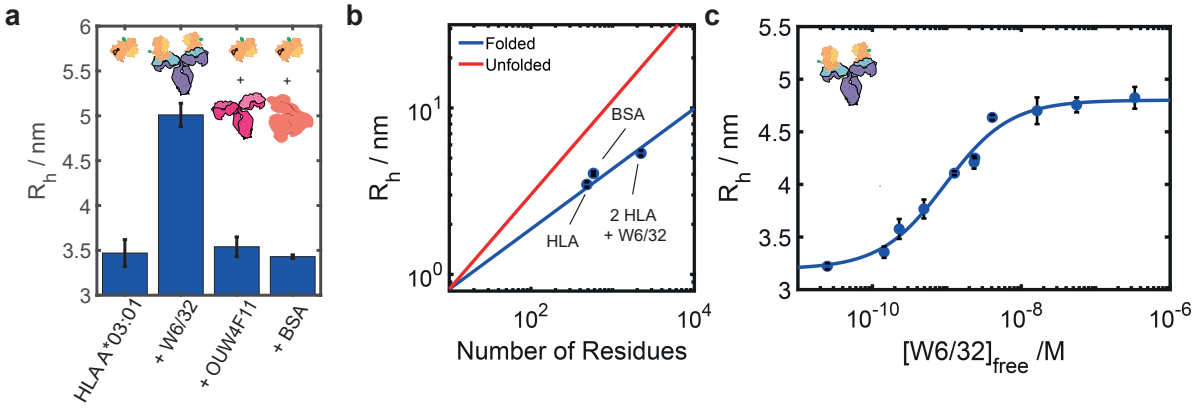

Figure 2: (**a**) Binding experiments of HLA A*03:01 using diffusional sizing. Bars show the average of triplicate measurements with the error bars representing the standard deviation. A significant change in hydrodynamic radius indicates binding of 5 nM HLA A*03:01 to 1.9 μM W6/32. In contrast, no binding can be observed between HLA and OUW4F11 or BSA. (**b**) Correlation of hydrodynamic radii with the number of residues.[61,62] The radii determined for HLA both free and bound to the antibody W6/32 agree well with the assumption of a folded protein. (**c**) Binding curve of 476 pM HLA A*03:01 with varying concentration of antibody W6/32. The blue points give the hydrodynamic radius of each equilibrated sample, averaged over the data of at least three replicates, and the blue curve is the best fit (see Materials and Methods for details). From the fit, the dissociation constant K_d = 0.7 [0.3, 1.6] nM (95% confidence intervals given in square brackets) could be determined with a ratio of two antigens per antibody.

which is expected for a bivalent IgG antibody which has two binding sites, and is consistent with the expected size for a natively folded protein complex of 260 kDa (Fig. 2b). Negative control experiments, including alloantibody against fluorescently labelled BSA (Fig. S4a), OUW4F11 (an alloantibody specific to HLA B*08:01) against HLA A*03:01 (Fig. 2a), and human IgG binding against HLA A*03:01 (Fig. S4b), did not show an increase in R_h and, therefore, confirmed that the complex formation is based only on specific interactions.

We next explored whether this approach could yield both the dissociation constant of the interaction and the concentration of the antibody. To this effect, an equilibrium binding curve for the interaction between HLA A*03:01 and antibody W6/32 was measured, yielding a $K_d = 0.7$ [0.3, 1.6] nM (95% confidence intervals from Bayesian inference given in square brackets) and consistent with a binding ratio of 1 to 2, i.e. a stoichiometry of 2 antigens per antibody (Fig. 2c and Fig. S5). Both cooperative and non-cooperative binding of antibodies have previously been described.[63] Thus, cooperativity was tested by a Hill plot (Fig. S5),[64] yielding a Hill parameter $h = 1.01 \pm 0.15$. This shows that the binding of the HLA and the antibody is non-cooperative, ergo binding events occur independently.

Characterisation of Alloantibody-HLA Interactions in Human Serum

We next determined the applicability of MAAP for the absolute quantification and characterisation of alloantibodies in human serum. We assayed two well-characterised, human monoclonal antibodies, SN23OG6 and OUW4F11, which specifically recognise HLA A*02:01 and HLA B*08:01, respectively,[65] both in human serum of non-transfused, healthy donors, which did not contain HLA-specific antibodies, and in buffer (PBS). During data processing, we corrected for a weak autofluorescence background signal from both the diffused and undiffused measurement channels. Serum autofluorescence has been reported for human serum in the spectral region of interest (Fig. S2)[66] and is likely to arise from natural aromatic compounds including haem complexes, found in haemoglobin or bilirubin, which are stabilised by human serum albumin.[67]

As shown in Fig. 3, the hydrodynamic radii of pure HLA obtained in human serum ($R_h = 3.27 \pm 0.11$ nm for HLA A*02:01 and $R_h = 3.22 \pm 0.19$ nm for HLA B*08:01), were found to be consistent with theoretical values for natively folded 50 kDa proteins, as

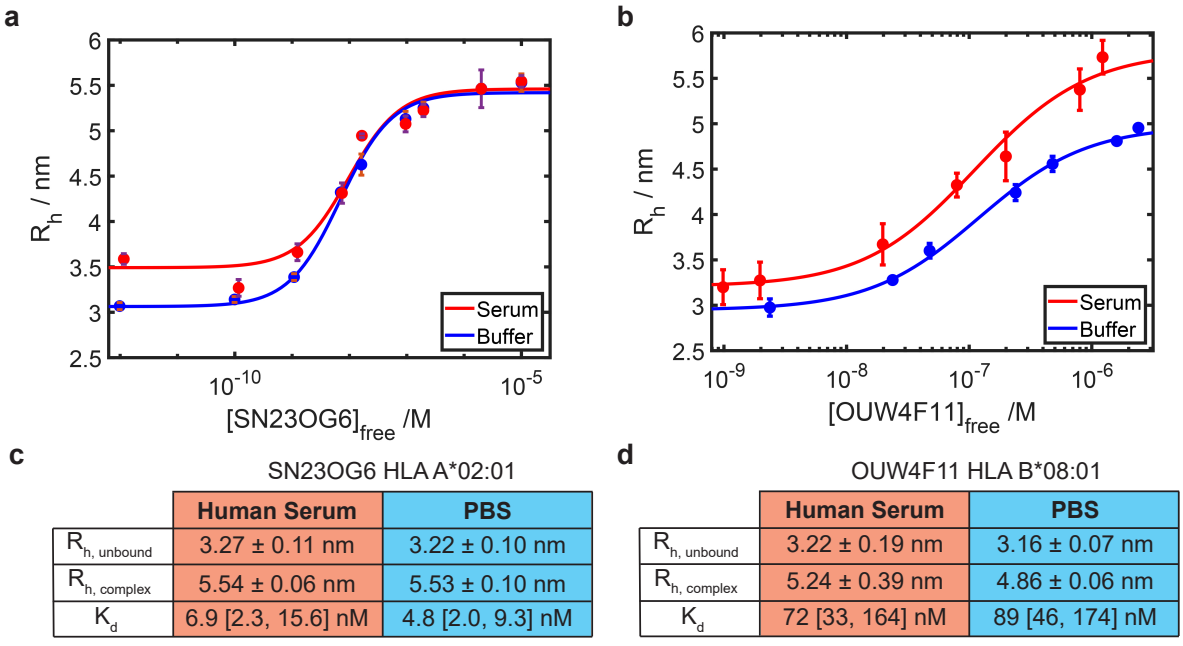

	Human Serum	PBS
$R_{h,\ unbound}$	3.27 ± 0.11 nm	3.22 ± 0.10 nm
$R_{h,\ complex}$	5.54 ± 0.06 nm	5.53 ± 0.10 nm
K_d	6.9 [2.3, 15.6] nM	4.8 [2.0, 9.3] nM

	Human Serum	PBS
$R_{h,\ unbound}$	3.22 ± 0.19 nm	3.16 ± 0.07 nm
$R_{h,\ complex}$	5.24 ± 0.39 nm	4.86 ± 0.06 nm
K_d	72 [33, 164] nM	89 [46, 174] nM

Figure 3: (**a**) Binding curve of 5 nM HLA A*02:01 against antibody SN23OG6 in human serum (red) and PBS (blue). The measurements in serum and PBS are in good agreement with each other, yielding K_d values of 6.9 [2.3, 15.6] nM and 4.8 [2.0, 9.3] nM, respectively, with a binding ratio of 2 antigens per antibody. (**b**) Binding curve of 1.2 nM HLA B*08:01 against antibody OUW4F11 in human serum (red) and PBS (blue). Again, the K_d = 72.1 [32.9, 163.6] nM in serum and K_d = 89.1 [45.7, 173.8] nM in PBS with a binding ratio of 1 to 2 are in good agreement. Summary of the hydrodynamic radii for the fully unbound antigens and of the dissociation constants in human serum in comparison to their values in pure buffer, demonstrating consistent values under both conditions (**c**) for SN23OG6 against HLA A*02:01 and (**d**) for OUW4F11 against HLA B*08:01 (Fig. S6).

well as with the radii obtained in buffer (R_h = 3.22 ± 0.10 nm for HLA A*02:01 and R_h = 3.16 ± 0.07 nm for HLA B*08:01), demonstrating the applicability of MDS for measurements in human serum. Importantly, this also shows that measurement in human serum did not affect the antigen size compared to the measurements in PBS, suggesting presence of serum proteins in the sample do not affect the measurements.

Assessment of these two alloantibody-HLA interactions showed that microfluidic affinity measurements were independent of the buffer conditions used (Fig. 3a-b). The interaction between SN23OG6 against HLA A*02:01 yielded a dissociation constant of K_d = 6.9 [2.3, 15.6] nM in human serum and was in good agreement with K_d = 4.8 [2.0, 9.3] nM in buffer. Similarly, for the interaction of antibody OUW4F11 against HLA B*08:01, the K_d = 72.1 [32.9, 163.6] nM in human serum which was consistent with K_d = 89.1 [45.7, 173.8] nM determined in buffer. The different saturation levels between the two media conditions are within the CI and most likely reflect minor conformational variations between individual antigens. Analysis of the above alloantibody-HLA interactions in PBS using biolayer interferometry showed dissociation constants in a similar order ($K_d = 5.6 \pm 0.03$ nM for SN23OG6 vs. HLA A*02:01 and $K_d = 314.9 \pm 0.04$ nM for OUW4F11 against HLA B*08:01, Fig. S7).

Taken together, these data show the general feasibility of binding measurements in complex media with diffusional sizing, with hydrodynamic radii, affinities and stoichiometric parameters consistent with theoretical values and measurements under unperturbed (buffer) conditions. The results show that the binding of HLA, even in the background of a complex solution such as human serum, is solely based on specific interactions and not influenced by any other protein species that are abundant in human serum including soluble HLA and β_2- microglobulin.[68] More generally, these results suggest that MAAP can be used as a platform for molecular level characterisation of protein-protein interactions in complex mixtures such as body fluids.

Quantification of Alloantibody-HLA Interactions in Human Serum

Simultaneous determination of both affinity and alloantibody concentration in patient samples is a key advantage of our method compared to traditional assays. Through varying the concentration of both labelled (i.e. HLA) and unlabelled (i.e. alloantibodies in human serum) species, it becomes possible to properly constrain the probability distribution of unknown parameters for the interaction (K_d and antibody concentration) as demonstrated by Bayesian inference analysis (see Methods). This is the key advance of this technology as compared to similar assays previously used to describe affinity measurements. In order to verify the robustness of our method for determination of absolute parameters for reactive antibody species, we spiked human serum from non-sensitised

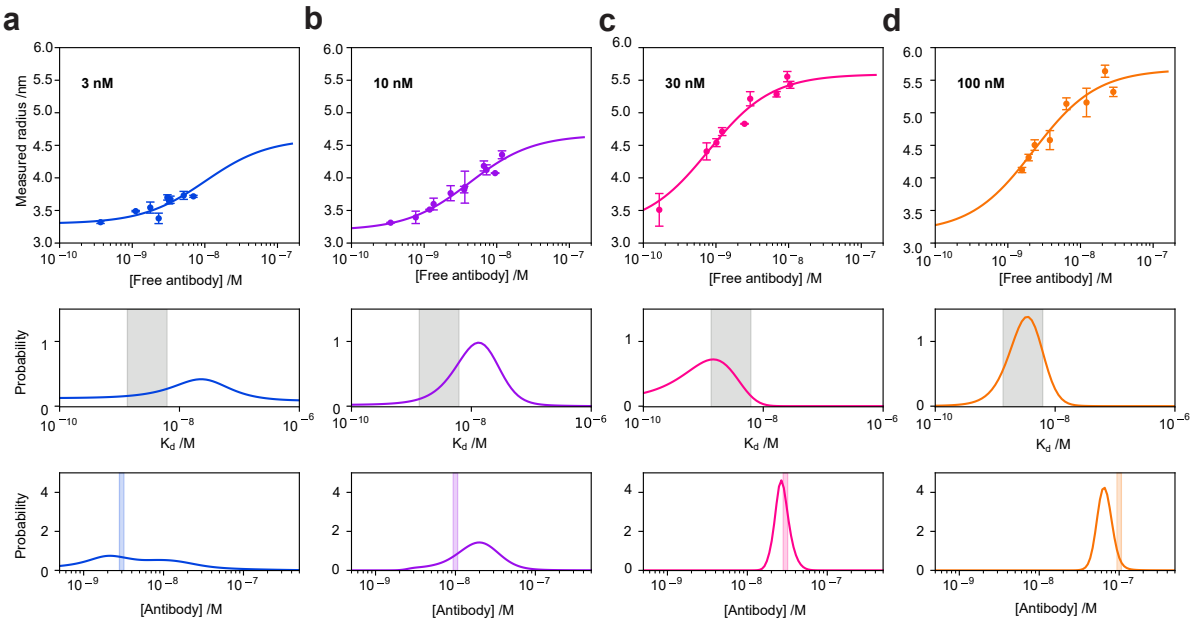

Figure 4: Binding curves (top row) of measured data and best fits for the interaction of A*02:01 against SN23OG6 antibody spiked into alloantibody-negative human serum at concentrations (**a**) 3 nM, (**b**) 10 nM, (**c**) 30 nM and (**d**) 100 nM. The analyses were performed assuming that both the antibody concentration and affinity were unknown. In all four cases, the Kd determined through MAAP is consistent with the K_d obtained through fitting all datasets combined, using the known concentrations; probability distributions over K_d resulting from each dataset are shown alongside the 95% confidence intervals (grey) obtained by considering all data (middle row). The experimentally determined antibody concentrations are also in good agreement with the known concentration (bottom row), assuming a binding stoichiometry of 1:2 antibody:HLA. Probability distributions over antibody concentration are overlaid with the experimental error range (shaded region) for the known antibody concentrations.

donors with HLA-specific monoclonal antibody in a blinded manner, i.e. the final antibody serum concentrations were not revealed to the person performing the analysis. The interaction investigated was that between alloantibody SN23OG6 and HLA A*02:01 (Fig. 4). For antibody concentrations of 1 nM or above, we were able to determine both the dissociation constant, K_d, and the concentration of specific antibody, $[\mathrm{Ab}]_{\mathrm{spec}}$, in doped serum simultaneously. The K_d determined in all cases was consistent with previous results for the interaction (as shown above), and the concentration determined was in good agreement with the expected antibody concentration (Fig. 4). This was the case even when the concentration of antibody binding sites was approximately equal to the dissociation constant, K_d (Fig. 4a), demonstrating that our method enables accurate determination of antibody concentrations around the K_d.

Quantification of Alloantibody-HLA Interactions in Patient Sera

We next investigated the ability of our immunoassay to quantify HLA-specific antibodies in the serum of a kidney transplant patient. The patient became sensitised after

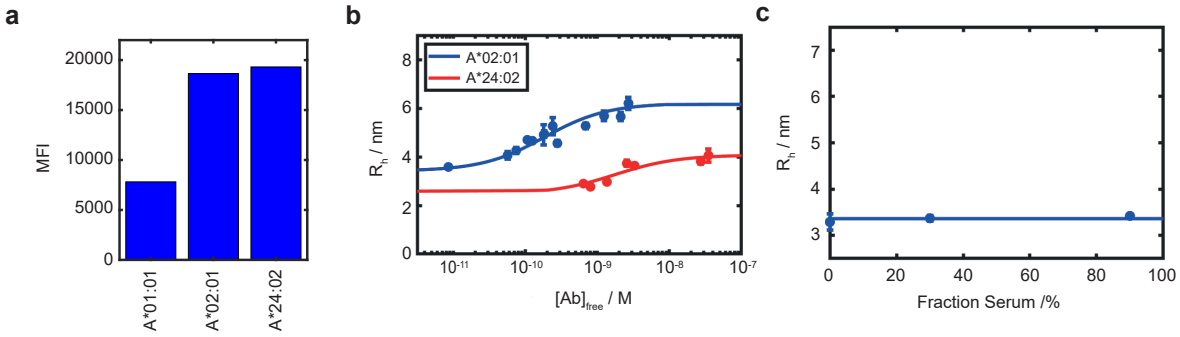

Figure 5: Quantification of reactivity against different HLA variants in serum from a transplant patient. (**a**) Antibody binding profile as detected on Luminex Single antigen beads for HLA A*01:01, HLA A*02:01 and HLA A*24:02 (MFI: Mean Fluorescence Intensity). (**b**) Binding Curves for the interaction of alloantibodies in patient serum against HLA A*02:01 and A*24:02, relating the hydrodynamic radius, R_h, to the measured concentration of antibody. The individual data points represent the measured data, the solid line the fit. The error bars report the standard deviation for triplicate measurements. For HLA A*02:01 isoform, an antibody concentration $[\text{Ab}]_{\text{spec}} = 3.0[1.2, 5.8]$ nM and a dissociation constant $K_d = 0.13\,[-,\ 1.38]$ nM were determined. For HLA A*24:02 isoform, we determined the $K_d = 1.3\,[0.2,\ 9.7]$ nM and $[\text{Ab}]_{\text{spec}}19.3 = [10.8, 49.3]$ nM. (**c**) Titration Curve for the same patient serum against 1 nM HLA A*01:01, with different serum concentration. As can be seen, no binding is detected.

transplantation with a kidney allograft expressing the HLA A*24:02 alloantigen. Analysis of post-transplant sera using the Luminex single antigen bead assay (standard of care in the clinical setting) showed a complex profile with reactivity against the priming antigen (A*24:02), cross-reactivity against A*02:01 (A*24:02 and A*02:01 are part of a common serological cross-reactive HLA epitope group), and additional reactivity to A*01:01 (no known serological cross-reactivity to A*24:02 and A*02:01[69]). The mean fluorescence intensity values detected by Luminex were 19314 a.u. for A*24:02, 18653 a.u. for A*02:01 and 7810 a.u. for A*01:01 (Fig. 5a). As shown in Fig. 5b, for the serum interaction with HLA A*02:01, we determined a concentration of alloantibody of $[\text{Ab}]_{\text{spec}} = 3.0$ [1.2, 5.8] nM and a $K_d = 0.13$ [0.01, 1.38] nM, assuming a binding ratio of 1 to 2. Similarly, for the same patient serum interaction with A*24:02, we detected an antibody concentration of, $[\text{Ab}]_{\text{spec}} = 19.3$ [10.8, 49.3] nM and an affinity of $K_d = 1.3\,[0.2,\ 9.7]$ nM. Thus, we were able to deconvolute the fundamental biophysical properties (affinity and alloantibody concentration) of the humoral response in a complex patient serum and differentiate the reactivity against the priming alloantigen (A*24:02) and a cross-reactive alloantigen (A*02:01) demonstrating higher antibody concentration against the priming HLA. Importantly, we could not demonstrate an interaction between HLA A*01:01 and the patient serum, despite a relatively high MFI value of 7810 a.u. from the Luminex assay. Output from the Luminex assay is avidity driven and is considered semi-quantitative;[40] accordingly, an interaction at the MFI level showed here against A*01:01 would be considered as clinically significant (e.g. potential donors expressing A*01:01 would typically be ex-

cluded for a patient with similar levels of reactivity on Luminex). Taken together, the data highlight the potential of MAAP to provide immunologically relevant information not attainable by currently available techniques and to quantify antibody interactions against proteins that share highly similar structures, such as the HLA system.

Conclusion

In this study, we have shown for the first time that, using an in-solution technique, namely Microfluidic Antibody Affinity Profiling (MAAP), it is possible to determine both dissociation constant, K_d, and the absolute concentration of antibody binding sites, which may manifest as the binding stoichiometry in samples of known antibody concentrations, or the total antibody concentration in unknown samples, through a measurement of effective hydrodynamic radii at different antibody and antigen concentrations. By applying this platform to measure immunologically-relevant interactions between specific antibodies and HLA, we were able to determine quantitative biophysical parameters describing the binding event fully, even in such a complex medium as human serum. The determined dissociation constants range between 10^{-10} M and 10^{-8} M and are consistent with previous work.[70] However, our in-solution approach avoids the commonly reported disadvantages of surface-based assays and does not require serum preparation to reduce non-specific binding thereby enabling determination of fundamental parameters of humoral responses under physiological conditions.

Our results suggest applicability of this method in a wide range of investigations aiming to understand the role of both abundance and dissociation constants implicated in clinically relevant immune responses. For example, further insights into the complex process of graft rejection may be obtained through investigations of the correlation of the concentration and affinity to the occurrence of an immune response. Finally, our results indicate that the platform can be of general use for diagnostics beyond histocompatibility testing, such as immuno-profiling in auto-immunity, in infectious diseases, and to monitor immune responses after vaccination, or the detection of biomarker levels for various diseases in human serum.[15,16]

Acknowledgement

The research presented in this manuscript has received funding from the European Research Council under the European Union's Seventh Framework Programme (FP7/2007-2013) through the ERC grant PhysProt (agreement no. 337969) and under European Union's Horizon 2020 research and innovation programme (ETN grant 674979-NANOTRANS).

We gratefully acknowledge financial support from the Engineering and Physical Sciences Research Council (EPSRC) and Frances and Augustus Newman Foundation. We also acknowledge funding from the NIHR Blood and Transplant Research Unit in Organ Donation and Transplantation at the University of Cambridge and from an NIHR Fellowship (PDF-2016-09-065, VK). The views expressed are those of the authors and not necessarily those of the National Health Service, the National Institute for Health Research, the Department of Health, or National Health Service Blood and Transplant. We are grateful to Dr Arend Mulder and Prof Frans Claas for provision of monoclonal antibodies SN23OG6 and OUW4F11. Ethical Approval for work involving human serum was granted from NRES Committee North-East York, IRAS number 167211.

Conflict of Interest

S.R.A.D. is an employee of Fluidic Analytics, which is developing and commercializing microfluidic diffusional sizing instrumentation including the Fluidity One-W Serum used here. V.K. is a consultant with Fluidic Analytics Ltd. T.P.J.K. is a member of the board of directors of Fluidic Analytics Ltd.

Supporting Information

The following files are available free of charge online.

References

1. King, N. P. *et al.* Computational Design of Self-Assembling Protein Nanomaterials with Atomic Level Accuracy. *Science* **336,** 1171–1174 (2012).
2. Edwardson, T. G. W., Mori, T. & Hilvert, D. Rational Engineering of a Designed Protein Cage for siRNA Delivery. *J. Am. Chem. Soc.* **140,** 10439–10442 (2018).
3. Esposito, L. *et al.* Crystal Structure of the Alcohol Dehydrogenase from the Hyperthermophilic Archaeon Sulfolobus solfataricus at 1.85A Resolution. *J. Mol. Biol.* **318,** 463–477 (2002).
4. Knowles, T. P. J. *et al.* An Analytical Solution to the Kinetics of Breakable Filament Assembly. *Science* **326,** 1533–1537 (2009).
5. Knowles, T. P. J., Vendruscolo, M. & Dobson, C. M. The amyloid state and its association with protein misfolding diseases. *Nat. Rev. Mol. Cell Biol.* **15,** 384 (2014).
6. Hartl, F. U. Protein Misfolding Diseases. *Ann. Rev. Biochem.* **86,** 21–26 (2017).
7. Goldberg, R. J. A Theory of Antibody—Antigen Reactions. I. Theory for Reactions of Multivalent Antigen with Bivalent and Univalent Antibody2. *J. Am. Chem. Soc.* **74,** 5715–5725 (1952).
8. Goldberg, R. J. A Theory of Antibody—Antigen Reactions. II. Theory for Reactions of Multivalent Antigen with Multivalent Antibody. *J. Am. Chem. Soc.* **75,** 3127–3131 (1953).
9. Patrick, G. L. *An Introduction to Medicinal Chemistry* (Oxford University Press, Oxford, 2013).

10. Huxley, H. E. The Mechanism of Muscular Contraction. *Science* **164,** 1356 (1969).

11. Westermarck, J., Ivaska, J. & Corthals, G. L. Identification of Protein Interactions Involved in Cellular Signaling. *Mol. Cell. Proteom.* **12,** 1752 (2013).

12. Suwinski, R. *et al.* Blood serum proteins as biomarkers for prediction of survival, locoregional control and distant metastasis rate in radiotherapy and radio-chemotherapy for non-small cell lung cancer. *BMC Cancer* **19,** 427 (2019).

13. Srivastava, A. & Creek, D. J. Discovery and Validation of Clinical Biomarkers of Cancer: A Review Combining Metabolomics and Proteomics. *Proteomics* **19,** 1700448 (2019).

14. Ivancic, M. M. *et al.* Conserved serum protein biomarkers associated with growing early colorectal adenomas. *Proc. Nat. Acad. Sci.* **116,** 8471 (2019).

15. Núñez, C. Blood-based protein biomarkers in breast cancer. *Clinica Chimica Acta* **490,** 113–127 (2019).

16. Shi, L. *et al.* A Decade of Blood Biomarkers for Alzheimer's Disease Research: An Evolving Field, Improving Study Designs, and the Challenge of Replication. *J. Alzheimers Dis.* **62,** 1181 (2018).

17. Chen-Plotkin, A. S. *et al.* Finding useful biomarkers for Parkinson's disease. *Sci. Transl. Med.* **10,** 454 (2018).

18. Huang, T. *et al.* A Network Analysis of Biomarkers for Type 2 Diabetes. *Diabetes* **68,** 281 (2019).

19. Killoran, A. & Biglan, K. Biomarkers for Huntington's disease: A brief overview. *Journal of Rare Diseases Research and Treatment* **1,** 46–50 (2016).

20. Sperling, R. A. *et al.* Toward defining the preclinical stages of Alzheimer's disease: Recommendations from the National Institute on Aging-Alzheimer's Association workgroups on diagnostic guidelines for Alzheimer's disease. *Alzheimers Dement.* **7,** 280–292 (2011).

21. Thambisetty, M. *et al.* Plasma Biomarkers of Brain Atrophy in Alzheimer's Disease. *PLOS ONE* **6,** e28527 (2011).

22. Hakki, Y., Cakmak, M., Ceydilek, B., Demir, C. & Aktas, A. Role of interlekin-35 as a biomarker in patients with newly diagnosed Hashimoto's thyroiditis. *Endocr. Regul.* **50,** 55–61 (2016).

23. Montgomery, R. A., Tatapudi, V. S., Leffell, M. S. & Zachary, A. A. HLA in transplantation. *Nat. Rev. Nephrol.* **14,** 558–570 (2018).

24. Loupy, A. & Lefaucheur, C. Antibody-Mediated Rejection of Solid-Organ Allografts. *N. Engl. J. Med.* **379,** 1150–1160 (2018).

25. Timofeeva, O. A. Donor-Specific HLA Antibodies as Biomarkers of Transplant Rejection. *Clin. Lab Med.* **39,** 45–60 (2019).

26. Terasaki, P. I. & Cai, J. Human leukocyte antigen antibodies and chronic rejection: from association to causation. *Transplantation* **86,** 377–83 (2008).

27. Taylor, C. J., Kosmoliaptsis, V., Summers, D. M. & Bradley, J. A. Back to the future: application of contemporary technology to long-standing questions about the clinical relevance of human leukocyte antigen-specific alloantibodies in renal transplantation. *Hum. Immunol.* **70,** 563–8 (2009).

28. Engvall, E. & Perlmann, P. Enzyme-Linked Immunosorbent Assay, Elisa: III. Quantitation of Specific Antibodies by Enzyme-Labeled Anti-Immunoglobulin in Antigen-Coated Tubes. *J. Immunol.* **109,** 129–135 (1972).

29. Ueda, H. *et al.* Open sandwich ELISA: A novel immunoassay based on the interchain interaction of antibody variable region. *Nat. Biotechnol.* **14,** 1714–1718 (1996).

30. Sakamoto, S. *et al.* Enzyme-linked immunosorbent assay for the quantitative/qualitative analysis of plant secondary metabolites. *J. Nat. Med.* **72,** 32–42 (2018).

31. Carson, R. T. & Vignali, D. A. A. Simultaneous quantitation of 15 cytokines using a multiplexed flow cytometric assay. *J. Immunol. Met.* **227,** 41–52 (1999).

32. Fulton, R. J., McDade, R. L., Smith, P. L., Kienker, L. J. & Kettman John R., J. Advanced multiplexed analysis with the FlowMetrixTM system. *Clin. Chem.* **43,** 1749–1756 (1997).

33. Joos, T. O., Stoll, D. & Templin, M. F. Miniaturised multiplexed immunoassays. *Curr. Opin. Chem. Biol.* **6,** 76–80 (2002).

34. Pei, R., Lee, J. H., Shih, N. J., Chen, M. & Terasaki, P. I. Single human leukocyte antigen flow cytometry beads for accurate identification of human leukocyte antigen antibody specificities. *Transplantation* **75,** 43–9 (2003).

35. Lyon, L. A., Musick, M. D. & Natan, M. J. Colloidal Au-Enhanced Surface Plasmon Resonance Immunosensing. *Anal. Chem.* **70,** 5177–5183 (1998).

36. Mullett, W. M., Lai, E. P. C. & Yeung, J. M. Surface Plasmon Resonance-Based Immunoassays. *Methods* **22,** 77–91 (2000).

37. Simon, A. & Macdonald, J. in *Wilson and Walker's Techniques of Biochemistry and Molecular Biology* (eds Hoffmann, A. & Clokie, S.) 500–534 (Cambridge University Press, Cambridge, 2018).

38. Tait, B. D. Detection of HLA Antibodies in Organ Transplant Recipients – Triumphs and Challenges of the Solid Phase Bead Assay. *Front. Immunol.* **7** (2016).

39. Reed, E. F. *et al.* Comprehensive Assessment and Standardization of Solid Phase Multiplex-Bead Arrays for the Detection of Antibodies to HLA. *Am. J. Transplant.* **13,** 1859–1870 (2013).

40. Gebel, H. M. & Bray, R. A. HLA antibody detection with solid phase assays: great expectations or expectations too great? *Am. J. Transplant.* **14,** 1964–75 (2014).

41. Henry, S. M., Sutlief, E., Salas-Solano, O. & Valliere-Douglass, J. ELISA reagent coverage evaluation by affinity purification tandem mass spectrometry. *mAbs* **9,** 1065–1075 (2017).

42. Butch, A. W. Dilution Protocols for Detection of Hook Effects/Prozone Phenomenon. *Clin. Chem.* **46,** 1719–1720 (2000).

43. Kosmoliaptsis, V., O'Rourke, C., Bradley, J. A. & Taylor, C. J. Improved Luminex-based human leukocyte antigen-specific antibody screening using dithiothreitol-treated sera. *Hum. Immunol.* **71,** 45–9 (2010).

44. Schnaidt, M. *et al.* HLA antibody specification using single-antigen beads–a technical solution for the prozone effect. *Transplantation* **92,** 510–5 (2011).

45. Anderson, N. L. & Anderson, N. G. The Human Plasma Proteome: History, Character, and Diagnostic Prospects. *Mol. Cell. Proteom.* **1,** 845–867 (2002).

46. Redman, E. A., Batz, N. G., Mellors, J. S. & Ramsey, J. M. Integrated Microfluidic Capillary Electrophoresis-Electrospray Ionization Devices with Online MS Detection for the Separation and Characterization of Intact Monoclonal Antibody Variants. *Anal. Chem.* **87,** 2264–2272 (2015).

47. Fan, R. *et al.* Integrated barcode chips for rapid, multiplexed analysis of proteins in microliter quantities of blood. *Nat. Biotechnol.* **26,** 1373 (2008).

48. Horton, R. *et al.* Gene map of the extended human MHC. *Nat. Rev. Genet.* **5,** 889–899 (2004).

49. Valenzuela, N. M. & Reed, E. F. Antibody-mediated rejection across solid organ transplants: manifestations, mechanisms, and therapies. *J. Clin. Invest.* **127,** 2492–2504 (2017).

50. Tait, B. D. *et al.* Consensus guidelines on the testing and clinical management issues associated with HLA and non-HLA antibodies in transplantation. *Transplantation* **95,** 19–47 (2013).

51. Gosset, C. *et al.* Circulating donor-specific anti-HLA antibodies are a major factor in premature and accelerated allograft fibrosis. *Kidney. Int.* **92,** 729–742 (2017).

52. Gebel, H. M., Bray, R. A. & Nickerson, P. Pre-transplant assessment of donor-reactive, HLA-specific antibodies in renal transplantation: contraindication vs. risk. *Am. J. Transplant.* **3,** 1488–500 (2003).

53. Tambur, A. R. *et al.* Sensitization in transplantation: Assessment of risk (STAR) 2019 Working Group Meeting Report. *Am. J. Transplant.* (2020).

54. Tambur, A. R. *et al.* Assessing Antibody Strength: Comparison of MFI, C1q, and Titer Information. *Am. J. Transplant.* **15,** 2421–30 (2015).

55. Konvalinka, A. & Tinckam, K. Utility of HLA Antibody Testing in Kidney Transplantation. *J. Am. Soc. Nephrol.* **26,** 1489–502 (2015).

56. Müller, T. *et al.* Particle-Based Monte-Carlo Simulations of Steady-State Mass Transport at Intermediate Péclet Numbers. *Int. J. Nonlin. Sci.* **17,** 175 (2016).

57. Arosio, P. *et al.* Microfluidic Diffusion Analysis of the Sizes and Interactions of Proteins under Native Solution Conditions. *ACS Nano* **10,** 333–341 (2016).

58. Linse, S. *et al.* Kinetic fingerprint of antibody therapies predicts outcomes of Alzheimer clinical trials. *bioRxiv,* 815308 (2019).

59. Scheidt, T. *et al.* Secondary nucleation and elongation occur at different sites on Alzheimers amyloid-β aggregates. *Sci. Adv.* **5,** eaau3112 (2019).

60. Kievits, F. & Ivanyi, P. Monomorphic anti-HLA monoclonal antibody (W6/32) recognizes polymorphic H-2 heavy-chain determinants exposed by association with bovine or human but not murine ß2-microglobulin. *Hum. Immunol.* **20,** 115–126 (1987).

61. Wilkins, D. K. *et al.* Hydrodynamic Radii of Native and Denatured Proteins Measured by Pulse Field Gradient NMR Techniques. *Biochemistry* **38,** 16424–16431 (1999).

62. Zhang, Y. *et al.* On-chip measurements of protein unfolding from direct observations of micron-scale diffusion. *Chem. Sci.* **9,** 3503–3507 (2018).

63. Yang, D., Kroe-Barrett, R., Singh, S., Roberts, C. J. & Laue, T. M. IgG cooperativity - Is there allostery? Implications for antibody functions and therapeutic antibody development. *mAbs* **9,** 1231–1252 (2017).

64. Hill, A. V. PROCEEDINGS OF THE PHYSIOLOGICAL SOCIETY: January 22, 1910. *J. Physiol. (Lond.)* **40,** i–vii (1910).

65. Mulder, A., Kardol, M., Regan, J., Buelow, R. & Claas, F. Reactivity of twenty-two cytotoxic human monoclonal HLA antibodies towards soluble HLA class I in an enzyme-linked immunosorbent assay (PRA-STAT). *Hum. Immunol.* **56,** 106–13 (1997).

66. Wolfbeis, O. S. & Leiner, M. Mapping of the total fluorescence of human blood serum as a new method for its characterization. *Anal. Chem. Acta* **167,** 203–215 (1985).

67. Blauer, G. & Wagniere, G. Conformation of bilirubin and biliverdin in their complexes with serum albumin. *J. Am. Chem. Soc.* **97,** 1949–1954 (1975).

68. DeVito-Haynes, L. D. *et al.* Soluble donor HLA class I and beta 2m-free heavy chain in serum of lung transplant recipients: steady-state levels and increases in patients with recurrent CMV infection, acute rejection episodes, and poor outcome. *Hum. Immunol.* **61,** 1370–82 (2000).

69. Rodey, G. E., Revels, K. & Fuller, T. C. Epitope specificity of HLA class I alloantibodies: II. Stability of cross-reactive group antibody patterns over extended time periods. *Transplantation* **63,** 885–93 (1997).

70. Visentin, J. *et al.* Measuring anti-HLA antibody active concentration and affinity by surface plasmon resonance: Comparison with the luminex single antigen flow beads and T-cell flow cytometry crossmatch results. *Mol. Immunol.* **108,** 34–44 (2019).

71. Yates, E. V. *et al.* Latent analysis of unmodified biomolecules and their complexes in solution with attomole detection sensitivity. *Nat. Chem.* **7,** 802 (2015).

72. Mallon, D. H. *et al.* Predicting Humoral Alloimmunity from Differences in Donor and Recipient HLA Surface Electrostatic Potential. *The Journal of Immunology* **201,** 3780 (2018).

Microfluidic Antibody Affinity Profiling for In-Solution Characterisation of Alloantibody - HLA Interactions in Human Serum

Matthias M. Schneider[1,*], Tom Scheidt[1,*], Ashley J. Priddey[2,*], Catherine K. Xu[1,*], Mengsha Hu[1,*], Sean R. A. Devenish[3], Georg Meisl[1], Christopher M. Dobson[1,†], Vasilis Kosmoliaptsis[1,4,5,+], Tuomas P. J. Knowles[1,6,+]

[1] Centre for Misfolding Diseases, Department of Chemistry, University of Cambridge, Lensfield Road, Cambridge CB2 1EW, United Kingdom
[2]Department of Surgery, University of Cambridge, Addenbrooke's Hospital, Hills Road, Cambridge CB2 0QQ, UK
[3]Fluidic Analytics, Unit A, The Paddocks Business Centre, Cherry Hinton Rd, Cambridge CB1 8DH, UK
[4] NIHR Blood and Transplant Research Unit in Organ Donation and Transplantation, University of Cambridge, Hills Road, Cambridge CB2 0QQ, UK
[5] NIHR Cambridge Biomedical Research Centre, Hills Road, Cambridge CB2 0QQ, UK
[6] Cavendish Laboratory, Department of Physics, University of Cambridge, JJ Thomson Ave, Cambridge CB3 0HE, UK
[*] contributed equally
[†] Passed away September 2019
[+] corresponding to vk256@cam.ac.uk and tpjk2@cam.ac.uk

Supplementary Information

Materials and Methods

Materials

HLA monomers were obtained through the NIH Tetramer Core Facility in Emory, Atlanta, US, in PBS. PBS and Alexa Fluor 647 was purchased from Thermo Fisher Scientific Inc., Waltham, US. Human IgG ab205198 was from Abcam, Cambridge, UK. All other chemicals were from Sigma Aldrich. All PBS was supplemented with NaN_3 (0.02 % (w/v)).

Plate reader experiments were performed on a Clariostar BMG Labtech, Ortenberg, DE instrument. Size exclusion chromatography was performed on a Superdex 200 increase 10/300 gL column (GE Healthcare, Chicago, US) on an AKTA Pure protein purification system (GE Healthcare, Chicago, US). All microfluidic experiments were performed on a Fluidity One-W Serum instrument(Fluidic Analytics, Cambridge, UK). The basic principle of MDS has been described before.[1] In brief, labelled protein and auxiliary buffer are introduced alongside one another at the beginning of an extended diffusion chamber. Due to the small channel size, laminar flow can be assumed, meaning that the particles can move into the buffer stream by diffusion only, whereby the rate depends on the size of the molecular complex (Fig. 1). At the end of the diffusion chamber, the stream is split and the fluorescence of both the diffused and the undiffused material is measured. From the ratio between the fluorescence in both chambers, the hydrodynamic radius, R_h, of the protein can be determined.

Determination of Autofluorescence in Human Serum

Human serum from non-sensitised volunteers (not containing HLA-specific antibodies) was supplemented with PBS and the fluorophore Alexa Fluor^{TM} 647 to yield fluorophore concentrations between 10 pM and 1 µM in serum. Similar dilutions of fluorophore in buffer were prepared for comparison. Subsequently, both absorption spectra (Fig. S2 a-b) and the emission spectra upon excitation at two wavelengths $\lambda_{ex,1}$ = 481 nm and $\lambda_{ex,2}$ = 632 nm (Fig. S2 c-d)were recorded on a plate reader.

Labelling of HLA with Alexa Fluor 647 fluorophore

To HLA (typically 1 nmol, 1 equiv.) in 0.1 M $NaHCO_3$ (pH = 8), Alexa Fluor 647 *N*-hydroxysuccinimide ester (in DMSO, 3 equiv.) was added. The reaction mixture was incubated for 1 h at ca. 20 °C, protected from light. The sample was purified by size exclusion chromatography with a flow rate of 0.5 mL/min and PBS as eluent buffer, to yield labelled HLA (typically around 0.8 nmol, DOL between 0.33 and 1.55).

MAAP measurements in PBS

Labelled HLA, together with a varying concentration of the antibody of interest, were added and diluted in PBS (supplemented with 0.02 % Tween-20). The samples were incubated at room temperature for approximately 30 minutes. Subsequently, the

size was determined by MDS. The same protocol was followed for negative controls with fluorescently labelled BSA.

Binding Experiments in Human Serum

All binding experiments in human serum were carried out using human serum from non-sensitised volunteers (not containng HLA-specific antibodies) or from a kidney transplant patient. For all binding experiments in human serum, HLA (typically at a total concentration of 5 nM) was incubated with a varying concentration of specific antibodies or serum fractions at room temperature for 30 minutes in human serum and measured by MAAP. When fitting the data, the background fluorescence intensity of both the diffused and the undiffused channel was subtracted from the sample values at the relevant serum concentration.

Bayesian Analysis

The dissociation constant, $K_d = \frac{[Ab][H]}{[AbH]}$, and where necessary the antibody binding site concentration, $[Ab]_0$, were determined through Bayesian inference. The hydrodynamic radii were measured based on the amount of protein that diffuses into the distal channel; in order to relate the measurements, we introduce the parameters ρ_f and ρ_b as the fractions of free and antibody-bound HLA, respectively, that diffuse into the distal channel. We can therefore express the fraction of HLA that diffuses into the distal channel, f_d, as:

$$f_d = \frac{([AbH]\rho_b + ([H]_0 - [AbH])\rho_f)}{[H]_0} \tag{1}$$

where $[AbH]$ denotes the equilibrium concentration of antibody-HLA complex, and $[H]_0$ the total HLA concentration. Considering mass-balance, we express $[AbH]$ as:

$$[AbH] = \frac{[Ab]_0 + [H]_0 + K_d - \sqrt{([Ab]_0 + [H]_0 + K_d)^2 - 4[Ab]_0[H]_0}}{2} \tag{2}$$

In the experiments where the total antibody concentration was unknown, we substitute $[Ab]_0$ for $\alpha[Ab]_{tot}$, where α is the fraction of serum used in the measurement, and $[Ab]_{tot}$ is the total concentration of antibody binding sites in the stock solution. Assuming a binding stoichiometry of 1:2 antibody:HLA, we therefore obtain the antibody concentration, $\frac{[Ab]_{tot}}{2}$. All confidence intervals used were 95% confidence intervals, corresponding to the standard derivation.

The priors used for ρ_f and ρ_b were flat in linear space, while flat priors in logarithmic space were used for K_d and antibody concentration, where applicable, where employed.

Luminex Single Antigen Beads

HLA-specific antibody reactivity in the patient serum was detected using LabScreen single antigen HLA class I detection beads (One Lambda, Canoga Park, CA), as previously described[2]. HLA single antigen bead-defined Ab reactivity was determined using a mean fluorescence intensity (MFI) cut-off threshold of 2000 (MFI cut-off level used

clinically in our center and elsewhere to define a positive alloantibody response to a given HLA).

Bio-Layer Interferometry

Monoclonal antibody affinity of binding to HLA was determined by bio-layer interferometry (BLI) using the Octet RED96 system (ForteBio, Fremont, California). Antibody was immobilised to anit-human IgG Fc kinetic biosensors. To determine the association phase, sensors were dipped into wells containing soluble, recombinant HLA in a 2-fold titration for 300 seconds so an equilibrium was reached. Next, sensors were placed into buffer alone-containing wells for further 1000 seconds to determine the dissociation phase. Affinity values (K_d) were calculated via steady-state analysis as the ratio of on- and off-rate constants ($\frac{k_{off}}{k_{on}}$. All experiments were carried out using standard kinetic buffer (PBS, 0.1% (w/v) bovine serum albumin, 0.02% Tween-20), at a temperature of 30°C and a constant plate shake speed of 1000 rpm.

Author Contribution

T.P.J.K., V.K., C.M.D., T.S., M.M.S. and A.J.P. designed the study. M.M.S., T.S., M.H., A.J.P. performed the experiments. A.J.P., S.R.A.D., V.K. and T.P.J.K. provided material. C.K.X., G.M., M.M.S., T.S., V.K. and T.P.J.K. analysed the data. M.M.S., T.S., C.K.X., G.M., V.K. and T.P.J.K. wrote the paper. All authors discussed the results and commented on the manuscript.

Supplementary Figures

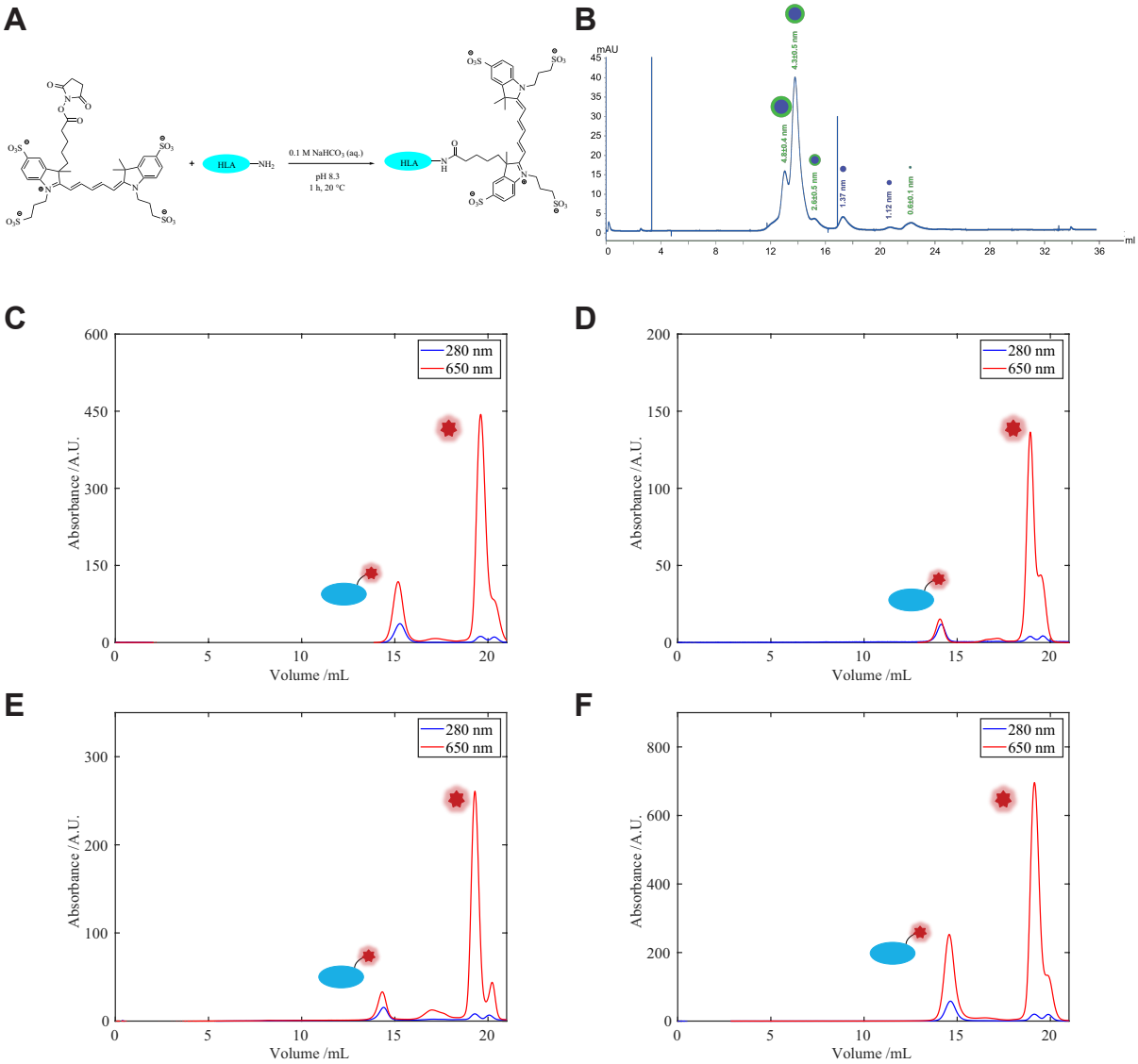

Figure 1: Strategy of Covalent labelling. (**A**) Reaction Mechanism of Linking an amine on a protein to Alexa Fluor 647, using an amide coupling. (**B**) Chromatogram for the purification of the streptavidin-HLA complex mixture. The blue circles represent different sizes of different streptavidin-HLA complexes; the green borders represent the Alexa Fluor^{TM} 488 label used in the mixture. (**C**) Chromatogram of the purification of Alexa Fluor 647 labelled HLA A*02:01 (degree of labelling (DOL) 1.22), (**D**) HLA A*03:01 (DOL 0.33), (**E**) HLA B*24:02 (DOL 0.96) and (**F**) HLA B*08:01 (DOL 1.55) after labelling, showing the elution of HLA (blue cartoon with red fluorophore) in one fraction around 14 mL and the excess fluorophore (red star) around 20 mL. The degree of labelling refers to the number of fluorophore per protein molecule.

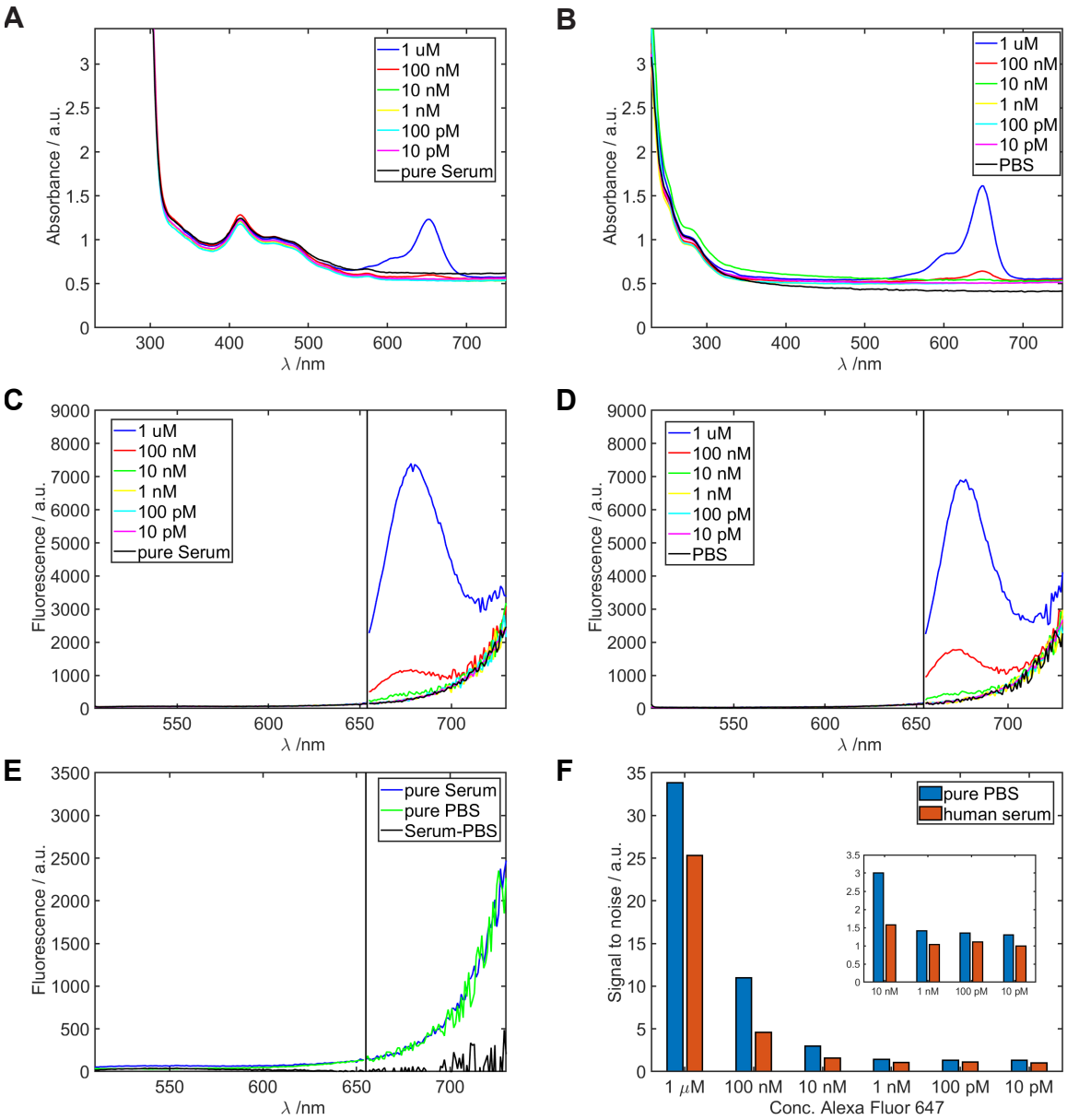

Figure 2: (**A**) Determination of the absorbance of varying concentration of Alexa Fluor 647 in human serum and (**B**) in buffer, showing no background absorbance around 663 nm in human serum. (**C**) Fluorescence emission of Alexa Fluor 647 in human serum and (**D**) in PBS. (**E**) Comparison of fluorescence emission of both human serum and PBS show no difference. (**F**) Signal to noise aspect ratios in human serum and in PBS. The signal-to-noise ratio is slightly reduced in human serum compared to PBS.

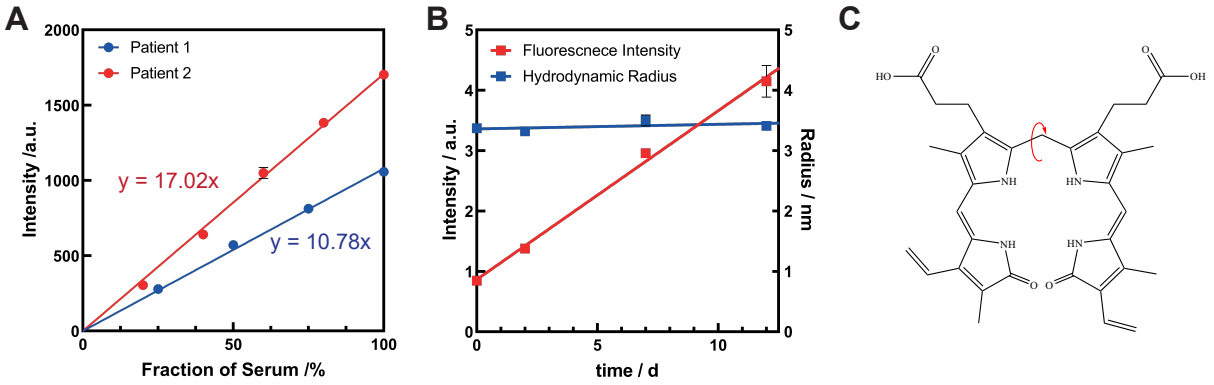

Figure 3: Fluorescence Emission of human serum, measured by microfluidic diffusional sizing. (**A**) Auto-fluorescence of human serum as a function of serum proportion for two different patients, showing that the behaviour varies among different individuals. (**B**) Increase in background intensity over time. As shown here, the background fluorescence increases linearly. The apparent hydrodynamic radius, R_h, remains unchanged. (**C**) Structure of bilirubin. The red arrow indicates the rotation which is hindered by complexation of bilirubin to HSA, a possible source of the fluorescence of the human serum.

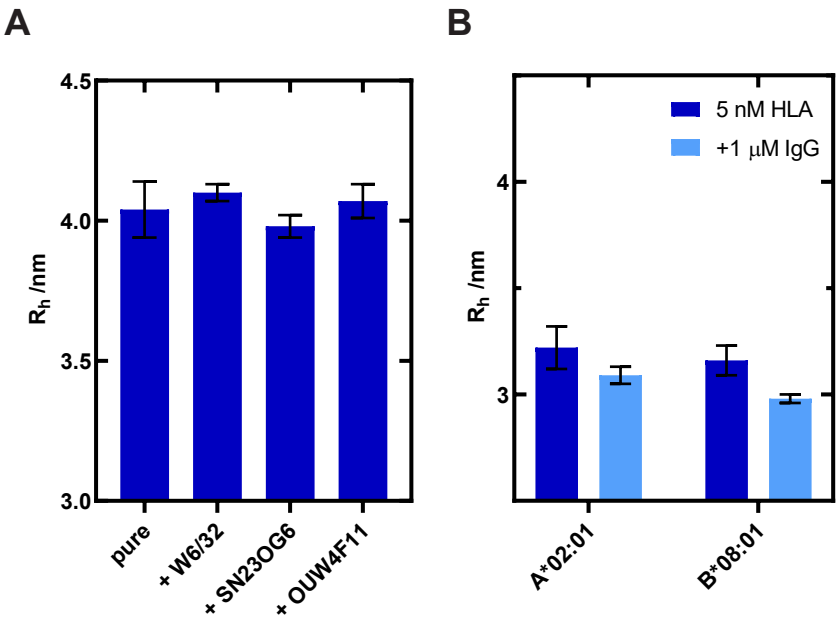

Figure 4: Control experiments testing specificity of binding interactions. (**A**) Comparison of hydrodynamic radii of Alexa Fluor 647 labelled BSA, both pure and after incubation with different antibodies. This demonstrates that the HLA specific antibodies do not recognise the fluorophore, thus, every binding interaction determined can be assumed to be specific. (**B**) Hydrodynamic radii of different HLA variants determined purely or after incubation with 200 nM IgG (ab205198), showing no size increase and, thus, suggesting selective interaction between these HLA variants and specific alloantibodies.

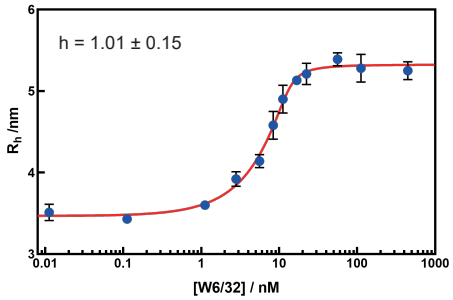

Figure 5: Binding curve of 25 nM HLA A*03:01 with varying concentration of antibody W6/32. The blue points are averages ofthree replicates, and the red line is the fit according to a Hill equation. From this data, the Hill coefficient $h = 1.01 \pm 0.15$ could be determined.

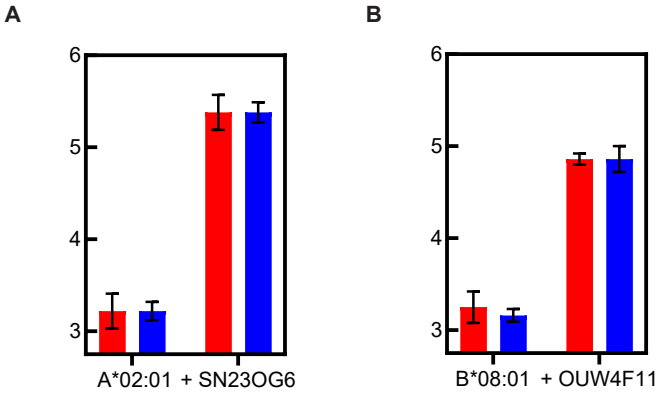

Figure 6: Hydroydnamic radii measured for (**A**) the interaction between 5 nM HLA A*02:01 and 1μM SN23OG6 and (**B**) the interaction between 5 nM HLA B*08:01 and 1μM OUW4F11, as shown in Fig. 3C-D. The data here, in comparison to the binding curves, were recorded on the same day, reducing batch-to-batch variability.

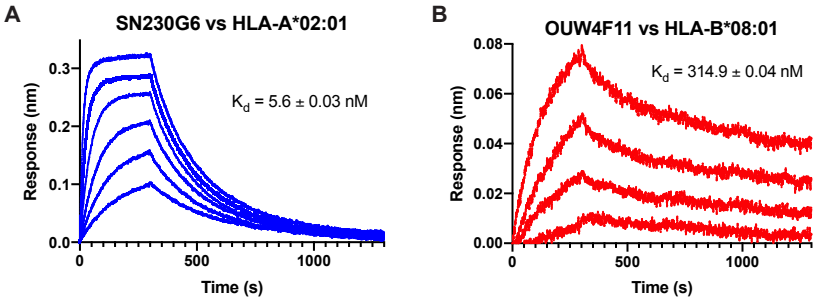

Figure 7: Biolayer Interferometry Curves for (**A**) the interaction between SN23OG6 vs. HLA A*02:01 ([HLA] = 100 nM, 50 nM, 25 nM, 12.5 nM, 6.25 nM and 3.125 nM) and (**B**) the interaction between OUW4F11 and HLA B*08:01 ([HLA] = 4000 nM, 2000 nM, 1000 nM, 500 nM).

References

1. Yates, E. V. *et al.* Latent analysis of unmodified biomolecules and their complexes in solution with attomole detection sensitivity. *Nat. Chem.* **7,** 802 (2015).

2. Mallon, D. H. *et al.* Predicting Humoral Alloimmunity from Differences in Donor and Recipient HLA Surface Electrostatic Potential. *The Journal of Immunology* **201,** 3780 (2018).

Received: 26 March 2019 | Revised: 11 July 2019 | Accepted: 9 August 2019

DOI: 10.1111/tan.13664

ORIGINAL ARTICLE

HLA Immune Response Genetics WILEY

Recombinant human monoclonal HLA antibodies of different IgG subclasses recognising the same epitope: Excellent tools to study differential effects of donor-specific antibodies

Cynthia S. M. Kramer[1] | Marry E. I. Franke-van Dijk[1] | Ashley J. Priddey[2] | Tamás Pongrácz[3] | Elena Gnudi[1] | Helena Car[1] | Gonca E. Karahan[1] | Els van Beelen[1] | Chalana C. C. Zilvold-van den Oever[4] | Hendrik J. Rademaker[4] | Noortje de Haan[3] | Manfred Wuhrer[3] | Vasilis Kosmoliaptsis[2] | Paul W. H. I. Parren[1,5] | Arend Mulder[1] | Dave L. Roelen[1] | Frans H. J. Claas[1] | Sebastiaan Heidt[1]

[1]Department of Immunohematology and Blood Transfusion, Leiden University Medical Center, Leiden, The Netherlands

[2]Department of Surgery, University of Cambridge, Cambridge, UK

[3]Center of Proteomics and Metabolomics, Leiden University Medical Center, Leiden, The Netherlands

[4]Genmab, Utrecht, The Netherlands

[5]Lava Therapeutics, 's-Hertogenbosch, The Netherlands

Correspondence
Cynthia Kramer, Department of Immunohematology and Blood Transfusion, Leiden University Medical Center, Albinusdreef 2, 2333 ZA, Leiden, The Netherlands.
Email: c.s.m.kramer@lumc.nl

In the field of transplantation, the humoural immune response against mismatched HLA antigens of the donor is associated with inferior graft survival, but not in every patient. Donor-specific HLA antibodies (DSA) of different immunoglobulin G (IgG) subclasses may have differential effects on the transplanted organ. Recombinant technology allows for the generation of IgG subclasses of a human monoclonal antibody (mAb), while retaining its epitope specificity. In order to enable studies on the biological function of IgG subclass HLA antibodies, we used recombinant technology to generate recombinant human HLA mAbs from established heterohybridomas. We generated all four IgG subclasses of a human HLA class I and class II mAb and showed that the different subclasses had a comparable affinity, normal human Fc glycosylation, and retained HLA epitope specificity. For both mAbs, the IgG1 and IgG3 isotypes were capable of binding complement component 3d (C3d) and efficient in complement-dependent cell lysis against their specific targets, while the IgG2 and IgG4 subclasses were not able to induce cytotoxicity. Considering the fact that the antibody-binding site and properties

Abbreviations: ADCC, antibody-dependent cell-mediated cytotoxicity; BCM, background corrected mean fluorescence intensity; CDC, complement-dependent cytotoxicity; C1q, complement component 1q; C3d, complement component 3d; DNA, deoxyribonucleic acid; DSA, donor-specific antibodies; ELISA, enzyme-linked immunosorbent assay; FcγR, Fc gamma receptors; HLA, human leukocyte antigen; IgG, immunoglobulin G; IgM, immunoglobulin M; IL, interleukin; LB, Lunia-Bertani; mAbs, monoclonal antibodies; MFI, mean fluorescence intensity; PBMCs, peripheral blood mononuclear cells; PBS, phosphate-buffered saline; PCR, polymerase chain reaction; PHA, phytohemagglutinin; RACE, rapid amplification cDNA ends; RNA, ribonucleic acid; SAB, single antigen beads; VH, heavy chain variable domain; VL, light chain variable domain.

remained unaffected, these IgG subclass HLA mAbs are excellent tools to study the function of individual IgG subclass HLA class I and class II-specific antibodies in a controlled fashion.

KEYWORDS

affinity, glycosylation, human leukocyte antigen, IgG subclass, monoclonal antibody, transplantation

1 | INTRODUCTION

In the field of transplantation, the induction of a humoural immune response to mismatched HLA antigens on the donor kidney is associated with graft rejection and inferior graft survival, but only in a subpopulation of patients.[1-3] The various clinical effects may be caused by the (mixture of) immunoglobulin G (IgG) subclass of produced donor-specific antibodies (DSA).[4-7] Indeed, various patterns of IgG subclasses have been observed in sera of transplanted patients that developed *de novo* DSA. However, their relative contribution to graft damage remains elusive, due to conflicting results on their clinical significance.[7,8]

The pathogenicity of an HLA antibody is determined by both the affinity for the HLA epitope recognised by the Fab part and the effector function of the antibody, defined by the Fc part. Indeed, the degree of complement activation and the binding capacity to Fc gamma receptors (FcγR) differs per IgG subclass.[9-11] In renal transplantation, DSA capable of complement activation, for example, IgG1 and IgG3, are associated with allograft loss.[7,12-14] However, other studies have implied that the presence of IgG2 and IgG4 can act either synergistically or inhibitory on complement activation, depending on the epitopes recognised.[15,16] Additionally, HLA IgG antibodies have been associated with graft damage independent of the complement cascade.[17-19] Binding of DSA to endothelial cells can lead to infiltration of macrophages causing antibody-mediated rejection, of which the severity is increased in case of IgG1 and IgG3 antibodies, due to their capacity to bind FcγR.[19] Furthermore, binding and crosslinking of HLA targets on endothelial cells can result in intracellular signalling, resulting in cell proliferation and initiation of coagulation.[18,20,21]

Thus, understanding the underlying mechanisms of IgG HLA antibody-mediated graft damage can contribute to the establishment of risk factors associated with antibody-mediated rejection. Several methodological studies on the effect of HLA antibodies in renal transplantation have been performed using human HLA monoclonal antibodies (mAbs).[16,19,22-25] However, these studies are restricted to the available human HLA mAbs, which are mainly of the IgG1 subclass. Therefore, we adapted a method to recombinantly generate and produce human mAbs of all four IgG subclasses, with the aim to generate HLA class I and class II-specific mAbs of all IgG subclasses recognising the same HLA epitope with the same affinity.

2 | MATERIALS AND METHODS

2.1 | B-cell heterohybridomas

Human B-cell heterohybridomas WIM8E5 (IgG1, κ) and RTLK1E2 (IgG1, κ), that had been established from two women who had been immunised during pregnancy by mismatched *HLA-A*11:01* and *HLA-DRB1*03:01*, respectively, were used to generate recombinant human HLA class I and class II-specific mAbs.[25] Heterohybridoma cells were cultured in Iscove's modified Dulbecco's medium supplemented with 100 μ/mL penicillin, 100 μg/mL streptomycin, 10% foetal bovine serum, 200 mM L-glutamine (all Gibco, Invitrogen, Paisley, UK), 50 μM 2 mercapto-ethanol (Sigma-Aldrich, Zwijndrecht, the Netherlands).

2.2 | Generation of human recombinant IgG1 HLA mAbs

RNA was isolated from heterohybridoma cells using RNeasy mini kit (Qiagen, Hilden, Germany). Next, SMART cDNA synthesis was performed using PrimeScript Reverse Transcriptase (Takara, Saint-Germain-en-Laye, France), and variable heavy chain (VH) IgG1, and variable light chain (VL) kappa (κ) or lambda (λ) gene products were amplified by 5′-RACE polymerase chain reaction (PCR). The VH and VL PCR products were purified with QIAquick gel extraction kit (Qiagen) and treated with T4 DNA polymerase (Bioké, Leiden, the Netherlands). Subsequently, the VH and VL products were ligation-independently cloned into pcDNA3.3 expression vectors[26] with the constant domains of the human IgG1 (*IGHG1*03*), κ (IGKC), or λ (*IGLC2*01*). The vectors were used for transformation of One Shot MAX Efficiency DH5α-T1R competent cells (ThermoFisher Scientific, Waltham, Massachusetts) by heat shock. The transformed cells were cultured on LB-agar plates supplemented with 50 μg/mL ampicillin (Sigma-Aldrich) and after overnight incubation at 37°C, multiple single colonies were picked and grown overnight in LB

medium containing ampicillin. From the cultures, plasmids were isolated using either QIAprep Spin Miniprep kit (Qiagen) or NucleoBond Xtra Midi EF (Bioké). The plasmids were sequenced by Sanger sequencing (Macrogen, Amsterdam, the Netherlands) to verify the hybridisation of VH and VL products with the expression vector. All kits were used according to manufacturer's instructions.

2.3 | Generation of human recombinant IgG subclass HLA mAbs

To generate recombinant IgG subclass HLA mAbs, the IgG1 plasmid was double digested with the appropriate restriction enzymes (Bioké). Simultaneously, pMK vectors containing IgG2 (*IGHG2*02*), IgG3 (*IGHG3*01*), or IgG4 (*IGHG4*01*) constant domains (ThermoFisher Scientific) were double digested the same way to obtain the constant domains. Next, the IgG subclass constant domain was ligated with the digested vector by T4 DNA ligase (Bioké). Subsequently, plasmids were generated as described above. Plasmids were sequenced to verify ligation of constant domain with the vector and to check if any mutations had occurred. No adaptation was made to the light chain.

2.4 | Production of human recombinant IgG HLA mAbs

For recombinant mAb production, heavy and light chain containing vectors were used for transient co-transfection of Expi293F cells with ExpiFectamine, Opti-MEM, and Expi293 expression medium (ThermoFisher Scientific) according to the instructions provided by the manufacturer. After 5 days of culture, supernatants containing the recombinant mAbs were harvested and filtered. The presence of IgG was determined by total IgG enzyme-linked immunosorbent assay (ELISA), as previously described.[27] IgG specificity of the different subclasses was confirmed by a human IgG subclass ELISA kit (ThermoFisher Scientific).

2.5 | Purification of recombinant IgG HLA mAbs

The recombinant mAbs were purified using Amicon ProAffinity Concentration Kit Protein G (Merck Millipore, Burlington, Massachusetts). A maximum of 1000 μg mAb was loaded onto 200 μL Protein G resin and incubated for 60 minutes at room temperature on a roller bench. After wash steps, mAb was eluted and neutralised. Next, the buffer was exchanged with phosphate-buffered saline (PBS, B Braun, Melsungen, Germany) using a Slide-a-lyzer 0.5-3 mL dialysis cassette (ThermoFisher Scientific) by incubating the cassette in beaker with PBS for 21 hours at 4°C, PBS was refreshed a couple of times during incubation. The concentrations of purified mAbs were measured using the protein A280 protocol of NanoDrop2000 (ThermoFisher Scientific), and molar concentration were calculated for each mAb.

2.6 | HLA antibody detection

For verification of the IgG subclasses, the supernatants were screened with Lifecodes Lifescreen Deluxe screening kit (Immucor Transplant Diagnostics, Stamford, Connecticut) modified by using anti-IgG1 (10 μg/mL; HP6001), anti-IgG2 (2.5 μg/mL; HP6002), anti-IgG3 (10 μg/mL; HP6050), and anti-IgG4 (2.5 μg/mL; HP6025) PE-conjugated detection antibodies (Southern Biotech, Birmingham, Alabama).

The HLA specificities of the recombinant mAbs were determined by screening the recombinant mAbs with Lifecodes HLA class I or II single antigen beads (SAB) using goat anti-human Pan-IgG PE-conjugated on a Luminex platform (Immucor). The ability of recombinant mAbs to bind complement component 3d (C3d) was tested with Lifedcodes C3d detection (Immucor). Both Lifecodes kits were used according to manufacturer's instructions. The data were analysed with Match It! Antibody software version 1.3.0 (Immucor).

2.7 | Bio-layer interferometry

Affinity of antibody to antigen was determined via bio-layer interferometry (BLI) using the Octet RED96 system (FortéBio, Fremont, California). HLA IgG subclasses from WIM8E5 were immobilised to anti-human IgG Fc kinetic biosensors with a response threshold of 0.6 nm. To determine the association phase, parallel sensors were dipped into wells containing soluble, recombinant *HLA-A*11:01* in a 2-fold titration from 200 to 6.25 nM for 300 seconds so an equilibrium could be reached. Next, sensors were placed into buffer alone-containing wells for a further 1000 seconds to determine the dissociation phase. Affinity values (K_D) were calculated via steady-state analysis, where the response equilibrium (R_{eq}) was plotted against the HLA analyte concentration for each sensor and K_D values were measured as the HLA concentration of 50% of the overall calculated maximum response (R_{max}). All experiments were carried out using standard kinetic buffer (1× PBS, 0.1% bovine serum albumin, 0.02% Tween-20), at a temperature of 30°C and a constant plate shake speed of 1000 rpm.

2.8 | Fc domain glycosylation profiling

Of WIM8E5 and RTLK1E2 IgG subclasses, 2 μg sample was added to a final volume of 20 μL PBS and affinity

captured with ProtG beads. After desalting, the mAbs were eluted with 100 µL 100 mM formic acid and subsequently vacuum dried at 60°C. The dried samples were resuspended in 40 µL digestion solution consisting of 25 mM ammonium bicarbonate and 5 ng/µL sequencing grade trypsin and followed by overnight digestion at 37°C to obtain tryptic glycopeptides. Fc glycosylation was measured by nano liquid chromatography-mass spectrometry of glycopeptides followed by data processing using LaCyTools as previously described.[28] From the relative abundances of the glycopeptides, the levels hybrid-type, high-mannose, and complex-type Fc *N*-glycans as well as the level of galactosylation, fucosylation, bisection, and sialylation were calculated.

2.9 | Cells

HLA-typed peripheral blood mononuclear cells (PBMCs) were isolated from buffy coats obtained from healthy donors after informed consent (Sanquin Blood Supply, Amsterdam, the Netherlands). PBMCs were isolated by Ficoll-Hypaque density gradient centrifugation and cryopreserved until further use. For the cytotoxicity experiment with RTLK1E2 mAbs, B cells were magnetically isolated from PBMCs using EasySep direct HLA cross-match B-cell isolation kit (Stemcell Technologies, Köln, Germany) with a purity of >90%.

2.10 | Complement-dependent cytotoxicity assay

Terasaki plates (Greiner) were oiled and filled with 1 µL of supernatant containing the mAb of interest in triplicate. Then, 3000 HLA typed PBMCs or B cells were added to each well and incubated for 60 minutes at 20°C. Next, 5 µL rabbit complement (Inno-train, Kronberg, Germany) was added and incubated for 60 minutes at 20°C. To visualise cytotoxicity, 5 µL propidium iodide ink was added to each well, and after 15 minutes incubation in the dark the plates were analysed with Patimed (Leica Microsystems, Amsterdam, the Netherlands).

2.11 | Statistical analysis

The Kruskal-Wallis test was used for unpaired analysis and the Friedman test was used for paired analysis. Statistical level of significance was defined as $P < .05$, and analyses were performed with GraphPad Prism, version 7.02 (GraphPad Software, La Jolla, California).

3 | RESULTS

3.1 | Recombinant human IgG subclass HLA mAbs

Genes encoding the variable heavy chain and light chain domains were cloned into expression vectors, after which recombinant antibodies can be expressed by transient co-transfection of both vectors.[29-31] Here, we generated recombinant human HLA class I and class II mAbs, WIM8E5, and RTLK1E2, respectively, of all four IgG subclasses. To verify IgG subclass, the supernatant of all four IgG subclass mAbs were screened with IgG subclass ELISA and a modified Luminex screening assay using detection antibodies specific for each IgG subclass. As shown in Figure 1, the specific IgG constant domains were recognised by the correct detection antibody, indicating that mAbs of all four IgG subclasses were produced.

To corroborate that HLA specificities remained unaffected by the recombinant technology, original hybridoma-generated mAbs and recombinant human IgG subclass mAbs were screened with HLA class I or II SAB Luminex assay. Upon comparison of the background corrected mean fluorescence intensity (BCM) values of both WIM8E5 (Figure 2A) and RTLK1E2 (Figure 2B) mAbs, no difference in HLA specificities was observed with the original hybridoma-generated mAb for both recombinant IgG subclass HLA mAbs.

3.2 | Affinity and Fc domain glycosylation is similar between IgG subclasses

As the recombinant IgG subclass HLA mAbs have the same HLA specificity, we next questioned whether these mAbs have the same affinity for the immunising HLA allele. Therefore, the recombinant IgG subclass WIM8E5 mAbs were tested with bio-layer interferometry (BLI). The affinity values (K_D) observed for the target *HLA-A*11:01* were in the range of 25 to 32 nM for all four IgG subclass WIM8E5 mAbs (Figure 3).

For mAb production Expi293F cells are used, so we wanted to determine if the correct human glycosylation was present on the Fc part of the generated mAbs. The glycosylation characterisation of the generated recombinant IgG subclass HLA class I and class II mAbs showed that the IgG subclasses have a similar profile (Figure 4). In addition, the observed glycosylation traits of the mAbs are in accordance with those found on IgG in human serum using the same method.[32] However, the relative levels of bisection (the presence of a bisecting *N*-acetylglucosamine) and sialylation are lower on the mAbs, as compared to what is generally found on IgG in human serum, while the abundance of high mannose-type species is higher.[32] For IgG3, we detected

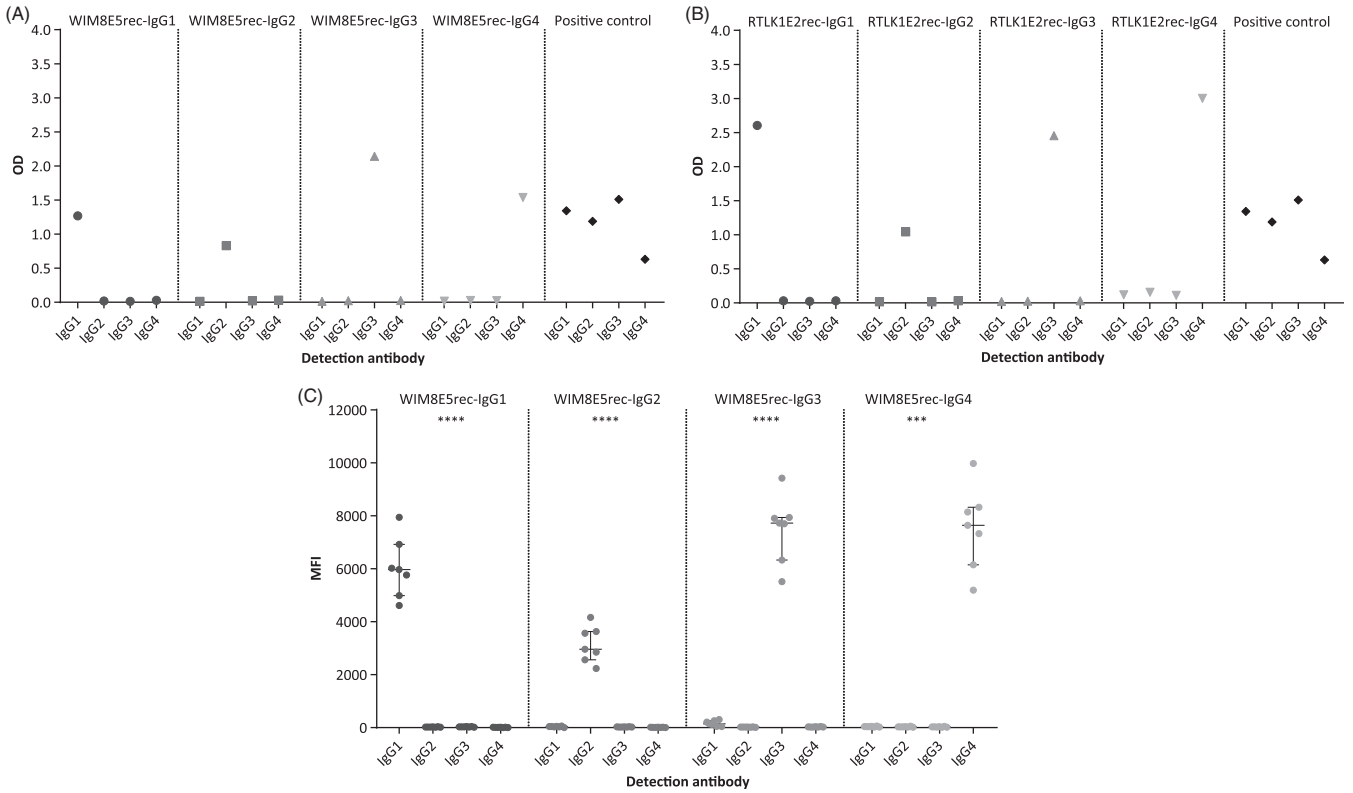

FIGURE 1 Recombinant IgG subclass HLA monoclonal antibodies (mAbs) could be detected by the corresponding IgG-specific detection antibody. IgG subclass could be detected with IgG subclass enzyme-linked immunosorbent assay (ELISA) kit for both WIM8E5rec-IgG mAbs (A) and RLTK1E2rec-IgG mAbs (B). Positive control is a human serum. (C) Similar findings were observed when screening recombinant WIM8E5 IgG subclass mAbs with Lifecodes Lifescreen Deluxe kit. The kit contains seven groups of HLA class I beads and each data point represents a single bead group. Kruskal-Wallis test was used to compare median of all four detection antibodies per IgG subclass mAb. Error bars represent median ± interquartile range. MFI is mean fluorescence intensity. OD is optical density. ***$P < .001$, ****$P < .0001$

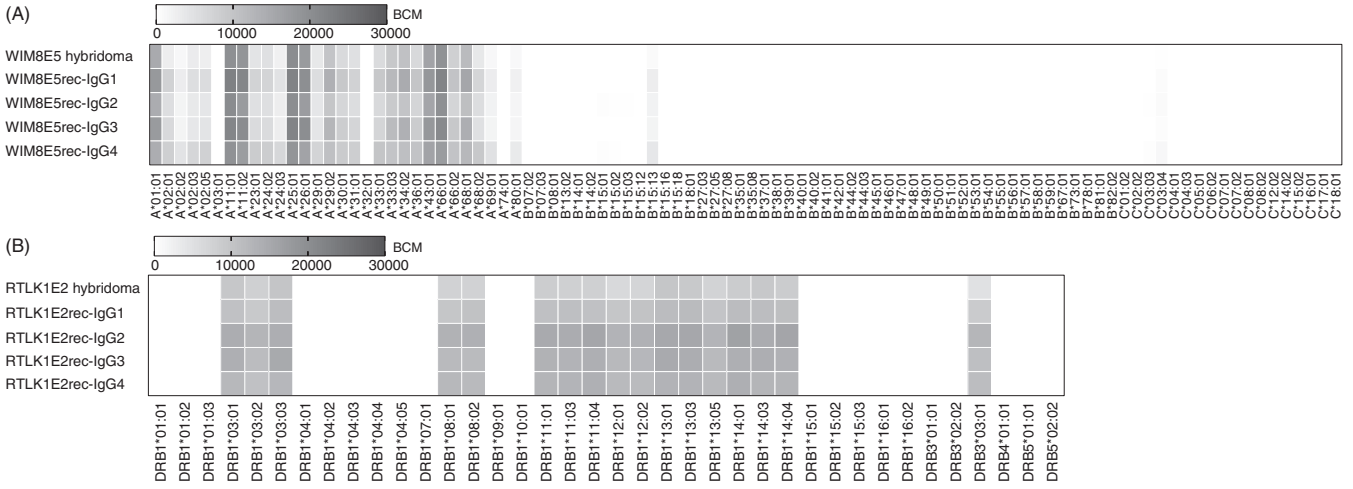

FIGURE 2 The same HLA epitope is recognised by the recombinant IgG subclass HLA monoclonal antibodies (mAbs). HLA specificities of recombinant IgG1, IgG2, IgG3, and IgG4 of WIM8E5 mAb (A) and RTLK1E2 mAb (B, only DRB1/3/4/5 beads are shown as all other loci were negative) as detected by Luminex SAB assay. Purified recombinant mAb concentration tested was 62.5 nM. BCM is background corrected mean fluorescence intensity

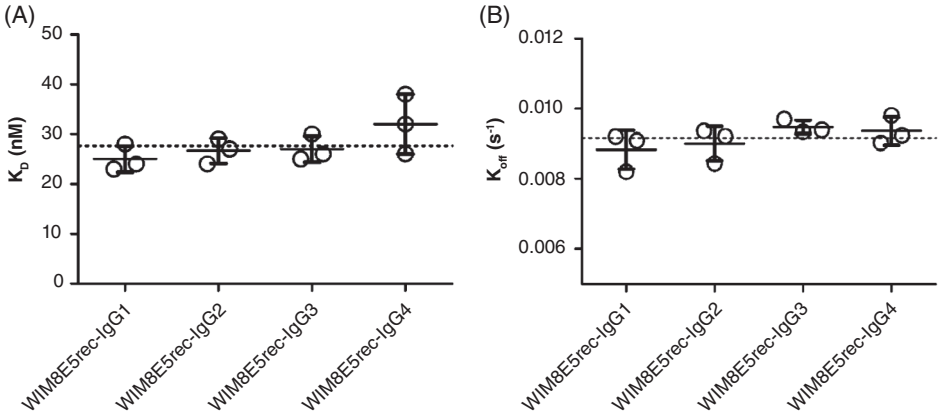

FIGURE 3 Recombinant IgG subclass HLA monoclonal antibodies (mAbs) have similar affinity. The affinity (A) and dissociation rates (B) of recombinant IgG subclass WIM8E5 mAbs were determined via bio-layer interferometry. Calculated values are consistently similar across all IgG subclasses against the target *HLA-A*11:01*. The dotted lines represent the affinity (A) and dissociation constant (B) average across all four IgG subclasses. Error bars represent the mean ± SD of three experiments

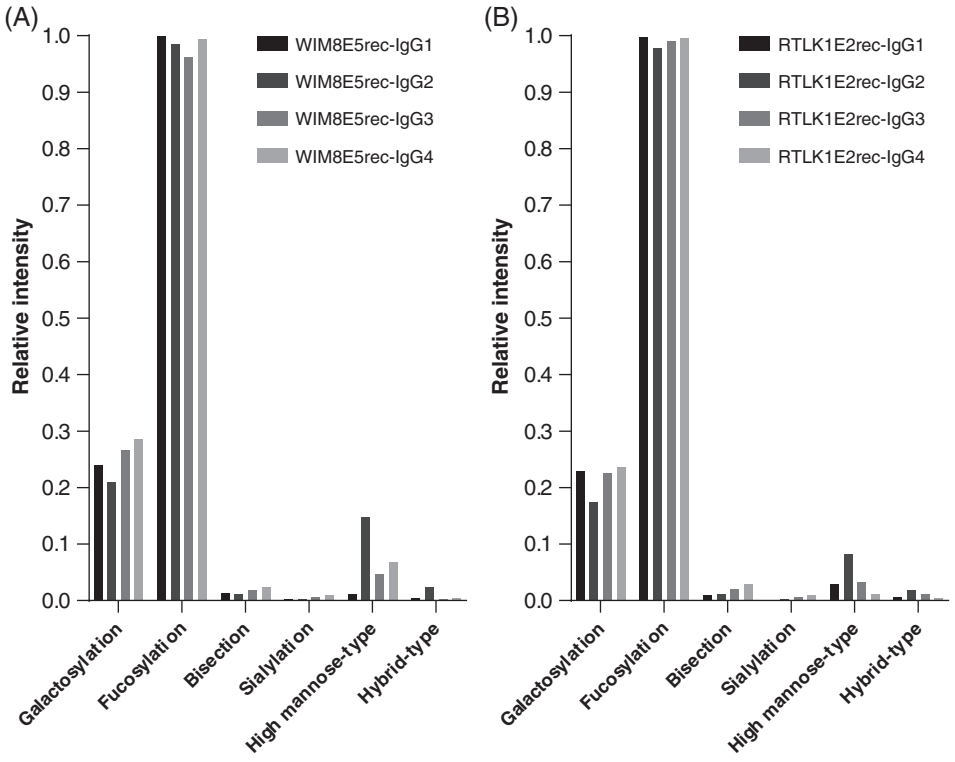

FIGURE 4 The glycosylation profile of recombinant IgG subclass HLA monoclonal antibodies (mAbs) is similar. Relative intensity values of derived traits for the recombinant IgG1, IgG2, IgG3, and IgG4 of WIM8E5 mAb (A) and RLTK1E2 mAbs (B) are shown

partial occupancy of the *O*-glycosylation sites in the hinge region (data not shown), which is in line with the hinge region *O*-glycosylation of IgG3 from the human circulation.[33]

3.3 | Cytotoxicity of recombinant human IgG subclass HLA mAbs

To determine whether the recombinantly generated IgG subclass HLA-specific mAbs showed the anticipated cytotoxicity patterns, we performed complement-dependent cytotoxicity (CDC) assays. Incubation of WIM8E5 recombinant IgG subclass mAbs with PBMCs expressing HLA antigens recognised by WIM8E5 (HLA-A11, -A1) showed that WIM8E5rec-IgG1 and -IgG3 mAbs were highly cytotoxic in a dose-dependent manner (Figure 5A). Both IgG2 and IgG4 subclasses did not show cytotoxicity. For the HLA class II mAb RTLK1E2, a CDC using purified B cells (HLA-DR17, -DR13) was performed. Both RTLK1E2rec-IgG1 and -IgG3 were highly cytotoxic (Figure 5B). While CDC with rabbit complement is standard practice in transplantation, it does not show if mAbs can also activate human complement.

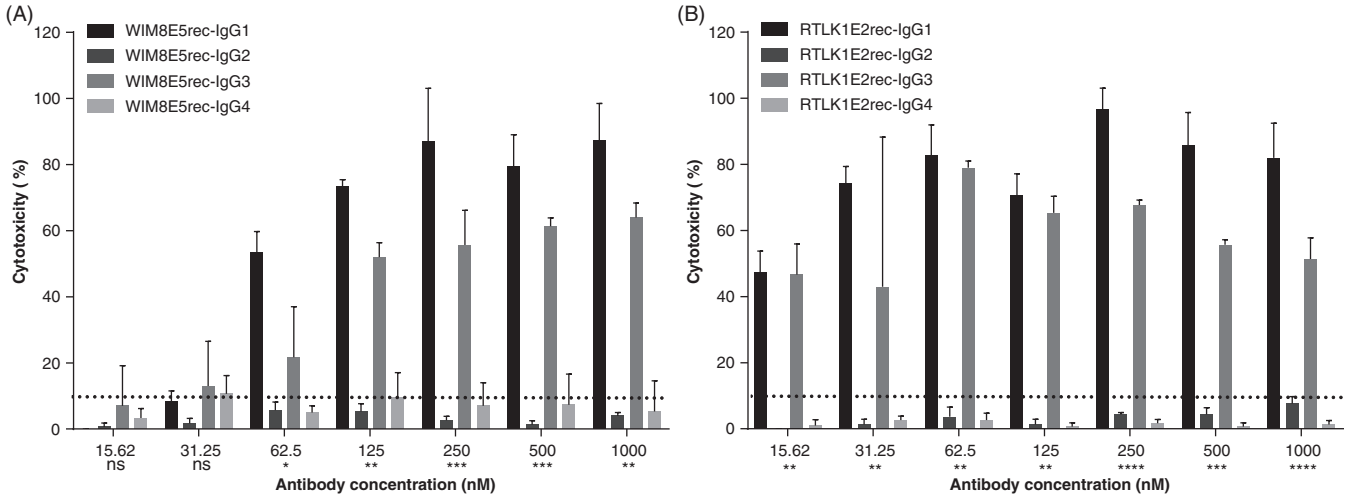

FIGURE 5 Recombinant IgG1 and IgG3 HLA monoclonal antibodies (mAbs) are cytotoxic. (A) Recombinant IgG subclass WIM8E5 mAbs were incubated with PBMC expressing HLA-A1, -A11, -B8, -B55, -Cw3, and -Cw7. WIM8E5rec-IgG1 and -IgG3 induced cell lysis (>60%), while IgG2 and IgG4 were unable to induce complement cytotoxicity. (B) Recombinant IgG subclass RTLK1E2 mAbs were incubated with B cells expressing HLA-DR17, -DR13, and -DR52. RTLK1E2rec-IgG1 (>80%) and -IgG3 (>60%) induced cell lysis, while no cell lysis was observed for RLTK1E2rec-IgG2 and RTKL1E2rec-IgG4. mAbs were added in various concentrations (1000, 500, 250, 125, 62.5, 31.25, and 15.62 nM). Error bars represent the mean ± SD of triplicate wells. The Kruskal-Wallis test was used per dilution to compare the IgG subclass HLA mAbs. Dotted line indicates background. ****$P < .0001$ ***$P < .001$, **$P < .01$, *$P < .05$

Testing the recombinant IgG subclass HLA mAbs with C3d SAB assay showed that only IgG1 and IgG3 mAbs are capable of binding human C3d (Figure S1), suggesting that these mAbs can activate human complement.

4 | DISCUSSION

In this study, we show the generation and production of recombinant human HLA class I and class II-specific mAbs of all four IgG subclasses from established B-cell heterohybridomas. The generated recombinant HLA mAbs of all four IgG subclasses recognise the same HLA epitope with the same binding affinity. Currently, we were only able to determine the affinity for the HLA class I mAbs, due to lack of recombinant HLA class II. Furthermore, we show that all recombinant IgG subclass HLA mAbs have human-type Fc glycosylation and the glycosylation profiles were similar between the mAbs. The conserved *N*-glycans located at asparagine 297 of the Fc part play a role in the function of an antibody and the different levels of specific glycosylation traits could have pronounced effects on complement activation and FcγR binding.[34,35] Both IgG1 and IgG3 HLA class I and class II mAbs are capable of complement activation, while a weak or no cytotoxicity was observed for the IgG2 and IgG4 mAbs. Preliminary data suggest that IgG1 and IgG3 can induce antibody-dependent cell-mediated cytotoxicity (ADCC), but only a low percentage of cell lysis was observed (Figure S2). This can be explained by the high levels of fucosylation (>96%) on the recombinant IgG subclass HLA mAbs, as it has been shown that high levels of fucosylation on IgG negatively influences ADCC activity.[36] Glyco-engineering of our recombinant IgG subclass HLA mAbs may further allow altering their functional properties.[37]

Currently available human HLA mAbs are mainly derived from multiparous women by Epstein-Barr virus transformation and electrofusion using mouse myeloma cell line, are primarily directed against HLA class I, and are restricted to an IgM or IgG1 isotype.[25,38,39] These human HLA mAbs have been widely used in various applications, such as flow cytometry assays,[40-42] B-cell ELISPOT assays,[43-45] blocking assays,[46] assays to determine HLA expression levels,[47-49] or functional assays of HLA antibodies.[16,19,22-24] Commercial chimeric IgG subclass HLA mAbs are available, but those have a mouse variable part, while W6/32 and F3.3 recognise all HLA class I molecules and majority of HLA class II molecules, respectively.[50]

Recently, Gu et al[51] elegantly characterised an HLA class I mAb generated by a germline phage display from a non-sensitised individual, resulting in an antibody that likely can be generated during an alloimmune response. In contrast, we have produced human recombinant HLA mAbs generated from heterohybridomas that were derived from B cells of immunised individuals. Therefore, the mAbs we produced are truly representative of HLA antibodies produced through alloimmunisation. In addition, we generated both human HLA class I and class II mAbs of all four IgG subclasses. Especially the latter is unique, as there are only a limited

number of HLA class II mAbs available and those are mainly IgG1.

Antibody effector function is determined by its isotype. As mentioned, complement binding HLA DSA is associated with graft loss, but in sera of renal transplant patients both complement binding, IgG1 and IgG3, as well as non-complement binding, IgG2 and IgG4 HLA antibodies are observed.[8,12-14] Previous studies have shown by mixing IgG subclass mAbs that IgG2 and/or IgG4 can inhibit complement activation of IgG1 and/or IgG3 when recognising the same epitope.[15,51] Others performed mixing experiments with human HLA mAbs directed against different epitopes of same HLA antigens and showed that combining these HLA mAbs promote complement activation, while individually the mAbs had no effect.[16] Additional mixture studies with human mAbs directed to HLA class I and class II molecules of different IgG subclasses, comparing different specificities and avidities, should be performed as this will allow greater understanding of the interaction of antibodies of different IgG subclasses recognising different epitopes on the same HLA molecules.

In addition, HLA mAbs have been used for functional assays to study HLA-antibody-induced graft damage independent of the complement cascade. HLA class I antibodies can cause crosslinking on endothelial and smooth muscle cells inducing intracellular signalling, resulting in inflammatory activation, and leukocyte recruitment such as P-selectin-induced monocyte adhesion.[17-19,52-54] Although crosslinking is irrespective of the IgG subclass, the level of P-selectin on endothelial cells and the monocyte recruitment via FcγR mechanism are increased with IgG1 and IgG3 antibodies. The levels of P-selectin and FcγR-dependent monocyte recruitment have been well studied with human IgG1 HLA mAb,[19] but due to lack of IgG3, IgG2, and IgG4 HLA mAbs, the exact influence of antibodies with these isotypes, especially the latter two, is not fully clear.

Human HLA mAb do not represent the polyclonal response observed in sera. However, due to the mixture of antibody specificities, concentrations and isotypes of HLA antibodies present in sera it is difficult to study the role and function of HLA antibodies. By using human HLA mAbs, mixture experiments can be performed in a controlled manner, even with normal human serum as matrix. For future studies, it is essential to extend the specificities of the available mAbs, since especially mAbs for HLA class II are currently lacking.

In conclusion, we show here that recombinant human HLA class I and class II mAbs of all four IgG subclasses recognising the same HLA epitope can be generated from established B-cell heterohybridomas. This method enables us to generate more IgG subclass HLA mAbs recognising different epitopes on the same HLA antigen, which can be used in mixing experiments to study the role and function of HLA DSA of different IgG subclasses in a controlled fashion. These IgG subclass HLA class I and class II mAbs can provide mechanistic insights into the role of DSA in renal transplantation and in other clinical settings.

ACKNOWLEDGMENTS

The authors thank the HLA typing and screening laboratory Leiden, the Netherlands, and Merve Uyar-Mercankaya for technical assistance and Geert W. Haasnoot for statistical advice.

CONFLICT OF INTEREST

C. C.C. Z.-v. d. O. and H. J. R. are Genmab employees and own Genmab stocks.

DATA ACCESSIBILITY

Data available on request from the authors.

ORCID

Cynthia S. M. Kramer https://orcid.org/0000-0003-1350-2336

REFERENCES

1. Everly MJ, Rebellato LM, Haisch CE, et al. Incidence and impact of de novo donor-specific alloantibody in primary renal allografts. *Transplantation*. 2013;95(3):410-417.
2. Hourmant M, Cesbron-Gautier A, Terasaki PI, et al. Frequency and clinical implications of development of donor-specific and non-donor-specific HLA antibodies after kidney transplantation. *J Am Soc Nephrol*. 2005;16(9):2804-2812.
3. Wiebe C, Gibson IW, Blydt-Hansen TD, et al. Evolution and clinical pathologic correlations of de novo donor-specific HLA antibody post kidney transplant. *Am J Transplant*. 2012;12(5):1157-1167.
4. Arnold ML, Ntokou IS, Doxiadis II, Spriewald BM, Boletis JN, Iniotaki AG. Donor-specific HLA antibodies: evaluating the risk for graft loss in renal transplant recipients with isotype switch from complement fixing IgG1/IgG3 to noncomplement fixing IgG2/IgG4 anti-HLA alloantibodies. *Transpl Int*. 2014;27(3):253-261.
5. Honger G, Hopfer H, Arnold ML, Spriewald BM, Schaub S, Amico P. Pretransplant IgG subclasses of donor-specific human leukocyte antigen antibodies and development of antibody-mediated rejection. *Transplantation*. 2011;92(1):41-47.
6. Khovanova N, Daga S, Shaikhina T, et al. Subclass analysis of donor HLA-specific IgG in antibody-incompatible renal transplantation reveals a significant association of IgG4 with rejection and graft failure. *Transpl Int*. 2015;28(12):1405-1415.

7. Lefaucheur C, Viglietti D, Bentlejewski C, et al. IgG donor-specific anti-human HLA antibody subclasses and kidney allograft antibody-mediated injury. *J Am Soc Nephrol*. 2016;27(1):293-304.
8. Lowe D, Higgins R, Zehnder D, Briggs DC. Significant IgG subclass heterogeneity in HLA-specific antibodies: implications for pathogenicity, prognosis, and the rejection response. *Hum Immunol*. 2013;74(5):666-672.
9. Tao MH, Smith RI, Morrison SL. Structural features of human immunoglobulin G that determine isotype-specific differences in complement activation. *J Exp Med*. 1993;178(2):661-667.
10. Bruhns P, Iannascoli B, England P, et al. Specificity and affinity of human Fcgamma receptors and their polymorphic variants for human IgG subclasses. *Blood*. 2009;113(16):3716-3725.
11. Bruggemann M, Williams GT, Bindon CI, et al. Comparison of the effector functions of human immunoglobulins using a matched set of chimeric antibodies. *J Exp Med*. 1987;166(5):1351-1361.
12. Loupy A, Lefaucheur C, Vernerey D, et al. Complement-binding anti-HLA antibodies and kidney-allograft survival. *N Engl J Med*. 2013;369(13):1215-1226.
13. Sutherland SM, Chen G, Sequeira FA, Lou CD, Alexander SR, Tyan DB. Complement-fixing donor-specific antibodies identified by a novel C1q assay are associated with allograft loss. *Pediatr Transplant*. 2012;16(1):12-17.
14. Viglietti D, Loupy A, Vernerey D, et al. Value of donor-specific anti-HLA antibody monitoring and characterization for risk stratification of kidney allograft loss. *J Am Soc Nephrol*. 2017;28(2):702-715.
15. Honger G, Amico P, Arnold ML, Spriewald BM, Schaub S. Effects of weak/non-complement-binding HLA antibodies on C1q-binding. *HLA*. 2017;90(2):88-94.
16. Kushihata F, Watanabe J, Mulder A, Claas F, Scornik JC. Human leukocyte antigen antibodies and human complement activation: role of IgG subclass, specificity, and cytotoxic potential. *Transplantation*. 2004;78(7):995-1001.
17. Jindra PT, Zhang X, Mulder A, et al. Anti-HLA antibodies can induce endothelial cell survival or proliferation depending on their concentration. *Transplantation*. 2006;82(1 Suppl):S33-S35.
18. Li F, Zhang X, Jin YP, Mulder A, Reed EF. Antibody ligation of human leukocyte antigen class I molecules stimulates migration and proliferation of smooth muscle cells in a focal adhesion kinase-dependent manner. *Hum Immunol*. 2011;72(12):1150-1159.
19. Valenzuela NM, Mulder A, Reed EF. HLA class I antibodies trigger increased adherence of monocytes to endothelial cells by eliciting an increase in endothelial P-selectin and, depending on subclass, by engaging FcγRs. *J Immunol*. 2013;190(12):6635-6650.
20. Kuo HH, Fan R, Dvorina N, Chiesa-Vottero A, Baldwin WM 3rd. Platelets in early antibody-mediated rejection of renal transplants. *J Am Soc Nephrol*. 2015;26(4):855-863.
21. Zhang X, Rozengurt E, Reed EF. HLA class I molecules partner with integrin beta4 to stimulate endothelial cell proliferation and migration. *Sci Signal*. 2010;3(149):ra85.
22. Duquesnoy RJ, Marrari M, Mulder A, Claas FH, Mostecki J, Balazs I. Structural aspects of human leukocyte antigen class I epitopes detected by human monoclonal antibodies. *Hum Immunol*. 2012;73(3):267-277.
23. Duquesnoy RJ, Mulder A, Askar M, Fernandez-Vina M, Claas FH. HLAMatchmaker-based analysis of human monoclonal antibody reactivity demonstrates the importance of an additional contact site for specific recognition of triplet-defined epitopes. *Hum Immunol*. 2005;66(7):749-761.
24. Daga S, Moyse H, Briggs D, et al. Direct quantitative measurement of the kinetics of HLA-specific antibody interactions with isolated HLA proteins. *Hum Immunol*. 2018;79(2):122-128.
25. Mulder A, Kardol M, Regan J, Buelow R, Claas F. Reactivity of twenty-two cytotoxic human monoclonal HLA antibodies towards soluble HLA class I in an enzyme-linked immunosorbent assay (PRA-STAT). *Hum Immunol*. 1997;56(1–2):106-113.
26. de Jong RN, Daniels MA, Kaptein R, Folkers GE. Enzyme free cloning for high throughput gene cloning and expression. *J Struct Funct Genomics*. 2006;7(3–4):109-118.
27. Heidt S, Roelen DL, Eijsink C, et al. Calcineurin inhibitors affect B cell antibody responses indirectly by interfering with T cell help. *Clin Exp Immunol*. 2010;159(2):199-207.
28. Falck D, Jansen BC, de Haan N, Wuhrer M. High-throughput analysis of IgG fc Glycopeptides by LC-MS. *Methods Mol Biol*. 2017;1503:31-47.
29. Vink T, Oudshoorn-Dickmann M, Roza M, Reitsma JJ, de Jong RN. A simple, robust and highly efficient transient expression system for producing antibodies. *Methods*. 2014;65(1):5-10.
30. van Berkel PH, Gerritsen J, van Voskuilen E, et al. Rapid production of recombinant human IgG with improved ADCC effector function in a transient expression system. *Biotechnol Bioeng*. 2010;105(2):350-357.
31. van der Neut KM, Schuurman J, Losen M, et al. Anti-inflammatory activity of human IgG4 antibodies by dynamic fab arm exchange. *Science*. 2007;317(5844):1554-1557.
32. Plomp R, Ruhaak LR, Uh HW, et al. Subclass-specific IgG glycosylation is associated with markers of inflammation and metabolic health. *Sci Rep*. 2017;7(1):12325.
33. Plomp R, Dekkers G, Rombouts Y, et al. Hinge-region O-glycosylation of human immunoglobulin G3 (IgG3). *Mol Cell Proteomics*. 2015;14(5):1373-1384.
34. Anthony RM, Wermeling F, Ravetch JV. Novel roles for the IgG fc glycan. *Ann N Y Acad Sci*. 2012;1253:170-180.
35. Dekkers G, Treffers L, Plomp R, et al. Decoding the human immunoglobulin G-glycan repertoire reveals a Spectrum of fc-receptor- and complement-mediated-effector activities. *Front Immunol*. 2017;8:877.
36. Shields RL, Lai J, Keck R, et al. Lack of fucose on human IgG1 N-linked oligosaccharide improves binding to human Fcgamma RIII and antibody-dependent cellular toxicity. *J Biol Chem*. 2002;277(30):26733-26740.
37. Dekkers G, Plomp R, Koeleman CA, et al. Multi-level glycoengineering techniques to generate IgG with defined fc-glycans. *Sci Rep*. 2016;6:36964.
38. Mulder A, Kardol M, Blom J, Jolley WB, Melief CJ, Bruning H. A human monoclonal antibody, produced following in vitro immunization, recognizing an epitope shared by HLA-A2 subtypes and HLA-A28. *Tissue Antigens*. 1993;42(1):27-34.
39. Mulder A, Kardol M, Blom J, Jolley WB, Melief CJ, Bruning JW. Characterization of two human monoclonal antibodies reactive with HLA-B12 and HLA-B60, respectively, raised by in vitro secondary immunization of peripheral blood lymphocytes. *Hum Immunol*. 1993;36(3):186-192.
40. Eijsink C, Kester MG, Franke ME, et al. Rapid assessment of the antigenic integrity of tetrameric HLA complexes by human

monoclonal HLA antibodies. *J Immunol Methods*. 2006;315(1–2): 153-161.
41. Romee R, Rosario M, Berrien-Elliott MM, et al. Cytokine-induced memory-like natural killer cells exhibit enhanced responses against myeloid leukemia. *Sci Transl Med*. 2016;8(357):357ra123.
42. Zoet YM, Eijsink C, Kardol MJ, et al. The single antigen expressing lines (SALs) concept: an excellent tool for screening for HLA-specific antibodies. *Hum Immunol*. 2005;66(5): 519-525.
43. Heidt S, Roelen DL, de Vaal YJ, et al. A NOVel ELISPOT assay to quantify HLA-specific B cells in HLA-immunized individuals. *Am J Transplant*. 2012;12(6):1469-1478.
44. Karahan GE, de Vaal YJ, Roelen DL, Buchli R, Claas FH, Heidt S. Quantification of HLA class II-specific memory B cells in HLA-sensitized individuals. *Hum Immunol*. 2015;76(2–3): 129-136.
45. Karahan GE, de Vaal YJH, Krop J, et al. A memory B cell Crossmatch assay for quantification of donor-specific memory B cells in the peripheral blood of HLA-immunized individuals. *Am J Transplant*. 2017;17(10):2617-2626.
46. van Bergen CA, van Luxemburg-Heijs SA, de Wreede LC, et al. Selective graft-versus-leukemia depends on magnitude and diversity of the alloreactive T cell response. *J Clin Invest*. 2017;127(2): 517-529.
47. Datema G, Stein S, Eijsink C, Mulder A, Claas FH, Doxiadis II. HLA-C expression on platelets: studies with an HLA-Cw1-specific human monoclonal antibody. *Vox Sang*. 2000;79(2):108-111.
48. Koelman CA, Mulder A, Jutte NH, et al. The application of human monoclonal antibodies for monitoring donor derived soluble HLA class I molecules in the serum of heart transplant recipients. *Hum Immunol*. 1998;59(2):106-114.
49. Koene G, Mulder A, van der Ven K, et al. Human monoclonal antibodies as a tool for the detection of HLA class I allele-specific expression loss in head-and-neck squamous cell carcinoma and corresponding lymph node metastases. *Hum Immunol*. 2006;67(9): 692-699.
50. Congy-Jolivet N, Drocourt D, Portet S, Tiraby G, Blancher A. Production and characterization of chimeric anti-HLA monoclonal antibodies targeting public epitopes as tools for standardizations of the anti-HLA antibody detection. *J Immunol Methods*. 2013;390 (1–2):41-51.
51. Gu Y, Wong YH, Liew CW, et al. Defining the structural basis for human alloantibody binding to human leukocyte antigen allele HLA-A*11:01. *Nat Commun*. 2019;10(1):893.
52. Valenzuela NM, Hong L, Shen XD, et al. Blockade of p-selectin is sufficient to reduce MHC I antibody-elicited monocyte recruitment in vitro and in vivo. *Am J Transplant*. 2013;13(2):299-311.
53. Valenzuela NM, Thomas KA, Mulder A, Parry GC, Panicker S, Reed EF. Complement-mediated enhancement of monocyte adhesion to endothelial cells by HLA antibodies, and blockade by a specific inhibitor of the classical complement cascade, TNT003. *Transplantation*. 2017;101(7):1559-1572.
54. Valenzuela NM, Trinh KR, Mulder A, Morrison SL, Reed EF. Monocyte recruitment by HLA IgG-activated endothelium: the relationship between IgG subclass and FcgammaRIIa polymorphisms. *Am J Transplant*. 2015;15(6):1502-1518.

SUPPORTING INFORMATION

Additional supporting information may be found online in the Supporting Information section at the end of this article.

How to cite this article: Kramer CSM, Franke-van Dijk MEI, Priddey AJ, et al. Recombinant human monoclonal HLA antibodies of different IgG subclasses recognising the same epitope: Excellent tools to study differential effects of donor-specific antibodies. *HLA*. 2019;94:415–424. https://doi.org/10.1111/tan.13664

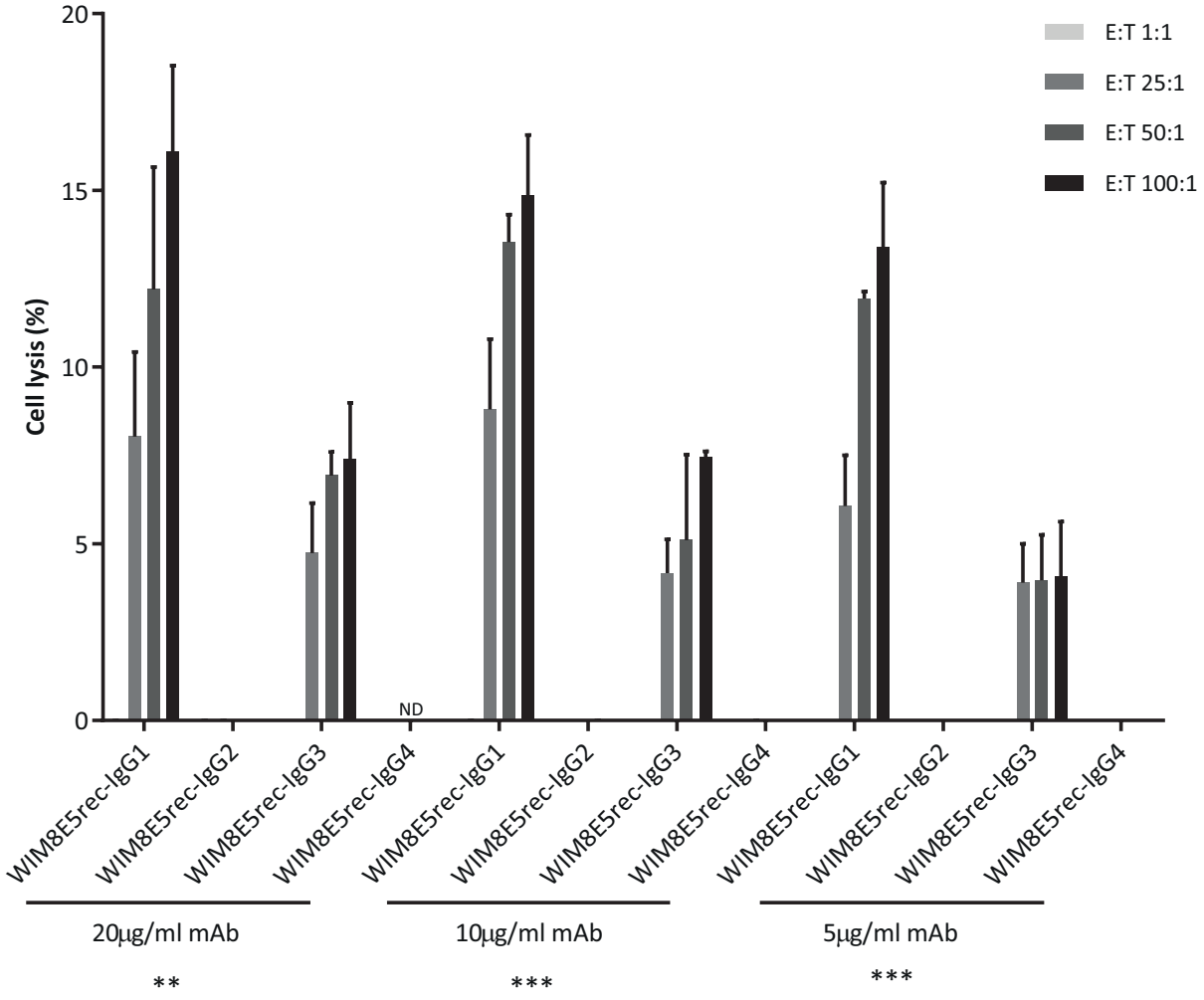

FIGURE S1 Human recombinant IgG1 and IgG3 HLA monoclonal antibodies (mAbs) can bind to human complement component 3d (C3d). Recombinant IgG subclass WIM8E5 mAbs (A) and RTLK1E2 mAbs (B, only DRB beads shown as all other loci were negative) were screened with Lifecodes C3d detection assay according to manufacturer's instructions. Purified recombinant mAb was tested with concentration of 62.5 nM. BCM is background corrected mean fluorescence intensity

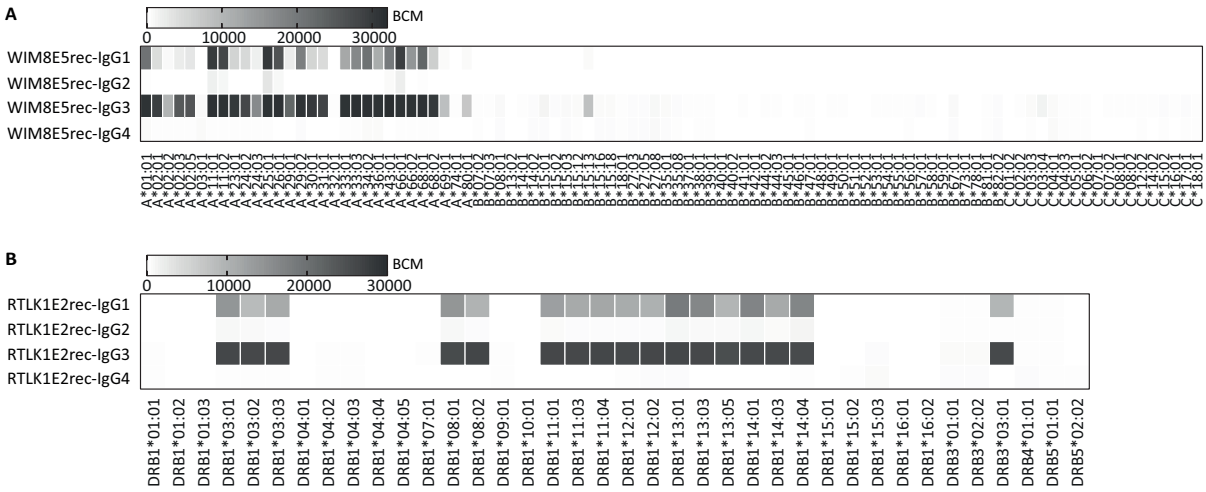

FIGURE S2 Human recombinant IgG1 and IgG3 HLA monoclonal antibodies (mAbs) can induce antibody-dependent cell lysis. HLA-typed phytohemagglutinin (PHA) blast cells expressing HLA-A11, −A24, -B35, -B40, -Cw10, and -Cw4 were generated by culturing peripheral blood mononuclear cells (PBMCs) for 7 days in RPMI 1640 medium (Gibco) containing 10% human serum S357, 200 mM L-glutamine, 10 CU/mL IL-2 (Proleukin Novartis, Arnhem, the Netherlands), and 4 µg/mL PHA (ThermoFisher Scientific). These PHA blasts were labelled with chromium-51 (^{51}Cr), and incubated with different concentrations non-purified WIM8E5rec-IgG1, -IgG2, -IgG3, and -IgG4 for 30 minutes at 37°C. Next, the effector cells, the HLA-typed PBMCs, were added and after 4 hours of incubation at 37°C, ^{51}Cr release was measured with γ-counter (PerkinElmer, Waltham, Massachusetts). The percentage of cell lysis was calculated by the following formula: (experimental ^{51}Cr release - spontaneous ^{51}Cr release)/(maximum ^{51}Cr release - spontaneous ^{51}Cr release) x 100. ^{51}Cr-labelled PHA blasts incubated with medium alone gave spontaneous ^{51}Cr release and maximum ^{51}Cr release was determined by adding TritonX100. Experiment was performed at different effector: target (E:T) ratios. Cell lysis was only observed with WIM8E5rec-IgG1 and -IgG3 induced cell lysis. Per mAb concentration the Friedman test paired for E:T ratio was performed to indicate difference between the four IgG subclass mAbs. Error bars represent the mean ± SD of triplicate wells. ND is not determined. ***P < .001, **P < .01, *P < .05